INVESTIGATING A NOVEL SMALL MOLECULE INHIBITOR OF NUCLEAR IMPORT AS AN ANTI-CANCER APPROACH

Ru-pin Alicia Chi

Thesis presented for the Degree of

DOCTOR OF PHILOSOPHY

In the Department of

Medical Biochemistry

UNIVERSITY OF CAPE TOWN

August 2016

DECLARATION

I, Ru-pin Alicia Chi, hereby declare that the contents of this thesis is my own unaided work, except where acknowledgements indicate otherwise; and that neither the whole work nor any part of it has been, is being, or is to be submitted for another degree in this or any other University. I am now presenting this thesis for academic examination towards the Degree of Doctor of Philosophy in Medical Biochemistry.

Signed: Signed by candidate Date: 14/August/2015

Signature removed

ACKNOWLEDGEMENTS

First, and foremost, I would like to express my most sincere and genuine gratitude to the two most important people in this journey; my father, Prof M.C. Chi, for his unconditional love and support, financially, emotionally and spiritually, words cannot describe my appreciation. My supervisor, A/Prof V. Leaner, for the inspiration, for the constant encouragement, for sharing her scientific expertise, and for providing indispensible guidance yet allowing me the freedom to conduct this research in my own way, as well as having faith in me through my ups and downs.

My co-supervisor, A/Prof D. Hendricks, for his excellent suggestions, creativity and support .

Dr P. van der Watt, for her countless help and advice, her patience and mentorship, both experimentally and conceptually.

Our laboratory technician, Robert Samuels, for making our work so much easier, and making sure that we never ran out of glassware and consumables even through public holidays and periods of student protesting.

Our laboratory manager, Hajira Guzgay, for keeping the lab running smoothly and spoiling us with treats from time to time.

To each and every member of the cancer lab family for making this work environment amicable and pleasant, for the generosity at sharing protocols and optimized experimental conditions. Special thanks to Liselotte Angus and Kate Hadley, for their eager and valuable contributions at each lab meeting; Liselotte Angus, Nina Holderness and Erin Strydom for always giving a helping hand when in need; Luke Esau for encouragements and support; Boris Krivochiev and Cleo Williams for adding a special dynamic to the lab environment; Hapiloe Maranyane and Tamlyn Shaw for all the laughter and entertainment, especially on the dreaded Friday afternoons; Tamara Stelma and Sarah Carden for the countless stimulating conversations over lunch hours, the source and inspiration which sparked many ideas in my work; and last but not the least, Liselotte Angus, Nelusha Shummoogam, Cherise Dunn, Tamara Stelma and Sarah Carden for friendship and immense support, it was their friendship and encouragement that kept me going through my worst times.

Dr Michael Birrer, for inviting me to, and accommodating me in his laboratory at the Gynecological Cancer Laboratory, Massachusetts General Hospital, Harvard Medical School, for 10 months. It was an experience so precious and irreplaceable, which taught me the clinical side of science. Special thanks to members for the Birrer Laboratory - Dr W. Wei, Dr Y.J. Na, Dr T.Y. Tsang, Dr G. Mohapatra and Dr V. Vathipadiekal, for their hospitality and warmth, as well as their scientific advices.

The animal technician, Rodney Lucas, for assistance in animal experiments, especially for overtime work during the countless weekends.

Susan Cooper, for assistance with the fluorescent microscope.

Mathew Njoroge, for assistance with the liver microsome assay and all the HPLC work.

A/Prof S. Prince and Dr A. Cooper, for kindly providing the pTIG-shTBX2 plasmid and pTIG-scr plasmid.

Che-Hang Yu, for his friendship, constant encouragement, faith, his patience and assistance on the confocal microscope.

William Michaud and Yu-shan Stephanie Hsiao, for their invaluable advice and suggestions, both scientifically and career-wise, as well as friendship.

Phoebe Hsieh, for friendship and constant support and encouragement.

National Research Foundation for the scholarship and financial assistance; and the University of Cape Town for the scholarships and bursaries which made my visit at Dr Birrer's lab possible.

"If we knew what it was we were doing, it would not be called research, would it?"

Albert Einstein

CONTENTS

ABBREVIATIONS

°C	Degree Celcius
%	Percentage
ABC	ATP-Binding Cassette
AKT	Protein Kinase B
APS	Ammonium Persulphate
ARH1	Aplasia Ras Homolog Member 1
ATM	Ataxia Telangiectasia Mutated
BCA	Bicinchoninic Acid
bp	Base pairs
BRCA	Breast Cancer Susceptibility Gene
BSA	Bovine Serum Albumin
CAS	Cellular Apoptosis Susceptibility Protein
CC3	Complement Component 3
CDDP	Cisplatin, cis-diamminedichloridoplatinum (II)
CDK	Cyclin-dependent Kinase
CHX	Cycloheximide
CI	Combination index
CMV	Cytomegalovirus
CO_2	Carbon dioxide
C-PARP	Cleaved Poly(ADP-Ribose) Polymerase
CRM1	Chromosomal Region Maintenance 1
Ctrl	Control
Cy	Cytoplasm/cytoplasmic

DAD	Diode array detector
DAPI	4',6-diamidino-2-phenylindole dihydrochloride
dH_2O	Destilled hydrogen dioxide
DMEM	Dulbecco's Modified Eagle's Medium
DMSO	Dimethyl sulfoxide
DNA	Deoxyribonucleic acid
dNTP	Deoxynucleotide
Dox	Doxycycline
E.coli	Escherichia coli
EDTA	Ethylenediaminetetraacetic acid
EGFR	Epidermal Growth Factor Receptor
EGTA	Ethylene glycol-bis(β-aminoethyl ether)-N,N,N',N'-tetraacetic acid
EMT	Epithelial-mesenchymal transition
Fa	Fraction affected
FG	Phenylalanine-glycine
FITC	Fluorescein isothiocyanate
G	Earth's gravitational force
Ga	Gauge
GAPDH	Glyceraldehyde 3-Phosphate Dehydrogenase
GFP	Green Fluorescent Protein
H_2O	Hydrogen dioxide
HCl	Hydrogen chloride
HEPES	4-(2-hydroxyethyl)-1-piperazineethanesulfonic acid
HER	Human Epidermal Growth Factor Receptor
HPLC-DAD-MS	High pressure liquid chromatography diode array detection mass spectrometry
HPLC-MS/MS	High pressure liquid chromatography tandem mass spectrometry

HPV	Human Papillomavirus
HRP	Horse Radish Peroxidase
i.p.	Intraperitoneal
IC_{50}	Half maximal inhibitory concentration
IGFR	Insulin-like Growth Factor Receptor
IgG	Immunoglobulin G
INI-43	Inhibitory of Nuclear Import-43
IPO	Importins
IRES	Internal ribosomal entry site
KCl	Potassium chloride
kDa	Kilodalton
Kpnβ1	Karyopherin Beta 1, Karyopherinβ1
LA	Luria agar
LB	Luria broth
LMB	Leptomycin B
Log	Logarithm
m/z	Mass-to-charge ratio
Mcl-1	Myeloid Cell Leukemia 1
$MgCl_2$	Magnesium chloride
$MgSO_4$	Magnesium sulphate
Min	Minutes
MRP1	Multidrug Resistance-associated Protein 1
MTA	Microtubule targeting agent
MTT	3-[4,5-dimethylthiazol-2-yl]-2,5-diphenyltetrazolium bromide
MXP	Mitoxantrone Resistance Protein
Na_3VO_4	Sodium orthovanadate

NaCl	Sodium chloride
NADPH	Nicotinamide adenine dinucleotide phosphate hydrogen
NaF	Sodium fluoride
NFκB	Nuclear Factor Kappa B
NLS	Nuclear localization signal/sequence
NPC	Nuclear Pore Complex
NSCLC	Non-small cell lung cancer
NTF2	Nuclear Transport Factor-2
Nu	Nucleus/Nuclear
Nup	Nucleoporin
OD	Optical density
PARP	Poly(ADP-Ribose) Polymerase
PBS	Phosphate Buffered Saline
PCR	Polymerase Chain Reaction
P-gp	P-glycoprotein
pmole	Picomole
Prdx-3	Peroxiredoxin 3
pTIG	pHIV7-TetR-IRES-GFP
RanGAP1	RanGTP-Activating Protein 1
RanGDP	Ran-Guanosine Diphosphate
RanGEF	Ran-Guanosine Nucleotide Exchange Factor
RanGTP	Ran-Guanosine Triphosphate
Rb	Retinoblastoma Protein
RCC1	Regulator of Chromosome Condensation-1
RIPA	Radioimmunoprecipitation assay
RISC	RNA-induced Silencing Complex

RNA	Ribonucleic acid
RNAi	RNA interference
RNase	Ribonuclease
rpm	Revolutions per minute
RPMI	Roswell Park Memorial Institute
Rt	Retention time
SAF	Spindle Assembly Factor
scr	Scramble
SDS	Sodium Dodecyl Sulfate
SDS-PAGE	SDS polyacrylamide gel electrophoresis
SEM	Standard Error Mean
shRNA	Small-hairpin RNA
SINE	Selective Inhibitors of Nuclear Export
siRNA	Small-interfering RNA
SLS	Sodium Lauryl Sulfate
$T_{1/2}$	Half-life
TAE	Tris-acetate EDTA
TBP	TATA-Binding Protein
TBS	Tris Buffered Saline
TBST	Tris Buffered Saline-Tween-20
TE	Tris-EDTA
U	Unit
V	Volts
XIAP	X-linked Inhibitor of Apoptosis Protein
XPO	Exportin
γH2AX	139-serine phosphorylated histone H2A.X

Units

M	Molar
mM	Millimolar
µM	Micromolar
nM	Nanomolar
kg	Kilogram
G	Gram
mg	Milligram
µg	Microgram
ng	Nanogram
L	Liter
mL	Milliliter
µL	Microliter
cm	Centimeter
mm	Millimeter
µm	Micrometer
nm	Nanometer
N	Normality

ABSTRACT

The identification of novel cancer-associated biomarkers against which drugs can be developed is anticipated to be beneficial in multiple ways; including their use as monotherapies and in combination with current chemotherapeutic agents for improved anti-cancer treatment outcome. Recently, research in our own laboratory and others have reported elevated expression of the nuclear transporter Kpnβ1 in multiple cancers. Using the cervical cancer model, we showed that its inhibition using small-interfering RNA (siRNA) resulted in cancer cell death via apoptosis while sparing normal cells, suggesting it has potential as a target for anti-cancer therapy. An *in silico* screen for Kpnβ1 inhibitors identified several small molecules that showed inhibitory effects on nuclear import as well as cancer killing activity.

In this study, we aimed to examine the potential of one such small molecule, the Inhibitor of Nuclear Import-43 (INI-43) as a lead compound with anti-cancer activities using multiple cancer models. Through culture-based *in vitro* assays, we demonstrated that INI-43 inhibited the proliferation of cancer cells grown anchorage-dependently and independently. These effects were similarly observed in Kpnβ1 knock-down cells, and Kpnβ1 over-expression was able to partially reverse these effects, suggesting that the anti-cancer effects of INI-43 is mediated through interference of the Kpnβ1 function. Toxicology studies and liver microsomal assay showed that INI-43 has an acceptable toxicity profile in nude mice and is metabolically stable, allowing its use in *in vivo* testing. Intraperitoneal administration of INI-43 significantly reduced the growth of subcutaneously xenografted cervical and oesophageal tumour cells in nude mice, supporting its anti-cancer activity *in vivo*.

To examine the potential of using INI-43 in combination therapy, we examined the effects of the combined treatment of INI-43 and Cisplatin (CDDP), a first-line chemotherapeutic agent used in the treatment of many cancers. INI-43 treatment at sub-lethal concentrations enhanced cancer cells' sensitivity to CDDP, which was similarly observed in Kpnβ1 knock-down cells. Using an ovarian cancer model, we demonstrated that CDDP treatment led to elevated expression and nuclear localization of Kpnβ1, suggesting that Kpnβ1 is involved in CDDP-induced stress response. INI-43 treatment impeded the CDDP-induced nuclear accumulation of Kpnβ1 which correlated with increased cell death, suggesting that nuclear localization of Kpnβ1 may be important for ovarian cancer cell survival when challenged with genotoxins such as CDDP. Using the cervical cancer model, we demonstrated that INI-43 enhanced CDDP-induced cell death synergistically, and that the enhanced cell death is mediated through stabilizing p53 protein. This associated with decreased levels of Myeloid Cell Leukemia 1 (Mcl-1), an anti-apoptotic factor negatively regulated by p53. Furthermore, INI-43 treatment reduced the nuclear import of NFκB, a stress-regulated response known to promote cancer cell survival. Decreased levels of various downstream pro-survival and DNA-repair targets of NFκB were observed, including cyclinD1, c-Myc and X-Linked Inhibitor of Apoptosis Protein (XIAP), which correlated with increased DNA damage and apoptosis. Taken together, we show that nuclear import inhibition using small molecules could have therapeutic benefits in the treatment of cancer, and that INI-43 is a promising candidate for further development to be used in anti-cancer monotherapy or combination chemotherapy.

CHAPTER 1

LITERATURE REVIEW

1.1. Global trend of cancer and cancer related deaths

The growing burden of cancer worldwide necessitates the continued and collaborative efforts in clinical and basic research, to understand this disease, and to set the grounds for improved preventative methods, early and accurate detection, as well as better and more accessible treatments. In a report issued by the International Agency for Research on Cancer, it has been estimated that approximately 14 million new cancer cases and 8.2 million cancer deaths were reported in 2012 worldwide, which is expected to rise to 22 million before reaching 2032, and cancer related death is expected to rise from 8.2 million to 13 million in the same timeframe (Globocan, 2012). In addition to this, developing countries such as Africa, parts of Asia, Central and South America accounts for over 60% of total cancer cases worldwide, and over 70% of cancer-related deaths worldwide. The alarming rate at which cancer cases and cancer related deaths are escalating worldwide, especially in developing countries present a global health concern.

In less developed countries such as Africa, cancer has received low priority in the health care system due mainly to the overwhelming load of other communicable diseases such as Human Immunodeficiency Virus infection/acquired immune deficiency syndrome (HIV/AIDS) and tuberculosis. The limited facilities for providing diagnosis and treatment coupled to the insufficient governmental health care budgets are contributing factors to the high rates of cancer-related mortality, which accounted for 65% of the global cancer-related deaths (Globocan, 2012). This

highlights the urgent need to identify novel strategies for cancer control with increased accessibility and decreased economical burden.

1.2. Improving the rate of survival for cancer patients

Whilst chances of developing cancer in an individual can be reduced by taking preventative measures, such as abstaining from smoking tobacco, living a healthy lifestyle, and getting vaccinated against certain cancer-causing infections, the risk cannot be completely eliminated due to involuntary risk factors such as genetic inheritance. Early detection and efficient treatments thus play key roles in the improvement of cancer survival. As an example, the introduction and wide use of the Papanicolaou test for the early detection of cervical cancer has successfully reduced cervical cancer related deaths by over 80% since the 1930s in the United States[1]. Unfortunately, with a limitation in facilities and trained cytologists in the poorer communities of the developing world, access to such screening programs is inadequate.

1.2.1. Current diagnostic tools and ongoing research

The general diagnostic tools for cancer include: (a) biopsies, where the target tissue is surgically removed and examined under the microscope for abnormalities; (b) endoscopies, where the suspicious tissue is viewed live *in situ*; (c) diagnostic imaging, where images of the internal organ is produced and analyzed for abnormalities; as well as (d) blood tests, in which the presence or concentration of cancer-specific biomarkers is investigated. The early detection of cancer relies on both the patient's initiative as well as sensitive and accurate diagnostic tools. These tests are used more commonly in combination to detect and confirm the presence of cancer, as single tests can sometimes be inconclusive. These form part of an intensive cancer research area, aimed at improving the accuracy of diagnosis using more cost-effective, rapid and less invasive methods.

Numerous reports have recently described preliminary findings of various protein and RNA molecules present in the serum, blood, saliva or vaginal fluid, indicating diagnostic usefulness in identifying cancer[2-9]. Correlation between genetic and cellular abnormalities (such as chromosome translocation and multinucleation) with disease state led to the proposal for the incorporation of these characteristic traits into routine assessment for certain cancers[10, 11]; and some research groups have recommended using a combination of markers to increase the accuracy of diagnosis[12-15]. The recent identification of exosomes and their implications in cancer have been widely recognized for diagnostic significance[16-20]. In addition to these, the continued testing and development of novel methods and technologies to detect possible signs correlating to cancer development is ongoing. Some of these include the detection of cancer-related gene mutations by using high resolution melting (HRM)[21] and amplicon-based next generation sequencing[22]; development of chemiluminescent immunoassays to identify presence of diagnostic biomarkers[23]; and nanoparticle-based sensors to detect cancer-related volatile organic compounds from exhaled breath[24]. Improving the current diagnostic tools, coupled to better means of result interpretation are also areas of intense research at present[25-30].

1.2.2. Contemporary anti-cancer therapies and shortfalls

A major determinant of cancer survival is treatment. Although treatment outcome depends heavily on factors such as the patient's age, health condition, the type and stage of cancer; adequate and efficient treatment is still nonetheless impactful on survival. The current treatments for cancer comprises various strategies, and the most commonly used are (A) surgery, (B) radiation therapy and (C) chemotherapy.

1.2.2.1. Current treatment options

(A) **Surgery** is the oldest type of cancer therapy and involves the operational removal of the tumour and surrounding tissues. Whilst this treatment method is direct and fast, its use is limited for disseminated and haematological tumours. Surgery is frequently combined with radiotherapy and/or chemotherapy, where the complete tumour removal is not possible due to metastasis or damage to the body.

(B) **Radiation therapy** makes use of photons or charged particles to induce DNA damage in tumour cells, thereby causing apoptosis[31]. Like surgery, radiation therapy is only effective at targeting tumour cells localized in one area, and is also used in combination with other therapies.

(C) **Chemotherapy** involves the use of chemical entities with cytotoxic properties administered orally or intravenously, and these can be categorized into the 'conventional' chemotherapeutic agents, which display systemic cytoxicity (C-i); targeted therapy (C-ii); and hormonal therapy (C-iii), which have narrower spectrum and more specific activities.

(C-i) **Conventional chemotherapy** acts by disturbing important mitotic functions, such as interference with DNA synthesis and replication. This is achieved by various first-line drugs, and different classes employ different mechanisms.

Platinum based agents are coordination complexes of platinum, and those frequently used in anti-cancer treatment include Cisplatin, Carboplatin and Oxaliplatin. Cisplatin (cis-diamminedichloridoplatinum(II), or CDDP) was the first platinum based drug to be identified in the 1840's by Italian chemist Michele Peyrone[32]. Its chemical structure was elucidated in 1893 by the

Swiss chemist Alfred Werner (Fig. 1.1)[33], and its inhibitory effects on cell division was first demonstrated in 1965 in *E.coli*[34]. CDDP subsequently gained scientific interest after its anti-tumour effects were shown in mice[35], and became the first FDA-approved platinum-based compound for treatment of cancer in 1978[36]. Since then, it has been used to treat a wide range of cancers including sarcomas, carcinoma and germ cell cancers. CDDP is composed of a charged platinum ion surrounded by two amine ligands and two chloride ligands[37]. Upon entry into the cell, CDDP is activated where the chloride atoms are displaced by water molecules, a process known as aquation which then permits the platinum to interact with DNA bases. This induces DNA damage in cells by causing intrastranded adducts and interstranded crosslinks, thereby inhibiting cell division which results in apoptotic cell death[38]. As such, the cytotoxic activities of CDDP is believed to be mediated mainly through DNA damage, although CDDP has also been shown to cause other effects such as inducing oxidative stress and disturbing the normal intracellular calcium homeostasis; as well as causing alterations in various important mediators of cell proliferation, apoptosis and signal transduction[38]. The success of CDDP in anti-cancer therapy has led to interest in other metal-containing compounds as potential anti-cancer drugs, and various platinum analogues have also been studied[39].

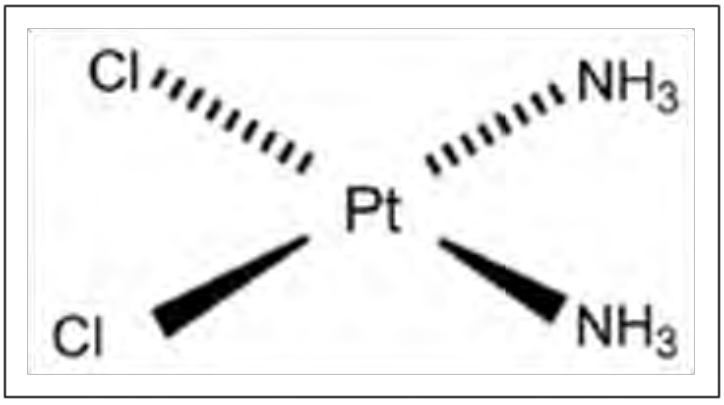

Figure 1.1. The chemical structure of the platinum-based agent Cisplatin (cis-diamminedichloridoplatinum(II), or CDDP).

There are other conventional chemotherapeutic agents targeting different processes important to cell division. Antimetabolites such as Methotrexate, Fluorouracil and Gemcitabine interferes with DNA replication by competing with nucleotides during DNA synthesis, or inhibiting crucial enzymes involved in this process[40, 41]. The anthracycline drugs such as Doxorubicin acts via DNA intercalation as well as damaging intracellular molecules by generating free radicals[42]. Inhibiting the DNA structure regulating enzyme topoisomerase is another class of agents including Irinotecan and Topotecan, and these drugs generate DNA breakage by preventing the religation step after replication and transcription[43]. Microtubule targeting agents (MTAs) are also effective cytotoxic agents. Microtubules are highly dynamic structures especially in mitotic cells where they are constantly undergoing polymerization and depolymerization[44]. MTAs comprises vinca alkaloids such as Vincristine and Vinblastine, which prevent polymerization of the tubulin subunits, and taxanes such as Paclitaxel and Docetaxel which prevents their depolymerization. These abnormalities in microtubule function render the cells incapable of dividing and induces cell cycle arrest, eventually leading to apoptosis[45].

(C-ii) **Targeted therapy**, as suggested by its name, is the use of chemical entities which interferes with specific molecules involved in tumourigenesis, rather than killing all rapidly dividing cells like conventional chemotherapeutic agents[46, 47]. A well-known example is the tyrosine kinase inhibitor Imatinib, which targets tyrosine kinase enzymes, including the fusion protein BCR-ABL1[48]. The BCR-ABL1 fusion is caused by the Philadelphia chromosome commonly observed in leukemic cancer cells, where a translocation from chromosome 9 to chromosome 22 results in the hybrid tyrosine kinase protein BCR-ABL1, which is constitutively active and causes uncontrolled cell proliferation[49]. Its exclusive presence in leukemic cancer cells allows the increased selectivity of Imatinib at targeting malignant cells only. Other well-known examples are Gefitinib and Erlotinib which are used in the treatment of non-small cell lung cancer (NSCLC) and pancreatic cancer[50-52]. Both compounds target the Epidermal Growth Factor Receptor (EGFR), a protein frequently over-active or mutated in

cancer[53]. An advantage of using targeted therapy over conventional chemotherapy is the reduced occurrence of adverse side effects[51, 52], as these agents are less toxic to non-cancer cells.

(C-iii) **Hormonal therapy** is commonly used for cancers that are derived from hormonally responsive tissues, such as breast and prostate, as these cancers present the opportunity for hormonal intervention[54, 55]. Success has been demonstrated using Aromatase inhibitors in treating breast cancer, which acts by decreasing the level of oestrogen[56], a hormone known to promote breast tumourigenesis through stimulating cell proliferation[54].

There are various other therapies currently in practice, such as immunotherapy, hyperthermia therapy, virotherapy and gene therapy. These different therapeutic approaches are frequently combined to optimize treatment outcome. Whilst early stage, localized tumours can be treated with radiation and surgery, disseminated cancer cells resulting from metastatic tumours presents difficulty as they may be present at multiple sites, some of which are not physically accessible. In these cases, chemotherapeutic agents that can be delivered via the circulatory system to otherwise unreachable sites may be beneficial.

1.2.2.2. Adverse side effects associated with chemotherapy

The use of chemotherapy, as outlined above, targets cellular functions important to cancer cells as well as rapidly-dividing normal cells, leading to their insufficient selectivity. Several side effects associated with their use directly reflect their toxic effects on non-cancer cells. This is a major concern in anti-cancer therapy, as the quality of life for patients undergoing chemotherapy is severely compromised[57]. Discomforts experienced as a result of chemotherapy encompass a wide range of symptoms, and some commonly reported ones include pain sensation in the lower back,

joint and stomach; swelling of body parts such as the extremities and face; abnormalities of the digestive and excretion systems such as nausea, vomiting, constipation, diarrhoea, pain and difficulty in urination which often accompanied with blood. Some organs of the body such as skin, heart and hair follicles; as well as visual, auditory and respiratory functions are also commonly affected areas. Unpleasant experiences such as fevers and chills, unusual bleeding, bruising and sores around the mouth are also frequently experienced by patients undergoing chemotherapy[58-62].

1.2.2.3. Resistance to chemotherapy

In addition to all the undesired side effects that accompanies chemotherapy, treatment outcome is frequently compromised as a result of resistance to anti-cancer drugs (chemoresistance). The mechanisms underlying such resistance have been extensively characterized and various causatives have been identified. These can be broadly categorized into two classes; the host factors, and the genetic/epigenetic alterations within the cancer cells[63]. Host factors include alterations which occur in the tumour-bearing patient, such as drug absorption, metabolism and excretion. In this class, resistance can arise as a result of decreased drug absorption, inappropriate metabolism leading to inactive derivative of the parent drug, such as the conversion of Irinotecan by CYP450[64, 65], rapid excretion[63] and failure to deliver drug to the target sites[66].

The more extensively researched mechanisms of chemoresistance is the genetic and epigenetic alterations, which occur in the actual cancer cells. These include alterations in cellular uptake, activation/sequestration, detoxification, suppression of apoptotic pathways, and drug-target mutations. The cellular entry of the drugs is dependent on their chemical structures, and various anti-cancer agents are known to enter the cells in receptor or transporter mediated ways. In these cases, decreased expression or mutation in the receptors or transporters can result in impaired drug

uptake, as demonstrated by the receptor Smoothened[67-69], nucleoside transporters[70, 71] and folate transporters[72], leading to impaired drug uptake which ultimately manifest a decreased response.

Upon cellular entry, the fate of the anti-cancer drugs is still vulnerable to numerous cellular actions leading to their sequestration or inactivation, rendering them ineffective. For example, Cytarabine which has been used to treat acute myeloid leukemia and non-Hodgkin Lymphoma requires activation through serial phosphorylation to form Cytarabine triphosphate by the enzyme Deoxycytidine Kinase. Its toxicity, however, can be evaded via decreased levels or expression of the mutant Deoxycytidine Kinase, thereby preventing the formation of the active form of the drug[73-76]. Whilst some drugs present cancer cells with the opportunity to prevent their activation, cancer cells have also formulated measures to inactivate active drugs, such as the conjugation of glutathione and metallothionine to platinum based agents and anthracyclines[77-83]. The consequences, whether through preventing drug activation or initiating drug inactivation, is decreased responsiveness to treatment with these agents.

Moreover, in the use of targeted therapies, resistance can arise as a result of disrupted binding of drugs to the target proteins against which they were designed for. This has been demonstrated for Imatinib[84], Erlotinib and Gefitinib[85-87]. In these settings, mutations occurring in the target proteins prevents drug-target associations, attributing to the drug-resistant phenotypes[88-96]. On the other hand, targeting the HER-2 protein in breast carcinoma using a monoclonal antibody, Trastuzumab has yielded resistant cancer cells via various mechanisms. Alterations in binding of Trastuzumab to HER-2 is attributed to two mechanisms; firstly, the expression of a truncated HER-2 which lacks the Trastuzumab binding epitope[97]; and secondly, the increased expression of the membrane associated Glycoprotein Mucin-4 (MUC4), which masks the Trastuzumab binding epitopes on HER-2, leading to decreased binding capacity[98, 99]. Other mechanisms have also been reported to confer Trastuzumab

resistance, including the elevated activation of HER-2 downstream PI3K/AKT pathway[100, 101], as well as the compensatory activation of parallel pathways such as Insulin-like Growth Factor-1 Receptor (IGFR1)[102, 103] and HER-3[104, 105].

Membrane transporter mediated drug elimination from cancer cells is accountable for resistance to a wide range of structurally and mechanistically diverse compounds, and has been reported in many types of cancers. This is caused by the increased expression or activity of the ATP-binding cassette (ABC) membrane transporters. Of the 49 transporters known in human, 3 have been shown to confer drug resistance, including P-glycoprotein (P-gp), Multidrug Resistance-associate Protein 1 (MRP1) and Mitoxantrone Resistance Protein (MXP). Together, these transporters actively pump out a wide range of clinically important chemotherapeutic agents from the cells, including Taxol, Vincristine, Vinblastine, Etoposide, Doxorubicin, Paclitaxel, Irinotecan, Methotrexate, topoisomerase inhibitors, anthracyclines, Fluorouracil and others[63, 106-108]. The modification of drugs by conjugation to glutathione leads to their recognition by these transporters and subsequent elimination from cancer cells[107]. The challenge posed by drug resistance of this nature presents even more clinical difficulty, as the resistance developed as a result of using one agent will result in resistance to a broad range of structurally and mechanistically unrelated agents limiting the subsequent treatment options[107].

Resistance to anti-cancer drugs can be inherent, where cancer cells are innately resistant prior to chemotherapeutic treatment; or acquired, where the resistant phenotype is a result of chemotherapy[107]. The acquired drug-resistance can arise with a small subpopulation of the tumour cells bearing intrinsic resistance or, alternatively developed resistance by random genetic/epigenetic alteration. By the Darwinian law of evolution, these resistant subpopulations become enriched under the selective pressure of chemotherapy. It is well-known that tumour development is tightly

linked to accumulation of genetic and epigenetic abnormalities, leading to high levels of intratumoural hetergeneity[109-112]. The diversity found within tumour subpopulations may account for cancer progression and malignant phenotypes such as invasiveness and metastatic potential. More importantly, it has been suggested to be the founding factor for drug resistance, which provides increased adaptability for the tumour population as a whole[109, 113]. Indeed, the heterogeneic nature of tumour cells have been demonstrated for many different types of cancers[114-119], which is associated with drug resistance. For this reason, the inclusion of heterogeneity assessment into prognostic evaluations had been proposed[117, 119]. The heterogeneous nature of tumour cells, coupled to the Darwinian evolution almost predicts the resistant fate of cancer cells subjected to chemotherapy.

1.2.3. Combination chemotherapy

Understanding the underlying mechanisms responsible for anti-cancer drug resistance is important, as this may provide guidance for future treatments. Successful attempts have been made in various cases to reverse chemoresistance. These include the co-administration of efflux pump inhibitors; and the use of second-generation drugs which are able to bind to the mutated target proteins in case of targeted therapy, where the causal mutation for resistance has been identified[120, 121].

The use of combination chemotherapy, in particular, is a powerful strategy with wider application in combating chemoresistance in general. The rationale of this approach is to use mechanistically different agents each targeting their respective susceptible cells to aim for maximum cell death in the heterogeneic tumour population. This is simplified in Fig. 1.2, where drug-A and drug-B is each active against a subset of a heterogeneous tumour population. The independent use of either drugs will result in enrichment of the resistant subpopulations, which can be avoided by the combined

treatment of drug-A and drug-B. True clinical cases are, however, more complicated with higher levels of heterogeneity, and combination regimens frequently involve the use of multiple agents. The direct correlation between the number of agents used and cure rate has been reported for acute lymphoid leukemia, where the use of up to 8 agents showed a cure rate of 80%, supporting the efficacy of using combination chemotherapy over monotherapy[†].

'Sequential' combination chemotherapy has also been proposed, where the use of each drug in the combination is separated temporally, rather than simultaneously. Whilst this may sound feasible, it must be taken into consideration that tumours cells are genomically unstable, where genetic and epigenetic changes are not static. Accumulation of mutations in these cells thus occur at a much faster rate than normal cells. Prolonged survival could therefore afford time for the development of an even more heterogeneic population with increased chance of resistance occurring, and potentially via mechanisms not targeted by neither drug-A nor drug-B as shown in Fig. 1.2. Sequential treatment could thus promote the sequential development of multidrug resistant cells. The ideal situation is therefore to target maximal cancer cell death in the shortest period possible. Though practically, this is often limited by adverse side effects tolerability, as intensive combination chemotherapy regimens can sometimes lead to severe side effects. For this reason, sequential treatment is sometimes favoured over simultaneous treatment[122]. Combination chemotherapy, whether through sequential or concurrent administration has nonetheless demonstrated success in several cases over single agent treatment, such as the combined use of Docetaxel and Capecitabine, compared to Docetaxel alone[123, 124]; and the combined use of Paclitaxel and Gemcitabine, compared to Paclitaxel alone[125], for breast cancer patients insensitive to anthracycline treatments. A combination of Erlotinib and Gemcitabine has also generated more favourable treatment outcome compared to Gemcitabine alone in advanced pancreatic cancer patients[126]. While increased efficacy

[†] Kufe, D.W., Pollock, R.E., Weichselbaum, R.R., Bast, R.C., Gansler, T.S.,Holland, J.F., Frei, E. (Eds). (2003) *Holland-Frei Cancer Medicine, 6th Edition*. Shelton, Connecticut: People's Medical Publishing House-USA.

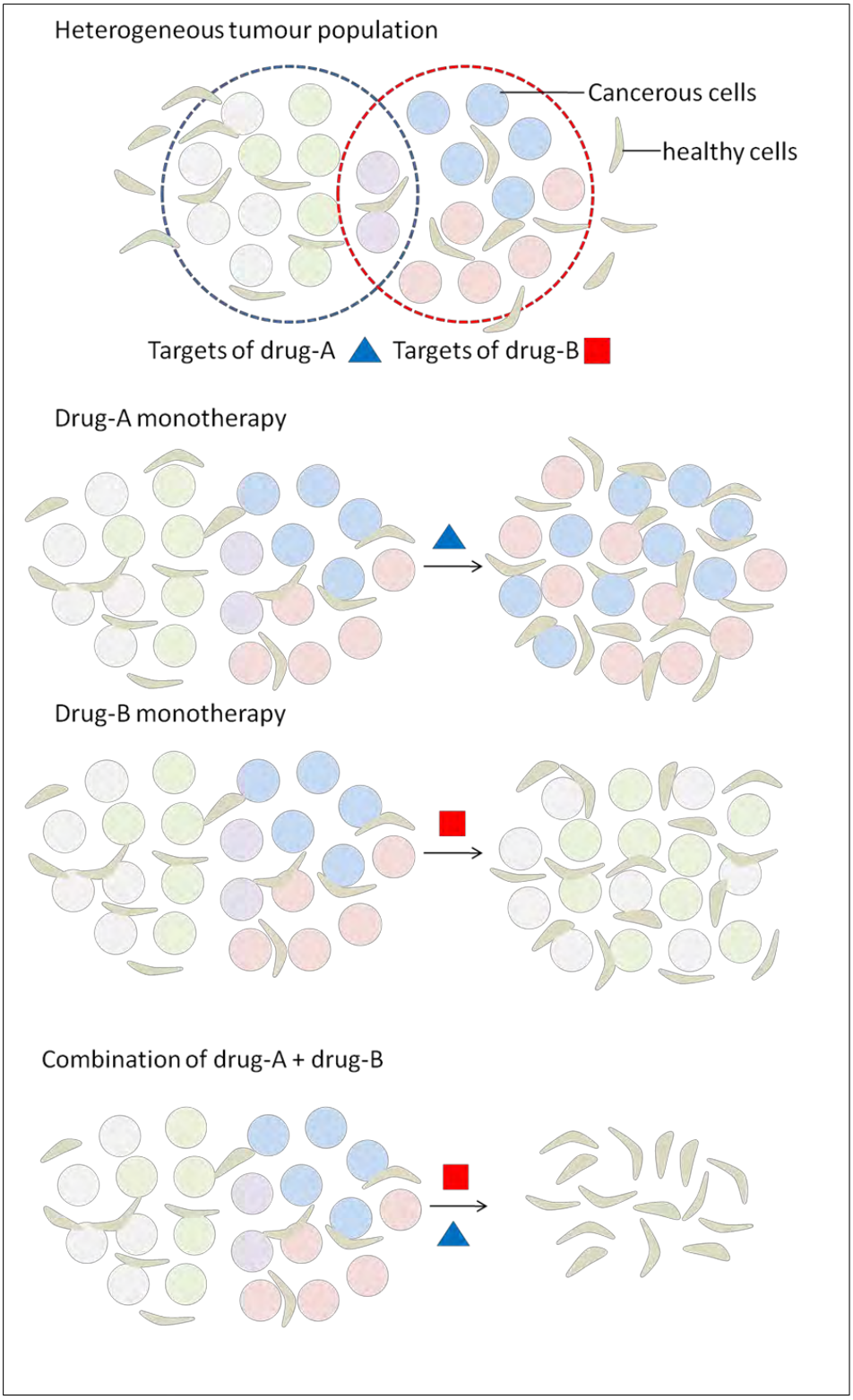

Figure 1.2. Single-agent chemotherapy versus combination chemotherapy. Drug-A and drug-B each targets a subset of the heterogeneous tumour population. Monotherapies using drug-A or drug-B alone promotes the growth of the resistant subpopulations. This can be avoided by a combined therapy of using drug-A and drug-B together.

is observed with various combinations, the toxic effects should also be taken into consideration. A phase III clinical trial reported that the addition of Gemcitabine to the Carboplatin-Paclitaxel pair in treating ovarian cancer was associated with more frequent grades 3-4 toxicity and decreased the quality of life, leading to no survival advantage compared to Carboplatin-Paclitaxel treatment[127].

In the battle against chemoresistance, the identification of novel, previously unexploited 'druggable' targets holds great potential, and may be a powerful strategy when used in combination with clinically relevant cytotoxic agents to improve treatment outcome. The designing of such treatment protocols require careful investigative planning and various factors need to be taken into consideration. These include the mechanism of action for each drug to be used in combination, nature of drug interaction (additive, synergistic or antagonistic), scheduling of administration and maintenance, as well as the severity of adverse effects to aim for a balance between benefits of treatment and harmful side effects. As this can vary from case to case, each combination should be investigated empirically.

1.3. Nuclear transport and cancer

The development of novel and more specific anti-cancer agents with reduced side effects has become a focus of various research organizations and pharmaceutical companies. The identification of cancer biomarkers for diagnostic and prognostic purposes, as well as elucidating molecular events on which cancer cells are reliant is of particular interest. Our laboratory has previously carried out a microarray study to investigate mRNA levels in patient-derived cervical cancer tissues and normal cervical specimens. Comparison of the expression profiles elucidated the differential expression of various genes between cancer and non-cancer[128]. Of those, three genes known to be involved in the nucleo-cytoplasmic trafficking system showed elevated levels in the cancer, namely *crm1*, *kpnβ1,*

kpnα2 and *Ran*. The nucleo-cytoplasmic trafficking system has gained increasing attention in recent years for their close correlation to cancer, as malfunction and dysregulation of this cellular process have been reported across a broad spectrum of cancers.

In eukaryotic cells, the genetic contents and processes associated with it, such as DNA replication and mRNA transcription are separated from the cytoplasm by the double membraned nuclear envelope. This compartmentalization of cellular contents is important, providing spatial control for important cellular processes which enables the cells to execute different activities simultaneously and efficiently. As such, the appropriate shuttling of macromolecules between the cytoplasm and nucleus play an important role in maintaining homeostasis and normal cellular functions. For example, transcription factors which are synthesized in the cytoplasm needs to enter the nucleus to induce gene expression, and mRNAs transcribed in the nucleus needs to exit the nucleus to be translated in the cytoplasm. Aberrantly regulated nucleo-cytoplasmic trafficking will lead to inappropriate accumulation of proteins and RNAs in these compartments at the incorrect time, and this is profoundly linked to pathogenesis[129-131].

The important participants in the nucleo-cytoplasmic trafficking system include the Nuclear Pore Complex (NPC), the Ras-related Nuclear protein (Ran) and the Karyopherin transporters. The nuclear pore complex is a large cylindrical and flexible structure embedded in the nuclear envelope, which provides passage for selective and bidirectional transport between the cytoplasm and the nucleus. Each NPC comprises a central channel lined with proteins, and peripheral filaments attached to the central core, extending into the cytoplasm and nucleoplasm. The majority of the proteins making up the components of the NPC are called nucleoporins (Nups), and those lining the central region are FG-Nups, as they contain phenylalanine-glycine (FG) motifs in tandem repeats[132, 133]. There are two

important functions provided by the NPC; to form a physical barrier with defined permeability for selected molecules, and to assist the traversing of larger macromolecules through its central channel.

The Ran protein on the other hand, is a small Ras-related nuclear guanine nucleotide binding protein responsible for supplying energy to facilitate nuclear transport. Inside the nucleus, Ran is present at high concentrations in the guanosine triphosphate bound state, RanGTP. This is due to the action of the Regulator of Chromosome Condensation 1 (RCC1, also known as Ran Guanosine Nucleotide Exchange Factor RanGEF), which exist in close proximity to the chromosomes. Outside of the nucleus, RanGTP becomes substrate for RanGTP-Activating Protein 1 (RanGAP1) and Ran-Binding Protein1 (RanBP1), which together causes GTP hydrolysis, leaving Ran in its guanine diphosphate bound state, RanGDP. RanGDP is imported into the nucleus by the Nuclear Transport Factor-2 (NTF2)[134], where nucleotide exchange by RCC1 returns Ran to its GTP bound state. This regulated system establishes a spatial gradient of RanGTP with the highest concentration around the chromosomes in the nucleus emanating outwards, eventually reaching the cytoplasm where concentration is the lowest. Such distribution of RanGTP is an important regulator for both nuclear transport and spindle assembly during mitosis[135, 136]. Ran is also known to regulate other cellular processes including nucleation and polymerization of microtubule during cell division[137, 138], nuclear envelope formation and cell-cycle checkpoint control[139, 140].

Both the NPC and Ran proteins play important roles in the nucleo-cytoplasmic trafficking system, and abnormalities in their presentation or function have been linked to tumourigenesis[141-144]. The oncogenic potentials of NPC is represented by its component Nups, where their mutations or altered expression have led to their mislocalization and ultimately impacted on signalling pathways and transcription profiles either through altered or diminished functionalities[141, 145]. Ran is frequently elevated in cancer and has been shown to be transcriptionally regulated by oncoprotein Myc[146]. Its

oncogenic role is mediated through altering various signalling pathways including the cyclins, CDKs, Retinoblastoma protein (Rb), Survivin, Bax and JNK[147, 148]. In fact, Ran over-activation alone has been shown to confer malignant phenotypes in fibroblast cells, indicative of its ability in cellular transformation[149, 150]. Furthermore, Ran directly mediates the nuclear entry of the E7 oncoprotein of Human Papillomavirus type 16 (HPV16), a high-risk cervical-cancer causing agent, thereby contributing to infection and possibly carcinogenesis known to be associated with HPV16[151].

Whilst the abnormal function of both Ran and NPC has been associated with cancer and cellular transformation, whether this is directly linked to their nuclear trafficking function has not yet been explicitly demonstrated. This likelihood, however, has been hypothesized by many. For example, the loss of function for one of the Nups making up the cytoplasmic filament, Nup88, leads to cytoplasmic accumulation of NFκB due to increased nuclear export[152]. It has been proposed that over-expression of Nup88, which is frequently observed in tumour cells[153], could reciprocally result in nuclear accumulation of NFκB and thereby promote oncogenesis[145], although experimental validation remain to be elucidated.

1.3.1. Cellular functions of the nuclear transporters: the Karyopherins

The transporters, the group of proteins that actively facilitate movement of cargoes across the NPC make up the Karyopherin superfamily. Although best known for their involvement in nucleo-cytoplasmic trafficking, they also participate in other vital cellular processes such as NPC and nuclear membrane assembly, cell cycle regulation, as well as replication and mitosis[154, 155]. Members of this family can be categorized into Importins (IPOs, Karyopherinβs), which functions to import cargoes into the nucleus; Exportins (XPOs, also Karyopherinβs and CAS) which shuttles the cargoes out of the

nucleus; Transportins known to engage in bidirectional transport; as well as the Karyopherinα adaptor proteins, which mediates the recognition between the Karyopherinβ and their cargoes.

In the classical import process, the Karyopherinα subunit recognizes and binds to the nuclear localization signal- (NLS-) bearing cargo[156], and Karyopherinβ facilitates the docking of the Karyopherinβ/α -cargo complex to the NPC. Karyopherinβ interacts with the FG-Nups present in the NPC, allowing the complex to transit through the channel[157]. Arrival at the nuclear side of the NPC allows RanGTP, which is present at high concentrations in the nucleus to bind to the trimeric complex, leading to its dissociation[158, 159]. The cargo is freed to perform its nuclear function, while Karyopherinβ and Karyopherinα is recycled back into the cytoplasm coupled to RanGTP, and CAS/RanGTP, respectively[160]. Back in the cytoplasm, RanGTP is hydrolysed by RanGAP and RanBP1 to form RanGDP, releasing Karyopherinβ and Karyopherinα from their respective receptors[161]. Karyopherinβ and Karyopherinα remain in the cytoplasm to initiate the next round of import while CAS and RanGDP re-enters the nucleus, where RanGDP is converted to RanGTP via the action of RCC1 (Fig.1.3). Import of cargo proteins can also occur in a non-classical manner, where direct association with cargo protein is made with Karyopherinβ itself independent of Karyopherinα[162, 163].

The exporting pathway involves the association of an Exportin and nuclear export signal- (NES-) bearing cargoes in the nucleus RanGTP-dependently, and transit through the NPC is made by the interaction between Exportin and the Nups. In the cytoplasm, hydrolysis of RanGTP to RanGDP allows the dissociation of the cargo protein from the Exportin, which then re-enters the nucleus. The action of RCC1 in the nucleus then converts RanGDP to RanGTP (Fig. 1.4)[164, 165].

The directional transportation for both import into and export out of the nucleus is conferred by two factors. Firstly, the asymmetrical distribution of both RCC1 and RanGAP/RanBP1 in the nucleus and

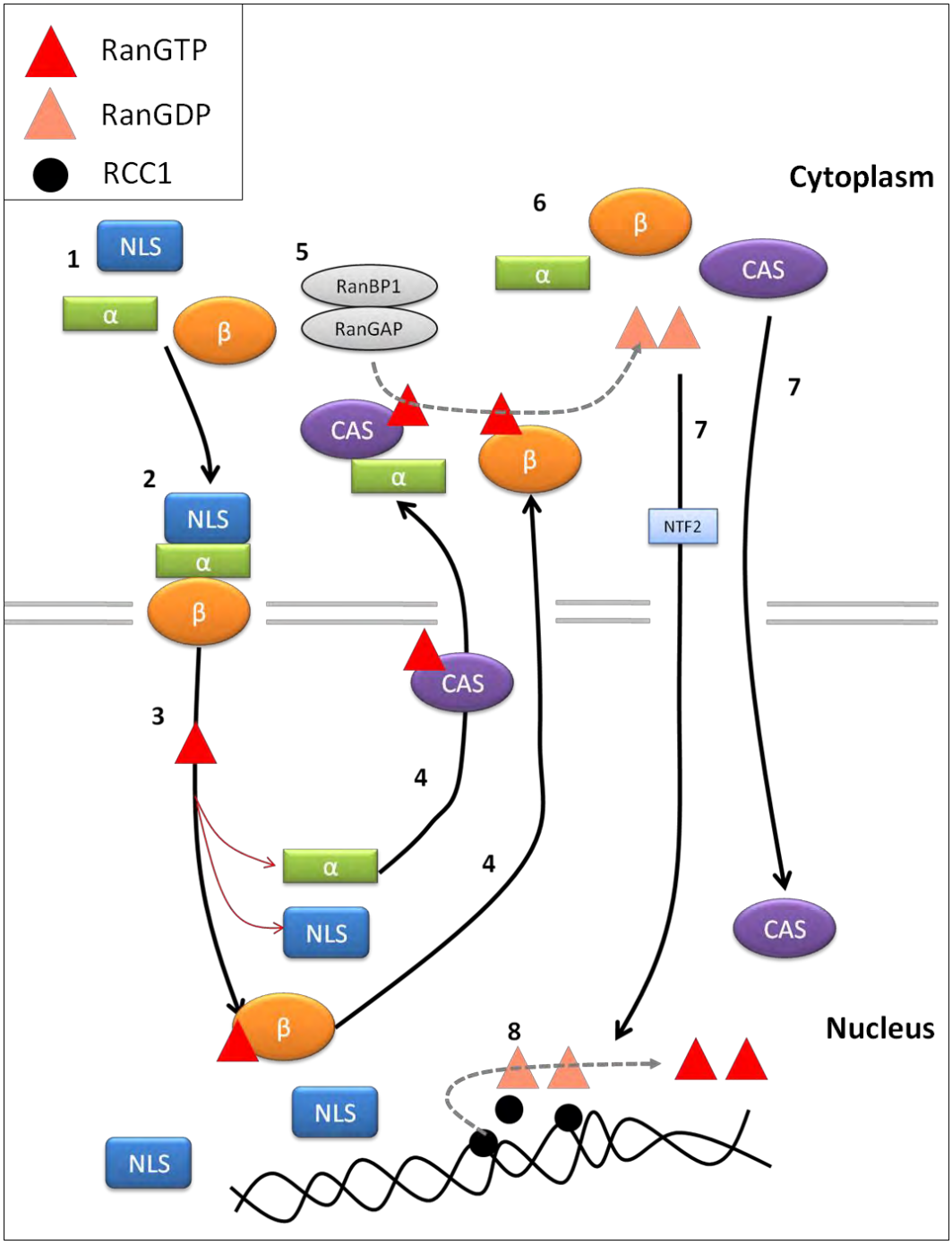

Figure 1.3 Schematic showing the Karyopherinβ/α mediated nuclear import cycle. Karyopherinβ (β), Karyopherinα (α) and import cargo (NLS) form a trimeric complex in the cytoplasm (1), and transit through the NPC (2). On the nuclear side, binding of RanGTP dissociates the complex (3), releasing the cargo while Karyopherinβ-RanGTP and Karyopherinα-CAS-RanGTP exits the nucleus (4). In the cytoplasm, hydrolysis of RanGTP to RanGDP via RanGAP and RanBP1 (5) releases Karyopherinβ, Karyopherinα/CAS (6). RanGDP, coupled to NTF2 together with CAS re-enters the nucleus (7), and via the action of RCC1 in the nucleus, RanGDP is converted to RanGTP (8).

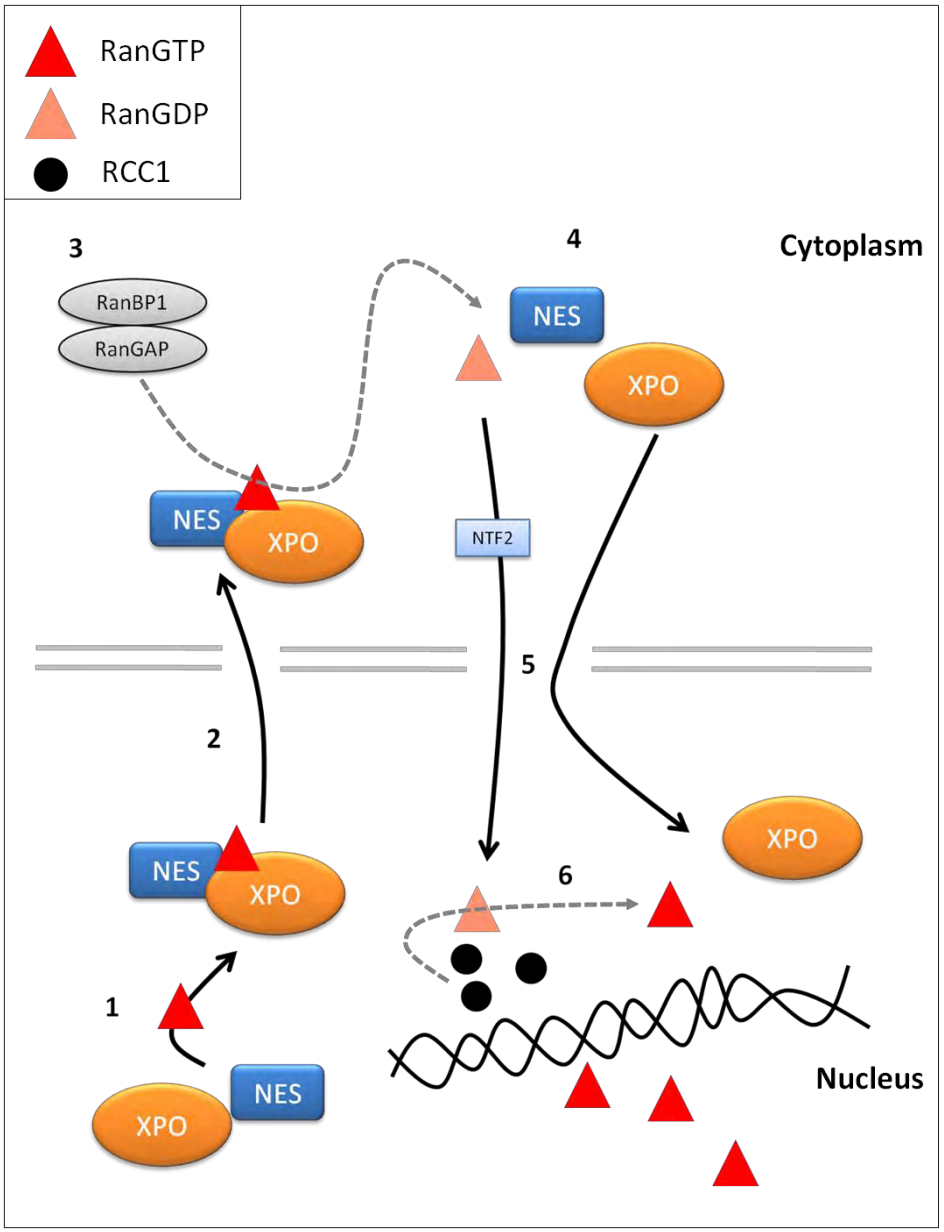

Figure 1.4. Schematic showing the Exportin-mediated nuclear export cycle. Exportin receptor (XPO) binds its export cargo (NES) in the presence of RanGTP (1), and the trimeric complex exit the nucleus through the NPC (2). The combined actions of RanGAP/RanBP1 hydrolyzes RanGTP to form RanGDP (3), releasing NES-cargo and XPO (4). RanGDP coupled to NTF2 and XPO re-enters the nucleus(5), and RCC1 in the nucleus converts RanGDP to RanGTP (6).

cytoplasm, respectively. This leads to high levels of nuclear RanGTP, which in turn is responsible for releasing the cargoes from Karyopherinβ/α in the nucleus. The cytoplasmic RanGAP and RanBP1 catalyzes RanGTP hydrolysis, allowing Karyopherinβ to be released from Ran and Karyopherinα from CAS/Ran in the cytoplasm[166]. The export pathway is essentially the reciprocal process. Secondly, the transit of the import complex through the NPC is made possible by the gradual increase in affinity between the Nups and Karyopherinβ from the cytoplasmic end to the nuclear end within the NPC, promoting a directional movement towards the nucleus[167].

Whilst smaller proteins and molecules can passively diffuse between the nucleus and cytoplasm, the majority of macromolecules (typically larger than 40 kDa) require facilitated nuclear entry and exit via the Karyopherin family. Although each Karyopherin protein possesses their own substrate specificity, some proteins are known to be transferred by multiple transporters, such as ribosomal proteins, core histone proteins and NFκB-p65[168-171].

As the correct cellular localization of various proteins at the correct time is a prerequisite for proper cell functioning, the Karyopherin proteins and their normal function have a key role in ensuring normal cellular processes. For example, the Exportin Chromosomal Region Maintenance 1 (CRM1) is known to transport various cell-cycle regulators such as p27, E2F and cyclinB. The appropriate transit through cell cycle therefore depends on the well-orchestrated regulation of CRM1 function[172-174], and indeed, dysregulation of CRM1 is correlated with abnormal cell cycle progression[175, 176]. It is therefore not surprising that the dysregulation or abnormal function of the Karyopherins is linked to pathogenesis, such as the development and progression of cancer[164].

Several studies have detailed the observation of protein mislocalization in association to a wide range of malignancies, including breast, stomach, colon, cervical, brain, skin, leukemia and others[177-

[183]. Although the inappropriate localization of these proteins may be due to fault in the cargo proteins themselves, for example, mutation or aberrant post translational modifications, but the aberrant functioning of the transport machinery is likely to cause global mislocalization of proteins, thereby promoting carcinogenesis.

Research done in our laboratory have previously shown that the levels of Karyopherin Beta 1 (Kpnβ1), Karyopherinα2 (Kpnα2) and CRM1 were elevated in cervical cancer cells compared to non-cancer cells, as well as in transformed lung fibroblast compared to their non-transformed counterparts[128], suggesting increased nuclear import and export in cancer and transformed cells[184]. The accelerated nuclear trafficking is thought to manage the increased metabolic and proliferative demands. Indeed, Kuusisto *et al*. have reported increased expression of the Importin Karyopherinβ1 (Kpnβ1) in correlation with increased rate of nuclear import activities in transformed breast epithelial compared to the non-transformed counterparts[185]. These suggest that increased expression, and thus function of the transporters is associated with cellular transformation. Supporting this, alterations in the expression and/or function of the Karyopherin proteins have been reported across a broad spectrum of cancers including oesophageal, breast, colon, pancreatic, prostate, ovarian, and hepatocellular carcinoma[128, 186-192].

1.3.2. Impaired nuclear transport regulation and cancer

Dysregulation of the nuclear trafficking system, mainly members of the Karyopherins has been reported in a many cancers, which can arise from various molecular alterations. Here we discuss a few mechanism known to induce abnormal nuclear trafficking associated with the transporters, including altered expression, aberrant post translational modification, mutation and disruption of the endogenous transporters (for more details, see review by Stelma *et al.*[193]).

Using the cervical cancer model, van der Watt *et al.* reported that over-expression of both Kpnα2 and Kpnβ1 results from the impaired E2F/Rb regulation, where the constitutively active E2F associated with increased expression of its downstream targets, including both Kpnα2 and Kpnβ1[194]. The E2F/Rb regulation is known to be disrupted in many human cancers[195], accounting for the increased expression of both proteins observed in multiple cancers. As the viral oncoprotein E7 is known to amplify E2F activity both Rb-dependently and independently[196, 197], it is likely that the increased Kpnα2 and Kpnβ1 expression is due to HPV infection in some cervical cancer cells[194]. In addition to the increased transcriptional activity, down-regulation of negative regulator micro-RNAs has also been reported to attribute to increased expression of both Kpnα2 and Kpnβ1 in other cancers[198, 199].

Another mechanism reported to impair regulation of Karyopherin family members is the genomic rearrangement of the 20q13 chromosome, which is known to accommodate amplifications linked to aggressive breast cancer[200]. In 1996, Brinkmann *et al.* mapped the CAS encoding gene, *cse*1, to chromosome 20q13, and amplification of *cse1* was detected in leukemia, colon cancer and breast cancer[201]. CAS and Kpnα2 have both been reported to be negatively regulated by p53 through induction of p21[202]. The loss of p53 function frequently observed in cancer could therefore account for increased CAS and Kpnα2 expression[203]. Indeed, increased CAS expression has been reported in colon cancer, lung cancer, leukemia, lymphoma, breast cancer and ovarian cancer[201, 204-206]. Brinkmann *et al.* investigated the expression of CAS in normal human tissues, and found that cells with increased proliferative activities manifested higher CAS expression[204], supporting the idea that increased expression of these transporter may be associated with increased proliferative demands of cancer cells.

Aberrant regulation of CRM1 expression in cervical cancer and transformed cell lines has been suggested to result from increased levels of NF-Y and Sp1 transcription factors[176]. Interestingly, all three subunits of NF-Y, namely NF-Ya, NF-Yb and NF-Yc are transported into the nucleus by Kpnβ1 and IPO13[207], suggesting a possible explanation as to why elevated expression of both Kpnβ1 and CRM1 is often observed in the same cancer[128, 208, 209]. Similar to CAS and Kpnα2, transcription of *crm1* has also been reported to be negatively regulated by p53 under DNA damaging conditions[176], the frequent loss of p53 function in cancer cells may therefore also attribute to elevated CRM1 expression. Interestingly, nuclear export of p53 is mediated by CRM1 under DNA damaging conditions[128], indicating a possible feed-back loop regulatory mechanism. In normal cells, increased p53 induced by DNA damage represses CRM1 expression, however, in cancer cells harbouring non-functional or suppressed p53, the repression on *crm1* transcription is alleviated, resulting in increased CRM1 expression, which then enhances nuclear exclusion of p53 thereby preventing p53-mediated suppression on CRM1 expression.

Various other causatives have also been identified to directly or indirectly interfere with the nuclear transport machinery. These include the inappropriate post-translational modification, such as that observed with the CAS protein where phosphorylation by both AKT and MEK-1 determines its localization[210, 211]. As nuclear CAS exhibited increased oncogenic properties compared to cytoplasmic CAS[210], the altered activities of the upstream kinases could therefore lead to inappropriate localization of CAS, resulting in pathogenesis. Mutations leading to impaired transport activities of the Karyopherins is another known factor to be linked to malignancy, and this has been reported for Karyopherinα and Exportin5, where the mutant versions of these proteins were unable to execute their respective functions leading to inappropriate p53 import and micro-RNA export, respectively[212, 213]. Endogenous negative regulators of the nuclear transporters, namely Aplasia Ras Homolog Member 1 (ARH1/DIRAS3/NOEY2), Complement Component 3 (CC3/TIP30) and Etoposide Induced Protein 2.4 (Ei24/PIG8) have been reported to show reduced levels or activity in many cancers[214-216],

which consequently led to elevated activities of the transporters and associated with carcinogenesis[217-220].

Together, these demonstrate the association between aberrant nuclear transport functions and cellular malignancy, and highlights the need of a well-organized, intricately regulated nuclear transport system. Mechanisms are devised through every step of the protein synthesis and regulatory pathway, including transcriptional and translational, as well as at the post-translational level. In healthy cells, they guard the smooth execution through each transporting cycle, ensuring the correct localization at the correct time for various cargoes. This does not only impact on protein localization, but virtually all cellular processes are reliant on a proper transport system for the correct execution of downstream pathways. The malfunction of this system strongly correlates with cancer progression, but at the same time provides opportunities for intervention, which will be discussed in the next section.

1.3.3. Therapeutic potential of the Karyopherins

Association of the Karyopherin proteins and cellular malignancy is a good indicator for their potentials as biomarkers. Indeed, various members have already been studied for their values in diagnosis, prognosis and therapy. The prognostic value of both the expression and localization of Kpnα2 has been well demonstrated in a variety of cancers[188, 190, 191, 221, 222]. However, its functional importance appears to be variable, as its inhibition does not always affect cancer cell proliferation and survival[128]. This is possibly due to the overlapping substrate specificities between the Karyopherinα members[170], and Kpnα2 has therefore been focussed on more as a prognostic tool. Although therapeutic potentials have been suggested for Kpnα2 in some cancers[188, 223], further experimental validation is required.

The Exportin protein CRM1, on the other hand, is the most extensively studied Karyopherin member as an anti-cancer target to date[193, 224-227]. Its increased expression has been reported in a multitude of cancers, including leukemia, breast cancer, prostate cancer, lung cancer, ovarian cancer, cervical cancer, glioma, pancreatic cancer, osteosarcoma and myeloma[128, 228-236]. CRM1 inhibition via genetic or chemical intervention resulted in growth inhibition and apoptosis in cancer cells, suggesting increased reliance of cancer cells on CRM1 function as opposed to non-cancer cells[128, 228, 230, 232, 237, 238]. Leptomycin B (LMB) was the first identified natural compound with anti-CRM1 activity[239], and acts by alkylating the cysteine-529 residue on CRM1, thereby inhibiting its function[240]. Although preliminary and preclinical studies were promising[241], LMB was eventually discontinued due to high toxicity in the phase I clinical trials[242]. Following that, various other CRM1 inhibitors were identified or developed, including LMB analogues[243] and CBS9106[244], both of which showed anti-tumour efficacies *in vitro* and *in vivo*. In addition, CRM1 has been shown to be the target of two natural-derived compounds Plumbagin and Piperlongumine, which were previously reported to show anti-cancer effects *in vitro* and *in vivo* [245, 246]. The clinical relevance of these compounds, however, remain to be defined.

More recently, a series of compounds termed the Selective Inhibitors of Nuclear Export (SINE) was generated by Karyopharm Therapeutic (Karyopharm Therapeutics, Inc., Boston, MA, USA) via *in silico* screening. These showed capacity to irreversibly modify the NES-binding groove of the CRM1 protein, thereby preventing its nuclear exporting function[228]. These bioavailable compounds showed great success in preclinical studies in various cancers including myeloid leukemia, kidney cancer, lymphoma, breast cancer, non-small cell lung cancer, melanoma and prostate cancer[229, 237, 247-252]. The clinical trials for selected SINE compounds, Selinexor (KPT-330) and KPT-335, which exhibited favourable pharmacokinetic and pharmacodynamic properties are ongoing, and have generated promising outcome so far in liposarcoma, multiple myeloma, glioblastoma and gynaecological cancers[224, 253].

The CRM1-inhibition phenotype has been proposed to result from a few mechanisms, such as the cytoplasmic retention of tumour suppressor proteins, and the reversal of EMT, an important process closely linked to malignant phenotypes[226, 254, 255]. CRM1 activity has also been associated with resistance to current chemotherapeutic interventions by preventing nuclear localization (thus activation) of tumour suppressors and chemotherapeutic responsive proteins[228, 256-258], suggesting a link between nuclear transport and drug resistance. In line with this, the combined therapy using conventional chemotherapeutic agents coupled to CRM1 inhibition via LMB, the SINE compounds or Piperlongumine have yielded promising results in reversing the chemoresistant phenotype[259-263]. In addition to its therapeutic values, ongoing research has also revealed prognostic potentials for CRM1, where its increased expression in tumour samples correlated with various malignant phenotypes and is generally associated with poor patient outcome[232-235, 264].

1.4. The Importin Karyopherinβ1

The nuclear transport system certainly present therapeutic opportunities in the current search for previously undescribed 'druggable' targets. The potential of Kpnβ1, one of the well-characterized Importin members is however, under-exploited. Kpnβ1 was first discovered in 1994 as a soluble factor that bridged the cargo recognition step in the cytoplasm to the translocation step at the NPC in the import pathway[265]. It was subsequently cloned independently by Gorlich *et al.* and Chi *et al*[266, 267]. Fluorescent *in situ* hybridization located the Kpnβ1 encoding gene, *kpnβ1* to chromosome 17q21[268], translating to a 97 kDa protein comprising 876 amino acids. Kpnβ1 is a superhelical structure composed of approximately 20 parallel HEAT repeat domains stacked together with a slight clock-wise twist. The N-terminal is responsible for interactions with RanGTP, while the inner concave and the C-terminal binds its Karyopherinα-independent cargoes and Karyopherinα, respectively[269].

Increased expression and activity of the protein itself is frequently observed in malignant tumour cells. Its contribution to carcinogenic activities has been proposed, most notably through the elevated nuclear import of other oncoproteins; such as NFκB in myeloma and hepatocellular carcinoma, Gli1 in glioma, and Stat1 in gastric cancer[192, 209, 270, 271]. Various proteins known to correlate with the cancer progression, such as those involved in EMT and inflammation have also been identified as Kpnβ1 cargoes, including EZH2, ING1, EGFR, STAT3, ETO, Smad3 and Nrf2, although the oncogenic contribution of their increased nuclear import by Kpnβ1 remain to be defined[199, 272-277]. In addition, the viral proteins L2 and E6 of HPV16, a high-risk cervical-cancer causing agent also relies on nuclear import by Kpnβ1, suggesting an aiding role of Kpnβ1 in the successful infection and reproduction of HPV16[278, 279].

Beyond its nuclear trafficking functions, Kpnβ1 is also important in the regulation of mitotic progressions, including spindle assembly and microtubule regulation, mitotic exit and nuclear membrane reformation after mitosis. Mitotic regulation is achieved by Kpnβ1 binding to and sequestering the activities of the spindle assembly factors (SAFs), and RanGTP promotes the release of SAFs from Kpnβ1, allowing them to participate in spindle assembly and microtubule regulation[280-283]. As RanGTP accumulates near the chromosomes, Kpnβ1, together with RanGTP provides a spatial control in SAF activity ensuring that they function at the appropriate cellular locations. Subsequently, Kpnβ1 engages in cellular exit from mitosis as well as regulating the reformation of interphase cell nuclear membrane[284, 285]. Whilst the elevated expression of Kpnβ1 in interphase cells may support the increased demands of cancer cells by increasing the rate of cargo import, some studies have reported a negative impact of Kpnβ1 over-expression in mitotic cells. These mitotic catastrophes were however, avoided by the co-over-expression of Kpnβ1 interacting partners, such as TPX2, Ran, RanBP2 and CRM1[282, 285, 286], suggesting that elevated expression of Kpnβ1 in cancer cells is coupled to increased expression of these proteins, allowing the uninterrupted progression through mitosis. Indeed, both TPX2 and Ran are known to be elevated in cancer cells compared to non-transformed

counterparts[287, 288]. Moreover, Kpnβ1 has also been shown to regulate other cellular properties and functions, such as the NPC permeability; the degradation of misfolded proteins in the endoplasmic reticulum; as well as preventing histone H1 cytoplasmic aggregation[289-291].

The function of Kpnβ1 can impact on a multitude of cellular functions from nuclear transport in interphase cells to division in mitotic cells, advocating the criticality of a well-orchestrated regulation for Kpnβ1. In line with this, intricate regulatory strategies have been reported to modulate the efficiency of Kpnβ1 and nuclear import, and some mechanisms where aberrancy have been associated to cancer were discussed above. In a report published by Yasuhara *et al.,* the Karyopherinβ/α mediated nuclear import efficiency is cell-cycle sensitive, exhibiting highest importing efficiency at late G1 and late S-phase[292]. Binding of both micro-RNA-9 and micro-RNA-30d has been demonstrated to negatively regulate Kpnβ1 expression by targeting its 3'-UTR in the mRNA, preventing its translation[199, 293]. The high intracellular level of calcium is another mechanism through which Kpnβ1 activity is modulated[294]. Recently, the newly characterized member of the Poly (ADP-Ribose) Polymerase (PARP/ARTD) family, ARTD15, a endoplasmic reticulum residing protein has been reported to directly bind to and ADP-ribosylate Kpnβ1, although the significance of this modification remains to be elucidated[295]. The impact of deregulated Kpnβ1 activity highlights the importance of its function in maintaining normal cellular functions, and abnormalities in its presentation or function may serve to indicate abnormalities in the cellular status.

1.4.1. Karyopherinβ1: a potential biomarker and therapeutic target for cancer

There is growing evidence in support of Kpnβ1 as a cancer biomarker, mainly as a prognostic marker and therapeutic target. This area of study, however, is still in its developing stage. The elevated Kpnβ1 levels has been reported in a many cancers, including cervical carcinoma, breast carcinoma,

myeloma, hepatocellular carcinoma, malignant peripheral nerve sheath tumour, gastric cancer and ovarian cancer when compared to their normal counterparts[128, 192, 199, 209, 270, 296, 297]. In a recent report by Kuusisto *et al.*, the extent of Kpnβ1 over-expression was found to directly reflect the disease state in the MCF10 breast tumour progression series, where increased malignancy was correlated to increased Kpnβ1 expression[296]. This finding illustrated the possible prognostic use of Kpnβ1, and indeed, elevated Kpnβ1 levels has been shown to significantly correlate to histological grade, metastasis, vein invasion and tumour size in hepatocellular cancer[192]; and tumour grade, Ki-67 staining and infiltration depth in gastric cancer[209].

As a therapeutic target, the inhibition of Kpnβ1 function through genetic or pharmacological interventions have yielded promising outcomes in various *in vitro* cancer models. To date, anti-cancer effects stemming from Kpnβ1 inhibition have been demonstrated for cervical carcinoma, myeloma, malignant peripheral nerve sheath tumours, hepatocellular carcinoma, breast carcinoma, head and neck carcinoma, lung carcinoma and gastric cancer[128, 192, 199, 209, 270, 296, 298, 299], suggesting that targeting Kpnβ1 may have broad-spectrum anti-cancer effects. Using the cervical cancer model, research in our laboratory demonstrated that Kpnβ1 inhibition led to a G2/M cell cycle arrest coupled to various mitotic defects, which ultimately triggered an apoptotic response via the intrinsic mitochondrial pathway[300]. The mechanism by which Kpnβ1 inhibition induces apoptosis in other cancer model, however, remains to be elucidated.

Targeting Kpnβ1 for cancer treatment has raised a few concerns. Firstly, various tumour suppressors are known to rely on Kpnβ1 for nuclear import, such as p53, BRCA1 and pRB[301-303]. The consequent prevention of their nuclear accumulation as a result of Kpnβ1 inhibition may thus not provide therapeutic benefits. These tumour suppressors, however, are frequently inactivated or non-functional in cancer cells to begin with. As such, Kpnβ1 inhibition is likely to reduce the actions of

oncoproteins which are highly active in cancer; more so than repressing tumour suppressors. Secondly, as the function of Kpnβ1 is utilized by both cancer and normal cells, targeting it for cancer therapy may induce undesired side effects as a result of cytotoxic effects to non-cancer cells. As cancer cells are derived from normal cells, most cellular machineries are used by both. Whilst some cancer-specific mutations can be targeted (like the BCR-ABL1 in leukemia), such mutations are not always present since most cancers arise from accumulative alterations in a multitude of different pathways rather than in a single protein. It is however, important to note that there exist an 'additional reliance' of cancer cells on certain cellular functions compared to normal cells, Kpnβ1-mediated nuclear import being one of them. This is supported by several experimental findings where cancer and transformed cells exhibited significantly higher sensitivity to Kpnβ1 inhibition compared to their normal counterparts[128, 270, 296, 300]. In addition, some proteins with important cellular functions have also proven to be effective targets in anti-cancer treatment, such as the 20S proteosome targeted by Bortezomib and Carfilzomib[304, 305]. van der Watt *et al.* and Kuusisto *et al.* both reported that siRNA mediated inhibition of other Karyopherin members, including Kpnα1, Kpnα2 and Kpnα3 has shown either no anti-cancer activity or no selectivity between malignant and benign cells, suggesting that the selective anti-cancer effects of Kpnβ1 inhibition was a result unique to Kpnβ1 inhibition[128, 296]. The results from these studies propose that targeting Kpnβ1 may have value as an anti-cancer strategy and requires further investigation.

In addition to its potential as a direct anti-cancer target, there is evidence suggesting that Kpnβ1 could mediate sensitivity to other chemotherapeutic agents. This was first described by Drinyaev *et al.*, where Avermectin (the parent compound of Ivermectin, a Karyopherinβ/α mediated nuclear import inhibitor) was found to enhance Vincristine-induced tumour growth suppression[306], although the underlying mechanism has not yet been defined. Moreover, Kpnβ1 has also been proposed to confer Docetaxel resistance, and its inhibition via siRNA enhanced the effect of Docetaxel treatment in cancer cells[209]. As CRM1 inhibition sensitized cancer cells to chemotherapeutic agents via

increasing nuclear retention of tumour suppressors[165, 257], there could exist a reciprocated role for Kpnβ1. Amongst the cargoes imported by Kpnβ1, many have been implicated to confer drug resistance such as STAT-1, Myc and NFκB[307-309]. As targeting Kpnβ1 will impair their nuclear entry, this could potentially interfere with survival mechanisms thereby enhancing drug sensitivity. Supporting this idea, there are evidence showing that suppression of NFκB enhanced chemosensitivity[310], and sensitization of cervical cancer cells to CDDP has been demonstrated in combination with Genistein, which acts by suppressing the NFκB response[311]. Furthermore, the inhibition of RelB:p52 nuclear import sensitized cancer cells to ionizing radiation[312]; and as radiation therapy acts mainly by causing DNA damage, this suggests a potential for nuclear import inhibition coupled to DNA-damaging agent as a combination chemotherapeutic regimen. Since none of the current chemotherapeutic agents target the nuclear import pathway, the combination of Kpnβ1 inhibition to a clinically relevant DNA-damaging agent thus fit the criteria where two agents are mechanistically different.

1.4.2. Intervening with Karyopherinβ1-mediated nuclear import

Attempts to alter the nuclear import system began in the 1990's, where a cell-permeable peptide mimicking the NFκB-p50 NLS, the SN50, was shown to inhibit nuclear translocation of NFκB-p50, AP1, NFAT, STAT1 and Nrf2[277, 313, 314]. SN50 was initially believed to inhibit import via targeting Karyopherinα, however, later works demonstrated its inhibitory effect on nuclear import of SREBP[315], a cargo imported into the nucleus Karyopherinα-independently[316]. This indicated that SN50 can also directly target Kpnβ1. By a similar approach, the inhibition of nuclear import of RelB:p52 was achieved using the SN52 peptide, which was shown to sensitize prostate cancer cells to radiotherapy[312]. With the intention of developing specific inhibitors for Kpnβ1/Karyopherinα mediated nuclear import, Kosugi *et al.* employed the peptide inhibitor design and developed Bimax1

and Bimax2, both of which targeted nuclear import via Karyopherinα, but were ineffective at inhibiting Kpnβ1-only mediated nuclear import[317].

There are three small molecules with nuclear import inhibitory effects described to date, namely Ivermectin, Karyostatin 1A and Importazole. Ivermectin, the oldest of the three was first discovered in the 1970's and came into clinical use in the 1980's for treating parasitic infections. Several years later, its anti-cancer effects were recognized against ascites and solid experimental tumours, although no correlation to nuclear import inhibition were made[306]. A few studies have since reported Ivermectin as an anti-cancer agent through alternative mechanisms[318, 319]. Only recently was its effect on nuclear import recognized, however, like the Bimax peptides, Ivermectin interfered with nuclear import only when Karyopherinα is involved[320, 321]. The first report linking Ivermectin, nuclear import inhibition and cancer was published earlier this year, wherein Ivermectin was shown to decrease tumour formation *in vitro* and *in vivo* for hepatocellular carcinoma. This study showed that Ivermectin was capable of inhibiting YAP1, an important mediator in the Hippo pathway, and proposed that this may result from decreased nuclear import of YAP1[322]. Whilst there are growing evidence to support the anti-cancer effects of Ivermectin, it has also been shown to induce the expression of P-gp, the membrane bound efflux pump closely associated with drug resistance, raising some concerns in its use for anti-cancer treatment[323].

Both Karyostatin 1A and Importazole are small molecules recently identified to specifically target for Kpnβ1/Karyopherinα mediated nuclear import, and both exerts its effect via disrupting the Kpnβ1-RanGTP interaction[324, 325]. Moreover, both small molecules specifically target the Kpnβ1 mediated nuclear import without affecting Transportin or CRM1 activity. Whilst effective at inhibiting nuclear import, their use mostly involves investigating cellular functions such as mitosis, and little work has been done in the cancer setting. Importazole has recently been shown to exhibit anti-tumour activity

in multiple myeloma and breast cancer *in vitro*[296, 298], although the underlying mechanisms still remain unclear.

Another potential Kpnβ1 inhibitor, 58H5-6, was identified from peptidomimetic libraries using permeabilized cell nuclear import assays, and is thought to act via disrupting the Kpnβ1-nucleoporin interactions. It also specifically targeted Kpnβ1/Karyopherinα mediated nuclear import, without affecting Transportin activity. This compound however, lacks *in vivo* efficacy, possibly due to low permeability or *in vivo* enzymatic activities, and further modifications are required before it can be used for biological assays[326].

These preliminary data are encouraging, yet the appropriate preclinical and clinical examinations are still lacking to demonstrate the feasibility and chemotherapeutic practicality of targeting nuclear import for anti-cancer therapy, and more extensive investigations should be executed.

1.4.3. The identification of a potential Karyopherinβ1 inhibitor: INI-43

In a search for novel small molecules with potential to bind to Kpnβ1 and inhibit its activity, a structure-based *in silico* screen was carried-out in our laboratory in collaboration with researchers at the Brown Cancer Centre (University of Louisville, Kentucky, USA). Based on the known crystal structure of Kpnβ1, a library of 12,662,570 small molecules were screened for their predicted ability to bind to the overlapping Karyopherinα and RanGTP binding sites within Kpnβ1, corresponding to amino acids 331-363. This region has previously been identified as essential for Kpnβ1 function, whereby its deletion rendered Kpnβ1 unable to import cargoes into the nucleus[158]. The search yielded 74 hits, and were numbered according to their predicted affinity for binding Kpnβ1. The 43rd compound in this series, *3-(1H-1,3-benzimidazol-2-yl)-1-[3-(dimethylamino)propyl]-1H-pyrrolol[2,3-*

b]quinoxalin-2-amine, which we named Inhibition of Nuclear Import-43 (INI-43), was a candidate chosen for further analysis, as it showed nuclear import inhibitory effects as well as half maximal inhibitory concentration (IC_{50}) values within the current chemotherapeutic range (less than 50 μM) as tested in cervical cancer cell lines.

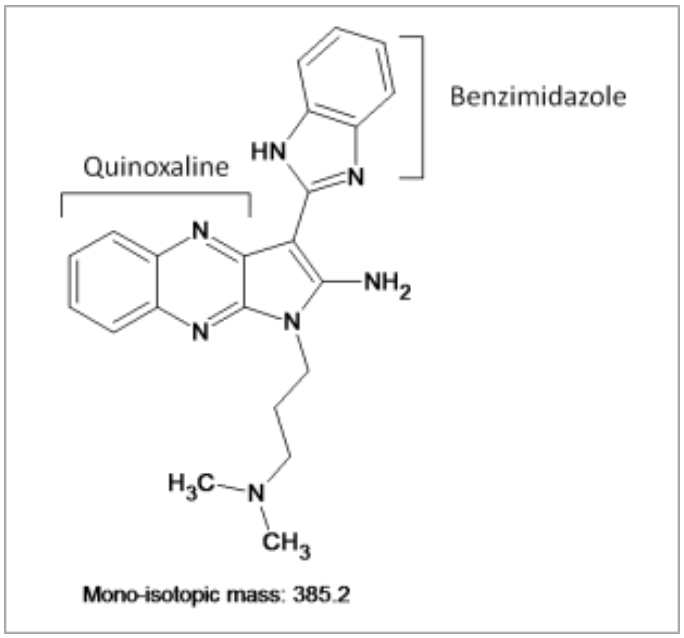

Figure 1.5. Structure of the small molecule Inhibitor of Nuclear Import-43 (INI-43). INI-43 is a quinoxaline derivative containing a benzimidazole side chain, with a molecular mass of 385g/mole.

INI-43 is an autofluorescent compound (emission peak around 519nm) possessing both quinoxaline and benzimidazole groups (Fig. 1.5). Quinoxaline is a heterocyclic compound made of a benzene ring and a pyrazine ring, and the benzimidazole side chain is a bicyclic compound consisting of a benzene and imidazole fused together. Interestingly, both quinoxaline and benzimidazole have been reported to show anti-cancer activities independently[327-332]. Pioneering work in our laboratory demonstrated that INI-43 impeded nuclear import of Kpnα2 in CaSki cells stably expressing the Kpnα2-GFP fusion

protein[‡], as well as Kpnβ1 in HeLa cells[333], indicating that INI-43 is able to impact on Kpnβ1/Kpnα2 mediated nuclear import. Supporting this, it was subsequently found that INI-43 treatment resulted in decreased transcriptional activity of a Kpnβ1 cargo protein NFAT as measured by a NFAT-luciferase reporter system. The inhibitory activity of INI-43 on nuclear import pathways was further shown for various known Kpnβ1/Karyoherinα cargoes, including AP1 and NFY. Excitingly, Kpnβ1 over-expression was found to rescue the repressed nuclear import of NFκB-p65 as a result of INI-43 treatment, suggesting that nuclear import inhibitory effect of INI-43 is exerted through Kpnβ1[333].

1.5. Significance

There are evidence to support that Kpnβ1-mediated nuclear import may have potential as a target for anti-cancer treatment, yet extensive research and appropriate preclinical modelling of the current nuclear import inhibitors are still lacking. This study verifies a newly identified small molecule INI-43 as a potential lead 'parent' compound in the nuclear import inhibitor class, by investigating its *in vitro* and *in* vivo efficacy. If successful, INI-43 can be further developed for future clinical use both as a single agent or in combination with other clinically relevant drugs in combating cancer.

[‡]Stowell, C. "Identification of Nuclear Import Inhibitors That Display Anti-cancer activity." University of Cape Town, 2011

1.6. Project aims

This project aims to:

(i) Investigate the anti-cancer potential of INI-43 as a lead compound, by examining the effects of INI-43 on cancer and non-cancer cell proliferation and viability using both cell culture system and an *in vivo* mouse xenograft model. In the *in vivo* model we aim to investigate its toxicity and anti-tumour activity.

(ii) Investigate the effects of INI-43 in combination with a clinically relevant cytotoxic agent Cisplatin (CDDP) on cancer cells. This will be done using two gynaecological cancer models; ovarian and cervical cancers. The molecular mechanisms associated with cell death as a result of the combination treatment was further explored.

CHAPTER 2

INVESTIGATING THE ANTI-CANCER EFFECTS AND DRUG PROPERTIES OF INI-43, A SMALL MOLECULE WITH POTENTIAL NUCLEAR IMPORT INHIBITORY ACTIVITY

2.1. Introduction

The identification of the altered Kpnβ1 expression in cancer versus normal, and its necessity in cancer growth and survival suggested that it has potential as a target for anti-cancer therapy. The subsequent *in silico* and biological screenings for potential inhibitors of Kpnβ1 identified various 'hits', one of which, the Inhibitor of Nuclear Import-43 (INI-43) was further examined. We have previously shown that INI-43 inhibited nuclear localization of both Kpnβ1[333] and GFP-tagged Kpnα2[§]. The nuclear import of various Kpnβ1-cargoes were prevented by INI-43 treatment, including AP1, NFY and NFκB. NFAT-luciferase reporter assays revealed that INI-43 treatment significantly reduced the transcriptional activity of the NFAT transcription factor, suggesting that the decreased nuclear import translated into functional relevance. Importantly, exogenously over-expressed Kpnβ1 alleviated the inhibitory effect of INI-43 on nuclear localization of NFκB. These data show that firstly, INI-43 had inhibitory effects on nuclear import activity, and secondly, these effects were likely mediated through interfering with Kpnβ1 function, making it an attractive compound for further investigation as an anti-cancer agent.

[§]Stowell, C. "Identification of Nuclear Import Inhibitors That Display Anti-cancer activity." University of Cape Town, 2011

Beyond its inhibitory effect on Kpnβ1-mediated nuclear import, preliminary findings in our laboratory have demonstrated the anti-cancer effect of INI-43 using the cervical cancer model. INI-43 showed a half maximal inhibitory concentration (IC_{50}) of 10 μM in cervical cancer cell lines HeLa and CaSki, which is within the range of chemotherapeutic agents in current practice. In addition, INI-43 treatment reiterated many phenotypes observed in Kpnβ1 knock-down cells. These included its anti-cancer effects, while causing less harm to non-cancer fibroblast cells; as well as cell cycle arrest at the G2/M checkpoint[300, 333]. The similar phenotypes observed between INI-43 treated and Kpnβ1 knock-down cells further support the idea that INI-43 is exerting its effect through perturbation of Kpnβ1 function.

Whilst the anti-cancer properties of INI-43 has been demonstrated using cervical cancer cells grown in culture[333], little is known about its mechanisms of action and *in vivo* effects. The aim of this chapter is therefore to investigate the phenotypic outcomes of INI-43 treatment both *in vitro* and *in vivo*. These included investigating cell viability and cell proliferation under various growth conditions; the apoptosis related release of mitochondrial cytochrome C and PARP-cleavage; the drug-properties of INI-43 including stability and toxicity in nude mice. Our data provides evidence that intraperitoneally administered INI-43 reduced tumour growth in an ectopic xenograft mouse model.

2.2. Results

2.2.1. Confirming the purity of commercially bought INI-43

The subject of this study, the small molecule INI-43 was purchased from Chembridge (San Diego, CA, USA) and MolPort (Riga, Latvia). Before using it in our investigation, we independently examined its purity by using high pressure liquid chromatography-diode array detection-mass spectrometry (HPLC-DAD-MS). Solutions of three different batches were prepared to a concentration of 100 µM in DMSO separately and together, and subjected HPLC-DAD-MS. The DAD chromatogram result showed two peaks at retention time (Rt) 1.05 and 5.95 which is representative of DMSO and INI-43 from the mix of all three batches (Fig. 2.1.A). The mass spectrum of the Rt 5.95 peak on the total ion chromatogram of the MS confirmed the mass of INI-43 to be 385Da from the$[M+H]^+$ ion at m/z ratio of 386 (Fig. 2.1.B). These results confirmed that all batches of INI-43 used in our laboratory were > 99% pure.

2.2.2. INI-43 reduced cancer cell viability and proliferation

To determine the effect of INI-43 on cell viability and proliferation in a panel of cancers and non-cancer cell lines, the half maximal inhibitory concentration (IC_{50}) was investigated for a treatment period of 48 hours. IC_{50} is a measure of the minimum concentration that is required to inhibit 50% of a specific biological or biochemical function, and in this case, cell viability was investigated using the MTT assay. Cells were treated with ranging concentrations of INI-43 for 48 hours and viable cells were determined for each INI-43 concentration. Cell viability was then converted to a numerical value, the 'fraction affected' (Fa), where Fa of 0 depicts 100% viable cells (i.e. no effect), and Fa of 1 is equivalent to complete cell death. The Log[Fa/(1-Fa)] is then plotted against Log INI-43 concentration, and the IC_{50} value was calculated using the formula $IC_{50} = 10^{x\text{-intercept}}$. When 50% of cell growth was inhibited, Fa and 1-Fa both equal to 0.5, equating to a y-value (Log[Fa/(1-Fa)]) of zero,

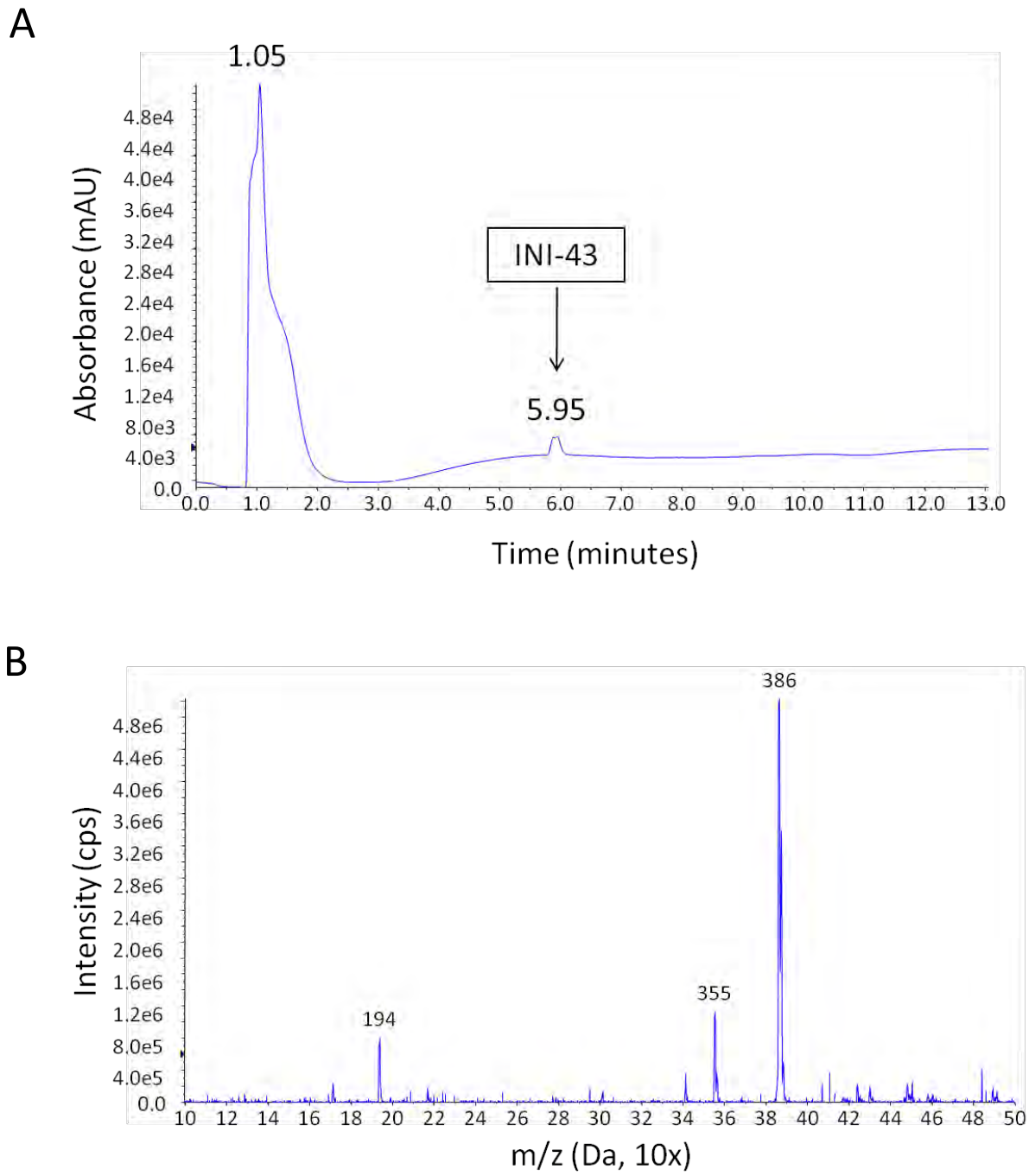

Figure 2.1. Purity and mass confirmation of INI-43. A DAD chromatogram showing the mixture of three different batches of INI-43, with peaks at Rt 1.05 and 5.95 representing DMSO and INI-43, confirming its purity (A). The mass spectrum of Rt 5.95 peak, confirming mass of INI-43 at [M+H]+ ion at m/z of 386 (B).

which is where the x-axis is crossed. As the x-axis represents the drug concentration in log scale, the actual drug concentration is calculated using $10^{x\text{-intercept}}$. Using this method, the INI-43 IC_{50} values were determined for ovarian cancer, oesphageal cancer and non-cancer cell lines. A representative for each cancer is shown (Fig. 2.2.A, for other cell lines refer to Appendix Fig. A.1), and the cervical cancer cell lines HeLa was included as a control and generated IC_{50} values similar to that previously observed[333]. The INI-43 IC_{50} values for each cell line are summarized in Fig. 2.2.B and Table 2.1. INI-43 exhibited IC_{50} values of between 5 μM and 10 μM in ovarian cancer cells, oesophageal cancer cells and transformed cells. The non-cancer fibroblast cell lines CCD-1068SK, FG_0 and DMB exhibited reduced sensitivity to INI-43 treatment, with IC_{50} values 2-3 fold higher than cancer cells (22 μM, 33 μM and 35 μM respectively).

In addition, cell viability after 5 μM, 10 μM and 15 μM INI-43 treatment were analyzed for each cell line, and in all cancer cell lines examined, 10 μM INI-43 treatment led to varying degrees of growth inhibitory effects, and 15 μM treatment caused complete cell death (Fig. 2.3). However, in the non-cancer cell lines CCD-1068SK, FG_0 and DMB, 10 μM INI-43 treatment had little effects, and more than 50% of the cells were still viable after 15 μM INI-43 treatment. These results illustrated increased sensitivity to INI-43 treatment in cancer cells compared to non-cancer cells.

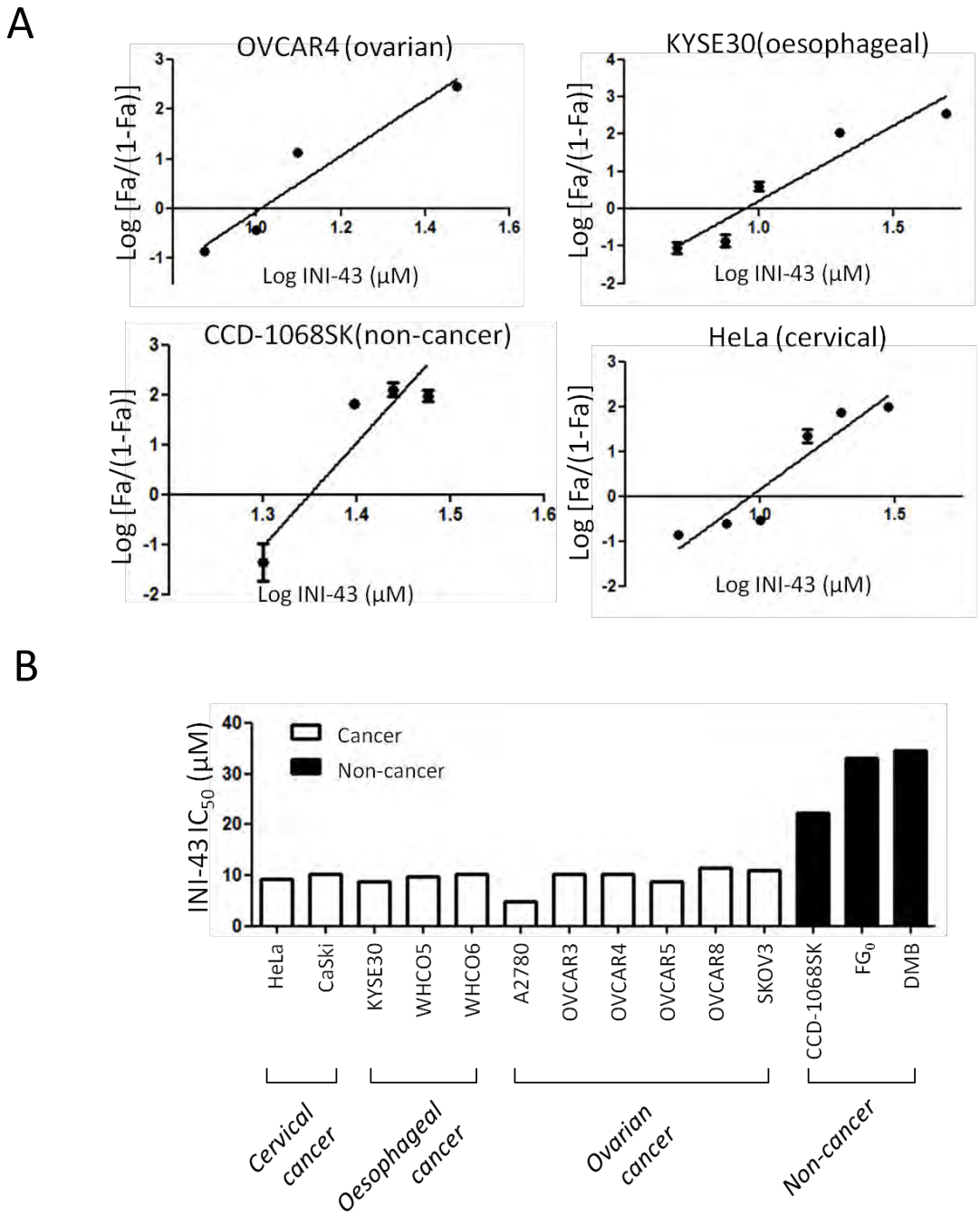

Figure 2.2. INI-43 IC_{50} determination in selected cancers and non-cancer fibroblast cells. Five-thousand cells were seeded per well in 96-well plates and allowed to adhere overnight, followed by INI-43 treatment at various concentrations. Viable cells were examined using the MTT reagent 48 hours later, and standardized to the untreated. The result are plotted as log [Fa/(1-Fa)] against the INI-43 concentration in log scale, where Fa = fraction of cells affected. IC_{50} values were calculated as $10^{x\text{-intercept}}$. One representative cell line is shown for each of the ovarian cancer, oesophageal cancer and non-cancer fibroblast (A, see the rest in Appendix Fig. A.1). For control, the cervical cancer cell line HeLa was included, and generated acceptable INI-43 IC_{50} value as previously established in our laboratory. Results shown are the mean ± SEM of experiments performed in 5 replicates, and repeated at least two times in each cell line (A), and IC_{50} values for each cell line shown are representatives of experiments performed in 5 replicates and repeated at least two independent times.

Table 2.1. INI-43 IC_{50} in cancer cell lines of different tissue origin and non-cancer cell lines

Origin	Cell line	INI-43 IC_{50} (μM)
Cervical cancer	HeLa	9.2
Cervical cancer	CaSki	10.2
Oesophageal cancer	KYSE30	8.9
Oesophageal cancer	WHCO5	9.9
Oesophageal cancer	WHCO6	10.1
Ovarian cancer	A2780	5.0
Ovarian cancer	OVCAR3	10.4
Ovarian cancer	OVCAR4	10.2
Ovarian cancer	OVCAR5	8.8
Ovarian cancer	OVCAR8	11.6
Ovarian cancer	SKOV3	10.9
fibroblast	CCD-1068SK	22.4
fibroblast	FG_0	33.0
fibroblast	DMB	34.6

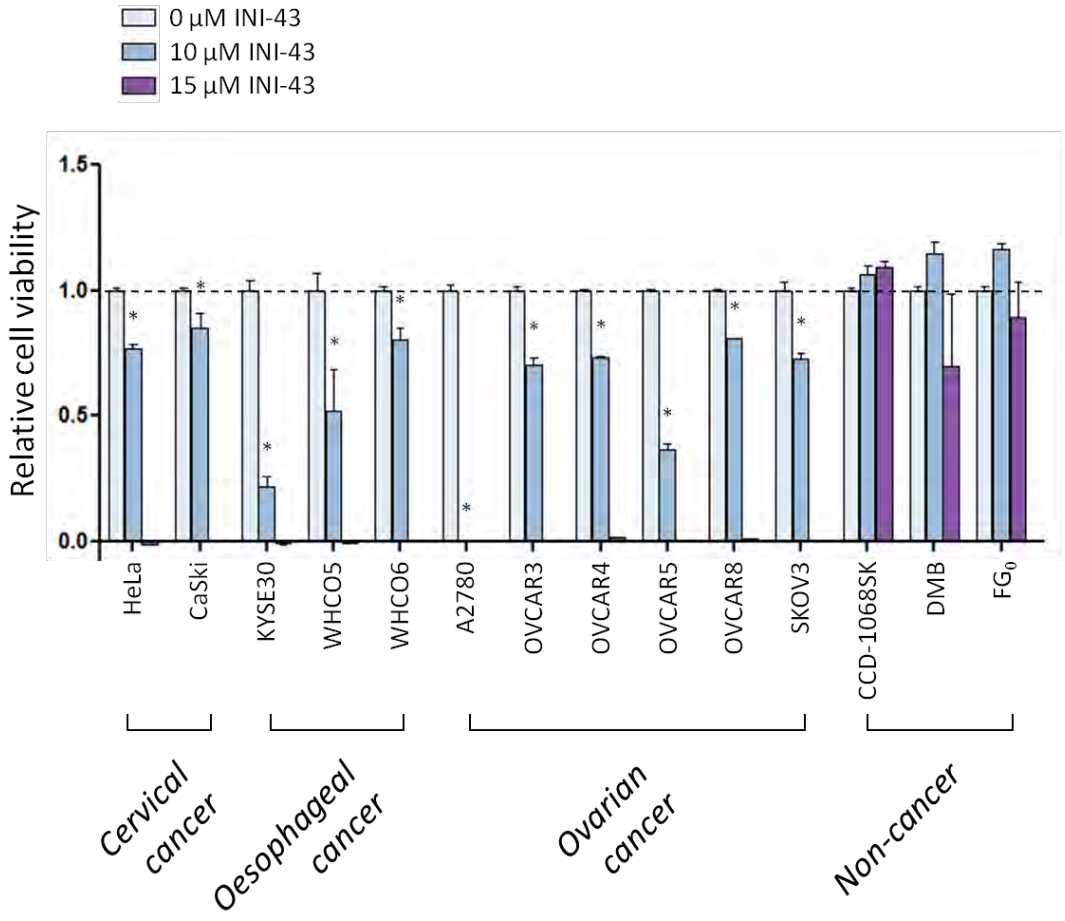

Figure 2.3. The effect of INI-43 on viability of cancer, transformed and non-cancer fibroblast cells. Cells were plated at 5000 per well in a 96-well dish and allowed to settle overnight, followed by incubation with 0 µM, 10 µM or 15 µM INI-43 for 48 hours. Viable cells were determined using the MTT reagent, and standardized to the untreated cells. Results shown are mean ± SEM of experiments performed in 6 replicates and repeated at least twice, *$p < 0.05$.

2.2.3. Anti-cancer properties of INI-43

Having shown that INI-43 selectively reduced cancer cell viability, we next investigated the effect of INI-43 on cell proliferation in a time-dependent manner, and under various growth conditions in selected cancer cell lines.

2.2.3.1. The effect of INI-43 on anchorage-dependent cell proliferation

To confirm the inhibitory effect of INI-43 on cell growth, representative cells of cervical cancer (HeLa and CaSki), oesophageal cancer (KYSE30 and WHCO6) and non-cancer (FG_0 and DMB) were grown under anchorage-dependent conditions in the presence of 1 μM, 5 μM and 10 μM INI-43, and proliferation was measured using the MTT assay over a period of four days. These assays showed that 10 μM INI-43 treatment significantly inhibited the proliferation of all cancer cell lines (Fig. 2.4). The inhibitory effect of INI-43 on cancer cell growth was maintained over the entire duration of the experiment, with no recovery observed. However, proliferation of both non-cancer fibroblast cell lines FG_0 and DMB were unaffected at 10 μM INI-43 (Fig. 2.4). These results support earlier findings that cancer cells appear more sensitive to INI-43 treatment compared to non-cancer cells. It should be noted that while 10 μM INI-43 led to complete inhibition of cell growth in this experiment, the same treatment rendered fractions of cancer cells viable shown in the viability assay (Fig. 2.3). This is likely due to the experimental set-up, as different cell numbers were seeded for these two experiments. In this experiment, we were interested in cell proliferation, and thus five-times less cells were plated to provide room for proliferation. The decreased confluency increased the drug to cell number ratio, possibly accounting for the different outcomes between the two experiments observed at the same INI-43 concentration. The net effect of INI-43 treatment, however, remains that it significantly inhibits cancer cell proliferation.

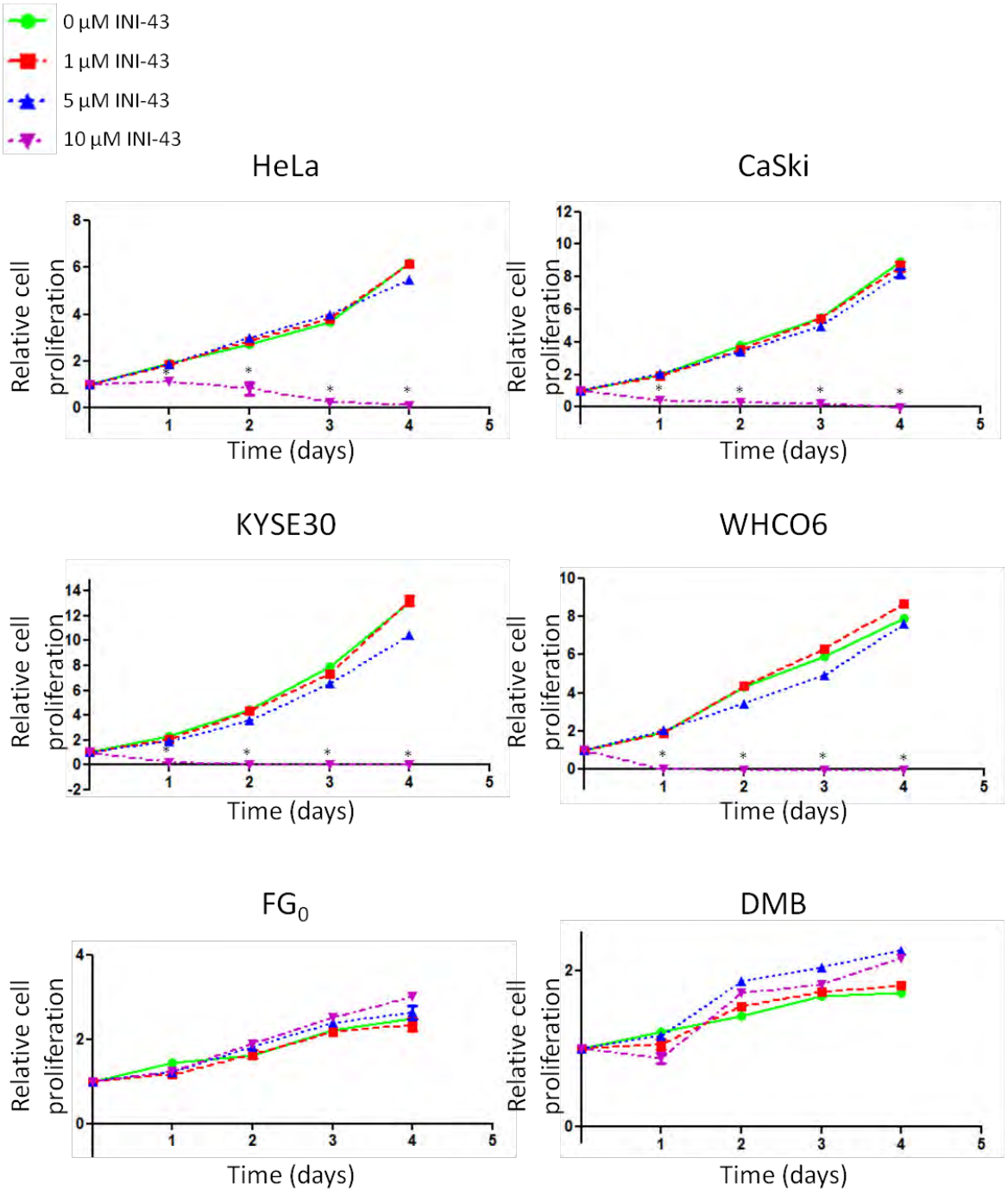

Figure 2.4. Proliferation of selected cancer and non-cancer cell lines treated with INI-43 over 4 days. Cells were seeded at 1000 per well in 96-well plates and treated with 0 µM, 1 µM, 5 µM and 10 µM INI-43 the following day. Proliferation was examined every 24 hours using the MTT reagent for 4 days after treatment, and normalized to the viable cells on day 0. Results shown are mean ± SEM of 6 replicates, and each experiment is repeated at least twice, *$p < 0.05$.

2.2.3.2. The effect of INI-43 on anchorage-dependent colony formation

We next examined the colony forming ability of cancer cells after INI-43 treatment by performing clonogenic assays as previously described[334]. Differing from the proliferation assay, which examined the proliferative activity of cells in the presence of a damaging agent, the colony formation assay assesses sensitivity by evaluating the reproductive viability of cells after the source of damage is removed. In order to form a colony, a single cell must survive and maintain its proliferative potentials to form a macroscopic colony. In this assay, cells were seeded sparsely allowing each cell to settle in isolation, thereby eliminating complexities caused by interactions between members of large cell population. Cells were then treated with INI-43 at various concentrations for 24 hours, after which the drug was removed from the growth media. The cells were then incubated over a period of 12 days, after which cells were stained with crystal violet and macroscopic colonies were visually examined[335]. Each macroscopic colony consists of more than 50 cells, and the number of macroscopic colonies is an indication of drug sensitivity. The clonogenic assays showed that in both HeLa and KYSE30 cells, 1 μM and 5 μM treatment did not cause significant differences in colony formation compared to the untreated cells (Fig. 2.5). However, 10 μM INI-43 completely inhibited colony formation, and no cells survived to produce colonies in both cancer cell lines. Coupled to the proliferation assay, this result confirmed that 10 μM INI-43 robustly prevented cancer cell survival and proliferation.

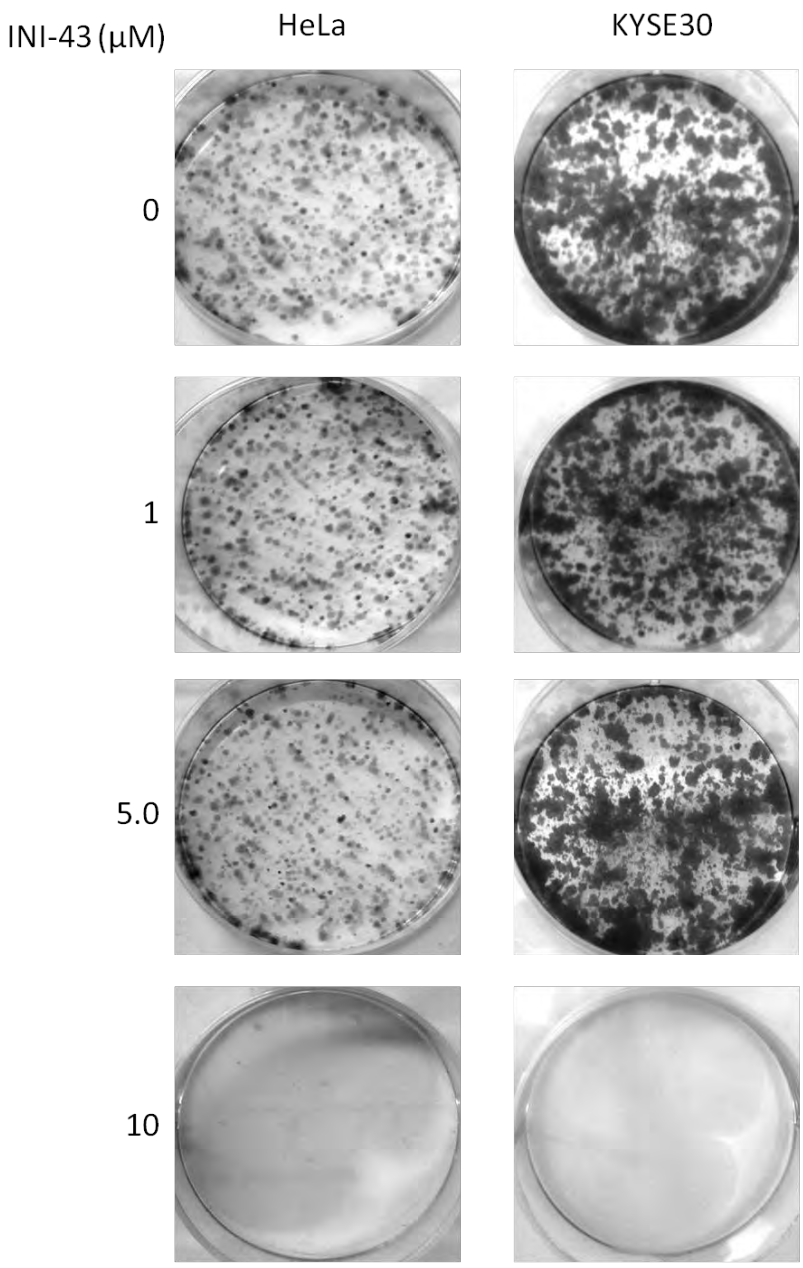

Figure 2.5. Survivability of HeLa and KYSE30 cells after INI-43 exposure. Cells were plated sparsely at 1000 per 35 mm dish followed by INI-43 treatment at 1 μM, 5 μM and 10 μM. After 24 hours, INI-43 was removed and media was replenished every second day for 12 days. Viable colonies were fixed and stained with crystal violet, and images were captured. Results shown are representatives experiments performed in triplicates and repeated two independent times.

2.2.3.3. The effect of INI-43 on anchorage-independent cell growth

One character of tumourigenic phenotype is the ability of cells to proliferate under substrate-free conditions (i.e. anchorage independently) by forming colonies[336]. We were therefore interested to examine whether INI-43 could affect the anchorage-independent cell growth of selected cancer cells by performing cell proliferation assays under non-adherent growth conditions. To do this, cells were resuspended in 1% methylcellulose in the absence or presence of INI-43 on poly-HEMA coated surfaces. While the methylcellulose prevented cells from migrating towards each other, the poly-HEMA prevented cells from adhering to the dish surface. Cells were left to proliferate and form colonies over a period of nine days, and subsequently treated with MTT reagent to identify viable colonies. In the untreated and 5 μM INI-43 treated cells, several MTT stained colonies were observed in both HeLa and WHCO6 cells, while 10 μM and 15 μM treatment resulted in smaller, non-viable colonies, shown by the lack of MTT staining (Fig. 2.6). This result indicated that 10 μM or higher concentrations of INI-43 prevented cancer cell proliferation in substrate-free media. In the 5 μM INI-43 treated cells, a slight reduction in colony size was observed, suggesting that at this concentration, INI-43 was able to exert inhibitory effects on cancer cell proliferation under substrate-free conditions. Taken together, these results showed INI-43 exhibited increased cytotoxicity in cancer cells compared to normal fibroblast cells, and that 10 μM INI-43 treatment reduced cell viability and inhibited cell proliferation in cancer cells grown both anchorage-dependently and independently.

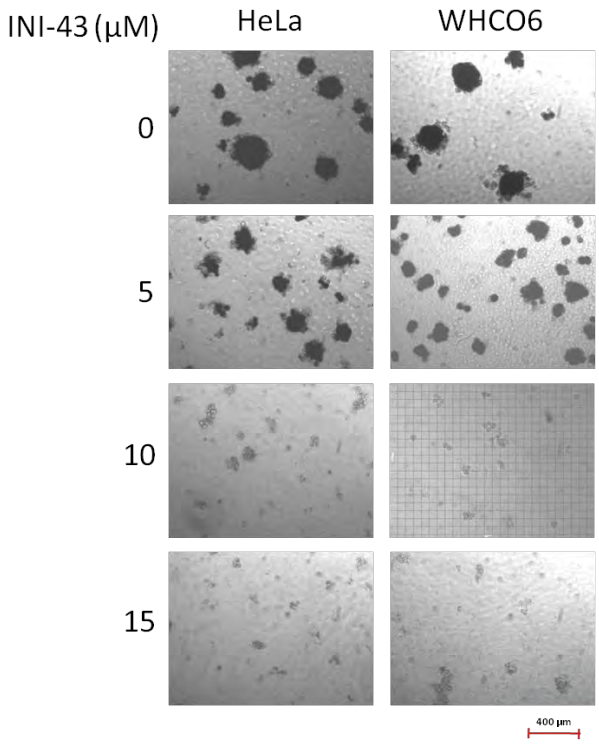

Figure 2.6. Effects of INI-43 on anchorage-independent proliferation in HeLa and WHCO6 cells. Cells were resuspended in 1% methylcellulose containing media and plated in poly-(HEMA) coated 96-well plates in the presence or absence of INI-43 for 9 days. Viable colonies were stained with MTT reagent and photographed under brightfield microscopy. Images shown are representative experiments performed in triplicates and repeated three times.

2.2.4. The effect of Kpnβ1 knock-down on cell proliferation

We next independently examined the effect of Kpnβ1 knock-down on cell proliferation using small (or short)-hairpin RNA (shRNA). The shRNA is an artificial RNA molecule resembling the structure of a hairpin, which potently inhibits the expression of its target gene via the RNA-induced silencing complex (RISC). The shRNA encoding plasmid is delivered into the host cells by viral-mediated infection or liposomal transfection. Upon entry into the cell, it uses the host cell's transcription machinery to produce shRNA molecules, which then becomes cleaved by Dicer, producing the sense and anti-sense strands. The anti-sense strand couples with the RISC complex, guiding it to the target

mRNA by complementary base-pairing. This ultimately results in the target mRNA degradation, preventing protein synthesis[337].

2.2.4.1. The doxycycline (dox) inducible pTIG-shKpnβ1 construct effectively reduced endogenous Kpnβ1 expression

In this study, we used the pHIV7-TetR-IRES-GFP plasmid (pTIG, a kind gift from Prof. S. Prince, University of Cape Town; and Prof M. Weinberg, University of Witwatersrand), which expresses the shRNA under the control of a doxycycline-inducible U6 promoter (see Appendix Fig. A.2)[338]. Kpnβ1-targeting shRNA (shKpnβ1) was designed and cloned into the pTIG vector, forming pTIG-shKpnβ1-1 as described in Materials and Methods. As the pTIG vector constitutively expresses GFP, GFP fluorescence was used as a read-out of the transfection efficiency. To determine the best transfection conditions, HeLa cells were transfected with pTIG-shKpnβ1-1 ranging from 0 ng/mL to 500 ng/mL, and shRNA expression were induced with 1 ng/μL doxycycline treatment. pTIG-shKpnβ1-1 uptake was examined using fluorescent microscopy, which showed concentration-dependent increase in transfection (Fig. 2.7.A). The results showed good transfection efficiency at 250 ng/mL and 500 ng/mL pTIG-shKpnβ1-1, and at 500 ng/mL the efficiency was close to 100%. To examine whether pTIG-shKpnβ1-1 caused efficient inhibition of Kpnβ1 expression, proteins were harvested and Kpnβ1 levels were analyzed by western blot. Corresponding to the transfection efficiency, Kpnβ1 knock-down occurred concentration-dependently, and were most visible in cells transfected with 250 ng/mL and 500 ng/mL plasmids (Fig. 2.7.B).

Having confirmed that pTIG vector effectively expressed the shRNA, two additional Kpnβ1 targeting shRNAs were designed, shKpnβ1-2 and shKpnβ1-3, and separately cloned into the pTIG vector, forming pTIG-shKpnβ1-2 and pTIG-shKpnβ1-3. All three pTIG-shRNA constructs, together with the control, the pTIG-scrambled (pTIG-scr) were transfected into HeLa cells and subsequently induced

A

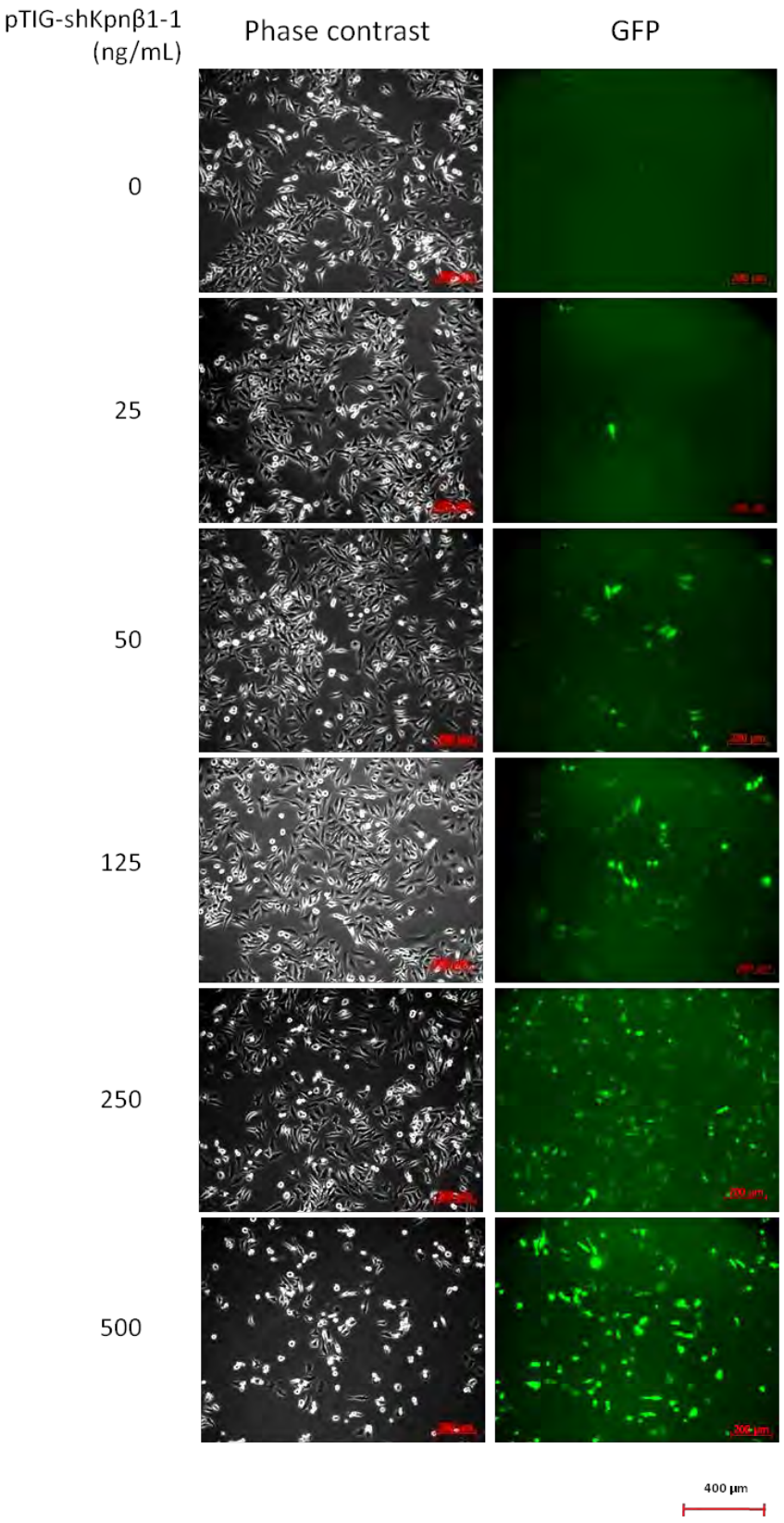
pTIG-shKpnβ1-1
(ng/mL)
Phase contrast
GFP
0
25
50
125
250
500
400 μm

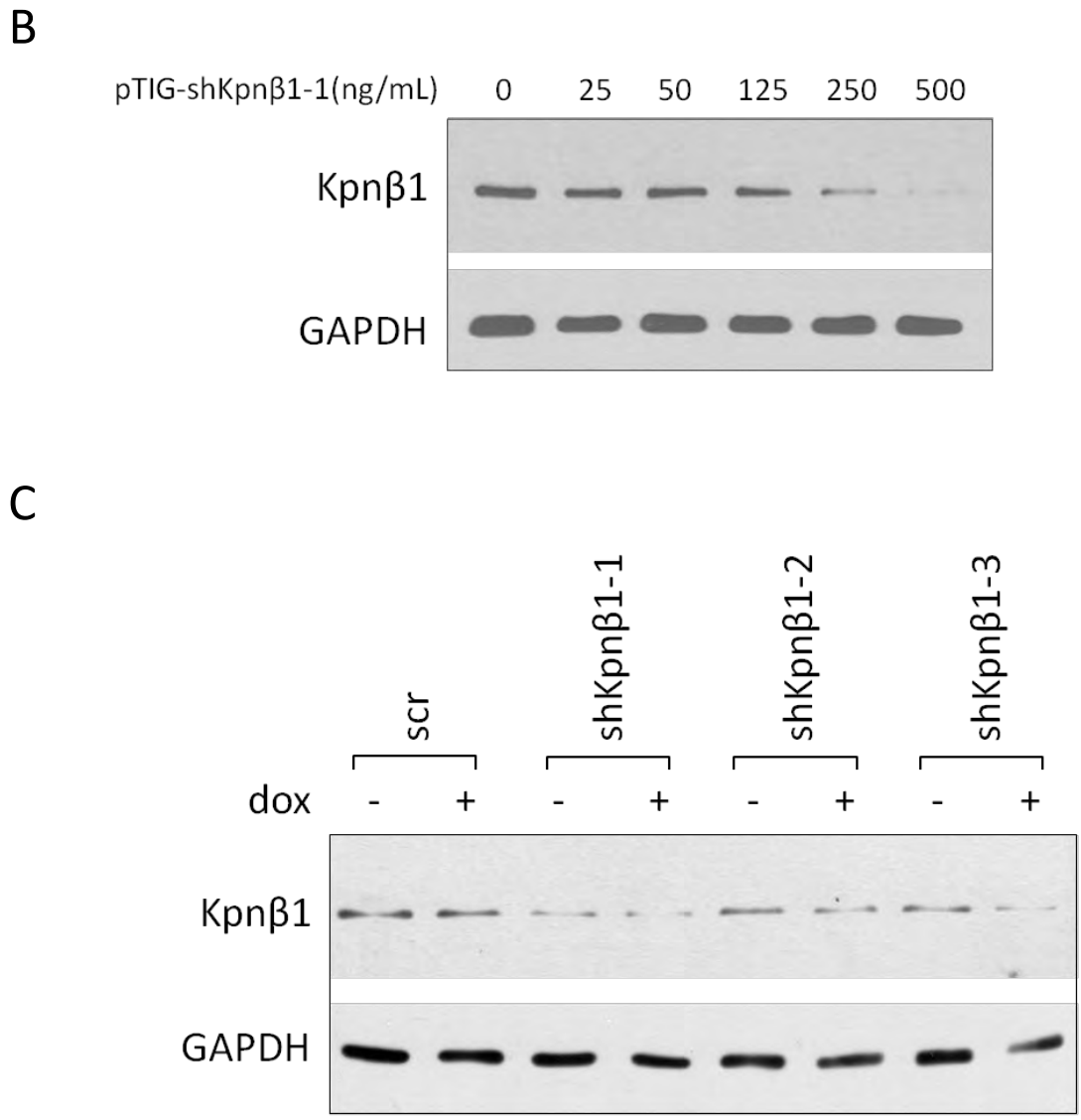

Figure 2.7. Transfection of HeLa cells with pTIG-shKpnβ1-1. HeLa cells were transfected with ranging concentrations of the pTIG-shKpnβ1-1 plasmid for 24 hours, followed by doxycycline (dox) induction at 1 ng/mL for 24 hours. The expression of GFP was examined using fluorescent microscopy as an indication of transfection efficiency (A). Kpnβ1 expression in pTIG-shKpnβ1-1 transfected cells (B), and Kpnβ1 expression in pTIG-scrambled, pTIG-shKpnβ1-1, pTIG-shKpnβ1-2 and pTIG-shKpnβ1-3 transfected cells with or without doxycycline induction (C). Results shown are representatives of experiments performed 3 independent times.

with doxycycline. Western blot analysis revealed that all three shKpnβ1s effectively down-regulated endogenous Kpnβ1 expression (Fig. 2.7.C). The inducible U6 promoter from which the shRNAs were expressed, however, appeared to be poorly regulated in HeLa cells, as Kpnβ1 levels were also reduced in the absence of doxycycline induction suggesting leakiness (Fig. 2.7.C). Various attempts

were made to reduce the U6 promoter leakiness, but were unsuccessful. For this reason, pTIG-scr transfected cells were used as a non-Kpnβ1 knock-down control.

2.2.4.2. shRNA-mediated Kpnβ1 knock-down reduced HeLa cell growth

Having shown that all the pTIG-shKpnβ1 constructs efficiently reduced Kpnβ1 expression, we next examined the effect of shRNA-mediated Kpnβ1 knock-down on cell proliferation in HeLa cells. Cells were transfected with pTIG-scr or pTIG-shKpnβ1 constructs for 24 hours, followed by 1 ng/mL doxycycline treatment to induce shRNA expression. Phase contrast images of the cells were captured 72 hours after doxycycline treatment, and results showed that cells transfected with pTIG-shKpnβ1-1, pTIG-shKpnβ1-2 and pTIG-shKpnβ1-3 all showed significant reduction in number of viable, adherent cells compared to the mock transfected control cells (Fig. 2.8.A). Quantification of the viable cells by MTT confirmed this, showing that in all Kpnβ1 knock-down cells, significant reduction in cell proliferation was observed in comparison to the control pTIG-scr transfected cells (Fig. 2.8.B). These results showed that shRNA-mediated Kpnβ1 inhibition resulted in similar inhibitory effects on cancer cell proliferation as observed with INI-43 treatment.

2.2.5. Kpnβ1 over-expressing HeLa cells exhibited increased tolerance to INI-43 treatment

INI-43 was initially identified as a potential inhibitor of Kpnβ1 based on *in silico* prediction of the known Kpnβ1 crystal structure. Furthermore, INI-43 showed inhibitory effects on both nuclear import and cancer cell proliferation[333], both of which were observed when Kpnβ1 was inhibited via RNAi[300]. In addition to this, Kpnβ1 over-expression reversed INI-43 induced inhibition on NFκB-p65 nuclear import, a known Kpnβ1 cargo[333], supporting that INI-43 acts via Kpnβ1 associated nuclear import. We therefore proposed that Kpnβ1 over-expression could rescue INI-43 induced inhibitory effect on HeLa cell viability. To examine this, a stable Kpnβ1 over-expressing cell line, HeLa-pEFIRES-

Kpnβ1-GFP which expresses Kpnβ1 tagged to GFP, and the control cell line HeLa-pEFIRES-GFP were used[333]. To confirm the expression of the appropriate proteins, western blot analysis was performed using both Kpnβ1 and GFP specific antibodies. HeLa-pEFIRES-Kpnβ1-GFP expressed Kpnβ1-GFP at similar levels to that of endogenous Kpnβ1 level, suggesting the presence of approximately twice as much Kpnβ1 as in the control cells (Fig. 2.9.A).

A

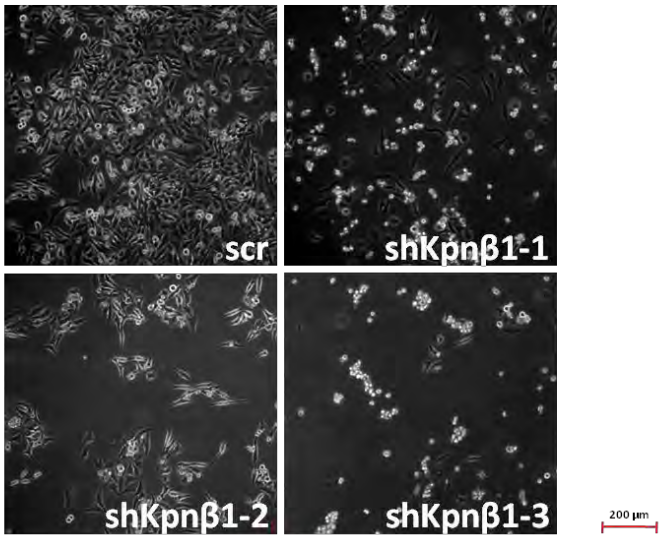

B

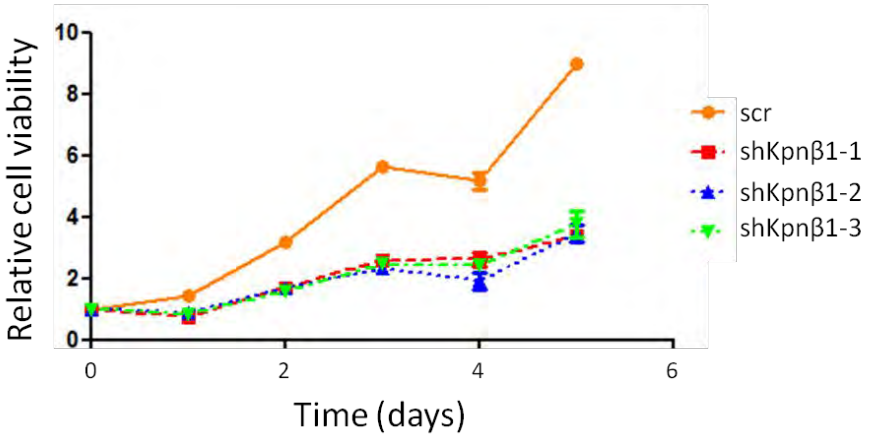

Figure 2.8. Proliferative activities in Kpnβ1 knock-down HeLa cells. HeLa cells were transfected with pTIG-scr, pTIG-shKpnβ1-1, pTIG-shKpnβ1-2 or pTIG-shKpnβ1-3, followed by 1 ng/mL doxycycline induction (day 0). Cells were photographed 72 hours after doxycycline induction (A), and cell proliferation was quantified every 24 hours for five days (B). Results shown are mean ± SEM of five replicates normalized to viable cells on day 0.

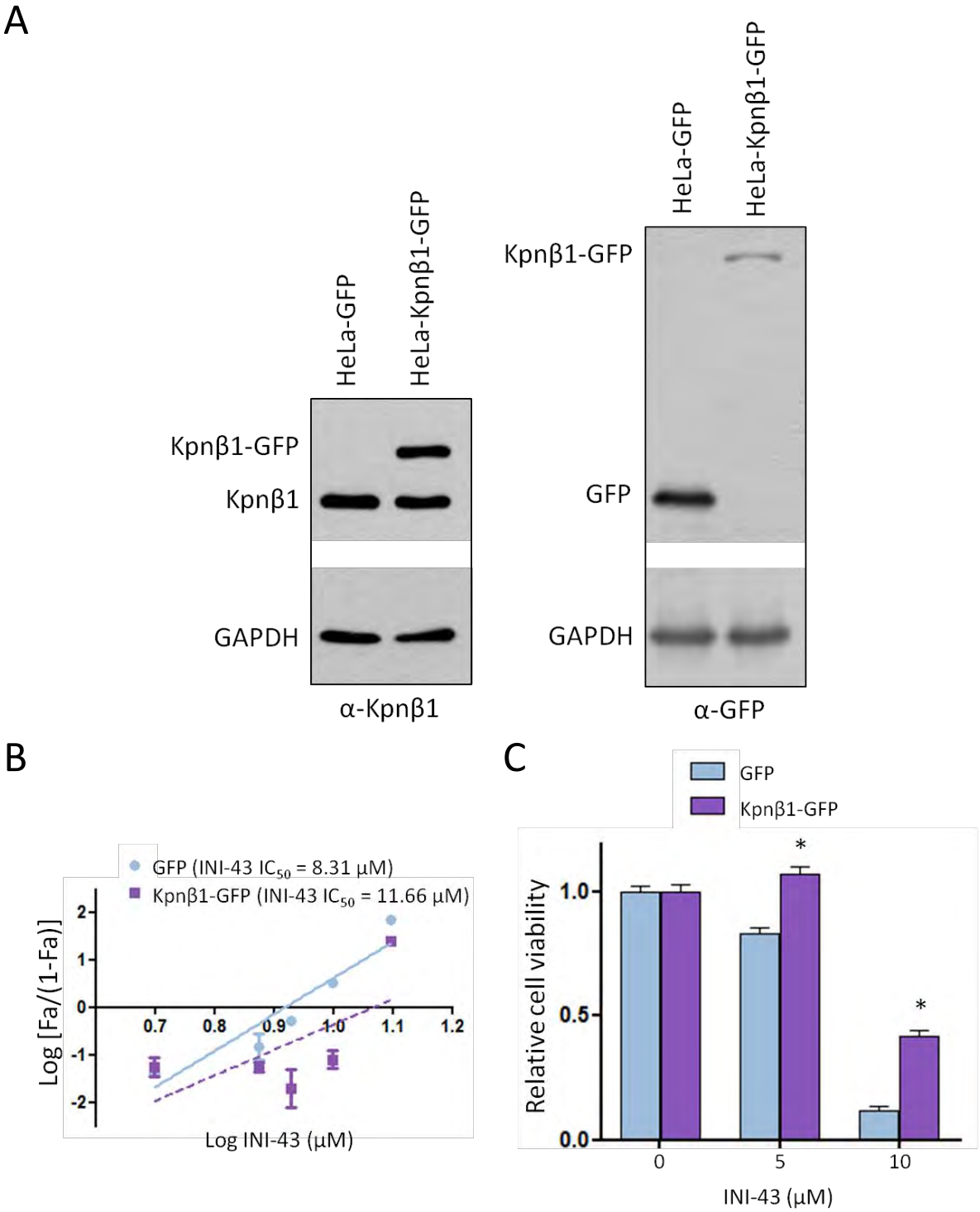

Figure 2.9. Kpnβ1 over-expressing HeLa cells showed decreased sensitivity to INI-43 treatment. Protein lysate from the HeLa-pEFIRES stable cell lines were examined via western blot to confirm the establishment of cells stably expressing GFP (HeLa-GFP) and Kpnβ1-GFP (HeLa-Kpnβ1-GFP). GAPDH was included as a loading control (A). INI-43 IC_{50} was examined for the GFP-expressing control and Kpnβ1-GFP over-expressing cells (B). The effect of INI-43 treatment on viability of HeLa-GFP and HeLa-Kpnβ1-GFP cells were examined, cells were seeded at 5000 per well in 96-well dishes followed by INI-43 treatment for 48 hours. Viable cells were determined using the MTT reagent, and OD_{595} readings were normalized to the untreated cells. Results shown are mean ± SEM of three independent experiments, with 6 replicates in each experiment, *$p < 0.05$.

Analysis showed that HeLa-pEFIRES-Kpnβ1-GFP exhibited significantly higher INI-43 IC_{50} value (11.7 μM) compared to the control cells (8.3 μM, Fig. 2.9.B), and that significantly more viable cells were observed in Kpnβ1 over-expressing cells compared to control cells after 5 μM and 10 μM INI-43 treatment (Fig. 2.9.C). These results showed that Kpnβ1 over-expression had a dampening effect on INI-43 induced cytotoxicity, thereby confirming that INI-43, at least in part, exerted its cancer killing effects by targeting Kpnβ1.

2.2.6. INI-43 causes cancer cell death via apoptosis

The mechanism of INI-43 induced cancer cell death was next investigated. We examined the cleavage of poly(ADP-ribose) polymerase (PARP), which is executed by caspase-3, a late event occurring in the apoptotic pathway. Cleavage of PARP into a 89 kDa product is an irreversible commitment to apoptosis, and is thus an accurate reflection of the apoptotic events[339]. Western blot analysis showed that INI-43 treatment caused PARP-cleavage both time and concentration dependently (Fig. 2.10.A). At both 1 x and 1.5 x INI-43 IC_{50} values, i.e. 10 μM and 15 μM, PARP-cleavage was already visible 3 hours after treatment. In the 10 μM treated cells, there was continual increase in cleaved PARP with the maximal cleaved PARP 24 hours after treatment. At 15 μM INI-43, GAPDH degradation was observed 12 hours after treatment, which became completely degraded by 24 hours after treatment, suggestive of global protein degradation which correlated with complete cell death observed. Treatment of HeLa cells with 1 x IC_{50} and 1.5 x IC_{50} concentrations of nuclear import inhibitors Importazole and Ivermectin similarly resulted in increased PARP-cleavage, but were only observed 24 hours after treatment for both drugs at their respective IC_{50} values (Fig. 2.10.B). These results showed that INI-43 induced apoptosis in cancer cells more rapidly than other known nuclear import inhibitors - where at their respective IC_{50} values, INI-43 induced PARP-cleavage within three hours, but Importazole and Ivermectin treatment only induced PARP cleavage after 24 hours.

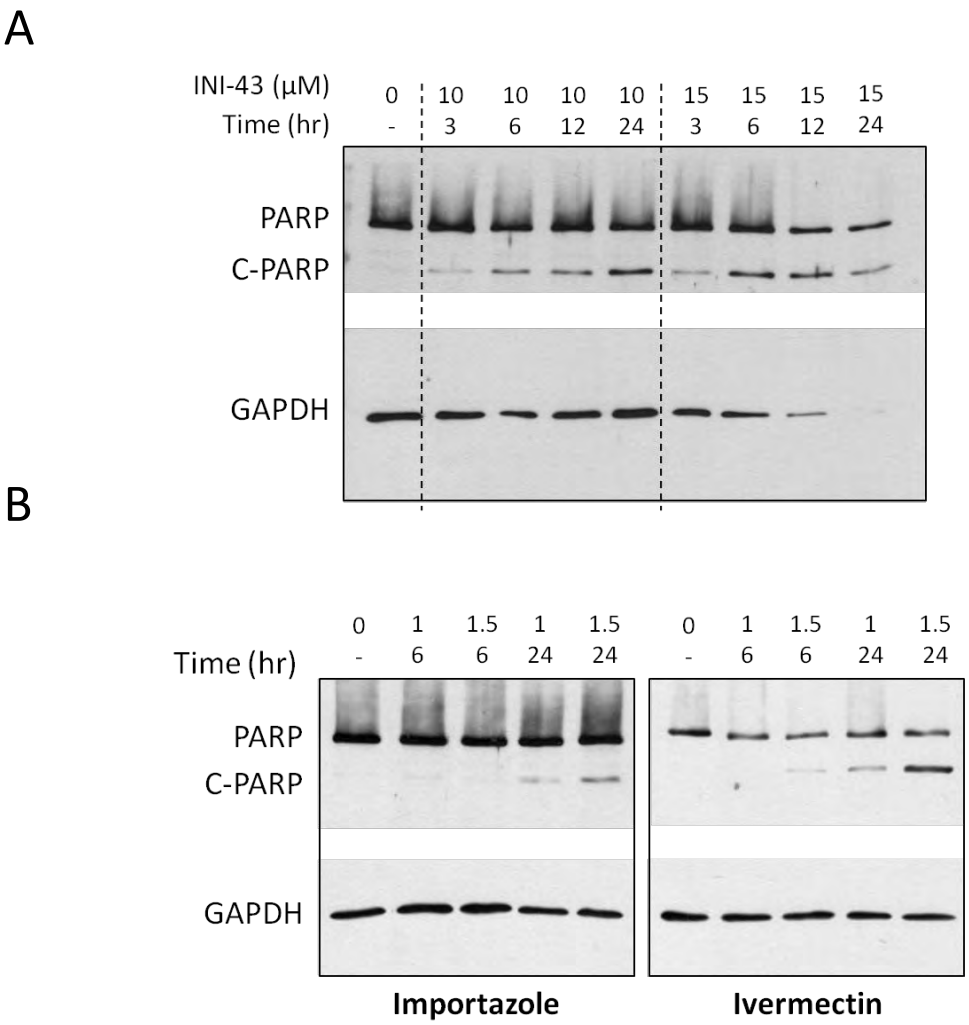

Figure 2.10. Cleavage of PARP in HeLa cells treated with nuclear import inhibitors. HeLa cells were treated with INI-43 at its 1 x and 1.5 x IC_{50} values and proteins were harvested 3, 6, 12 and 24 hours after treatment. PARP status was analyzed by western blot (A). The effect of two additional nuclear import inhibitors, Importazole and Ivermectin on PARP cleavage were also examined at 1 x and 1.5 x their respective IC_{50} 6 and 24 hours after treatment (B). GAPDH were included for loading control. PARP-cleavage analysis using INI-43 in HeLa cells was conducted two independent times.

To determine whether INI-43 induced apoptosis was associated with the intrinsic mitochondrial pathway, the mitochondrial content of cytochrome C was examined, as cyctochrome C release from the mitochondria is an event preceding PARP cleavage in the intrinsic apoptotic pathway. Corresponding to the PARP-cleavage event, decreased mitochondrial cytochrome C was observed in HeLa cells after 10 μM INI-43 treatment time-dependently (Fig. 2.11.A). A subtle decrease of

cytochrome C was observed 3 hours after INI-43 treatment, which continued to decrease with increasing time of drug incubation, and the lowest mitochondrial cytochrome C was observed 24 hours after INI-43 treatment (Fig. 2.11.A and B). These results support the idea that INI-43 treatment induced apoptotic events in cancer cells via activating the intrinsic mitochondrial pathway, leading to mitochondrial release of cytochrome C and the subsequent cleavage of PARP.

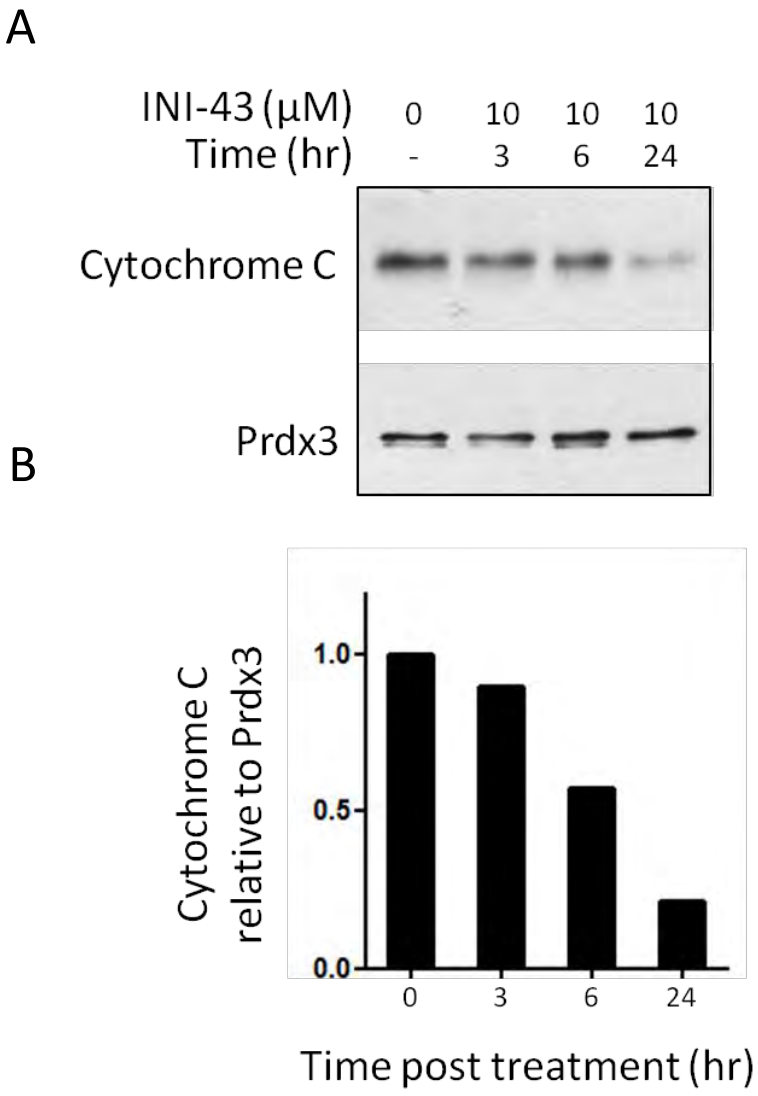

Figure 2.11. Mitochondrial levels of cytochrome C in HeLa cells treated with INI-43. HeLa cells were treated with 10 µM INI-43, and mitochondrial cytochrome C was examined 3, 6 and 24 hours after treatment with western blot. Peroxiredoxin-3 (Prdx3) was included as the mitochondrial loading control (A). cytochrome C levels were densitometrically quantified relative to Prdx3 (B). Results shown are representative of two independent experiments.

2.2.7. Investigating drug properties of INI-43 for further use in animal studies

Whilst commercially available nuclear import inhibitors such as Importazole and Ivermectin have been widely used in biological assays to investigate the functional relevance of nuclear import, little work has been done to investigate their anti-cancer properties, and intensive examination in animal models is still lacking. We thus examined the stability of INI-43, and focussed more extensively on the drug toxicity in an animal model system.

2.2.7.1. INI-43 exhibited moderate stability in liver microsome assays

Metabolically unstable drugs are rapidly degraded upon administration into the living system, thereby not allowing enough time for candidate drugs to reach the target site. For this reason, we first examined the metabolic stability of INI-43 by performing the liver microsome assay. The liver microsome assay is an *in vitro* assay used to predict possible break-down products of the compound of interest, as well as examining the stability of the parent compound in the presence of metabolizing enzymes from the liver. The concept behind this experiment it to incubate the compound of interest with enzymes isolated from the hepatocytes, as the liver is largely responsible for drug metabolism in the living system. Liver microsomes are processed liver tissues to remove other cellular components, leaving behind the concentrated liver enzymes. It consists mostly of vesicle-like artefacts formed from the endoplasmic reticulum where the most active enzymes are found, and is prepared by homogenizing liver tissues followed by differential centrifugation thereby separating the cell membrane, cytoplasm and organelles. An advantage of removing cell membranes is that the active enzymes are readily exposed to the compound of interest upon addition, allowing the reaction incubation time to be significantly reduced, as the compound of interest is not required to cross the cell membrane. To ensure that INI-43 exhibits sufficient stability for animal testing, liver microsome was first carried out to assess its metabolic stability.

INI-43 was incubated with liver microsomes under the appropriate physiological conditions, and the resulting samples were subjected to HPLC-MS/MS to determine the percentage of un-metabolized, intact INI-43 remaining. The percentage remaining was then used to calculate its half-life ($T_{1/2}$) which is tabulated in Table 2.2. Two additional compounds with known stabilities, Midazolam and Propranolol were included as the controls, and gave values within their acceptable ranges. As shown in Table 2.2, 88% of the parental INI-43 compound remained intact after 30 minutes incubation period, projecting to a half-life of 161.2 minutes in human liver microsomes. It exhibited decreased stability in mouse microsome, with 59% parental compound remaining after incubation, and the half-life was calculated to be 39.4 minutes. In both human and mouse liver microsomes, INI-43 showed greater stability than Propranolol, which is considered to be a moderately stable compound, suggesting that INI-43 is sufficiently stable for use in preclinical studies.

Table 2.2. Microsomal turnover of INI-43

Drug	% remaining		Half-life (minutes)	
	Human	**Mouse**	**Human**	**Mouse**
INI-43	87.90	59.00	161.23	39.41
Midazolam	0.77	1.53	5.12	4.96
Propranolol	62.00	5.33	43.80	7.09

Data presented are the mean of triplicate (for % remaining) and the half-life was calculated based on the average % remaining values (see Materials and Methods, section .6.2.12).

2.2.7.2. Assessing INI-43 cytotoxicity in athymic nude mice

In *in vitro* studies, the efficacy of INI-43 is examined by addition of drug directly to cells, which does not take into account the possible interactions between INI-43 and other cells *in vivo*. These interactions may lead to toxic side effects, which can sometimes be fatal. Indeed, toxicity has been reported to be one of the major reasons for failure of developing drugs to reach the market, as well as withdrawal of drugs already on the market[340]. For this reason, possible undesired side effects should be carefully and extensively scrutinized. Here, we examined the possible side-effects by performing toxicology analysis, where mice receiving a dose of INI-43 were compared to the vehicle DMSO receiving control mice. Drugs were administered intraperitoneally (i.p.) every second day for a period of 28 days (14 treatments in total, Fig. 2.12.A), during which the mice's body mass and behaviour was monitored daily as an indication of the animals' wellbeing. The experiment began with 1 mg/kg INI-43 treatment (low dose), and the control mice were treated with equivalent volumes of DMSO. Throughout the entire experiment, no signs of distress or abnormal behaviour were observed with the animals, and body mass fluctuations between the two groups of mice were similar (Fig. 2.12.B). No significant difference in body mass gain between control and 1 mg/kg INI-43 receiving mice were observed (20% versus 15%, Fig. 2.12.E). Similarly, control and 10 mg/kg INI-43 (intermediate dose) treated mice showed no significant differences in body mass changes, with approximately 22% and 24% gain in body mass at the end of the study for the control and treated mice, respectively (Fig. 2.12.C and E). Lastly, we also examined adverse effects at 50 mg/kg INI-43 (high dose). While the INI-43 treated mice showed no signs of discomfort or sickness, a decrease was observed in body mass gain compared to the controls (22% in INI-43 treated mice versus 39% in control mice, Fig. 2.12.D and E), although the difference was not statistically significant. The treated mice in this group, however, gained body mass which was within acceptable range, and the difference observed between the control and treated mice was likely attributed to the control mice gaining more weight than usual.

A

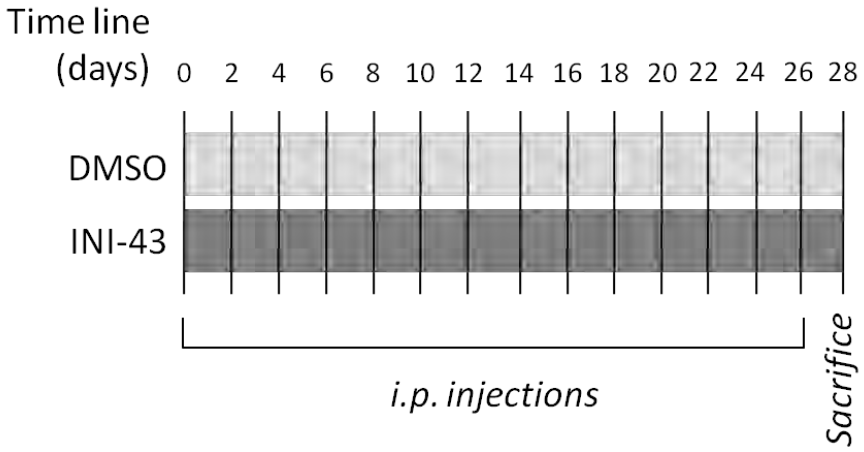
Time line
(days)
0 2 4 6 8 10 12 14 16 18 20 22 24 26 28
DMSO
INI-43
i.p. injections
Sacrifice

B

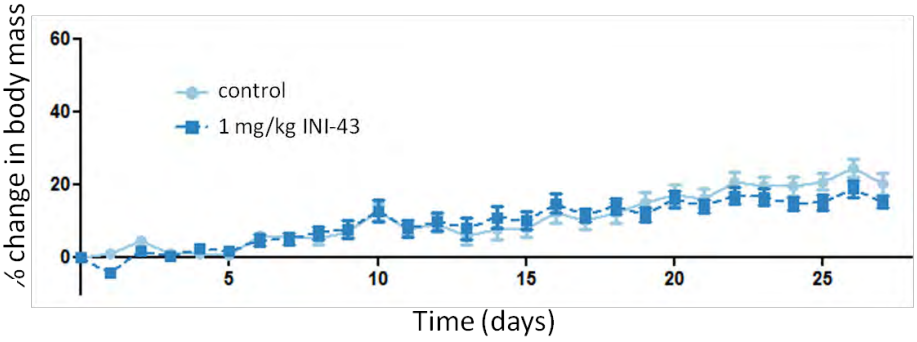
% change in body mass
60
40
20
0
control
1 mg/kg INI-43
5
10
15
20
25
Time (days)

C

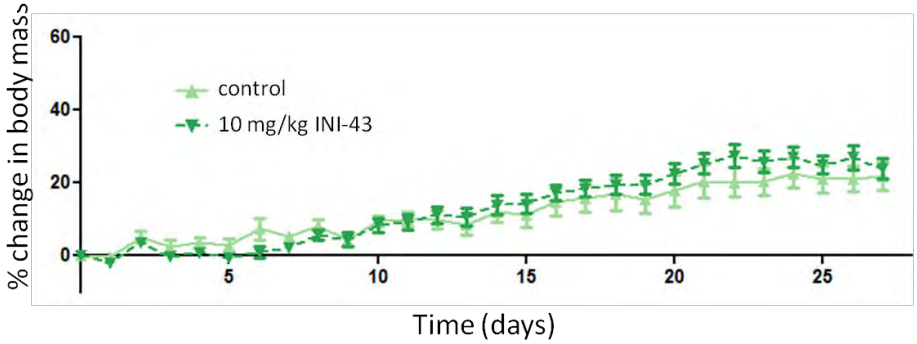
% change in body mass
60
40
20
0
control
10 mg/kg INI-43
5
10
15
20
25
Time (days)

D

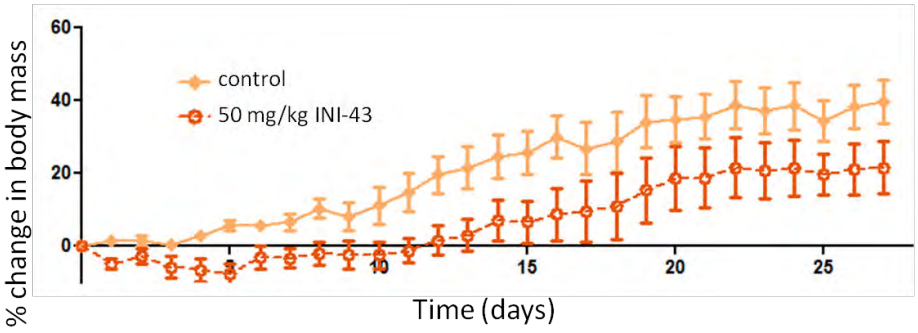
% change in body mass
60
40
20
0
control
50 mg/kg INI-43
10
15
20
25
Time (days)

E

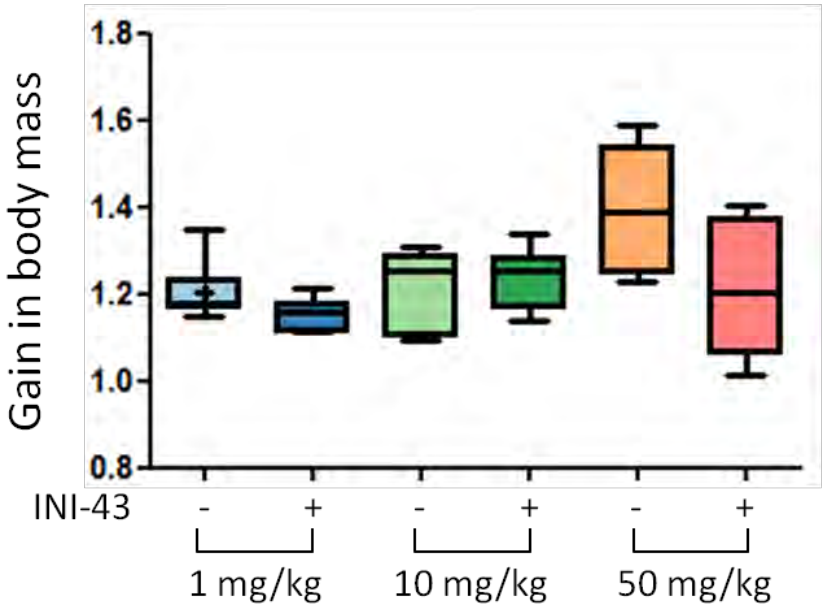

Figure 2.12. Toxicology analysis of INI-43. The toxicology study was carried out in three sequential stages, starting with 1 mg/kg, followed by 10 mg/kg and 50 mg/kg. All three experiments were executed in identical format (A). Body mass were measured on the day treatment started, and everyday thereafter. Body mass was calculated as percentage increase from the initial measurement for 1 mg/kg (B), 10 mg/kg (C) and 50 mg/kg (D). Results shown are mean ± SEM for six mice in each group. The gain in body mass at the end of the study are presented in a Box-and-Whiskers plot showing median, minimum and maximum values, N = 6 (E).

Post mortem evaluation of the INI-43 treated mice by an animal technician concluded no abnormalities in the lung, spleen, ovaries, kidneys, liver and heart. As enlargement of the liver has been reported to be a sign of toxicity[341], the liver mass were measured from the control and INI-43 treated mice for all dose groups, and expressed relative to their body mass, which showed no significant difference at all three INI-43 doses examined (Fig. 2.13). In addition, histological evaluations of liver sections showed no pathology within the parenchyma, no lesions were observed and morphological assessment were consistent with normal architecture of the murine liver. These results demonstrated that nude mice tolerated INI-43 up to, but not necessarily restricted to 50 mg/kg. For this reason, 50 mg/kg INI-43 were used in the subsequent tumourigenesis assays.

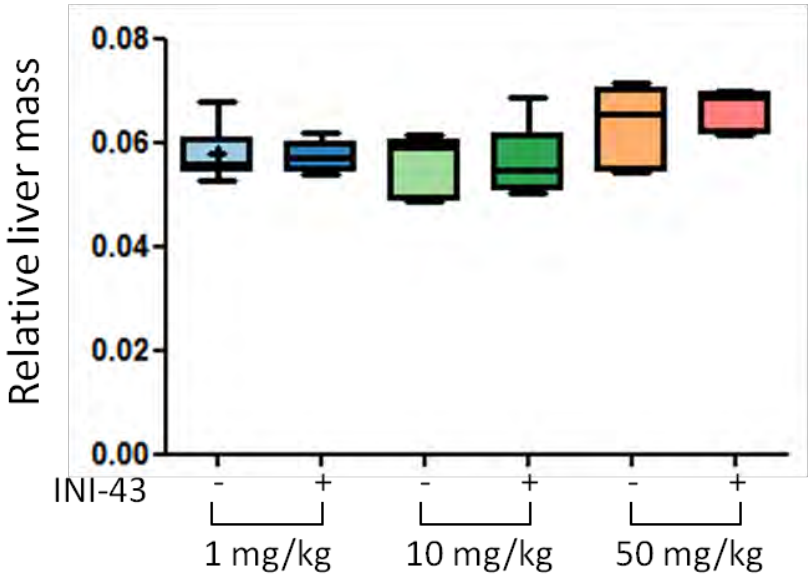

Figure 2.13. Liver size at the end of the toxicology study. The mice's liver mass at the end of each toxicology study was measured and normalized to each mouse's body mass for the 1 mg/kg group, 10 mg/kg group and 50 mg/kg group. Results are presented in Box-and-Whisker plots showing the median, minimum and maximum values in each group of mice, N = 6.

2.2.8.The effect of INI-43 treatment on induced tumour growth in nude mice

In order to determine the effect of INI-43 on tumour development *in vivo*, we employed the ectopic xenograft mouse model, where cancer cells of the human origin were injected subcutaneously into nude mice.

2.2.8.1. Pilot study to determine the optimal number of cells to inoculate for tumour induction

A pilot study was carried out to determine the optimal number of cells to inoculate in order to induce tumour formation. As our initial attempt of subcutaneous injection of 1 million HeLa cells failed to induce tumour formation, we investigated the injection of 5, 7.5 and 10 million cancer cells. Nine mice were used for each cell line (HeLa, CaSki, WHCO6 and KYSE30), which was divided into

three groups of 3 mice each, and each group received the same number of cells at inoculation. To minimize the suffering of the animals, they were euthanized upon tumour size reaching 20 mm in any dimension, observation of severe necrosis in the tumour tissue, or observation of distress in the animals, whichever occurred first. The endpoint of the study was marked by the euthanization of the last mouse for each cell line.

Tumour induction using HeLa cells were unsuccessful at all cell numbers tested (data not shown). The other cervical cancer cell line, CaSki, started forming visible tumours around 80 days after inoculation of 5 million cells (Fig. 2.14.A, top). All three animals formed tumours and grew uniformly, and was only euthanized at the study endpoint of the study as the tumours did not exceed 20 mm in any dimension, and only one tumour developed necrosis. Mice inoculated with 7.5 million CaSki cells exhibited major inconsistency in tumour formation and development. Of the three mice inoculated, one mouse did not develop any visible tumour by the study endpoint, which was 110 days after inoculation, and the other two mice formed visible tumours approximately 25 days after inoculation (Fig. 2.14.A, middle). Of those two that formed tumours, the tumours grew at very different rates - while one mouse developed a tumour of 1360mm^3 by day 84 and had to be euthanized prematurely, the other mouse formed a tumour of only 163.09mm^3 by the study endpoint. Interestingly, none of the mice inoculated with 10 million CaSki cells formed any visible tumours (Fig. 2.14.A, bottom), suggesting that inoculation of more cells does not necessarily result in faster tumour growth. Based on these observations, 5 million cells was selected for the actual tumourigenesis assay.

WHCO6 cells developed tumours more uniformly with all inoculations leading to tumour formation (Fig. 2.14.B). All tumours were visible within one week after treatment, and tumours grew more rapidly in mice inoculated with 7.5 million and 10 million cells. In both groups, all animals were euthanized on or before day 35 (Fig. 2.14.B, middle and bottom). Mice inoculated with 5 million cells

showed slower tumour growth, and were euthanized 46, 49 and 76 days after inoculation (Fig. 2.14.B, top).

Inoculation of KYSE30 cells led to tumour formation in all but one mouse (Fig. 2.14.C). Of the three mice inoculated with 5 million KYSE30 cells, two successfully formed tumours and were euthanized on days 39 and 46 due to necrosis, and one mouse never developed a visible tumour by the end of the study, which was 79 days after inoculation (Fig. 2.14.C, top). Inoculation of 7.5 million and 10 million KYSE30 cells developed visible tumours within one week, and were all euthanized prematurely due to either large tumour size or necrotic development (Fig. 2.14.C, middle and bottom). As mice inoculated with 7.5 million and 10 million cells showed extremely aggressive growth with high necrotic occurrence (4 out of 6), 5 million cells were selected for inoculation of the tumourigenesis assay.

Interestingly, the tumours formed from the three different cell lines showed different characteristics. CaSki cells developed tumours that were softer, and two out of the five tumours showed signs of necrosis (Fig. 2.15, (i, arrow). WHCO6 cells induced tumours were firm, but instead of forming one round tumour like CaSki, WHCO6 cells tend to form irregularly shaped, fractured tumours with no necrotic signs (Fig. 2.15, (ii)). KYSE30 tumours were larger, firmer, showed a blister-like appearance, and four of eight tumours developed necrosis (Fig. 2.15, (iii) and (iv, arrow)). The necrotic occurrence in tumour tissues is an indication of aggressiveness and often associated with metastatic potentials[342]. The use of these three cell lines in tumourigenesis assays provided an opportunity for the effect of INI-43 to be tested against tumours of different aggressiveness.

A

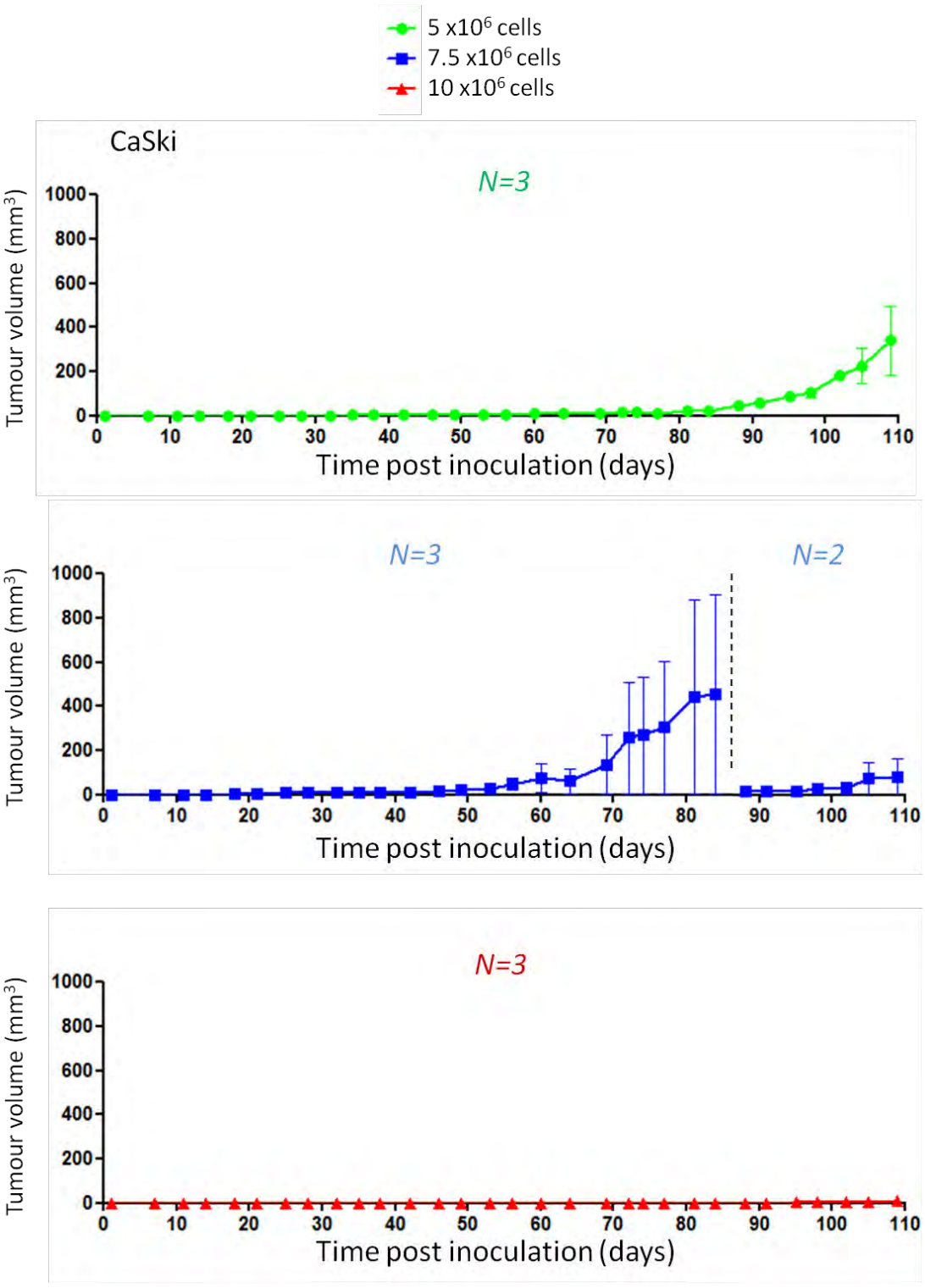
5 x10^6 cells
7.5 x10^6 cells
10 x10^6 cells
CaSki
N=3
Tumour volume (mm3)
Time post inoculation (days)
N=3
N=2
Tumour volume (mm3)
Time post inoculation (days)
N=3
Tumour volume (mm3)
Time post inoculation (days)

B

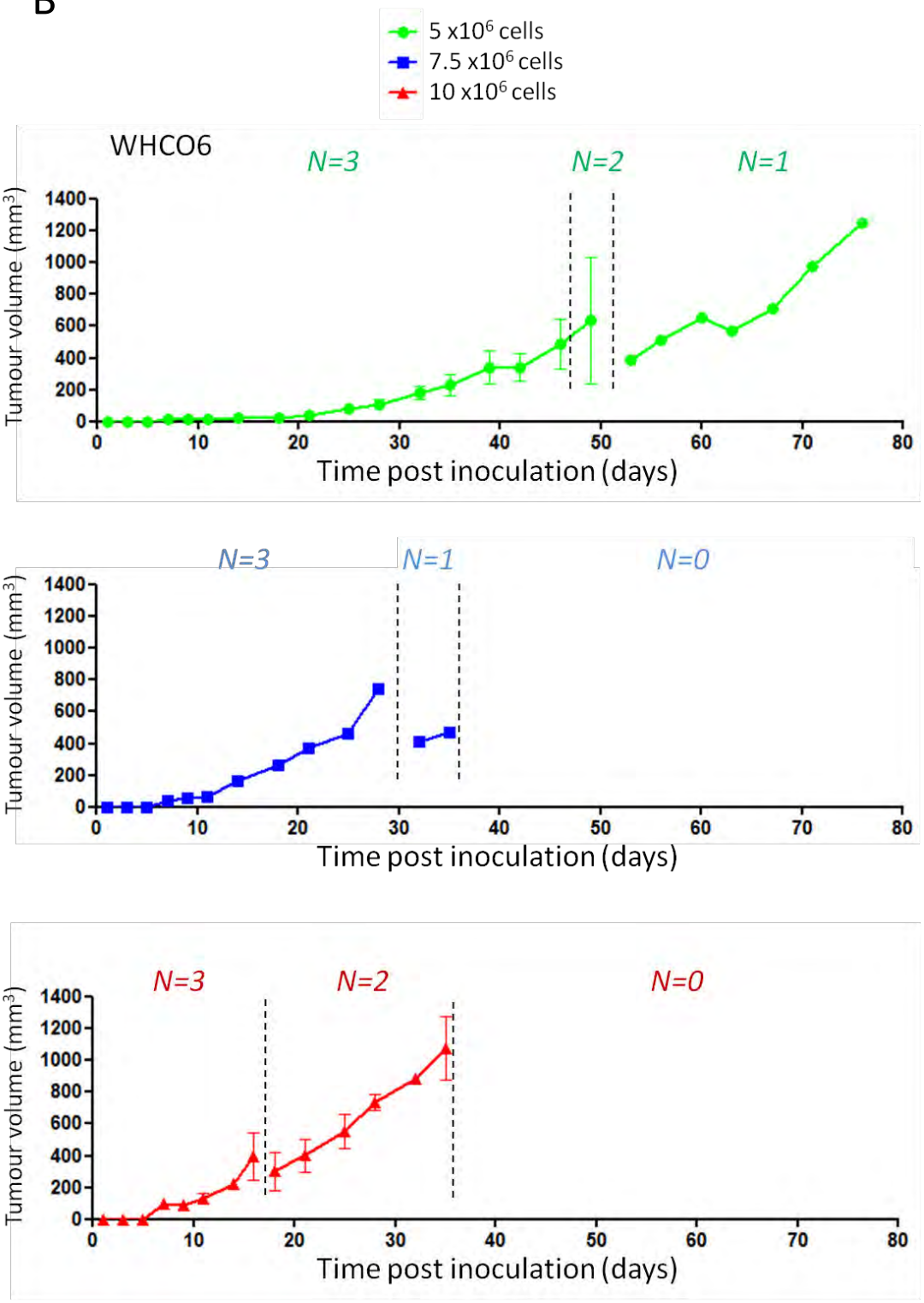
5 x10^6 cells
7.5 x10^6 cells
10 x10^6 cells
WHCO6
N=3
N=2
N=1
Tumour volume (mm3)
Time post inoculation (days)
N=3
N=1
N=0
Tumour volume (mm3)
Time post inoculation (days)
N=3
N=2
N=0
Tumour volume (mm3)
Time post inoculation (days)

C

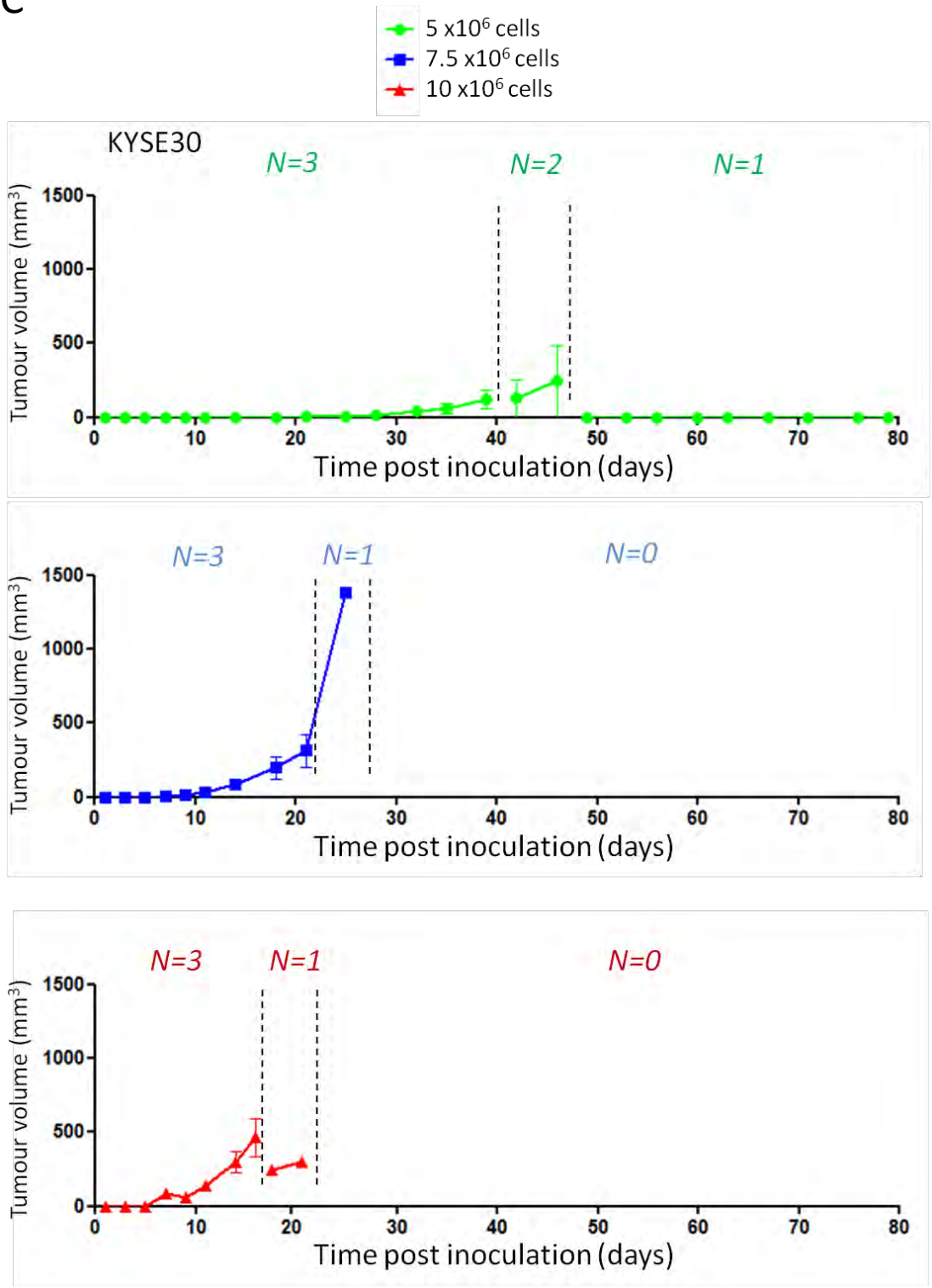

Figure 2.14. Tumour growth rates in nude mice inoculated with cancer cells. Nine mice were randomized into three groups of three each, and subcutaneously inoculated with 5 million (top), 7.5 million (middle) and 10 million (bottom) CaSki (A), WHCO6 (B) and KYSE30 (C) cells on day 0. The length (L) and width (W) of tumours were measured twice a week, and converted to tumour volume by the formula $V = (LxW^2)/2$. Results shown are mean ± SEM of N, where N = the number of animals alive at each time point.

Figure 2.15. Tumours formed from the different cancer cell lines. Tumour growth induced with CaSki, WHCO6 and KYSE30 were photographed after euthanization. (i) CaSki tumour formed 110 days after inoculation with 5 million cells, (ii) WHCO6 tumour formed 16 days after inoculation with 10 million cells, (iii) KYSE30 tumour formed 28 days after inoculation with 7.5 million cells, and (iv) KYSE30 tumour formed 23 days after inoculation with 10 million cells. Arrows indicates observation of visible signs of necrosis in the tumour.

2.2.8.2. Tumourigenesis assay in nude mice: Effect of INI-43 on tumour development

Having established the cell numbers required for xenograft tumour formation in nude mice, we next examined the effect of intraperitoneally administered INI-43 on tumour development, using CaSki, KYSE30 and WHCO6 cells. Mice were inoculated with 5 million cancer cells, and treated with DMSO or INI-43 upon palpable tumour formation. As the different cell lines formed tumours at different rates, the day which treatment began was marked as day 0 in each experiment. Mice were treated three times a week (CaSki and KYSE30, Fig. 2.16.A and 2.16.C) or every second or third day (WHCO6, Fig. 2.16.B), and tumour sizes were measured twice a week for 4 weeks in CaSki-tumour bearing mice, 3 weeks for WHCO6-tumour bearing mice and 2.5 weeks for KYSE30-tumour bearing mice.

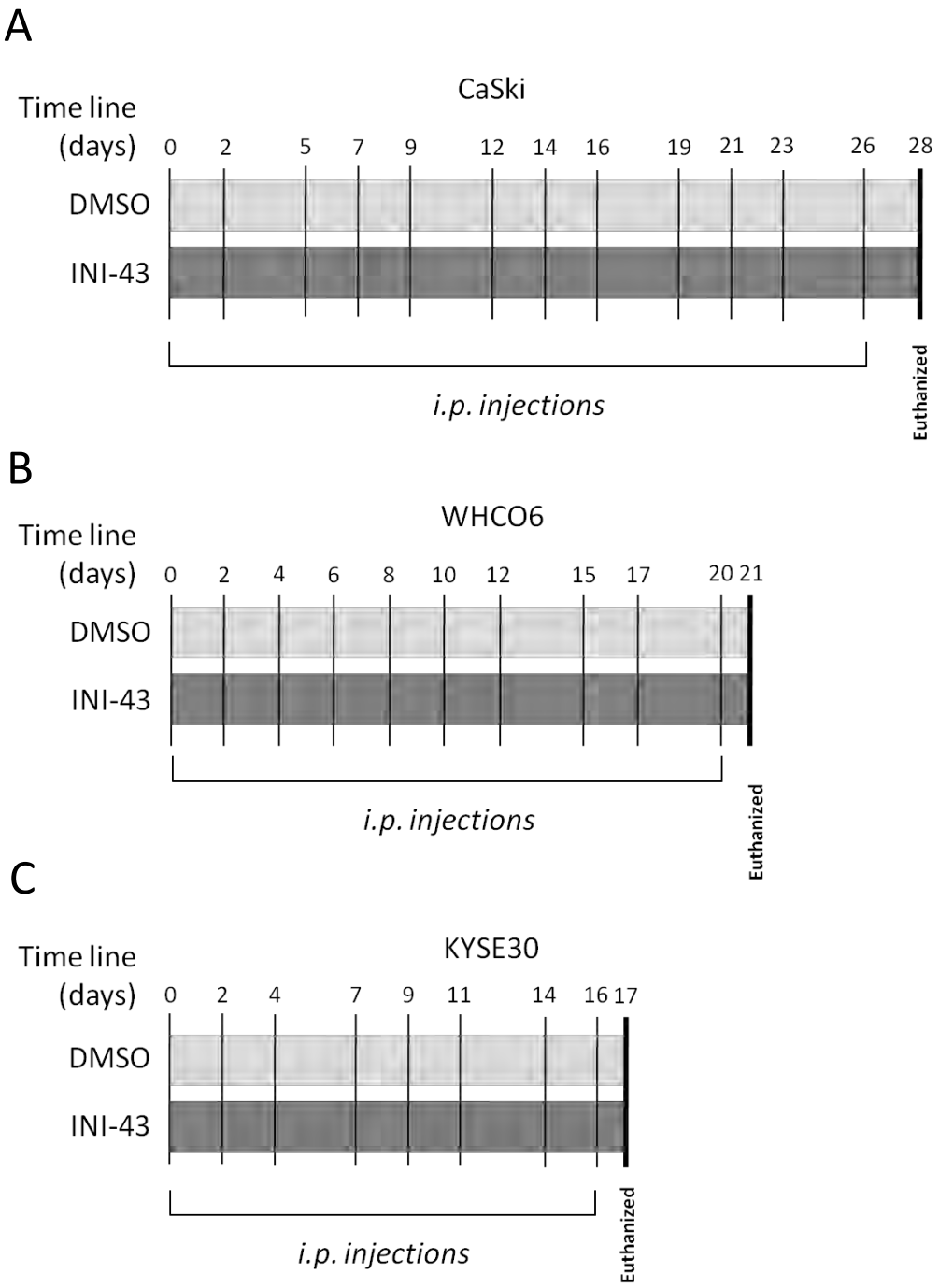

Figure 2.16. Timelines showing treatment protocols for the tumourigenesis assays. Five million cancer cells were subcutaneously inoculated in nude mice for CaSki (A), WHCO6 (B) and KYSE30 (C). Upon palpable tumour formation, mice were randomized into the DMSO control group and INI-43 test group (N = 6), followed by treatment as indicated from day 0. Treatments were administered via intraperitoneal (i.p.) injections, and the animals were euthanized at the study endpoint.

Continual observation and measurements of the tumour sizes revealed that INI-43 treated mice showed a decreasing trend in tumour growth rate when compared to the DMSO-treated control group for all three cell lines (Fig. 2.17). Moreover, the difference reached significance for CaSki and WHCO6 tumours (Fig. 2.17.A and B). A decrease in KYSE30 tumours was observed (Fig. 2.17.C), the difference was however, not significant. The fold change in tumour volume between day 0 and the last day showed a significant difference for both CaSki and WHCO6 tumours (Fig. 2.18.A). In mice bearing CaSki tumours, the control mice showed a 4.9-fold increase in tumour volume while INI-43 treatment group showed only 2.3-fold increase. Similarly for the WHCO6 tumours, 5.7-fold increase and 1.9-fold increase in tumour volumes were observed for control and INI-43 treated mice, respectively. In addition, comparison of tumour mass at the end point also showed decreased tumour mass in all INI-43 treated mice compared to DMSO treated mice in all three cell lines (Fig. 2.18.B). In the course of the experiment performed with WHCO6 cells, one mouse was euthanized prematurely due to unexpected illness before day 21 excluding it from the last day's measurements. For this reason, measurements on day 21 were excluded from the data, making day 18 the endpoint for this experiment. Taken together, these results suggest that INI-43 significantly reduced CaSki and WHCO6 cancer cell growth *in vivo*, but had less effects on tumour size of highly aggressive KYSE30 cancer cells.

In addition to reducing tumour growth, INI-43 treated mice also showed less frequent necrotic development in tumour tissues compared to the control mice (Fig. 2.19). Necrotic tissues can vary in appearance depending on its severity. Mild necrosis manifests a doughnut-shaped tumour, where a collapse in the tumour centre is observed. More severe necrosis is characterized by darkened and liquefied tissue at the tumour centre, and in some extreme cases, destruction of tumour tissues is visible. As previously shown, both CaSki and KYSE30 tumours showed necrotic potentials (Fig. 2.19, A and C). In CaSki cells, the onset of necrosis was observed as early as 10 days into treatment for the control mice, while the first necrotic signs in INI-43 treated mice were only observed on day 19. At

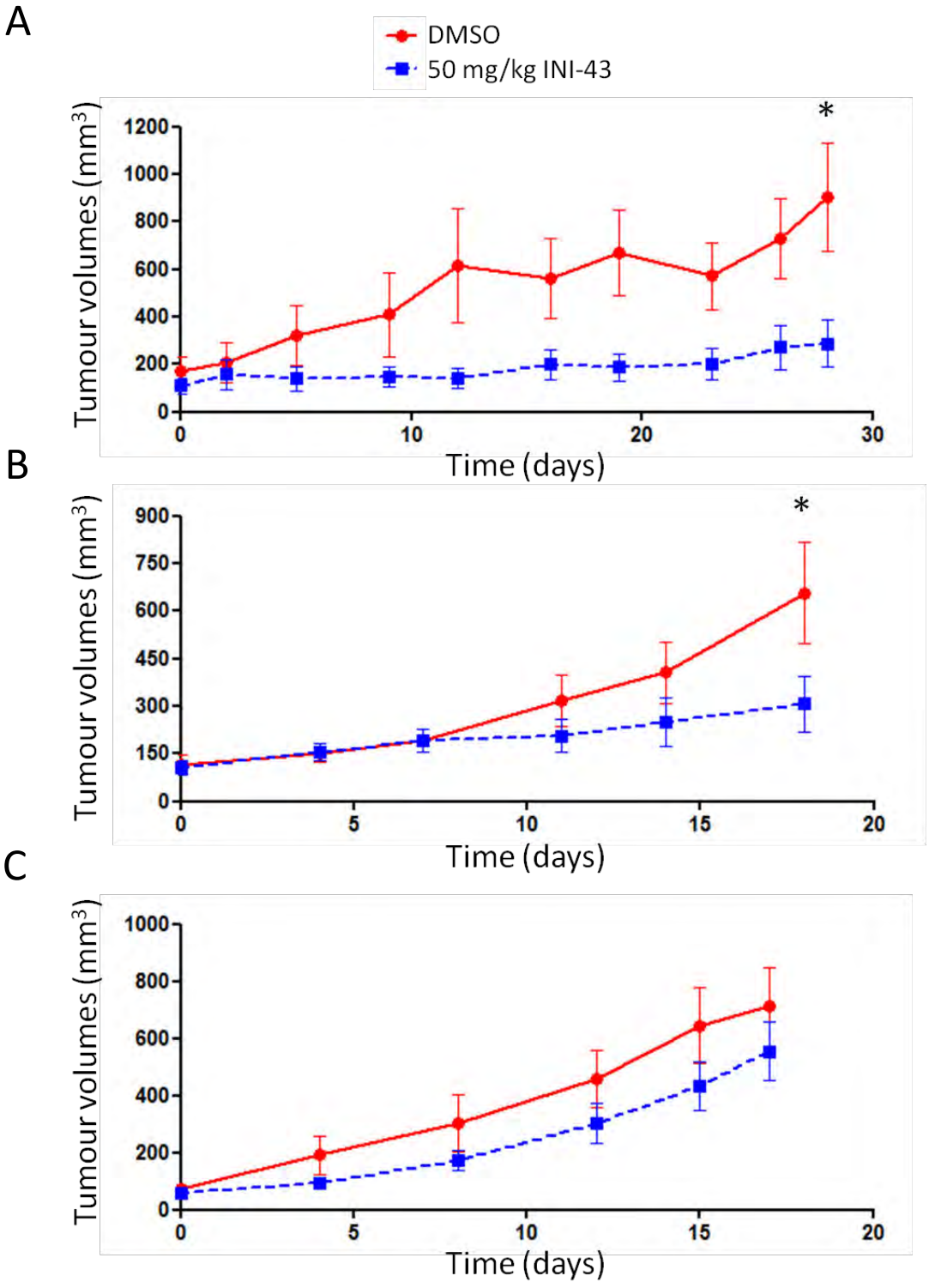

Figure 2.17. The effect of INI-43 treatment on xenografted tumour growth in nude mice. Tumour development for control (DMSO) and INI-43 treated mice bearing CaSki (A), WHCO6 (B) and KYSE30 (C) tumours. Results shown are mean ± SEM for 6 mice in each group, *$p < 0.05$.

the experimental endpoint, necrotic tumours were observed in four out of six control mice, including one severe, two moderate and one mild necrosis. On the other hand, INI-43 treated mice showed only two out of six necrotic tumours, and one was only observed on the last day of the study (Fig. 2.19.A, asterisk marks). Paralleling this, KYSE30 tumours had four out of six necrotic tumours in the control group, and two out of six in the INI-43 treated group (Fig. 2.19.C, asterisk marks). WHCO6 tumours did not show any obvious signs of necrosis in both control and INI-43 treated groups (Fig. 2.19.B).

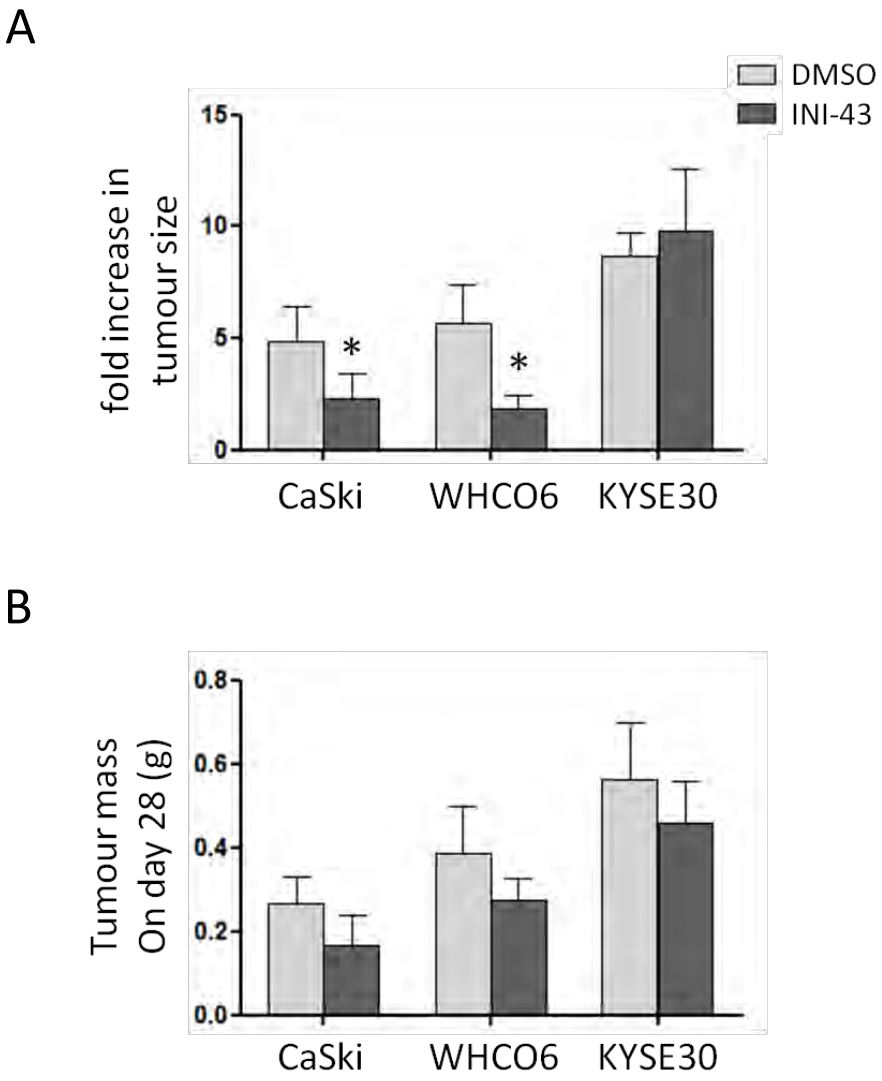

Figure 2.18. Analysis of tumour size at the end of the treatment schedule. The fold increase in tumour size at the end of the study relative to the starting tumour size (A), and the tumour mass at the end of the study for all groups of mice (B). Results shown are mean ± SEM for 6 mice in each group, *$p < 0.05$.

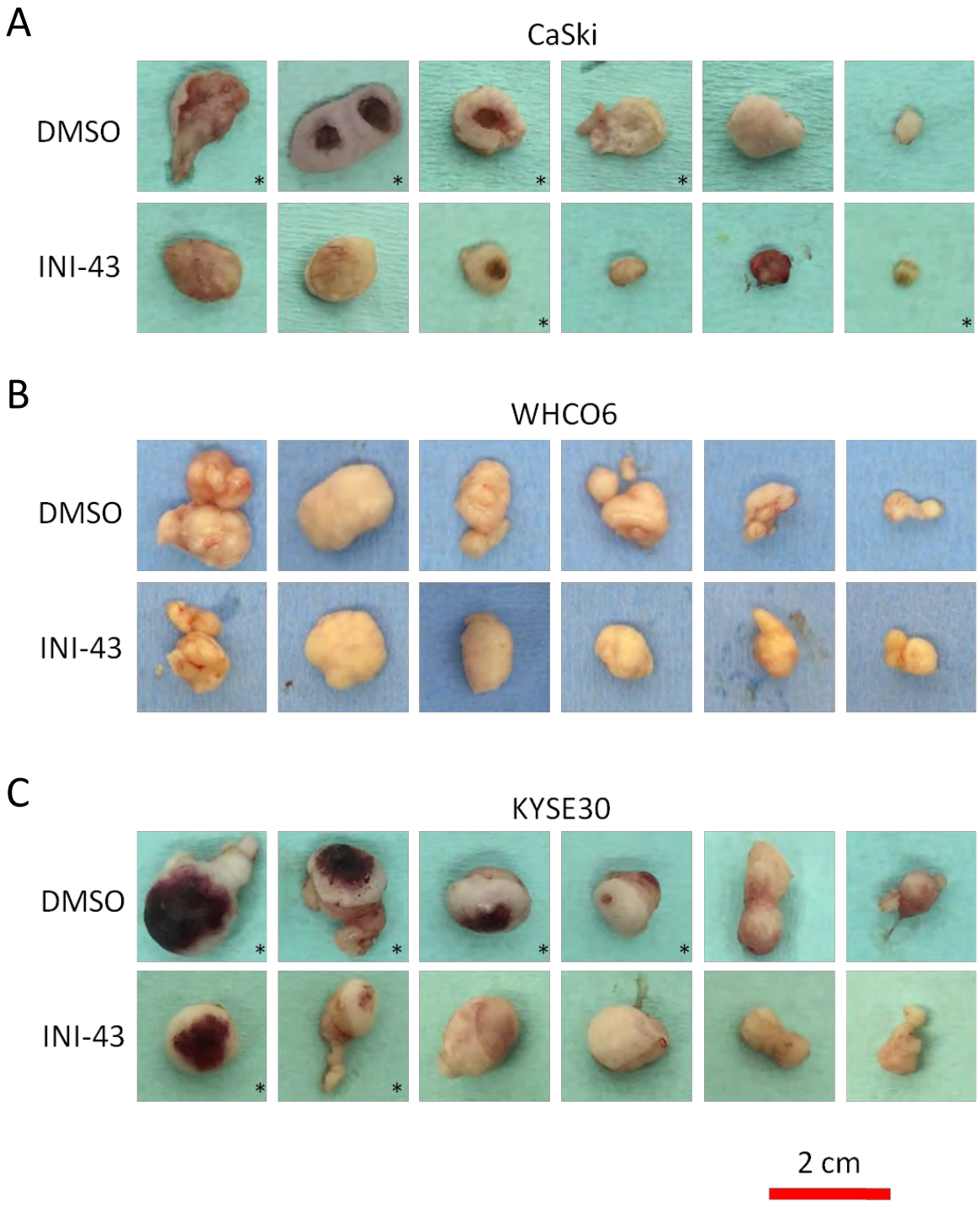

Figure 2.19. Tumours at the end of the tumourigenesis assay. At the endpoint of the tumourigenesis assay the mice were euthanized and tumours were dissected out. Tumours from both DMSO and INI-43 treated groups were photographed for CaSki (A), WHCO6 (B) and KYSE30 (C) tumours. Asterisk marks indicates observation of necrosis in the tumour mass.

The change in mice body mass and behaviour were monitored daily alongside to ensure that minimal distress was experienced by the animals (Fig. 2.20). No abnormalities were observed in behaviour of mice in both DMSO control and INI-43 treated groups, and similar fluctuation of body mass which is likely a result of intraperitoneal injections were observed in both groups of mice, confirming that INI-43 treatment at 50 mg/kg does not appear to compromise the animals' wellbeing (Fig. 2.20, A-C). Furthermore, the total gain in body mass between DMSO and INI-43 treatment groups were similar for all three experiments conducted with CaSki, KYSE30 and WHCO6 cells (Fig. 2.20, D-F), supporting that INI-43 is tolerated in the nude mice model. Taken together, these results showed that INI-43 demonstrated inhibitory effect on cancer cell growth both *in vitro* and *in vivo* without causing intolerable toxicity in nude mice.

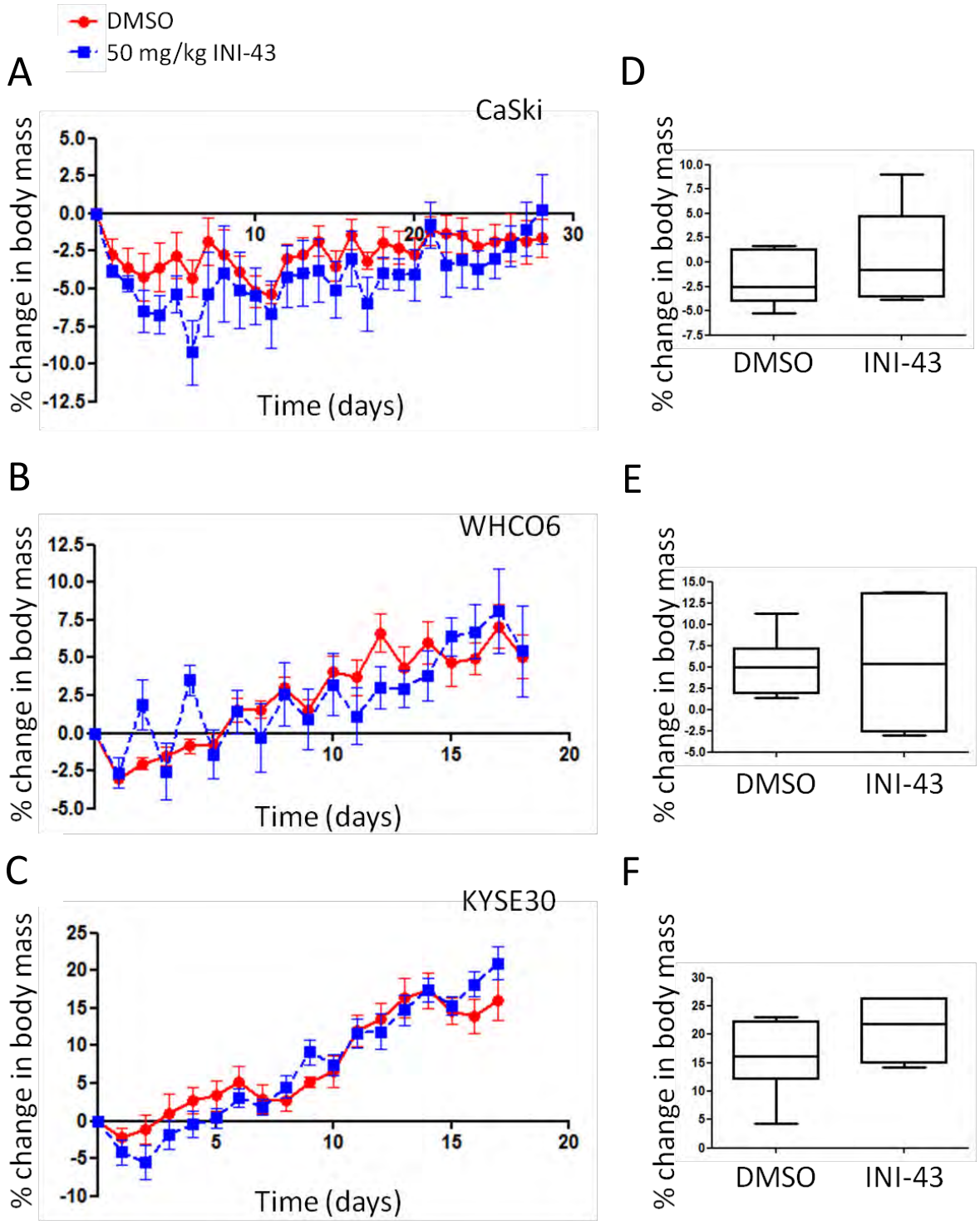

Figure 2.20. Body mass change in mice. During the tumourigenesis assay, the animals' body mass were monitored daily for both DMSO and INI-43 treatment groups for CaSki (A), WHCO6 (B) and KYSE30 (C) tumour bearing mice. Body mass was expressed as percentage change to the body mass measured on day 0 of each experiment, and shown as mean ± SEM, with 6 mice in each group. The percentage gain in body mass for control and treated mice are shown for each cell line (D-F). Results are presented in Box-and-Whisker plots showing median, minimum and maximum values generated by Graphpad Prism.

2.3. Discussion

Conventional chemotherapy has been employed for decades in anti-cancer therapies, and may be used for curative or palliative purposes. In general, chemotherapy involves the use of chemical substances and is often combined with radiotherapy or surgery. Various classes of chemotherapeutic agents exist, such as alkylating agents, taxanes, anthracycline, antimetabolites and others. Whilst each class of agents achieve cytotoxicity via different mechanisms, the commonality (and shortfall) of all chemotherapeutic agents is that they target all rapidly dividing cells, thereby killing cells such as those in the gut lining and hair follicles, resulting in severe undesired side effects such as hair loss and vomiting. The insufficient selectivity of current chemotherapeutics is a major drawback in cancer treatment, and the identification of novel anti-cancer agents with increased specificity for cancer cells is anticipated to provide better and more efficient therapeutic means.

In recent years, interference of the nuclear transport system has gained increasing attention as an anti-cancer approach, with the focus mainly on the inhibition of CRM1-mediated nuclear export[128, 229, 230, 237, 245, 343-347]. Here, we have identified and examined a novel inhibitor of nuclear import designated INI-43, potentially through inhibition of Kpnβ1, and showed that it is effective at inducing cancer cell death both *in vitro* and *in vivo*. Supporting its role as an inhibitor of the Kpnβ1 protein, RNAi mediated Kpnβ1 inhibition displayed similar selective cancer killing effects via cell cycle arrest and apoptotic induction as observed with INI-43 treatment[300, 333]. Moreover, INI-43 displayed inhibitory effects on the nuclear import of various Kpnβ1 cargoes, including AP1, NFAT and NFY, and exogenous Kpnβ1 over-expression was able to partially reverse the inhibitory effect of INI-43 on NFκB-p65 nuclear import as well as cell viability[333]. These results suggest that INI-43 causes selective cancer killing effects via inhibiting Kpnβ1 function. Other Kpnβ1 inhibitors such as Ivermectin and Importazole have been reported to exhibit anti-cancer effects in ovarian cancer and multiple

myeloma[298, 318]. The mechanisms and selectivity of these agents, however, remain to be investigated. It has been reported that CRM1 inhibition via small molecules specifically induced apoptosis in cancer cells with minimal effects in non-cancer cells[238, 243, 348], suggesting that interfering with the nuclear transport system, i.e. members of the Karyopherin family, may be an effective strategy to intervene with cancer growth and development. In this study we showed that INI-43 was significantly more toxic to cancer cells compared to non-cancer fibroblast cells, supporting that INI-43 could be selective in its cytotoxic activities. However, the possibility that the difference observed is due to other reasons should not be ruled out - as the control cells used in this study were isogenically different to the cancer cells (fibroblast versus epithelial). Our laboratory has, however, previously shown that siRNA mediated Kpnβ1 inhibition showed higher killing effects in cancer cells compared to normal epithelial cells EPC2[128], suggesting that targeting Kpnβ1 is selective. The specificity of nuclear transport inhibition against cancer cells may be attributed to the increased reliance on nuclear trafficking which has been associated with cellular transformation and cancerous phenotypes[128, 185, 231, 347].

In this study, the effect of INI-43 on cancer cell growth and viability was assayed under various conditions, and this showed inhibitory effects on both cell proliferation and survival when grown anchorage-dependently and independently. Examination of the mitochondrial content of cytochrome C and the apoptotic related cleavage of PARP demonstrated that INI-43 induced apoptosis via the intrinsic mitochondrial pathway. Similarly, the intrinsic apoptotic pathway was also found to be activated in cervical cancer cells when Kpnβ1 was inhibited via RNAi[300], confirming that INI-43 treatment and Kpnβ1 inhibition resulted in similar cell death mechanisms. Whilst sufficient evidence exist to show that inhibition of nuclear import activates apoptotic pathways, this does not rule out the possibility that other cell death pathways may also be involved, such as autophagy.

The discovery and development of novel drugs, at some stage, involves pharmacokinetic and pharmacodynamic evaluations, including properties such as absorption, distribution, metabolism excretion and toxicity (ADMET). More often than not, promising candidates fail at this stage due to adverse findings, halting the process when a great deal of efforts and money have already been dedicated. In a study authored by van de Waterbeemd and Gifford, 39% of total drug discovery failure is attributed to suboptimal pharmacokinetic properties and 11% were a result of animal toxicity, suggesting that these two areas should be evaluated as early as possible in the drug discovery process[340]. While the *in vivo* pharmacokinetic and pharmacodynamic is currently under investigation in our laboratory, in this study we assessed the metabolic stability and animal toxicity. The examination of microsomal stability of the drug was particularly important prior to animal testing, as various candidates which showed promising results *in vitro* quite often fail to produce significant effects *in vivo*. In some cases, this is not due to lack of drug efficacy, but rather lack of metabolic stability. Since the majority of drug metabolism takes place in the liver, we evaluated the stability of INI-43 using both human and mouse liver microsomes. We showed that INI-43 exhibited good stability, with half-lives in both human and mouse liver microsomes longer than that of propranolol, a moderately stable compound. Next, possible adverse effects of INI-43 were studied at three different doses sequentially, and the result suggested that nude mice could tolerate INI-43 at least up to 50 mg/kg, at which dose the mice showed no obvious signs of discomfort or stress, and body mass gain were within acceptable range. The moderate stability and lack of toxicity of INI-43 at the concentrations tested, coupled to the promising *in vitro* anti-cancer activities set the premise for preclinical testing.

Subsequent tumourigenesis assays using an ectopic xenograft mouse model revealed that INI-43 displayed anti-tumour effect *in vivo*. Reduced growth rate as well as reduced necrotic tumour occurrence were observed in mice treated with INI-43 compared to the control mice treated with DMSO. The necrotic occurrence is likely a result of tumour growth beyond its vasculature supply,

and is generally associated with aggressive phenotypes such as invasion and metastasis[342, 349]. Although necrotic tumours represents death in the tumour tissue, it often induces powerful inflammation responses, resulting in increased growth in the surrounding tumour tissues due to the stimulatory effects of inflammation[350]. Indeed, it has been suggested that necrotic cell death and inflammation promote tumour growth in adult-related cancers[351]. Moreover, the association between poor prognosis and necrotic tumours have been demonstrated in urothelial carcinoma[352-354], renal cell carcinoma[349, 355], colorectal cancer[356],non-small cell lung cancer[357] and pancreatic cancer[358]. The ability of INI-43 to reduce necrotic events may be an indication of its inhibitory effects on the aggressiveness of certain types of tumours.

Taken together, these findings demonstrated that interference of nuclear import activities via the use of INI-43, potentially through inhibiting Kpnβ1 function induced apoptosis in cancer cells *in vitro* and decreased tumour growth rate *in vivo*. These anti-tumour effects of INI-43 makes it an attractive candidate to further pursue and develop for chemotherapeutic purposes, and in the next sections we explore the possibility of combining INI-43 with an established chemotherapeutic drug Cisplatin (CDDP) in treating gynaecological cancers.

CHAPTER 3

INVESTIGATING THE COMBINATION TREATMENT OF INI-43 AND CDDP IN OVARIAN CANCER

3.1. Introduction

Ovarian carcinoma, although not the most frequently diagnosed, exhibits the highest mortality rate of gynaecological cancers[359]. This is attributed to two main reasons; firstly, the lack of symptoms which often lead to late diagnosis when the cancer has advanced already and treatment is difficult[360]. Secondly, the emergence of drug resistance is frequently observed in women receiving chemotherapy[360], compromising treatment outcome and most patients relapse within two years of initial treatment[361]. The latter has remained one of the main challenges in treating ovarian cancer today.

Platinum-based agents such as CDDP and Carboplatin form the important backbone in treating ovarian cancer[36], and in the last two decades, research and clinical trials have demonstrated favourable outcome in their combined use with taxanes, compared to their monotherapy or combination with non-taxanes[362-364]. The combined use of CDDP or Carboplatin with Paclitaxel have become the standard approach for treatment and is generally effective[365]. While both combinations have similar treatment outcome in terms of survival[366], Paclitaxel paired with Caboplatin is favoured over CDDP due to better toxicity profiles in clinical studies[367]. The combined use of CDDP and Etoposide has also been studied in relapsed patients, which was shown to be effective[368, 369], although some concerns have been raised regarding its high rate of toxicity[370]. The incorporation of

molecularly targeted therapies into the standard platinum-taxane treatment is also a subject of study, and in particular, addition of Bevacizumab, an angiogenic inhibitor into the treatment regimen have shown improved progression-free survival in two clinical studies[371, 372].

While Kpnβ1 has not been extensively studied in ovarian cancer, there is literature describing increased Kpnβ1 expression at both mRNA and protein levels, suggesting increased reliance of ovarian cancer on the nuclear import function[297]. We were able to show that ovarian cancer cells exhibited sensitivity to INI-43 at IC_{50} values similar to that of cervical and oesophageal cancer, indicating a similar dependence of ovarian cancer on Kpnβ1 associated function. In addition, there is evidence showing elevated expression of other members of the Karyopherin family, including CRM1[232] and Kpnα2[191, 373], suggesting a link between nuclear transport and ovarian cancer. Various studies have addressed the therapeutic role of CRM1 in ovarian cancer[175, 344, 346] and examined Kpnα2 as a prognostic marker[374], while Kpnβ1 is beginning to be explored.

More recently, CRM1 inhibition via the KPT compounds or Piperlongumine has been examined in combination with various cytotoxic agents[263, 375], which showed additive or synergistic effects when partnered to CDDP, Topotecan, Doxorubicin, Paclitaxel and Bevacizumab *in vitro*, and combined use with Topotecan, Paclitaxel and Bevacizumab demonstrated effectiveness in preclinical mouse models[376, 377], indicating a role for nuclear transport in chemoresistance. These suggest that co-targeting the nuclear transport system with other cytotoxic agents may yield better treatment outcome compared to monotherapy.

In this study, we investigated whether INI-43 can cooperate with the platinum based drug CDDP to achieve better therapeutic outcome. This is, to the best of our knowledge, a first study aimed at investigating a novel approach of combining a potential nuclear import inhibitor and CDDP.

3.2. Results

3.2.1. The effect of INI-43 on nuclear import in ovarian cancer

We have previously shown in cervical cancer cells that INI-43 exhibited inhibitory effects on nuclear import of various Kpnβ1 cargoes as well as Kpnβ1 itself[333]. These data showed that INI-43 negatively impacted nuclear import activities, and this is likely mediated through interfering with Kpnβ1 function. To determine whether INI-43 could similarly interfere with Kpnβ1 in the ovarian cancer model, we investigated the effect of INI-43 on Kpnβ1 localization, as well as a pseudo-cargo protein, the nuclear localization signal (NLS) bearing mCherry protein (NLS-mCherry).

3.2.1.1. INI-43 decreased nuclear localization of Kpnβ1 in ovarian cancer cell lines OVCAR4 and OVCAR8

To examine Kpnβ1 localization in the presence and absence of INI-43, cells were treated accordingly for 1 hour, followed by immunofluorescence staining for Kpnβ1 and analyzed by confocal microscopy. Kpnβ1 staining in the DMSO-only treated control cells showed mostly an equal distribution between the cytoplasm and nucleus, with stronger signal in the peri-nuclear region (Fig. 3.1.A, arrows indicate position of the nuclei). In cells treated with 5 μM INI-43, the cytoplasmic fluorescence became distinctively stronger compared to the nucleus (Fig. 3.1.A). This result suggests that 5 μM INI-43 treatment for 1 hour is sufficient to decrease the nuclear translocation of Kpnβ1. Cells were scored as either showing cytoplasmic or equal distribution of Kpnβ1, and plotted as a percentage, which revealed that INI-43 treatment led to an increase in percentage of cells showing cytoplasmic Kpnβ1 compared to the control cells (19% versus 67%, Fig. 3.1.B). To confirm the visual interpretation of the data, Kpnβ1 fluorescence intensity was quantified along the linear axis for two selected cells from each treatment (Fig. 3.1.C, line indicates position along which fluorescence intensity was quantified, and quantification path was drawn to avoid the nucleolus). Quantification

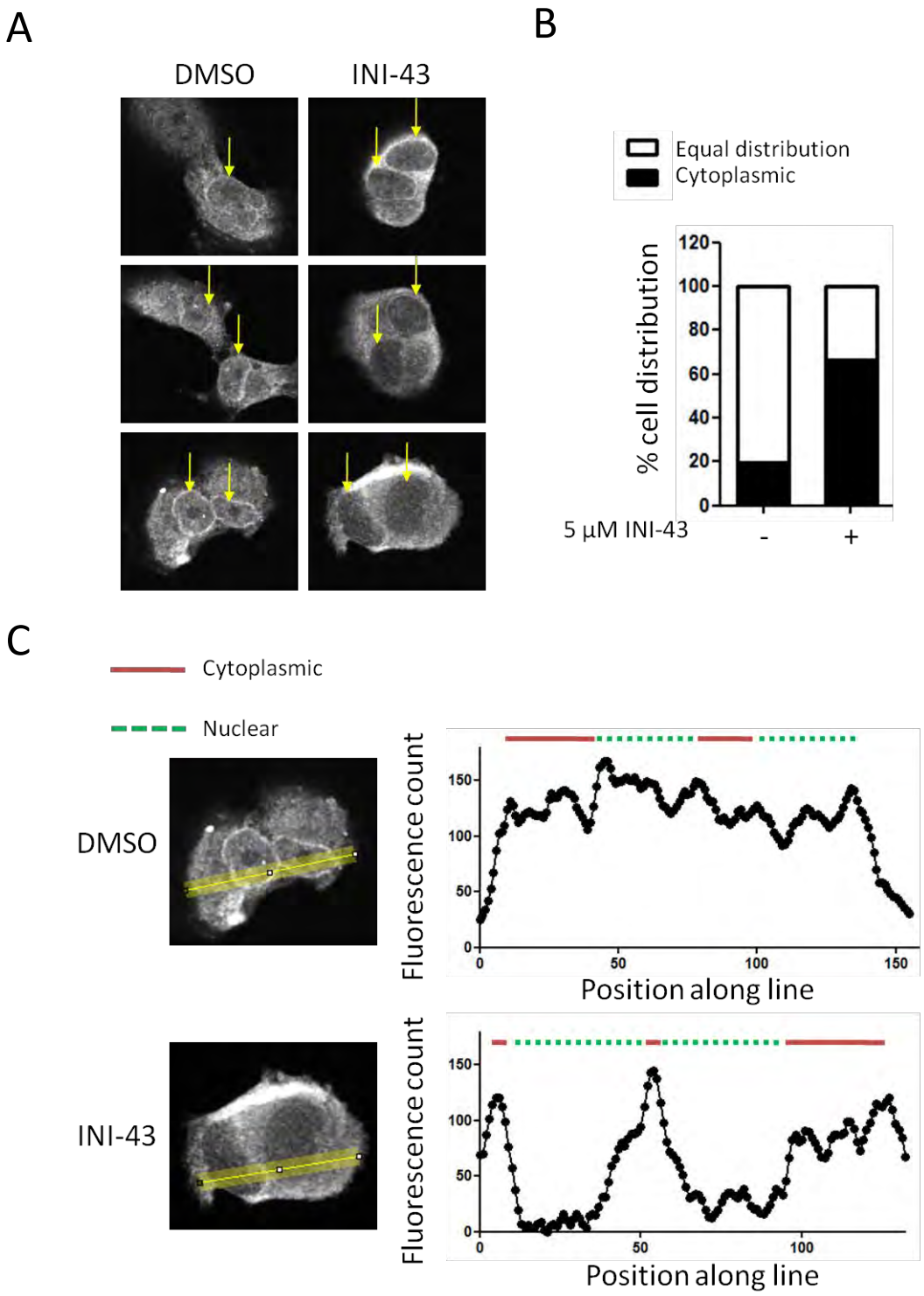

Figure 3.1. INI-43 treatment decreased nuclear Kpnβ1. OVCAR4 cells were treated with DMSO or 5 µM INI-43 for 1 hour, followed by fixation and immunofluorescence staining and confocal microscopy (A). For both untreated and INI-43 treatment, at least 100 cells were scored as showing either cytoplasmic distribution or equal distribution (equal intensity in the nucleus and cytoplasm), and plotted as a percentage (B). Kpnβ1 fluorescence intensity along the cell linear axis (indicated by yellow line) was quantified and plotted. Positions of the nucleus and cytoplasm was shown with red solid line and green dotted line, respectively (C). Data shown are representative of three independent experiments.

of Kpnβ1 fluorescence showed two distinct profiles; in the DMSO treated cells, there were smaller fluctuations in fluorescence intensity along the length of the cell which did not correlate to cytoplasmic or nuclear positions, suggesting a more uniform distribution of Kpnβ1 throughout the entire cell. In the INI-43 treated cells, there was a clear biconcave distribution, with the two nuclear regions showing a marked decrease in Kpnβ1 concentration (green dotted line) compared to the cytoplasmic region (red solid line), confirming the visual interpretation that INI-43 treatment led to decreased nuclear Kpnβ1 localization.

To independently confirm these results, cytoplasmic and nuclear proteins were harvested separately after treatment with or without INI-43 from OVCAR4 and OVCAR8 cells, and Kpnβ1 content analyzed via western blotting. In both cell lines, a decrease in nuclear Kpnβ1 after one hour treatment with 5 μM INI-43 was observed (Fig. 3.2). Histone H3, a marker for nuclear proteins remained unchanged. No change in nuclear Kpnβ1 was noticeable after 1 μM INI-43 treatment, suggesting a minimal concentration of INI-43 is required for inhibitory effects to occur. To confirm that the nuclear fraction was not contaminated with cytoplasmic proteins, β-tubulin was probed and compared against a cytoplasmic fraction 'C'.

3.2.1.2. INI-43 increased the cytoplasmic accumulation of NLS-mCherry in OVCAR4

Having shown that INI-43 treatment interfered with the nuclear localization of Kpnβ1, we next examined whether INI-43 affected the localization of a classical NLS-tagged mCherry fluorescent reporter protein (NLS-mCherry), as this type of NLS containing cargoes are known substrates for Kpnβ1[378]. OVCAR4 cells were transfected with the pQC-NLS-mCherry-IX plasmid (Addgene plasmid 37354, see Appendix Fig. A.3), which constitutively expresses NLS-mCherry under the control of CMV promoter. Cells were then treated with 5 μM and 10 μM INI-43 48 hours after transfection for 1

hour, followed by fixation and fluorescent microscopy was used to examine mCherry localization. In the

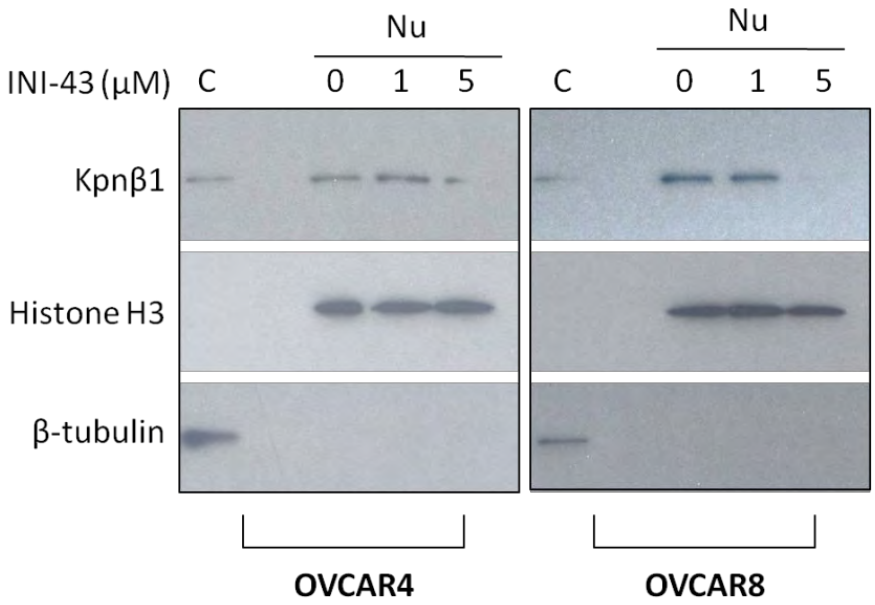

Figure 3.2. INI-43 lead to decreased nuclear Kpnβ1. Nuclear and cytoplasmic proteins were independently harvested from OVCAR4 and OVCAR8 cells after treatment with 0 μM, 1 μM or 5 μM INI-43 for one hour, and Kpnβ1 levels in the nuclear fraction (Nu) was analyzed by western blot. Histone H3 and β-tubulin serve as loading control for nucleus and cytoplasm, respectively. A cytoplasmic sample 'C' was included to confirm proper separation of nuclear and cytoplasmic fractions. Results shown are representative of two independent experiments.

untreated cells, mCherry was predominantly localized inside the nucleus, and INI-43 treatment resulted in increased cytoplasmic retention of NLS-mCherry (Fig. 3.3.A). Interestingly, INI-43 did not block nuclear localization of NLS-mCherry completely, this could be due to the experimental setup, as cells were treated with INI-43 48 hours after transfection. It is likely that by then mCherry was already expressed and imported into the nucleus, and the INI-43 treatment affected mainly the newly synthesized mCherry, preventing it from entering the nucleus leading to increased cytoplasmic retention. The mCherry fluorescence intensity was quantified and expressed as cytoplasmic mCherry fluorescence relative to nuclear mCherry fluorescence (Fc(Cy/Nu)). This

showed a significant increase in cytoplasmic mCherry after 5 µM and 10 µM INI-43 treatment compared to the untreated cells (Fig. 3.3.B).

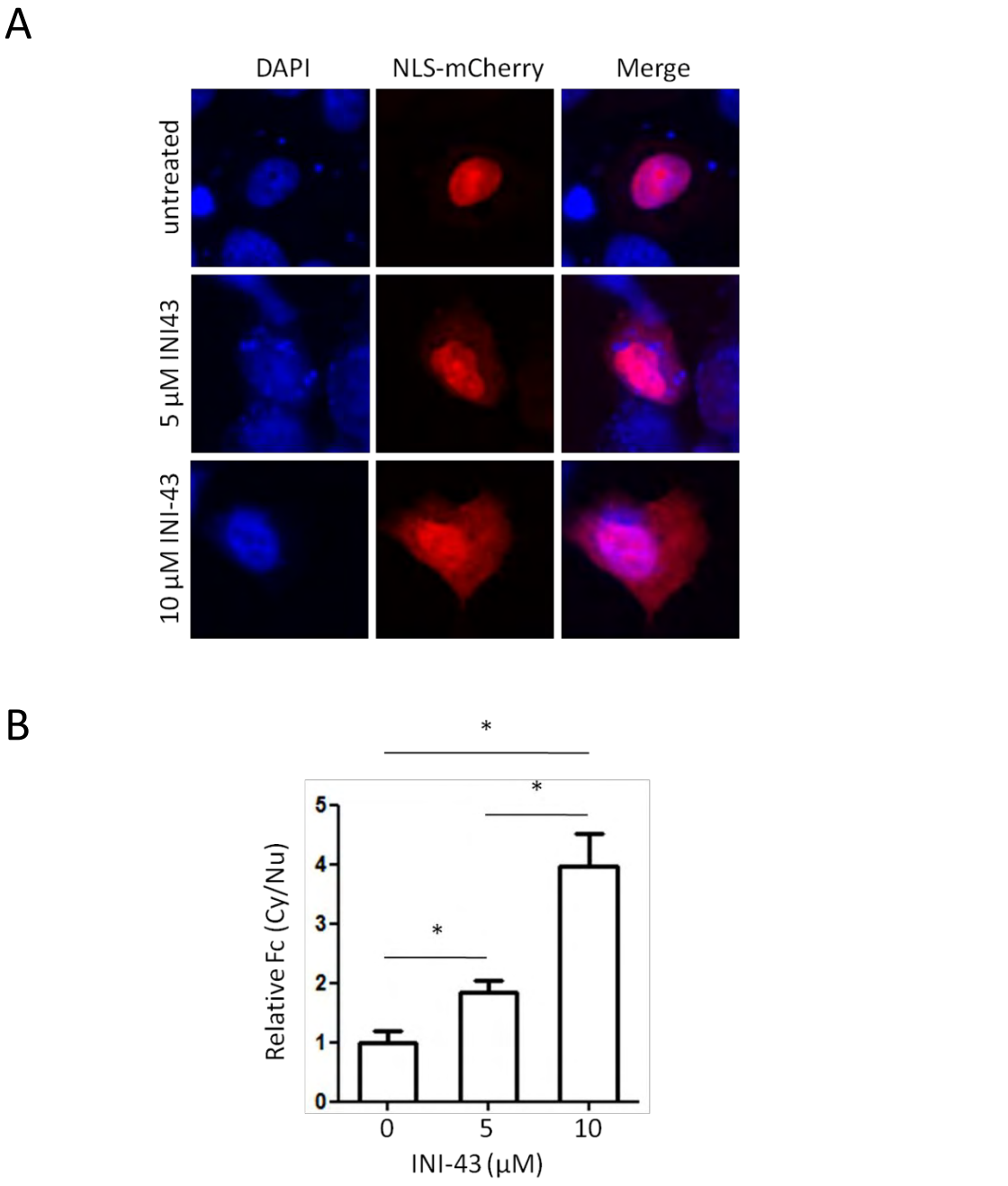

Figure 3.3. INI-43 treatment leads to increased cytoplasmic retention of NLS-mCherry. OVCAR4 cells were transfected with the constitutive NLS-mCherry expressing construct, pQC-NLS-mCherry-IX for 48 hours followed by 5 µM or 10 µM INI-43 treatment for 1 hour. Cells were fixed and stained with DAPI, and fluorescent microscopy were performed to examine localization of NLS-mCherry (A). NLS-mCherry fluorescence intensity was quantified using ImageJ and expressed as cytoplasmic fluorescence relative to nuclear fluorescence (Fc(Cy/Nu)), and normalized to the untreated cells (B, $*p < 0.05$). Results shown are mean ± SEM of 6 cells, the experiment was repeated two independent times.

Taken together, these results showed that INI-43 increased the cytoplasmic retention of a NLS-bearing protein as well as Kpnβ1 itself, supporting the idea that INI-43 has an inhibitory effect on nuclear import, and that this is possibly mediated through interfering with Kpnβ1.

3.2.2. INI-43 pre-treatment sensitized ovarian cancer cells to CDDP

3.2.2.1. INI-43 pre-treatment led to decreased CDDP IC_{50} in OVCAR4 and OVCAR5

Having shown that INI-43 caused an inhibitory effect on nuclear import similar to that observed in cervical cancer, we next assessed whether interference of the nuclear import system can affect cancer cells' response to DNA damage stress by examining CDDP sensitivity. To test this, three ovarian carcinoma cell lines OVCAR4, OVCAR5 and OVCAR8 were pre-treated with vehicle control DMSO or 5 μM INI-43 for 2 hours, a concentration which is sufficient to decrease nuclear import as shown in section 3.2.1, but does not cause significant cell death. After INI-43 pre-treatment, CDDP IC_{50} was determined for both control (single treatment) and INI-43 pre-treated (combination treatment) cells without removing INI-43 from the growth media. In all three cell lines, there was a significant reduction in CDDP IC_{50} (8.8 μM to 6.1 μM, 9.4 μM to 6.2 μM, and 14.8 μM to 10.2 μM for OVCAR4, OVCAR5 and OVCAR8 cells, respectively, Fig.3.4.A). This effectively represented 30%, 34% and 31% reduction in CDDP concentration which is needed to inhibit cell viability by 50% for OVCAR4, OVCAR5, and OVCAR8 respectively. A representing IC_{50} determination plot is shown for each cell line, and the IC_{50} values were calculated using the formula $IC_{50} = 10^{x\text{-intercept}}$ as previously described (Fig. 3.4.B).

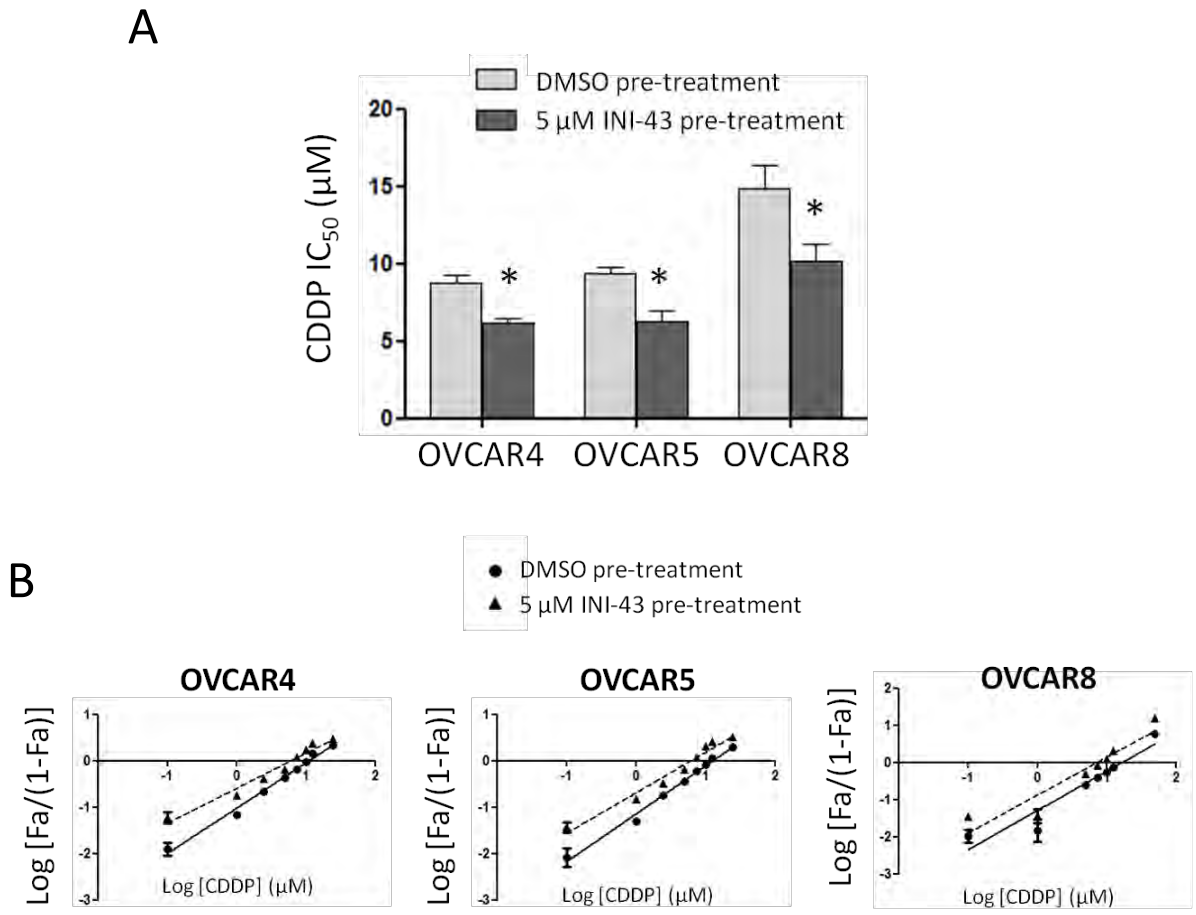

Figure 3.4. INI-43 pre-treatment decreased CDDP IC_{50} in ovarian cancer cell line OVCAR4, OVCAR5 and OVCAR8. Cells were pre-treated with DMSO (single treatment) or 5 µM INI-43 (combination treatment) before CDDP IC_{50} determination. (A) Average CDDP IC_{50} for single and combination treatments (*$p < 0.05$). (B) One representing experiment for CDDP IC_{50} determination for single and combination treatment is shown for each cell line. Results shown are mean ± SEM of experiments performed in 6 replicates and repeated at least three times.

3.2.2.2. INI-43 pre-treatment augmented CDDP-induced cytotoxic effects in OVCAR4 and OVCAR5

To assess whether the difference in CDDP IC_{50} between single and combination treatment translated into a relevant difference in CDDP sensitivity, cell viability was examined in OVCAR4, OVCAR5 and OVCAR8 cells. Cells were pre-treated with DMSO or 5 µM INI-43 for 2 hours, followed by addition of CDDP to the growth media without removing INI-43. Viable cells were quantified using the MTT assay 48 hours later. The results demonstrated that while 5 µM INI-43 on its own caused negligible cell death, when coupled to CDDP it enhanced the inhibitory effect of CDDP on cell viability (Fig. 3.5).

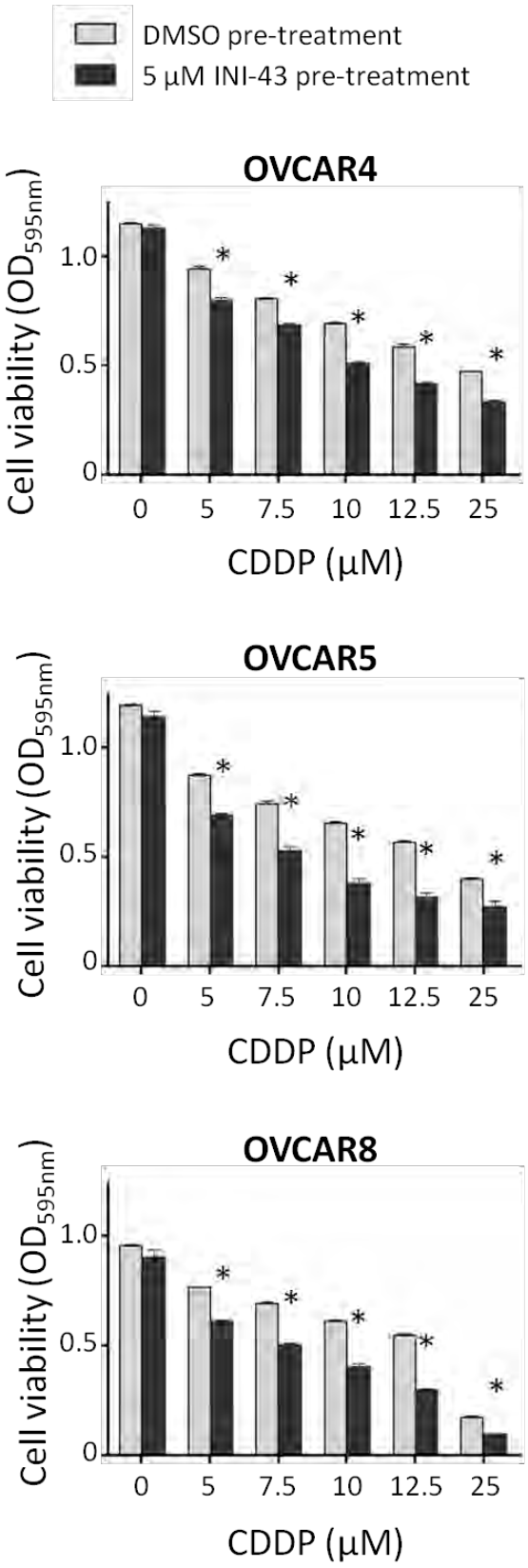

Figure 3.5. INI-43 pre-treatment sensitized OVCAR4 and OVCAR5 cells to CDDP. OVCAR4, OVCAR5 and OVCAR8 cells were pre-treated with DMSO (light grey bars) or 5 µM INI-43 (black bars) before CDDP treatment at various concentrations. Cell viability was determined by MTT 48 hours after CDDP treatment (*$p < 0.05$). Results shown are representative experiments of three repeats for each cell line, mean ± SEM of 6 replicates.

3.2.2.3. INI-43 pre-treatment enhanced CDDP-induced cell death via increased apoptosis in OVCAR4 and OVCAR5

Next, we investigated whether the reduced cell viability observed in the combination treatment was due to increased apoptosis. To examine apoptotic events in single and combination treated cells, PARP-cleavage was analyzed. Cells were pre-treated with DMSO or INI-43 for 2 hours followed by 48-hour CDDP incubation, and the PARP status was determined by western blot. Results showed that INI-43 pre-treatment led to enhanced PARP cleavage at both 5 μM and 10 μM CDDP, compared to cells receiving CDDP only for both cell lines (Fig. 3.6). In addition, 5 μM INI-43 pre-treatment alone caused no PARP cleavage, confirming previous findings that this concentration of INI-43 does not significantly affect cell viability. These results indicated that INI-43 pre-treatment increases CDDP-induced cell death via increasing apoptosis.

Together, our data shows that INI-43 pre-treatment sensitized ovarian cancer cells to CDDP, implicating the importance of the nuclear import function in response to DNA damage stress. We speculate that when this function is perturbed, the cells became less tolerant to CDDP treatment.

3.2.3. Kpnβ1 inhibition via siRNA sensitized OVCAR4 and OVAR5 cells to CDDP

As described in Chapter 1, INI-43 was identified in an *in silico* screening as a potential inhibitor of Kpnβ1, and we have shown that INI-43 treatment decreased nuclear import as well as induced cancer cell death similar to that observed in Kpnβ1 knock-down cells[128, 300, 333]. Furthermore, we showed that INI-43 treatment decreased nuclear Kpnβ1[333], suggesting that its inhibitory effect on nuclear import is possibly mediated through Kpnβ1. So we next verified whether the enhancing effect of INI-43 on CDDP cytotoxicity is mediated directly through Kpnβ1 inhibition, and not possible

off-target effects of INI-43. To address this, we inhibited Kpnβ1 expression by siRNA transfection and examined CDDP sensitivity.

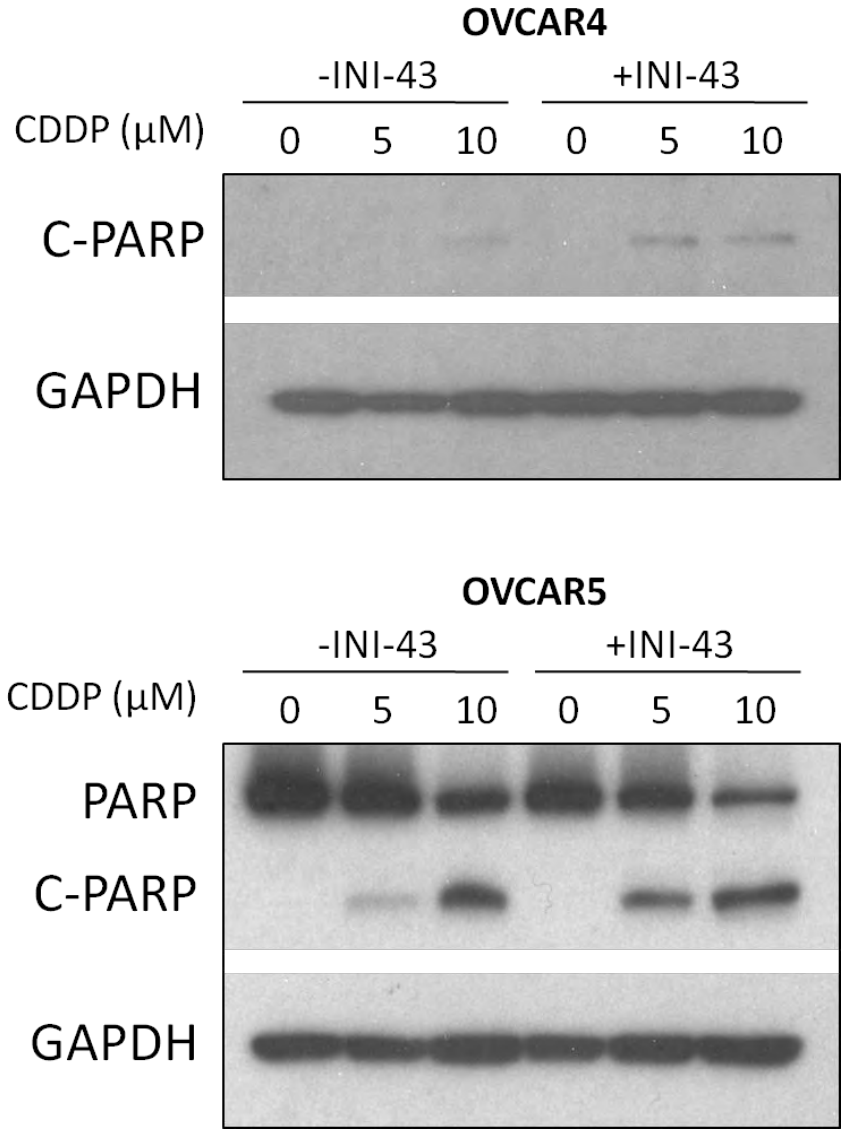

Figure 3.6. INI-43 pre-treatment enhanced CDDP-induced PARP cleavage. OVCAR4 and OVCAR5 cells were subjected to single or combination treatment at 5 μM and 10 μM CDDP for 48 hours. Proteins from both live and dead cells were collected and analyzed by western blot for PARP cleavage. For OVCAR4 cells, cleaved PARP was probed using an antibody specific for cleaved PARP, and for OVCAR5 cells, an antibody which recognized total PARP was used. GAPDH was used as loading control. Results shown are representative experiments performed at least two independent times.

3.2.3.1. Kpnβ1 knock-down with siRNA leads to decreased CDDP IC_{50} in OVCAR4 and OVCAR5

CDDP IC_{50} was evaluated in cells transfected with 20 nM control siRNA (si-ctrl) and Kpnβ1 siRNA (si-Kpnβ1), and knock-down was confirmed by western blot in OVCAR4 and OVCAR5 cells (Fig. 3.7.A). CDDP IC_{50} was determined using the standard MTT assay, and results showed a decrease in CDDP IC_{50}, from 10.3 µM to 5.7 µM for OVCAR4 cells and from 12.6 µM to 4.7 µM for OVCAR5 cells (Fig. 3.7.B). These represented 44% and 63% reduction in CDDP concentration that is required to kill 50% of the cells in OVCAR4 and OVCAR5, respectively.

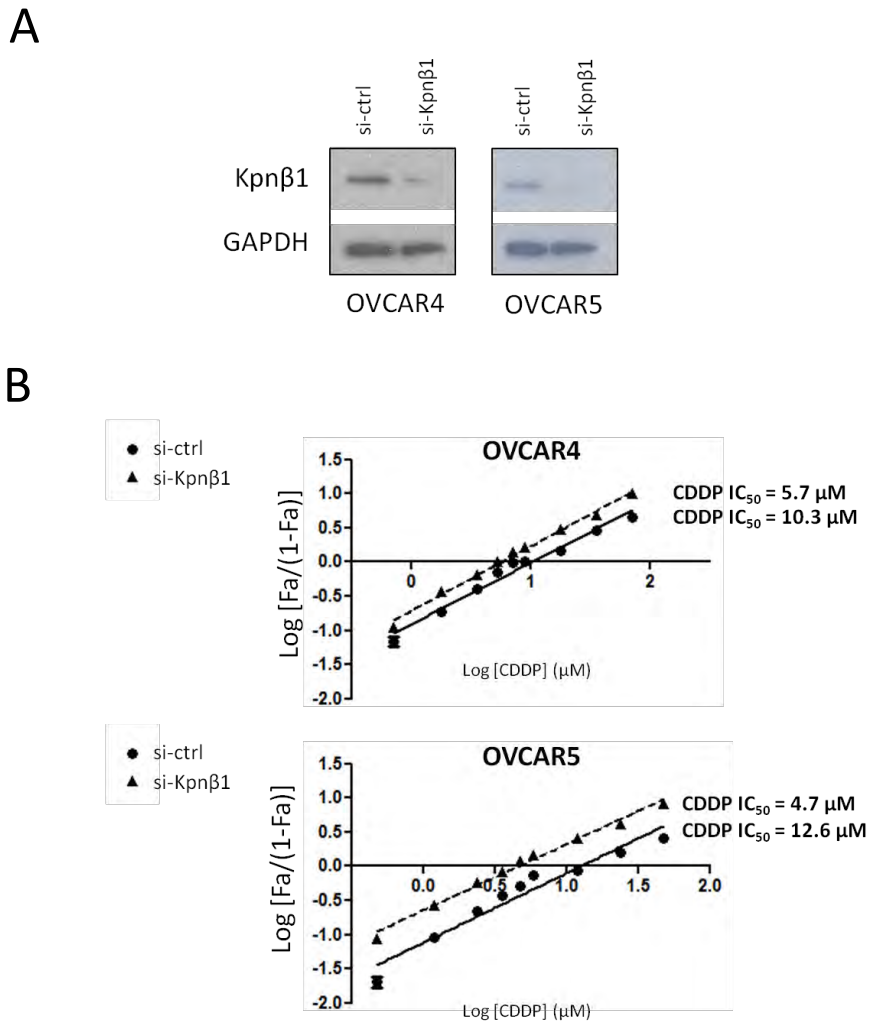

Figure 3.7. Kpnβ1 knock-down decreased CDDP IC_{50} in OVCAR4 and OVCAR5 cells. Cells were transfected with 20 nM control siRNA (si-ctrl) or Kpnβ1 targeting siRNA (si-Kpnβ1) for 48 hours, and Kpnβ1 knock-down was confirmed via western blot (A). Representing CDDP IC_{50} determination plots for control and Kpnβ1 knock-down cells are shown for both cell lines. Results shown are mean ± SEM of 6 replicates, the experiment was repeated two independent times.

3.2.3.2. Kpnβ1 knock-down enhanced CDDP cytotoxicity in ovarian cancer

Next we examined the effect of CDDP on cell viability in Kpnβ1 knock-down cells and control cells. The knock-down conditions were carried out as previously described in section 3.2.3.1, and cell viability was examined after CDDP treatment at various concentrations using the standard MTT assay. In OVCAR4 cells, Kpnβ1 knock-down led to decreased cell viability compared to the control cells, including those that were not treated with CDDP (Fig. 3.8.A, compare viability at 0 μM CDDP treatment). These cell death were likely due to potent inhibition of Kpnβ1 achieved by siRNA[128, 300], and to eliminate the cell death that was caused by Kpnβ1 inhibition only, cell viability was normalized to the CDDP-untreated cells in each transfection group. The corrected results showed a significant decrease in cell viability in the Kpnβ1 knock-down cells compared to the control cells at all CDDP concentrations tested (Fig. 3.8.B). This was similarly observed in OVCAR5 cells (Fig. 3.8.C and D).

Having shown that siRNA mediated Kpnβ1 knock-down enhanced the cytotoxicity of CDDP, we next examined whether transient Kpnβ1 inhibition affected cell growth at a lower CDDP concentration. Control and Kpnβ1 knock-down OVCAR5 cells were seeded sparsely (2000 cells/35 mm dish) and incubated with 1 μM CDDP for 24 hours, before CDDP-containing media was replaced with fresh growth media and cell growth was examined nine days later. Whilst the conventional MTT assay examines cell viability in the presence of the damaging source for a short period of time, this experiment inspects the cell's ability to survive a damaging agent after the source is withdrawn. The result showed that cell growth was able to recover nine days after transient Kpnβ1 knock-down (Fig. 3.8.E, compare (i) and (ii)), however, low concentration CDDP treated cells with transient Kpnβ1 knock-down showed a substantial decrease in cell number after nine days of culture, compared to the control cells (Fig. 3.8, compare (iii) and (iv)). These results demonstrated that cells with transient

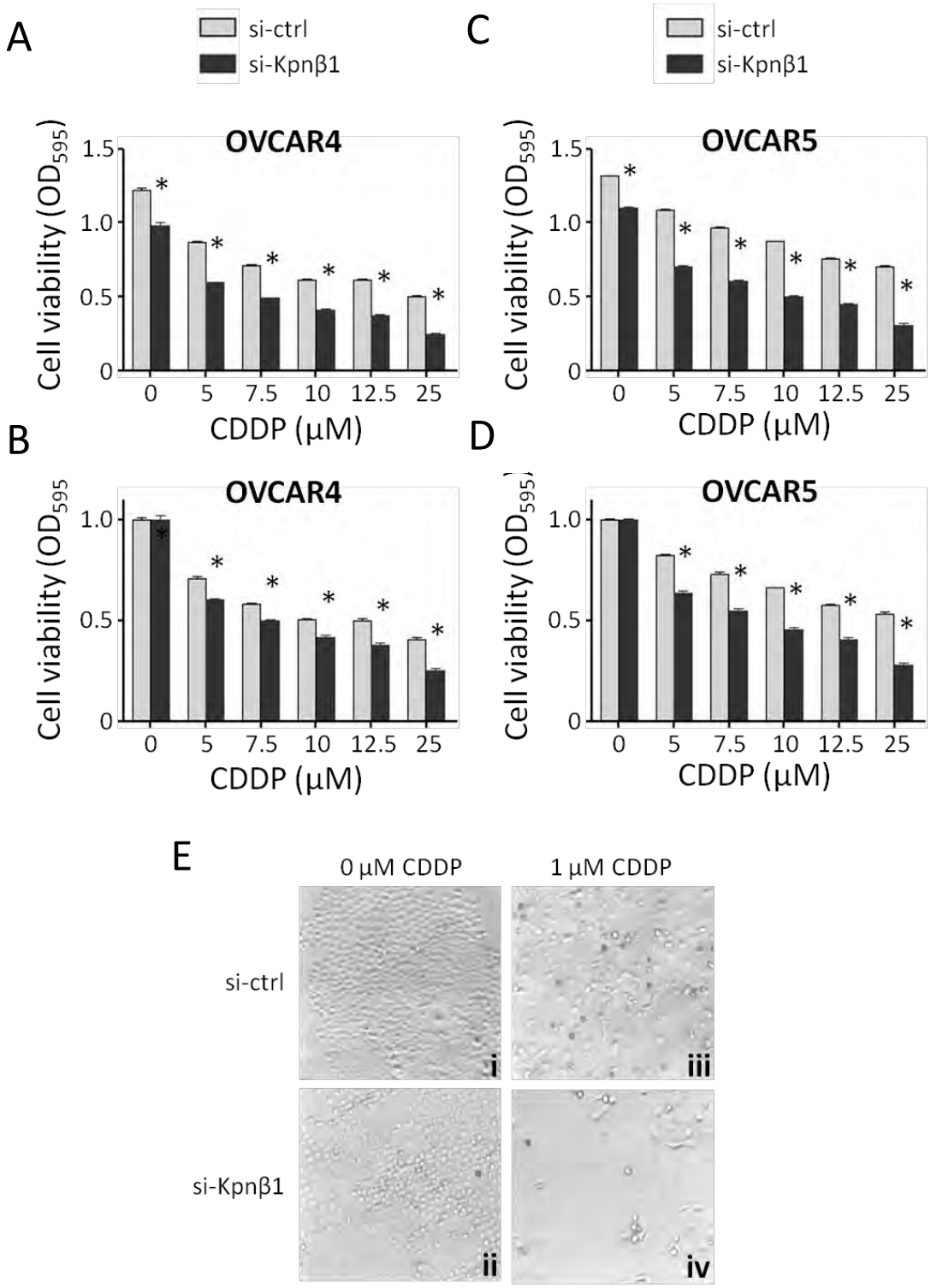

Figure 3.8. Kpnβ1 knock-down enhanced CDDP cytotoxicity in OVCAR4 and OVCAR5 cells. Cells were first transfected with 20 nM si-ctrl or si-Kpnβ1, followed by CDDP treatment at various concentrations. Cell viability was examined using MTT assay after 48 hours of CDDP treatment (A and C). Cell viability was corrected to the untreated cells for each transfection group to eliminate the effect that were specific to Kpnβ1 knock-down (B and D, *$p < 0.05$). Phase contrast images showing si-ctrl and si-Kpnβ1 transfected cells 9 days after 24 hours exposure to 1 μM CDDP (E). Results shown are mean ± SEM of 6 replicates (A-D), and each experiment was repeated two independent times.

Kpnβ1 knock-down showed decreased survival compared to the control cells with an intact nuclear import system. As the Kpnβ1 knock-down effect would be long lost by day 9, it is likely that the low CDDP concentration was able to kill more of the initial population in the Kpnβ1 knock-down cells compared to the control cells, thereby leaving less cells to proliferate and thus less cells were observed after nine days.

3.2.3.3. Kpnβ1 knock-down enhanced PARP cleavage in CDDP treated OVCAR5 cells

Next we investigated whether the enhanced cell death observed after CDDP treatment in Kpnβ1 knock-down cells resulted from an increase in apoptosis as observed with INI-43 pre-treatment. si-ctrl and si-Kpnβ1 transfected OVCAR5 cells were treated with CDDP for 48 hours and the amount of cleaved PARP present in each cell population was analyzed by western blot. Of the cells which received the same CDDP concentration, those with Kpnβ1 knock-down showed higher levels of PARP-cleavage compared to the control cells (Fig. 3.9.A). Densitometry analysis was used to quantify cleaved PARP to total PARP, and this confirmed that elevated cleaved PARP was present in Kpnβ1 knock-down cells compared to control cells at the same CDDP concentration (Fig. 3.9.B).

Taken together, these results showed that Kpnβ1 knock-down cells resulted in sensitization of ovarian cancer cells to CDDP similar to that observed in INI-43 treated cells, supporting the hypothesis that INI-43 augmented CDDP-induced apoptosis via interfering with Kpnβ1 function.

3.2.4. CDDP treatment increased Kpnβ1 expression in ovarian cancer cells, but not non-cancer cells

As shown in the previous sections, INI-43 pre-treatment followed by CDDP treatment resulted in a increase in sensitivity and cell death in ovarian cancer cells. This suggests that when cancer cells are

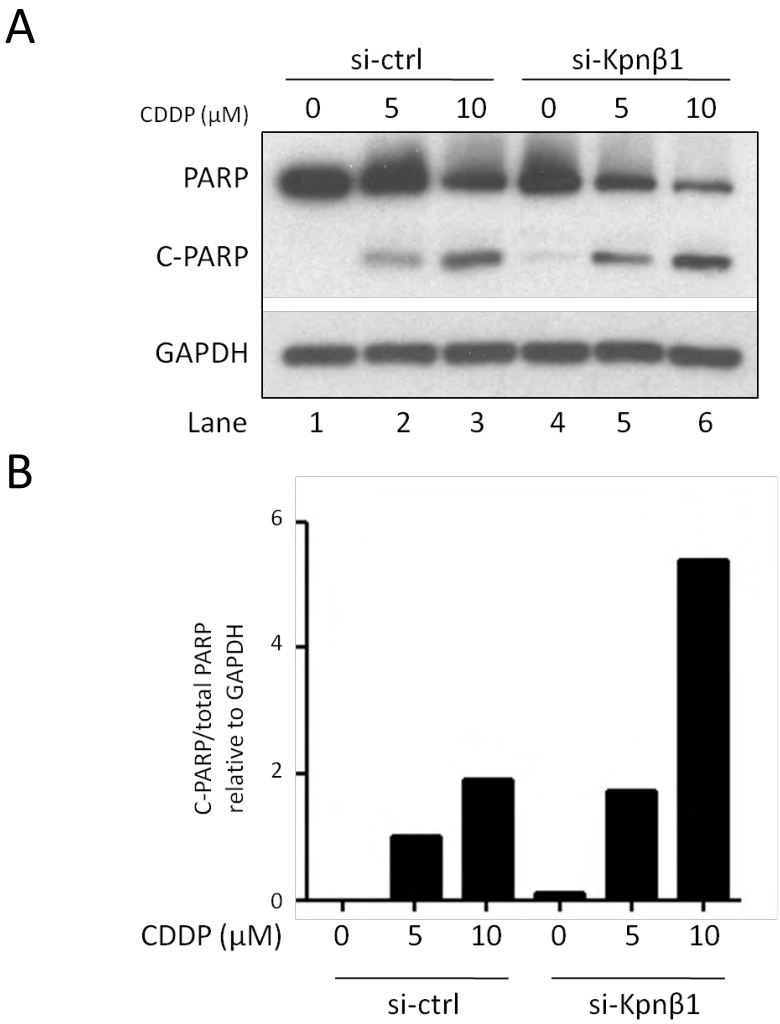

Figure 3.9. Kpnβ1 knock-down enhanced CDDP-induced apoptosis. Kpnβ1 knock-down OVCAR5 cells were treated with CDDP for 48 hours, followed by protein collection from both live and dead cells. PARP and cleaved PARP (C-PARP) were examined using western blot, GAPDH served as loading control (A). Densitometric quantification of protein bands in (A), expressed as C-PARP relative to total PARP, and corrected to GAPDH levels (B). Result shown is representative of 2 independent experiments.

challenged with genotoxic stress such as that caused by CDDP treatment, they rely on Kpnβ1 function more so than the unchallenged cells. Based on this, we hypothesized that Kpnβ1 may be responsive to genotoxic stress caused by CDDP treatment. To test this, OVCAR4 and OVCAR5 cells were treated with CDDP at different concentrations for 24 hours, followed by protein extraction which was then subjected to western blot analysis. To confirm DNA damage, the phosphorylated form of histone H2A.X (γH2AX) was detected alongside Kpnβ1. Histone H2A.X is known to be

phosphorylated at serine-139 by kinases such as Ataxia Telangiectasia Mutated (ATM), and it is a well-established marker for DNA damage[379]. Analysis revealed that Kpnβ1 expression increased with CDDP treatment in a concentration dependent manner for both cell lines, which correlated with the amount of DNA damage, as indicated by increased γH2AX (Fig. 3.10).

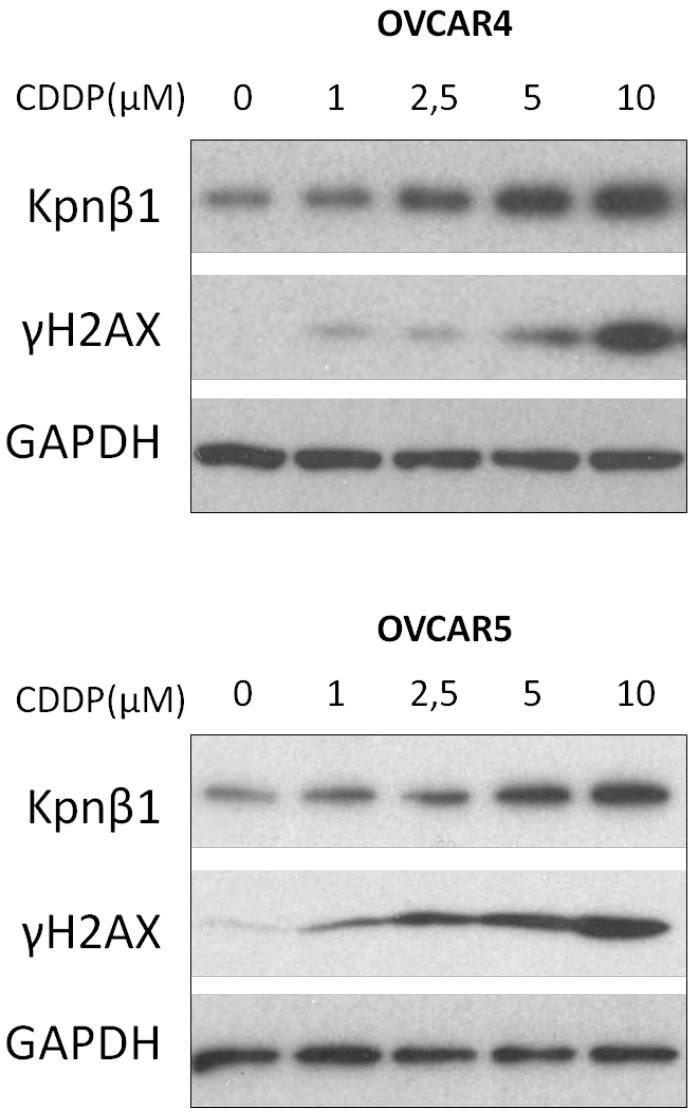

Figure 3.10. CDDP treatment increased Kpnβ1 expression in OVCAR4 and OVCAR5 cells. OVCAR4 and OVCAR5 cells were treated with CDDP at various concentrations for 24 hours, and Kpnβ1 expression was analyzed using western blot. Levels of γHA2X were examined alongside to confirm CDDP-induced DNA damage, and GAPDH served as loading control. Results shown are representatives of two independent experiments from each cell line.

We further investigated whether Kpnβ1 elevation in response to CDDP treatment occurs in other ovarian cancer cell lines; including A2780, OVCAR8 and CP70; as well as the immortalized nontumourigenic human ovarian surface epithelial cell line T29[380]. The cells were either untreated or treated with a concentration of CDDP similar to their own CDDP IC_{50} (Fig. 3.11.A, 0.9 μM, 13.3 μM, 11.6 μM and 4.9 μM for A2780, OVCAR8, CP70 and T29 respectively). Our results showed a clear induction of Kpnβ1 expression in both A2780 and OVCAR8 cells, and a weaker induction in CP70 cells when treated with CDDP at their own IC_{50} (Fig. 3.11.B), which was confirmed by densitometrical quantification (Fig. 3.11.C). Interestingly, the nontumourigenic cell line T29 did not show increased Kpnβ1 levels after CDDP treatment, suggesting that it is possibly less reliant on the nuclear import system under DNA-damaging conditions. Indeed, INI-43 pre-treatment of T29 cells did not significantly improve the outcome of CDDP treatment in T29 cells, shifting the CDDP IC_{50} values from 5.4 μM to 5.3 μM (Fig. 3.11.D).

3.2.5. CDDP treatment induced Kpnβ1 nuclear localization in OVCAR4 and OVCAR5 cells

Having shown that Kpnβ1 expression was responsive to CDDP treatment, we next examined its localization in the presence and absence of CDDP. OVCAR4 and OVCAR5 cells were treated with CDDP at 0.5 x and 1 x its IC_{50} values for 24 hours, followed by fixation and Kpnβ1 was stained using a FITC conjugated secondary antibody. Fluorescent microscopy analysis showed that without treatment, most cells showed an even distribution of Kpnβ1 in both the cytoplasm and nucleus with stronger signal in the peri-nuclear region (Fig. 3.12.A). In cells treated with 5 μM or 10 μM of CDDP, localization of Kpnβ1 became more nuclear for the majority of cells (Fig. 3.12.A). The Kpnβ1 fluorescence intensity (FC-Kpnβ1, FITC) was correlated to the nucleus (FC-nucleus, DAPI) for a random cell from each treatment, as previously described. This demonstrated an overlap of Kpnβ1 fluorescence and DAPI fluorescence in the presence of 5 μM and 10 μM CDDP compared to the control cell, where Kpnβ1 intensity fluctuated around a baseline value (Fig. 3.12.B). Furthermore,

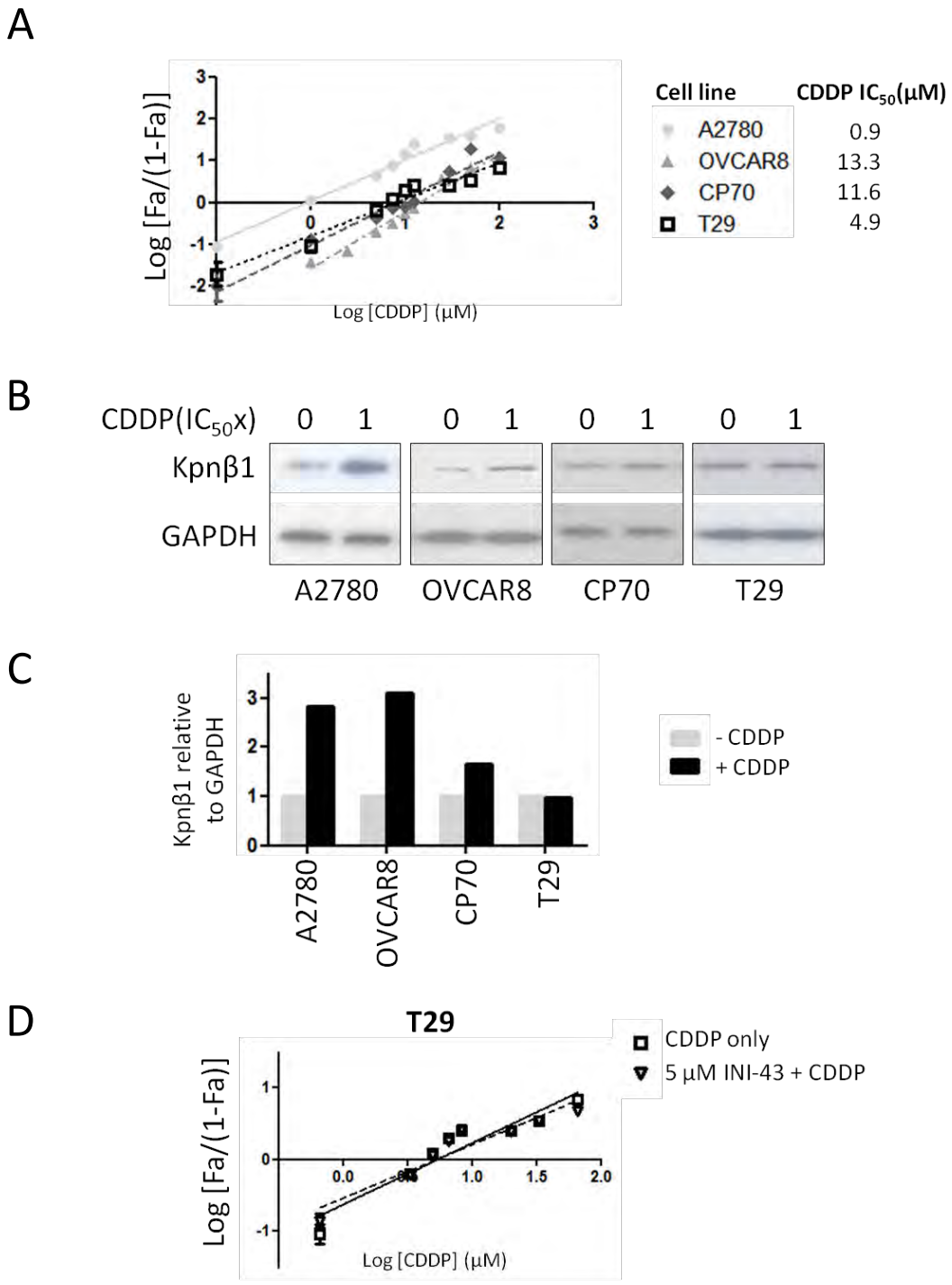

Figure 3.11. CDDP treatment increased Kpnβ1 expression in ovarian cancer cells but not the non-cancer cell line T29. CDDP IC_{50} values were determined in ovarian cancer cell lines A2780, OVCAR8, CP70 and non-cancer cell line T29 (A), and Kpnβ1 expression were then examined for each cell line at their respective CDDP IC_{50} values (B), with GAPDH as the loading control. Kpnβ1 expression was densitometrically quantified and expressed relative to GAPDH for each cell line (C). A representative of CDDP IC_{50} determination plot for T29 cells pre-treated with and without INI-43, the experiment was repeated twice (D). Data shown here are representatives of experiments performed at least two independent times (A, B and D), and values plotted are mean ± SEM of 6 replicates from the representative experiment (A and D).

cells treated with 5 μM and 10 μM showed significant correlation between the nucleus (DAPI) and Kpnβ1 (FITC) fluorescence intensities, with R^2 values of 0.91 and 0.91, compared to 0.17 in the untreated cells. Similar observations were made in OVCAR5 cells, where untreated cells exhibited poor correlation between Kpnβ1 and DAPI fluorescence (Fig. 3.12.C). When cells were treated with CDDP, there was a noticeable increase of Kpnβ1 in the nucleus (Fig. 3.12.C), and fluorescence intensity quantification confirmed co-localization of FITC and DAPI, indicating nuclear accumulation of Kpnβ1 in the CDDP treated cells (Fig. 3.12.D). Correlation analysis of the DAPI and FITC intensity was only significant in the 5 μM and 10 μM treated cells, and R^2 values were 0.026, 0.79 and 0.84 for untreated, 5 μM CDDP treated and 10 μM CDDP treated cells, respectively.

To independently validate the results obtained from the immunofluorescence experiments, nuclear proteins were harvested separately from the cytoplasmic proteins for both OVCAR4 and OVCAR5 cells after treatment with CDDP. The amount of Kpnβ1 present in the nuclear fraction was examined using western blot, and results confirmed an increase in nuclear Kpnβ1 after CDDP treatment in both cell lines (Fig. 3.13).

Taken together, these results show that in ovarian cancer cells, the uniform distribution of Kpnβ1 between the cytoplasmic and nuclear compartments is disrupted by CDDP treatment, as increased nuclear accumulation of Kpnβ1 is observed after CDDP treatment.

A

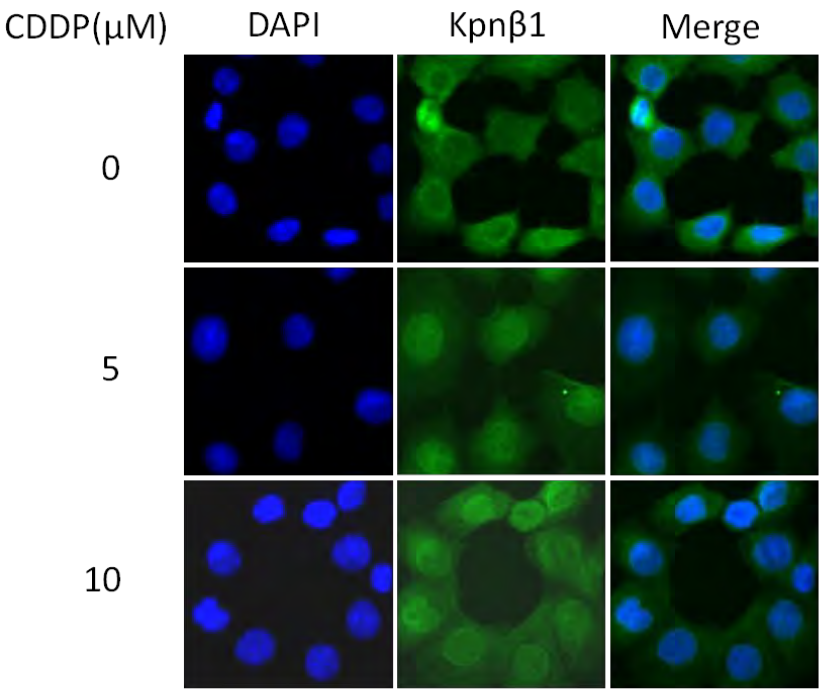
CDDP(μM)
DAPI
Kpnβ1
Merge
0
5
10

B

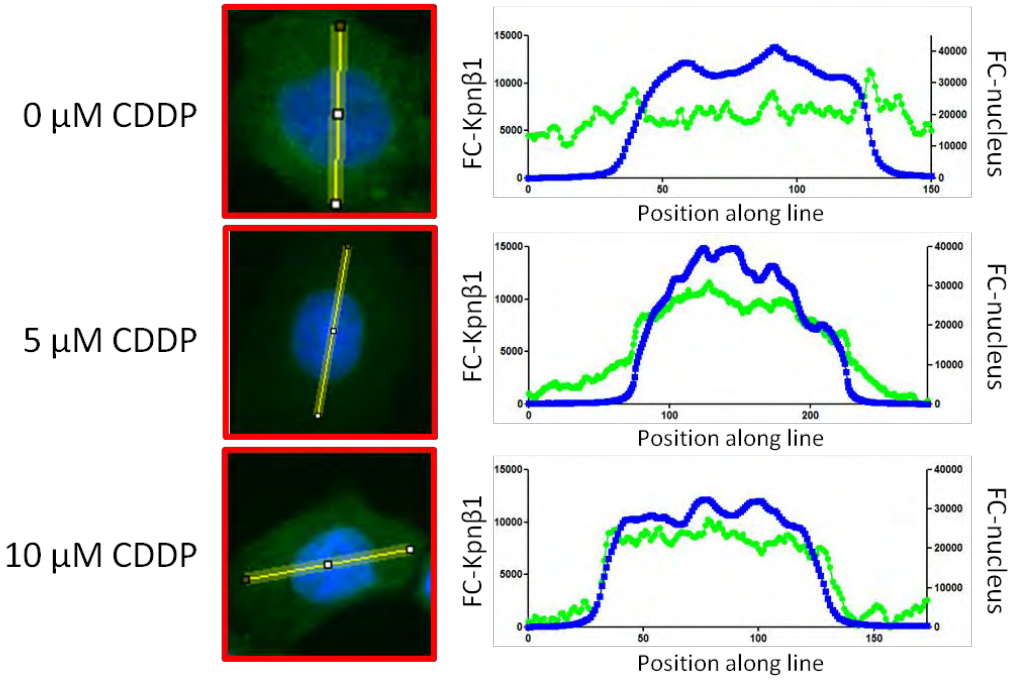
0 μM CDDP
5 μM CDDP
10 μM CDDP
FC-Kpnβ1
FC-nucleus
Position along line

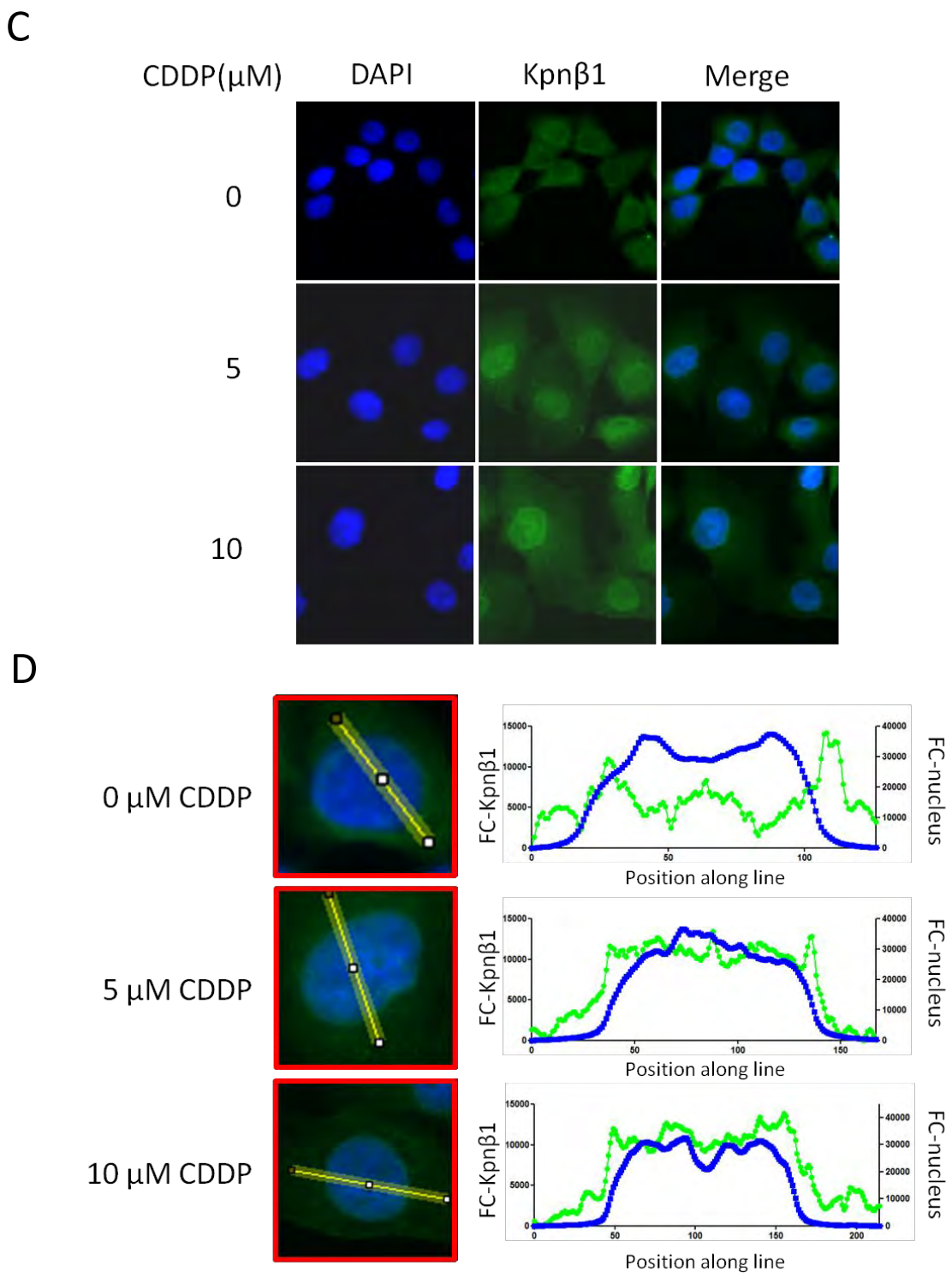

Figure 3.12. CDDP treatment induced nuclear accumulation of Kpnβ1 in OVCAR4 and OVCAR5 cells. Cells were treated with CDDP for 24 hours, followed by fixation and staining with FITC (Kpnβ1) and DAPI (nucleus). Images were captured using a fluorescent microscope and a representing image for each treatment was shown for OVCAR4 (A) and OVCAR5 (C) cells. Correlation between FITC (Kpnβ1) and DAPI (nucleus) fluorescence intensity were performed using ImageJ for OVCAR4 (B) and OVCAR5 (D) cells. The experiment was repeated two independent time, and representative images from one experiment is shown.

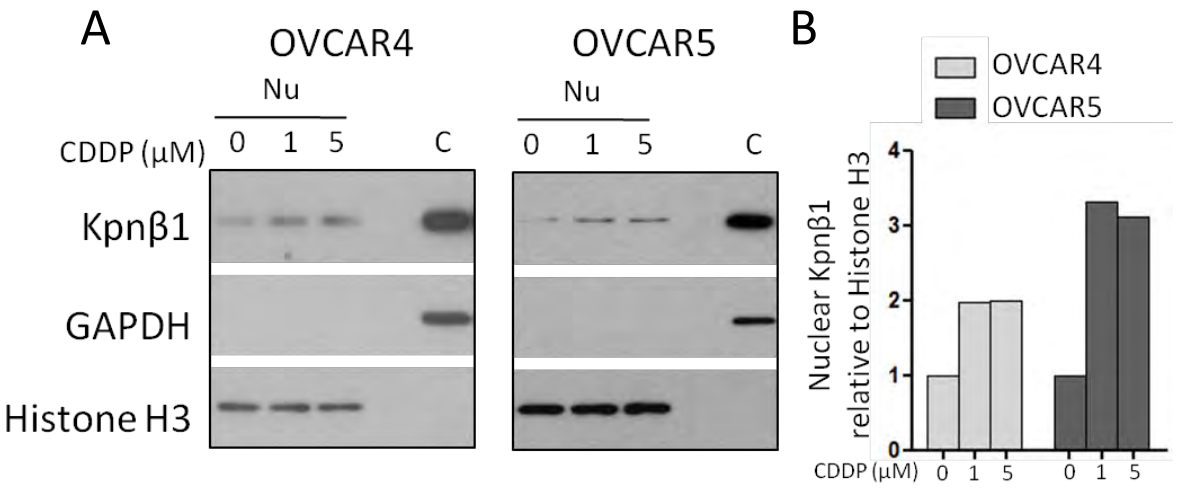

Figure 3.13. CDDP treatment led to increased nuclear Kpnβ1. Western blot analysis of nuclear proteins (Nu) treated with CDDP for 24 hours in OVCAR4 and OVCAR5 cells. GAPDH and Histone H3 serve as cytoplasmic and nuclear loading controls, respectively, and a cytoplasmic fraction 'C' was included to confirm non-cross contamination of the two cellular compartments. Results were densitometrically quantified and shown as Kpnβ1/Histone H3, relative to the untreated in each cell line (B). Results shown are representative of experiments repeated three independent times.

3.2.6. INI-43 pre-treatment reduced CDDP-induced nuclear import of Kpnβ1

We have shown so far that OVCAR4 and OVCAR5 cells responded to CDDP treatment by elevating Kpnβ1 expression as well as nuclear accumulation. We have also presented evidence showing that nuclear import inhibition by INI-43, whose action is likely mediated through Kpnβ1, sensitized ovarian cancer cells to CDDP. Based on these, we next investigated whether, and how, INI-43 affected CDDP-induced alternations in Kpnβ1.

To do this, we used immunofluorescence to examine Kpnβ1 distribution via an Alexa-Fluor 647 labelled antibody. Cells were pre-treated with DMSO or INI-43 for 2 hours, followed by 24 hours of CDDP treatment (with the DMSO or INI-43 kept in the media). Cells were then fixed and stained with the Kpnβ1 primary antibody and fluorescently labelled secondary antibody. Control (untreated) cells and cells treated only with INI-43 were included for comparison. Images were then captured using a

fluorescent microscope and analyzed by a scoring system where cells were categorized into three different populations: (i) where Kpnβ1 fluorescence intensity was higher in the cytoplasm (cytoplasmic), (ii) where Kpnβ1 fluorescence was higher in the nucleus (nuclear), or (iii) where Kpnβ1 was equally distributed between the two compartments, including those with strong peri-nuclear signal (equal distribution). One-hundred cells were scored for each treatment (Fig. 3.14), and numbers are tabulated in Table 3.1.

Table 3.1. Cellular distribution of Kpnβ1 after treatment with INI-43, CDDP or a combination of both

Treatment		Kpnβ1 distribution (%)		
INI-43 (μM)	**CDDP (μM)**	**Cytoplasmic**	**Nuclear**	**Equal distribution**
0	**0**	31	5	64
5	**0**	81	8	11
10	**0**	90	2	8
0	**5**	18	42	40
5	**5**	57	11	32
10	**5**	68	4	28
0	**10**	7	85	8
5	**10**	29	35	36
10	**10**	60	8	32

Data shown are quantification of 100 cells from multiple field of views photographed using a fluorescent microscope for each treatment.

Without any treatment, Kpnβ1 was present in both cellular compartments with roughly equal intensity for the majority of the cells (64%, Fig. 3.14.A), suggesting an equal distribution. Kpnβ1 became predominantly cytoplasmic with INI-43 treatment (81% and 90% for 5 μM and 10 μM, respectively, Fig. 3.14.A). Without INI-43 pre-treatment, 5 μM CDDP markedly increased the percentage of cells showing nuclear Kpnβ1, from 5% to 42%. On the other hand, pre-treatment with INI-43 decreased CDDP-induced Kpnβ1 nuclear localization in a concentration dependent manner - from 42% in the single treatment to 11% and 4% for 5 μM and 10 μM INI-43 pre-treatment, respectively. The same was observed when cells were treated with 10 μM CDDP - whilst single treatment led to 85% of the cells showing nuclear Kpnβ1, INI-43 pre-treatment reduced it to 35% and 8% for 5 μM and 10 μM INI-43 pre-treatment, respectively. A representative image for each treatment is shown, and the fluorescence intensities for Alexa-647 (representing Kpnβ1 concentration) and DAPI were quantified as previously described (Fig. 3.14.B and C). Fluorescence quantification showed that in the untreated cells, Kpnβ1 fluorescence intensity was poorly associated to DAPI intensity, suggesting that Kpnβ1 was not particularly localized to either compartment (Fig. 3.14.C). INI-43 treated cell showed a clear decrease in Kpnβ1 intensity where DAPI intensities were maximal, suggesting decreased Kpnβ1 localization in the nucleus. In the CDDP-only treated cell, Kpnβ1 and DAPI fluorescence signal exhibited similar trends, suggesting higher Kpnβ1 in the nucleus. Lastly, in the combination treated cell, a profile similar to the INI-43 only treated cell was observed, whereby the nuclear concentration of Kpnβ1 was lowest in the nuclear region (Fig. 3.14.C). These plots supports the accuracy of the scoring system which was carried out visually. Taken together, these results showed that INI-43 pre-treatment suppressed the CDDP-induced nuclear accumulation of Kpnβ1.

A

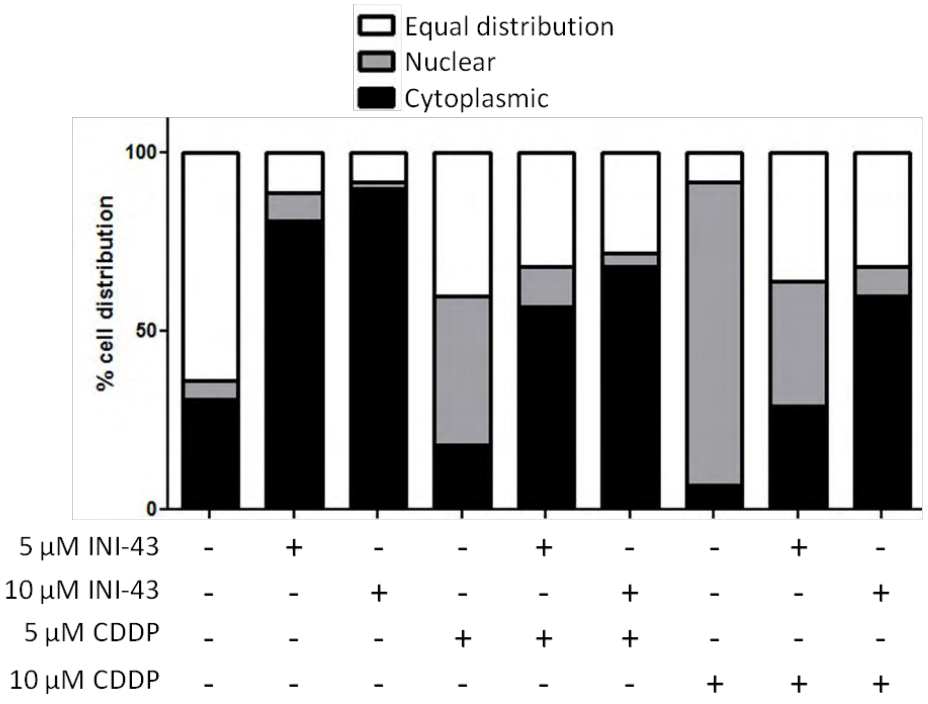
Equal distribution
Nuclear
Cytoplasmic
% cell distribution
100
50
0
5 μM INI-43 - + - - + - - + -
10 μM INI-43 - - + - - + - - +
5 μM CDDP - - - + + + - - -
10 μM CDDP - - - - - - + + +

B

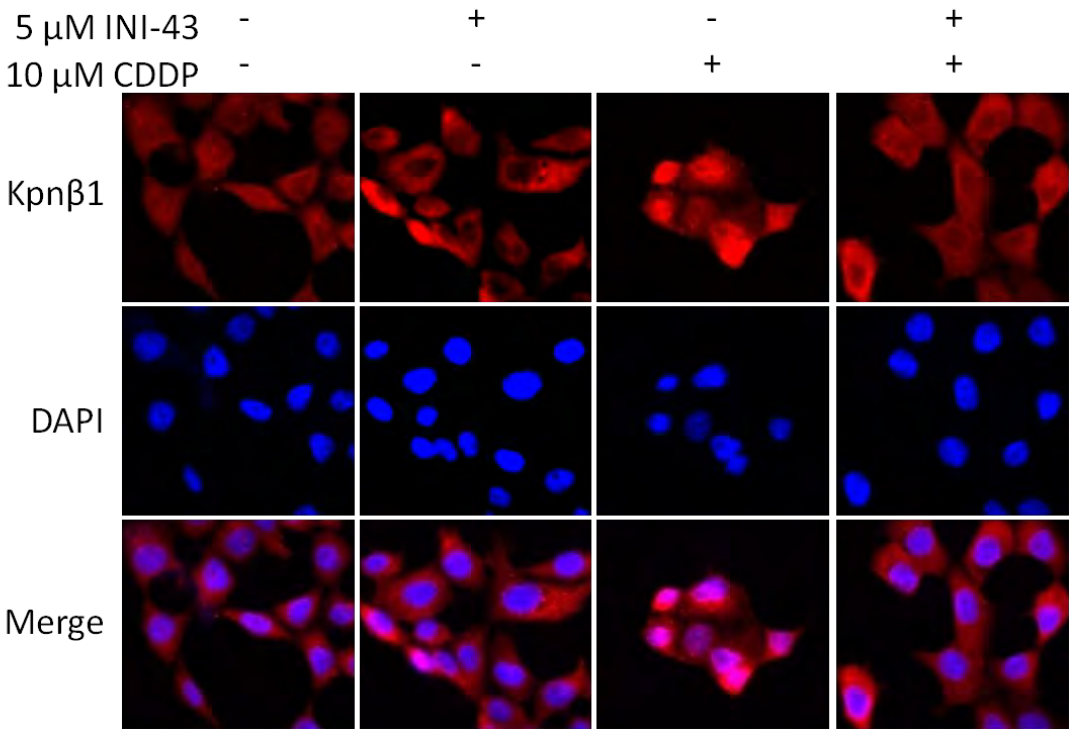
5 μM INI-43 - + - +
10 μM CDDP - - + +
Kpnβ1
DAPI
Merge

C

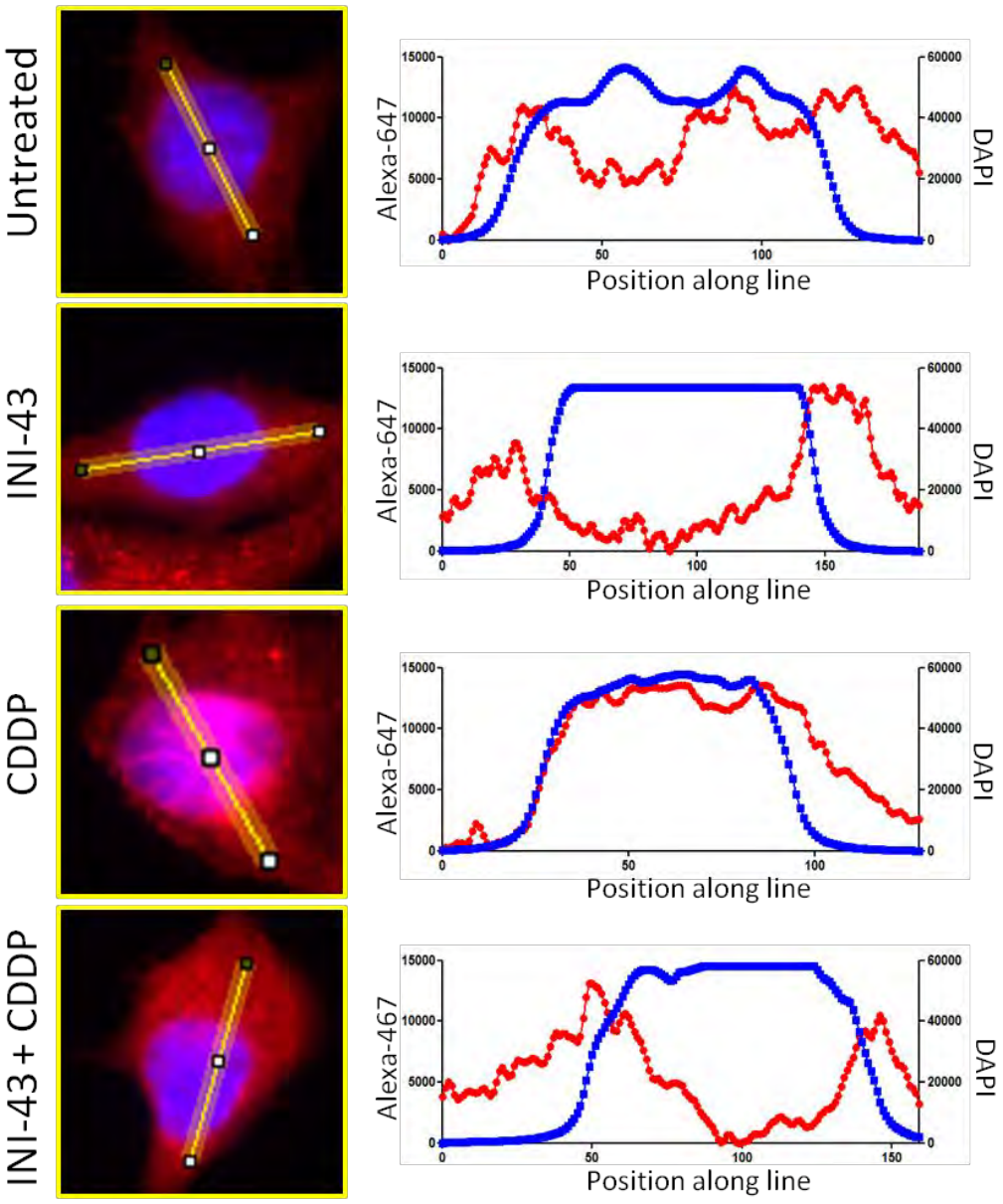

Figure 3.14. INI-43 pre-treatment suppressed CDDP-induced nuclear accumulation of Kpnβ1. OVCAR5 cells were subjected to INI-43 only, CDDP or a combination of INI-43 and CDDP as previously described. Cells were then fixed and Kpnβ1 was stained with Alexa-647, and Kpnβ1 localization was analyzed using fluorescent microscopy. For each treatment, 100 cells were scored either as showing nuclear Kpnβ1, cytoplasmic Kpnβ1 or even distribution of Kpnβ1 (A). A representative image for each type of treatment is shown (B), and the fluorescence intensity for Kpnβ1 (Alexa fluor-647) and the nucleus (DAPI) are plotted as previously described (C). Results showed that INI-43 pre-treatment decreased CDDP-induced nuclear import of Kpnβ1.

3.3. Discussion

An effective combination therapy is one where using both drugs together provides an outcome that is greater than the combined effect of both drugs when used alone. In this chapter, we presented evidence showing that a combination treatment where cancer cells are first exposed to INI-43 at a sub-lethal concentration sufficient to reduce nuclear import, followed by CDDP treatment resulted in greater killing effect compared to the combined effect of both drugs when used alone. Furthermore, the enhanced cell death occurred via the apoptotic pathway, a desired mechanism for cell death in anti-cancer therapy.

As previously discussed, INI-43 is a small molecule identified based on its predicted ability to bind to functional sites of Kpnβ1, thereby acting as an inhibitor of Kpnβ1. Data generated from our laboratory have shown that INI-43 manifested inhibitory effects on the nuclear import of various transcription factors, including AP1, NFκB and NFAT in cervical cancer cells[333]. These results suggest that INI-43 decreases nuclear import via interfering with Kpnβ1 function, as those are all known cargoes of Kpnβ1. The role of INI-43 on nuclear transport in ovarian cancer, however, has not been explored to date. Here, we report novel findings showing that it affected the cellular distribution of mCherry protein tagged with the classical NLS, which under normal circumstances accumulates in the nucleus via Kpnβ1/Karyopherinα dependent importing activity. In INI-43 treated cells, we observed increased cytoplasmic retention of NLS-mCherry, confirming that INI-43 is interfering with the nuclear import system in ovarian cancer. Furthermore, the localization of Kpnβ1 itself was altered by INI-43 treatment, suggesting that INI-43 interferes with nuclear import via Kpnβ1 in ovarian cancer cells.

INI-43 treatment, as well as Kpnβ1 knock-down both enhanced CDDP sensitivity in ovarian cancer cells, which was evident through the decreased viability and increased apoptosis. The degree of this enhancement is more prominent in Kpnβ1 knock-down cells compared to INI-43 pre-treated cells, which is likely due to the greater inhibitory effect achieved with 20 nM siRNA compared to the dose of INI-43 used in the experiments.

We also report elevated Kpnβ1 levels and increased nuclear accumulation in response to CDDP treatment, and this could be interpreted in different ways. Firstly, the increased expression could suggest increased reliance on Kpnβ1 function under DNA damage conditions. However, the general consensus is that nuclear trafficking is repressed in stressed cells[381-383]. Whilst this may seem contradictory to our findings, there could be alteration in transport substrate specificity under DNA damage conditions, so that although the overall nuclear trafficking activities are reduced, trafficking of selected proteins could still be elevated. This is supported by two factors; firstly, Kodiha *et al*. showed that although nuclear import was repressed in response to oxidative stress, it was not completely abolished and some facilitated nuclear import is still supported by the cell[381]. Secondly, nuclear trafficking of various proteins have been reported to be induced by stress signals[384-387]. The alteration in substrate specificity may derive from modifications of the substrate themselves rather than the nuclear transporters, but importantly, they still rely on the transporters for appropriate localization. These findings suggest that under stressed conditions, even though nuclear transport machinery may be repressed but they still play important roles in regulating stress response.

Interestingly, Kodiha *et al.* demonstrated that Kpnβ1 was more prone to proteosme-dependent degradation under oxidative stress conditions leading to decreased levels; however, their results were obtained after one hour exposure to oxidative stress. Our observation of elevated Kpnβ1 24 hours after CDDP treatment could be a result of later events occurring in the stress response

pathway. Alternatively, it could be a result specific to stress induced by CDDP-treatment, as CDDP specifically induces DNA damage whereas the oxidants have damaging effects on a broader spectrum.

We also demonstrated increased nuclear accumulation of Kpnβ1 after CDDP treatment. In the cargo import process, whether executed with or without Karyopherinα, Kpnβ1 itself needs to enter the nucleus, and may then stay in the nucleus or exit the nucleus coupled with RanGTP. Kpnβ1 is thus constantly shuttled between the two cellular compartments, which is supported by our observation that under normal conditions, it is present in both the cytoplasm and the nucleus, with some accumulation at the peri-nuclear region, possibly associated with the Nups during transit. The increased nuclear accumulation of Kpnβ1 observed after CDDP treatment could result from increased nuclear import rate or decreased nuclear export by RanGTP. As the global nuclear trafficking is reported to be repressed in stressed cells, it is more likely that the increased Kpnβ1 nuclear accumulation is due to its decreased export rather than increased nuclear import. Indeed, similar findings have been reported in oxidative stressed cells, which was attributed to a dissipation of RanGTP gradient[381]. However, whether this is true in our CDDP-treated ovarian cancer system remain to be elucidated. Our findings showed that INI-43 interfered with Kpnβ1 translocation into the nucleus after CDDP treatment, and that this associated with greater cell death as observed in the combination treatment. We speculate that this relocalization may be a 'rescue mechanism' associated with cell survival, and may be related to altered importing activities of Kpnβ1. There exist, however, a possibility that these two observations were two independent events. If Kpnβ1 accumulation inside the nucleus in CDDP treated cells was a result of loss of RanGTP gradient, this would prevent nuclear exit of most Kpnβ1 (possibly contributing to the decreased global importing activity), and INI-43 treatment would simply diminish the importing activity of the residual Kpnβ1 that is still able to exit the nucleus. So even though an antagonistic effect on Kpnβ1 localization was observed with INI-43 and CDDP treatments, INI-43 in essence just suppressed nuclear import

irrespective of CDDP-induced nuclear accumulation of Kpnβ1. Furthermore, the increased Kpnβ1 levels after CDDP treatment could be a response to ensure that sufficient importing activity can still occur even when the majority of the Kpnβ1 is trapped in the nucleus.

A question that arises, is how the perturbation of Kpnβ1 function affects the cellular response to CDDP, resulting in enhanced killing. Recent studies have suggested targeting DNA repair pathways in combination with DNA-damaging agents to achieve synergism[388, 389], which highlights the potential role of the DNA-repair function in anti-cancer therapy. Indispensible to this process is the nuclear transport function, which plays an integral part in DNA-repair, as re-organization of protein distribution is known to be a response of cells under replication stress, such as DNA damage caused by CDDP[390]. Indeed, various proteins involved in DNA repair pathways have been reported to undergo nucleo-cytoplasmic translocations when exposed to DNA-damaging agents. For example, the p38 Mitogen-Activated Protein Kinase (MAPK)[391], both Rad51 and its interacting protein Rad51C[392], p21[393], the damage-specific DNA Binding Protein (DDB)[394], and the MDM2 homolog protein MDMX[395] are all DNA damage response proteins known to localize to the nucleus after DNA damage. On the other hand, the cell cycle regulator Cdc25[396] and precursor microRNAs[397] have been reported to show accelerated export out of the nucleus upon DNA damage. All of these findings highlight the importance of the nuclear transport function in response to stressful conditions.

Whilst Kpnβ1 is not responsible for the entire transport network within the cell, it is a key mediator of nuclear import for macro-molecules, which can occur with or without the Karyopherinα adaptors. This could explain why stressed cells become more reliant on the nuclear import (and export) system, as this allows them to redistribute proteins to the right locations where they can react to the stress appropriately. Supporting this, various DNA damage response proteins possess NLS, amongst which many even contain multiple NLSs, including ERCC6, XPC and Rep-3/Duc-1[398]. More recently it has

been reported that a non-classical bipartite NLS, which was previously thought to be absent, has been identified in XCRR1, another DNA-repair protein[399]. As the NLS is a sequence used for cargo recognition by Kpnβ1/Karyopherinα, these findings suggest that those proteins are imported in a Kpnβ1-dependent manner. This may provide an explanation as to why Kpnβ1 inhibition via siRNA or INI-43 resulted in greater killing at the same dosage of CDDP, and may result from an impaired response mechanism of cancer cells with its Kpnβ1 function is deprived.

In addition to its nuclear importing function in interphase cells, Kpnβ1 is also an important regulator of many aspects of mitosis, and manipulation of its expression, whether elevated or repressed causes mitotic defects[282, 286, 300]. Kpnβ1 inhibition via siRNA or INI-43 could therefore sensitize cancer cells to CDDP through inducing genomic instability, which could render cancer cells more sensitive to DNA damage.

In this chapter, we presented novel findings to suggest that combining nuclear import inhibition with a DNA-damaging agent could have enhanced therapeutic benefits. Whilst CDDP alone has been used widely to treat a variety of cancers, its off-target effects are a long-standing challenge in cancer therapy[400, 401]. Lowering the dose of CDDP and combining it with a nuclear import inhibitor could provide viable alternatives to treatment and could be useful in minimizing the off-target effects of CDDP, warranting further studies.

CHAPTER 4

INVESTIGATING THE COMBINATION TREATMENT OF INI-43 AND CDDP IN CERVICAL CANCER

4.1. Introduction

Cervical cancer is the third most common cancer in women worldwide, and according to the International Agency for Research on Cancer (World Health Organization), it has been estimated that in the year 2020, over 120 000 diagnosis and over 75 000 deaths will occur in Africa alone. The current treatment options for cervical cancer include surgery, radiation therapy, chemoradiation (combination of chemotherapy and radiation) and chemotherapy. Early stage tumours are frequently treated with surgery and radiation therapy, and locally advanced cancers are treated with chemoradiation. Metastatic, late stage cervical cancer appearing at distant sites cannot be surgically removed, in which case the use of chemotherapeutic agents becomes necessary[402]. In addition, recurrent disease with increased chemoresistance and decreased response rate in cervical cancer patients present further clinical difficulty as treatment options become limited[403].

Chemotherapeutic options include several platinum-based, anthracycline and microtubule targeting agents[404]. While CDDP is considered the most effective and form part of the standard care[404], its use is often compromised due to its toxicity profile and resistance in previously irradiated patients[405, 406]. Combination chemotherapy is an effective approach to increase treatment response, and survival advantage has been demonstrated for platinum-based combinations incorporating Topotecan, Irinotecan, Gemcitabine and Docetaxel compared to the use of single agents[407-410]. Recently,

sensitization of cervical cancer cells to CDDP has been demonstrated using natural-derived compounds such as Melatonin, Epigallocatechin Gallate and Genistein, as well as the autophagy inhibitor 3MA *in vitro*[311, 411-413]. These findings demonstrated potentials for exploring novel CDDP-based combination chemotherapy which could increase the effectiveness of CDDP treatment in cervical cancers, or alternatively, enable lower doses of CDDP to minimize associated toxicity.

We have recently reported data supporting the role of INI-43 as an inhibitor of nuclear import potentially mediated through Kpnβ1[333]. Furthermore, INI-43 treatment sensitized ovarian cancer cells to CDDP-induced death signals. This proposed a novel approach of combining nuclear import inhibition and CDDP in the treatment of ovarian cancer. In this chapter, we investigated the combination of INI-43 and CDDP treatment on a panel of cervical cancer cell lines. In addition, the molecular pathways underlying cancer cell's response to CDDP in Kpnβ1-inhibited cells was investigated. This aspect of the study focussed on the HPV18 positive HeLa cells and HPV16 positive SiHa cells, the latter having been reported as CDDP-resistant[414]. We used the same treatment protocol as previously described, where combination treatment refers to pre-exposing cells to a dose of INI-43 sufficient to reduce nuclear transport, but insufficient to induce cell death on its own, followed by CDDP treatment.

4.2. Results

4.2.1. INI-43 treatment sensitized cervical cancer cells to CDDP

To investigate whether nuclear import inhibition via INI-43 sensitized cervical cancer cells to CDDP, we investigated the effect of single and combination treatments. Briefly, cells were pre-treated with vehicle control DMSO (single treatment) or sub-lethal dose of INI-43 (combination treatment) for 2 hours before CDDP treatment, followed by various different experiments to determine CDDP sensitivity. The pre-treatment was performed for two hours as we have recently shown that INI-43 repressed nuclear import of Kpnβ1 cargoes within 1.5 hours in cervical cancer cells[333].

4.2.1.1. INI-43 pre-treatment decreased CDDP IC_{50} in HeLa and SiHa cells

To examine whether nuclear import inhibition sensitized cervical cancer cells to CDDP, CDDP IC_{50} values were determined for control DMSO or INI-43 pre-treated cells. Of the four cell lines tested, both HeLa and SiHa cells showed significant decreased in CDDP IC_{50} values when pre-treated with INI-43 in a concentration dependent manner. (Fig. 4.1.A). CaSki cells showed a smaller reduction of CDDP IC_{50} when pre-treated with 5 μM INI-43, although the difference was not significant. The C33A cells did not show significant changes in CDDP sensitivity when pre-treated with INI-43 at both concentrations tested (Fig. 4.1.A). In HeLa cells, the average CDDP IC_{50} was approximately 18.0 μM, which was decreased to 11.8 μM and 10.1 μM after 2.5 μM and 5 μM INI-43 pre-treatment, respectively. Similarly for SiHa cells, CDDP IC_{50} reduced from 30.8 μM for single treatment to 23.0 μM and 16.9 μM for 2.5 μM and 5 μM INI-43 pre-treated cells, respectively. This effectively represented 44% and 46% decrease in CDDP IC_{50} when pre-treated with 5 μM INI-43 for HeLa cells and SiHa cells. A representing CDDP IC_{50} determination plot for single and combination treatment is shown for each cell line (Fig. 4.1.B).

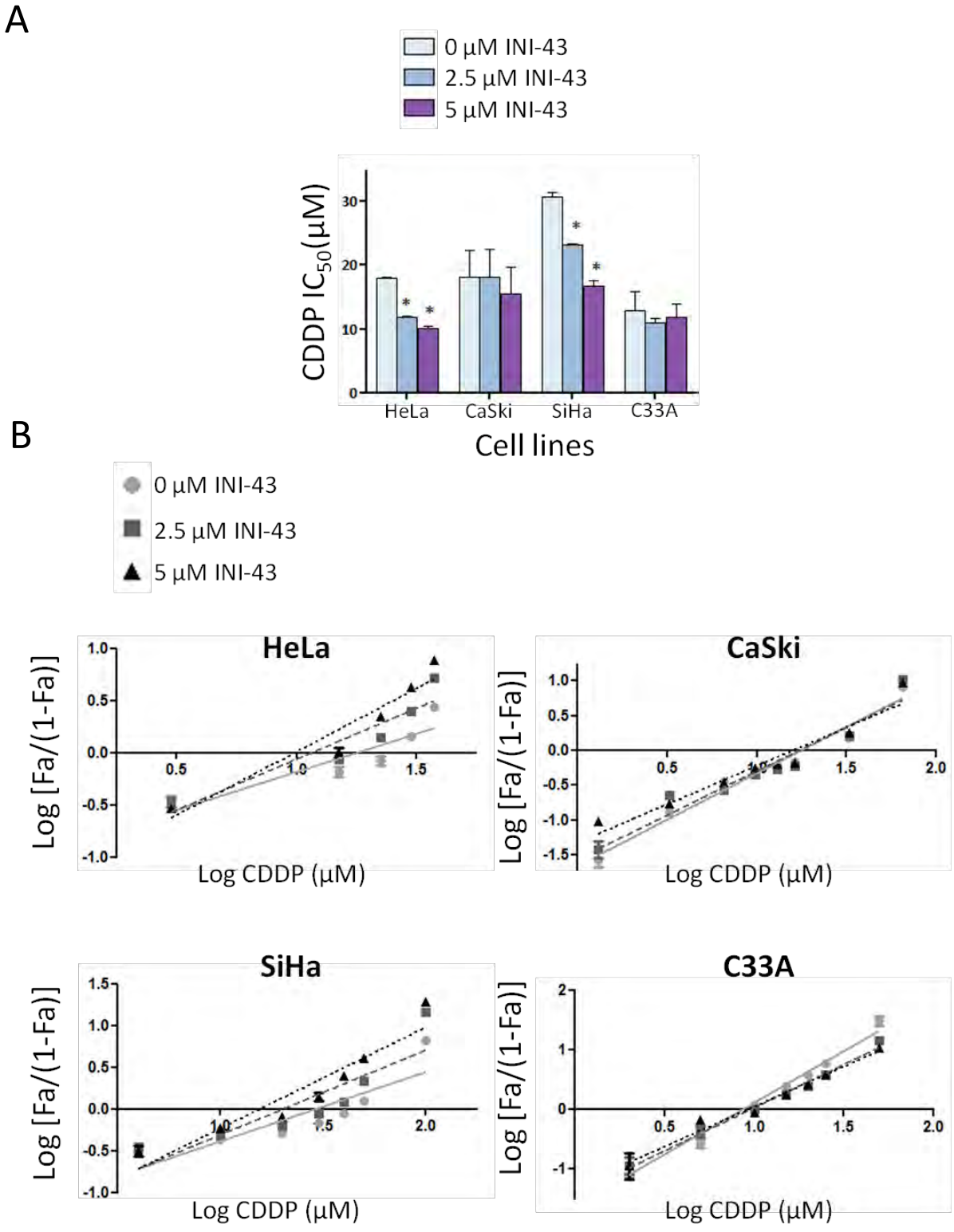

Figure 4.1. CDDP IC_{50} in cervical cancer cells with or without INI-43 pre-treatment. CDDP IC_{50} values were determined for cervical cancer cell lines HeLa, Caski, SiHa and C33A in single and combination treatments as previously described (A). Results shown are mean ± SEM of three independent experiments, each performed with 6 replicates, and the mean ± SEM for one representing experiment is shown for each cell line (B), *$p < 0.05$.

Interestingly, SiHa cells which has been reported as a CDDP-resistant cervical carcinoma showed a CDDP IC_{50} that is approximately 1.5-2 fold higher compared to HeLa, CaSki and C33A[414, 415]. As SiHa cells showed significantly increased sensitivity to CDDP after INI-43 pre-treatment, this suggests that the combined use of these two agents could be an effective approach in treating CDDP-resistant cervical cancer cells.

To confirm the IC_{50} results, cell viability was examined in response to CDDP with or without INI-43 pre-treatment. Cells were pre-treated with DMSO or 5 μM INI-43 for 2 hours prior to CDDP treatment at their respective CDDP IC_{50} values, and viable cells were quantified using the MTT assay. The results showed that in HeLa, CaSki and SiHa cells, 5 μM INI-43 pre-treatment enhanced the cell killing effect of CDDP, whereby cell viability was significantly lower in the INI-43 pre-treated cells compared to the control cells (Fig. 4.2, A-C). Treatment with 5 μM INI-43 alone had negligible effects on cell viability (Fig. 4.2). The most significant effects were observed in HeLa and SiHa cells, with 67% and 50% reductions in cell viability in the combination treatment, respectively (Fig. 4.2.A and C). CaSki cells showed enhanced CDDP effect, but to a lesser degree, with a 28% decrease in cell viability for combination treatment compared to single treatment (Fig. 4.2.B). In line with the IC_{50} results, C33A cells showed no further reduction in cell viability when subjected to combination treatment (Fig. 4.2.D).

4.2.1.2. INI-43 pre-treatment enhanced CDDP-induced apoptosis in HeLa and SiHa cells

To determine whether the decreased cell viability observed in the combination treatment was a result of increased apoptosis, caspase-3/7 activity and PARP cleavage were examined. Various signals can trigger an apoptotic response, which leads to a series of well-coordinated events culminating in caspase-3/7 activation, leading to cleavage of various substrates including PARP[416].

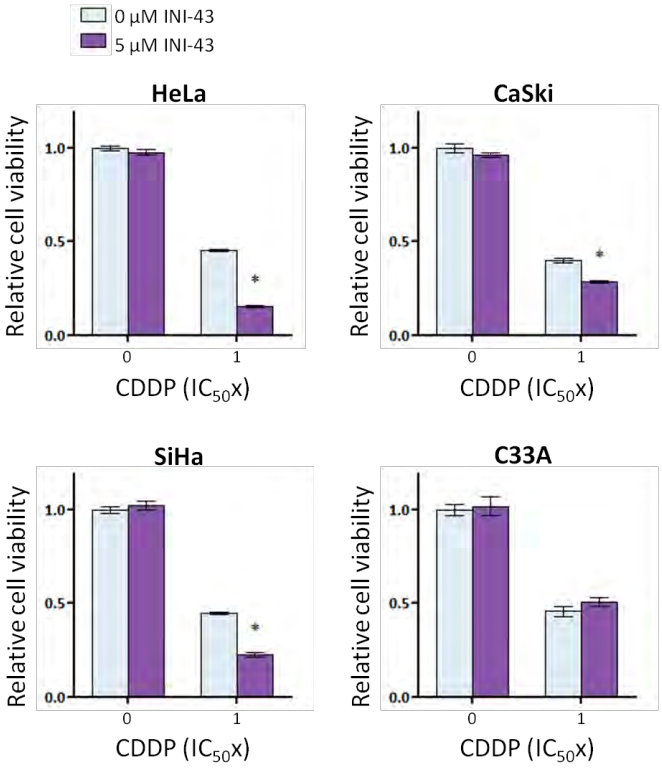

Figure 4.2. The effect of single and combination treatment of cervical cancer cell viability. Cervical cancer cell lines HeLa, CaSki, SiHa and C33A were seeded overnight, and cells were sequentially treated with 5 µM INI-43 or DMSO followed by CDDP as previously described. Viable cells were determined 48 hours after CDDP treatment, and expressed as a normalized value to the viability of untreated cells. Results shown are mean ± SEM of 6 replicates, and each experiment was repeated at least twice, *$p < 0.05$.

Caspase-3/7 activation and PARP cleavage thus serve as good indicators of apoptosis. SiHa cells were subjected to single or combination treatment as previously described for 48 hours, and the cell lysates were harvested for caspase-3/7 assays and western blots. Results showed that CDDP-induced caspase-3/7 activity was significantly augmented by INI-43 pre-treatment, with more than two-fold increase observed after 30 µM and 60 µM CDDP treatment (Fig. 4.3.A). In line with this, enhanced PARP cleavage was observed for cells receiving the INI-43 pre-treatment, compared to those which received CDDP only (Fig. 4.3.B). Similar results were observed in HeLa cells, where INI-43 pre-treated cells showed enhanced PARP cleavage compared to their single treatment counterparts (Fig. 4.3.B). These results were densitometrically quantified and showed elevated PARP cleavage in response to INI-43 and CDDP combination treatments (Fig. 4.3.C).

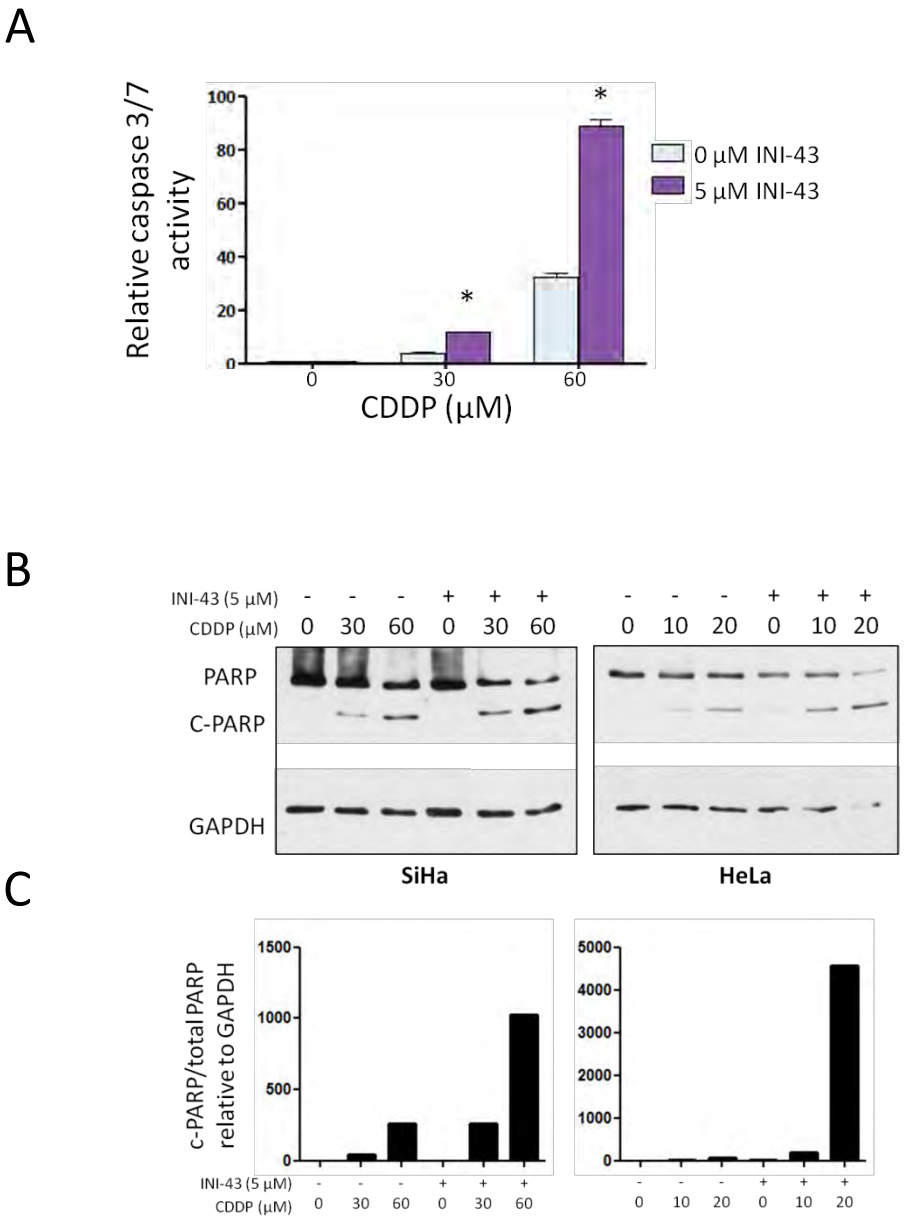

Figure 4.3. The effect of single and combination treatment on apoptosis in SiHa and HeLa cells. To determine if the enhanced effect of CDDP on cell viability observed in INI-43 pre-treated cells was due to increased apoptosis, caspase-3/7 activity and PARP cleavage were examined. The caspase-3/7 activity in SiHa cells subjected to single and combination treatment were examined using the Caspase-GloR 3/7 assay, and expressed as a normalized value to viable cells as determined by MTT assay performed in parallel (A). SiHa and HeLa cells were subjected to single and combination treatment at various CDDP concentrations for 48 hours, and PARP cleavage was analyzed by western blot, GAPDH was included for loading control (B). Densitometrical analysis of cleaved PARP relative to total PARP, normalized to GAPDH (C). Results shown are mean ± SEM of triplicates (A), and each experiment was repeated at least two independent times (A and B), *$p < 0.05$.

These results showed that a combination treatment where pre-exposure to INI-43 in cervical cancer cells resulted in significant enhancement of CDDP-induced cell death. This was observed in CDDP-

sensitive cell lines HeLa and CaSki, as well as the reported CDDP-resistant cell line SiHa. The concentration of CDDP needed to achieve a 50% of killing was significantly lowered, as indicated by the decrease in CDDP IC_{50}. The increased apoptotic activity shown by increased caspase-3/7 activity and PARP cleavage accounted for the decreased cell viability observed in combination treatment compared to single treatment.

4.2.2. Kpnβ1 inhibition sensitized SiHa cells to CDDP

To confirm that the enhanced cell death observed in the combination treatment was a result specific to Kpnβ1 inhibition, we investigated whether Kpnβ1 knock-down cells could similarly increase CDDP sensitivity. Control and Kpnβ1 siRNA transfected SiHa cells were subjected to CDDP IC_{50} determination, cell viability assay and PARP cleavage analysis.

Successful Kpnβ1 knock-down was confirmed using western blot 48 hours after transfection, at which time point CDDP treatment began (Fig. 4.4.A). The IC_{50} determination revealed that in Kpnβ1 knock-down cells, there was a reduction in CDDP IC_{50} compared to the control cells (19.3 μM versus 30.5 μM, Fig. 4.4.B), suggesting increased CDDP sensitivity in Kpnβ1 knock-down cells. Investigation of cell viability showed that Kpnβ1 knock-down cells were significantly less viable compared to control cells even without CDDP treatment (data not shown). To eliminate the cell death that was caused by si-Kpnβ1 transfection, viable cells at each CDDP concentration was normalized to the untreated cells in each transfection group. The results showed a significant decrease in cell viability in the Kpnβ1 knock-down cells at all CDDP concentrations tested compared to the control cells (Fig. 4.4.C). To investigate whether the decreased cell viability associated with increased apoptosis, PARP cleavage was examined via western blot. The result showed enhanced cleaved PARP in Kpnβ1 knock-down cells treated with CDDP, which is particularly evident at 60 μM CDDP (Fig. 4.4.D).

Densitometrical quantification of cleaved PARP relative to total PARP confirmed this result (Fig. 4.4.E). These results showed that Kpnβ1 knock-down similarly sensitized SiHa cells to CDDP as observed with INI-43 pre-treatment, providing supporting evidence that INI-43 enhanced CDDP treatment by interfering with Kpnβ1 associated functions.

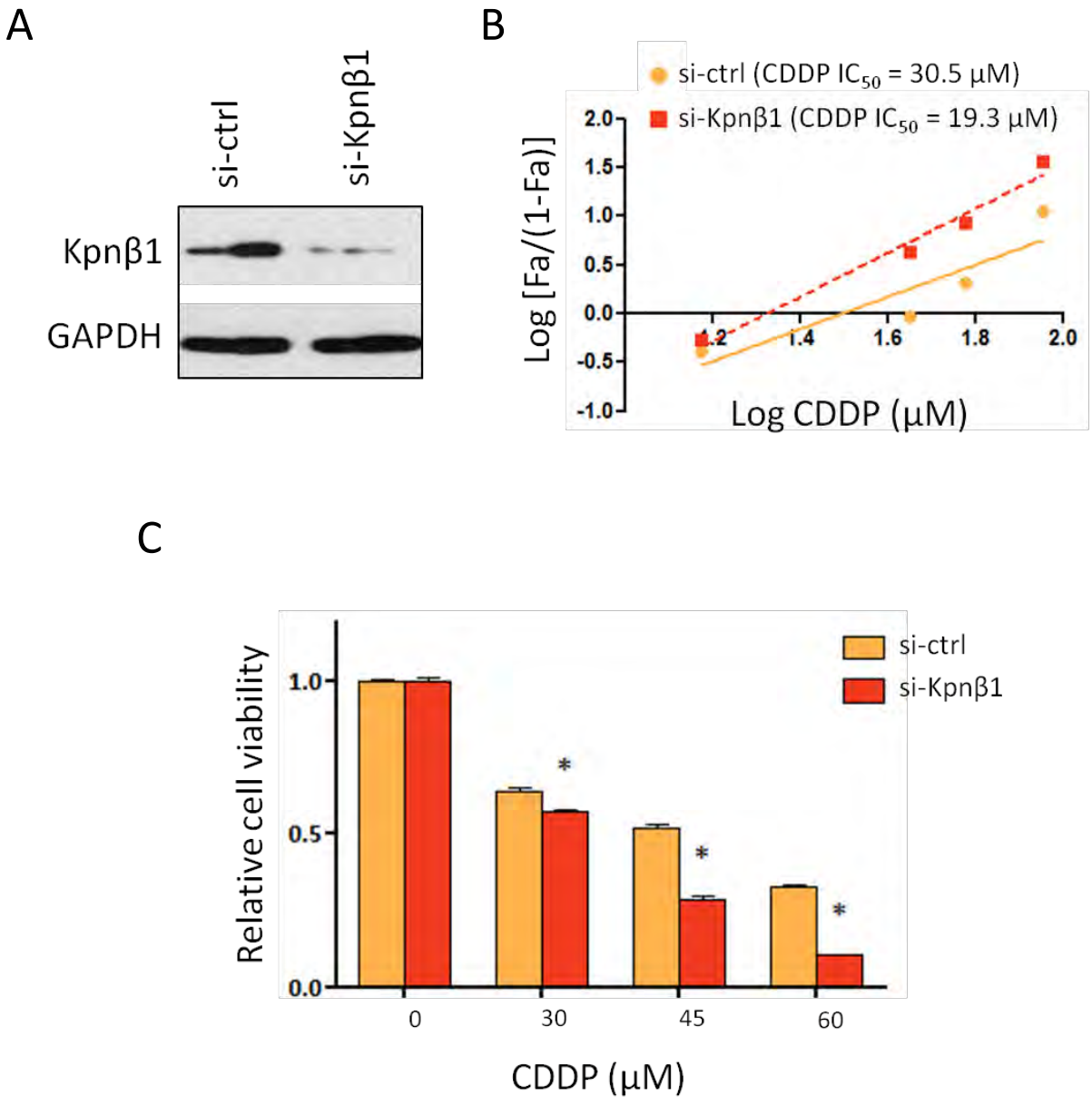

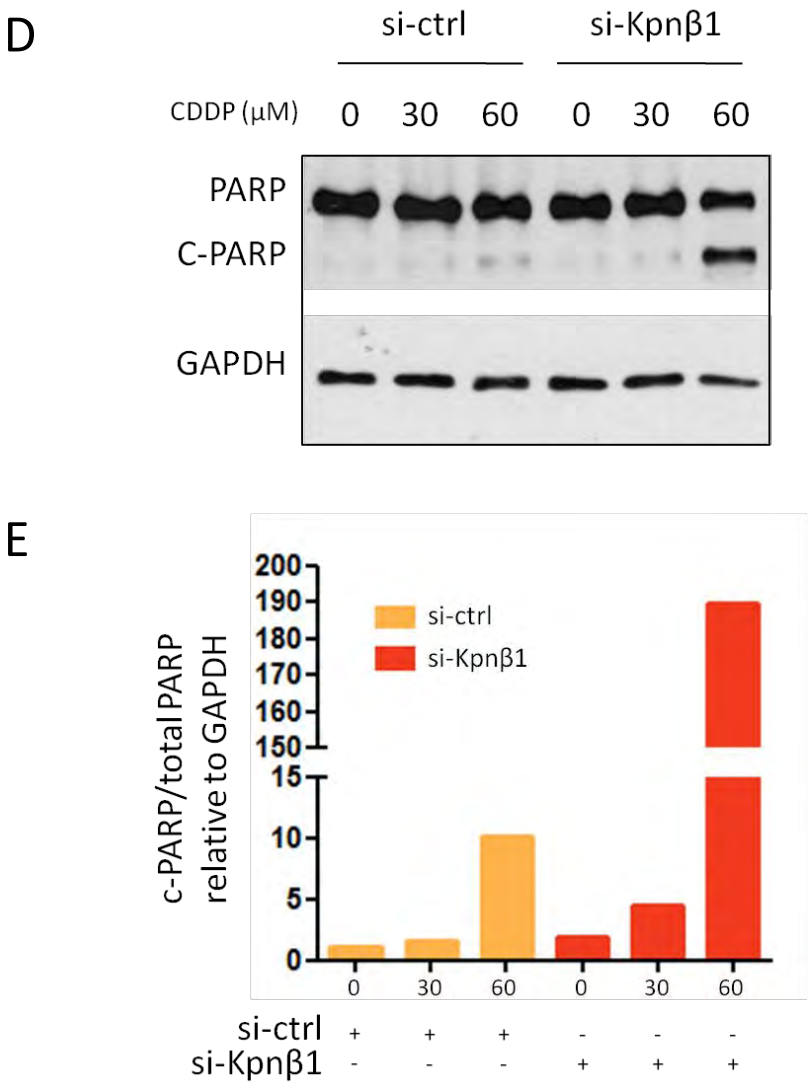

Figure 4.4. The effect of Kpnβ1 knock-down on CDDP sensitivity in SiHa cells. Cells were transfected with 20 nM of control or Kpnβ1 targeting siRNA (si-ctrl and si-Kpnβ1), and knock-down was confirmed 48 hours post transfection (A). CDDP IC_{50} was determined in si-ctrl and si-Kpnβ1 transfected cells (B), and cell viability at 1 x, 1.5 x and 2 x CDDP IC_{50} treatment were analyzed by MTT assay, and expressed as a normalized value to the viability of untreated cells in each transfection group (C). PARP cleavage was examined in si-ctrl and si-Kpnβ1 transfected cells treated with CDDP for 48 hours, with GAPDH as the loading control (D), and densitometrical quantification are shown for cleaved PARP relative to total PARP, normalized to GAPDH (E). Results shown are mean ± SEM of 6 replicates (B and C), and each experiment was repeated at least two independent times (B, C and D), $*p < 0.05$.

4.2.3. INI-43 and CDDP synergistically enhanced cell death in SiHa cells

Combination treatments can lead to various outcomes, which can generally be categorized into antagonism, additivity or synergism. Antagonism describes an interaction where two agents cancel the effects of each other, producing a combined effect less than the sum of effects produced by each individual agent when used individually. An additive effect refers to two agents producing an effect which is equivalent to the sum of effects of each when used individually. Synergism depicts a combination treatment outcome which is greater than the sum of the effects of each individual agent used independently, which is primarily what combination treatment is aiming to achieve.

Various methods have been proposed to model antagonism, additivity and synergism, of which the Chou-Talalay method has been the most widely used. This method is based on the median effect equation, where the combination index value (CI) defines the interaction of two drugs[417]. The CI is calculated using the equation $CI = \frac{CDx.A}{IDx.A} + \frac{CDx.B}{IDx.B}$, where IDx.A and IDx.B represents the concentration of each drug (A and B) needed to achieve a certain effect when used alone, and CDx.A and CDx.B refers to the dose of A and B in combination required to produce the same effect. A CI value of less than one, equal to one and greater than one suggest synergistic, additive and antagonistic interactions of the two drugs, respectively[418].

In order to determine the nature of the interaction for INI-43 and CDDP, CI values were calculated using dose-response curves, where SiHa cells were treated with INI-43 and CDDP singly and in combination, after which cell viability was determined. A range of concentrations for both drugs were used, and paired in such a way that the ratio between the two drugs remain fixed in each experiment. As the IC_{50} for INI-43 and CDDP is approximately 10 µM and 30 µM for SiHa cells, respectively, we tested INI-43:CDDP ratios of 1:3, 1:4 and 1:5 (for detail of concentrations used, see

Appendix Table A.1). Combination treatments were performed in the same way as previously described, where cells were exposed to INI-43 for 2 hours prior to CDDP treatment, and cell viability was quantified via MTT reagent 48 hours after CDDP treatment. The results showed evident enhancement of cell death in INI-43 pre-treated cells at 22.5 μM and higher CDDP concentrations for the 1:3 ratio, and 30 μM and higher CDDP concentrations for 1:4 and 1:5 ratios (Fig. 4.5.A, see arrow). For both 1:4 and 1:5 ratios, CDDP cytotoxicity was particularly amplified especially at higher concentrations of CDDP, as INI-43 alone at those concentration caused no cell death, but in combination it was able to augment CDDP-induced cell death.

Based on the viability result, CI values were then calculated for each combination ratio using the CompuSyn software (ComboSyn, Inc., Paramus, NJ). The synergistic interaction of the two drugs, which is indicated by CI values of less than one, was apparent when the fraction affected (x-axis, fraction affected of 1 = complete cell death) was greater than a threshold value indicated by X (Fig. 4.5.B). These results confirmed that INI-43 synergized with CDDP in SiHa cells at CDDP concentrations greater than 22.5 μM.

4.2.4. CDDP treatment does not alter Kpnβ1 expression and nuclear localization in HeLa and SiHa cells

In the ovarian cancer model, we found CDDP treatment led to increased Kpnβ1 expression and nuclear accumulation, suggesting that Kpnβ1 is responsive to DNA damage stress in this model. To investigate whether this is similar in cervical cancer, we investigated Kpnβ1 expression and localization in response to CDDP treatment.

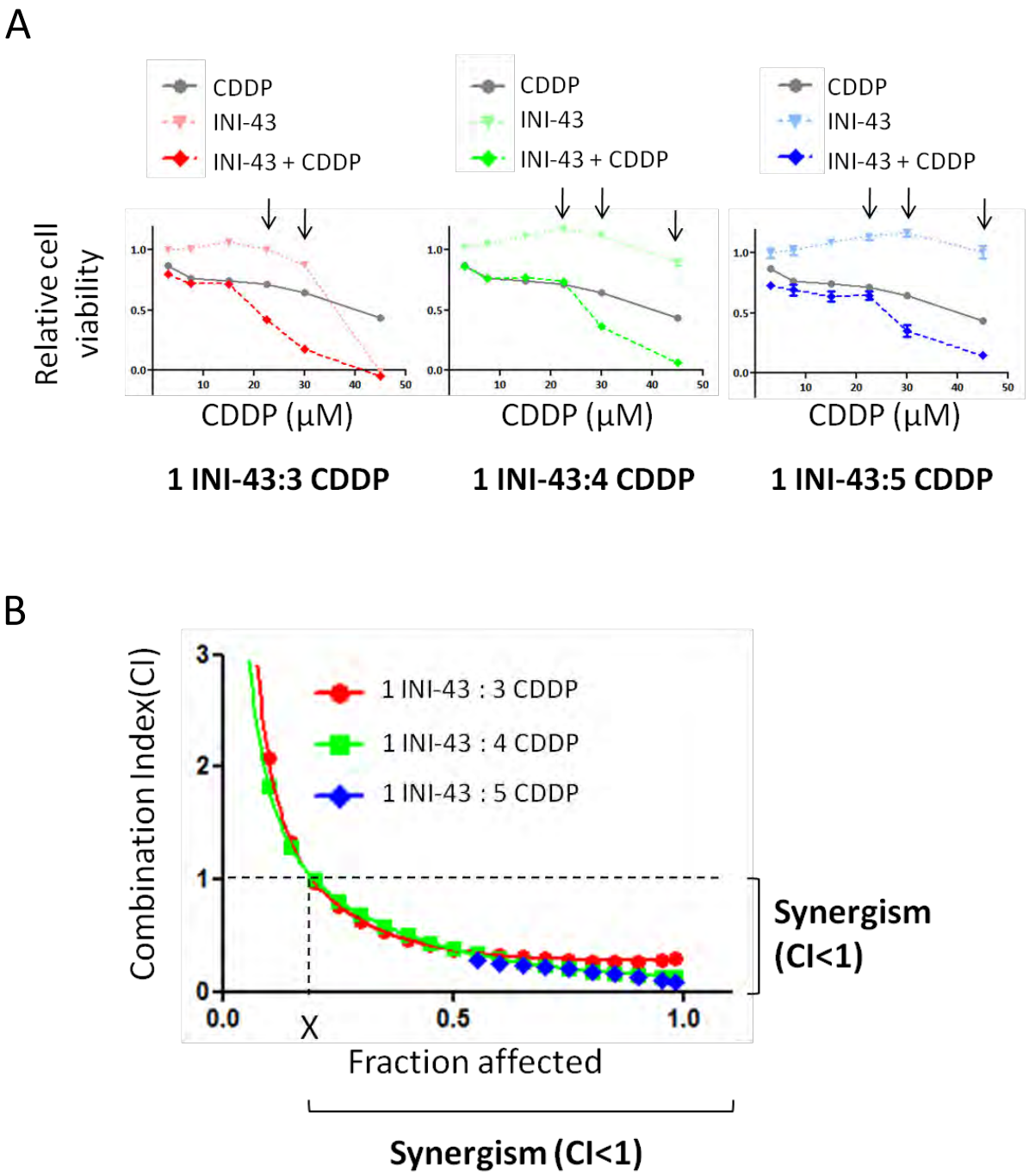

Figure 4.5. Combination index (CI) evaluation for the INI-43 and CDDP combination treatment in SiHa cells. Cells were subjected to INI-43 only, CDDP only and INI-43 plus CDDP combined treatments at INI-43:CDDP ratios of 1:3, 1:4 and 1:5 (see Appendix Table A.1 for drug concentrations used). Cell viability was assayed after 48 hours of drug treatment, and expressed as a normalized value to the untreated (A, arrows indicate enhanced cell death). The calculated CI values were plotted for each INI-43:CDDP ratio examined against the fraction affected, where fraction affected of 1 = 100% cell death (B). Results shown are mean ± SEM of 5 replicates of 1 experiment which was repeated two independent times.

HeLa and SiHa cells were treated with CDDP at their respective IC_{50} values for 24 hours, and proteins were harvested for western blot analysis using a Kpnβ1 specific antibody. To confirm that CDDP treatment was effective, γH2AX levels were examined alongside as a confirmation for CDDP-induced DNA damage. The results showed that while increased γH2AX was observed in both cell lines, Kpnβ1 expression remained unaltered (Fig. 4.6). We then examined Kpnβ1 localization in CDDP-treated HeLa and SiHa cells, using concentrations around their respective IC_{50} values. Nuclear and cytoplasmic proteins were harvested separately, and nuclear Kpnβ1 levels was analyzed by western blot. Our results revealed similar Kpnβ1 levels in the nucleus for both HeLa and SiHa cells after CDDP treatment (Fig.4.7.A). This result was independently confirmed by immunostaining and fluorescence microscopy, which showed similar Kpnβ1 distribution between control and 30 µM CDDP treated SiHa cells (Fig. 4.7.B).

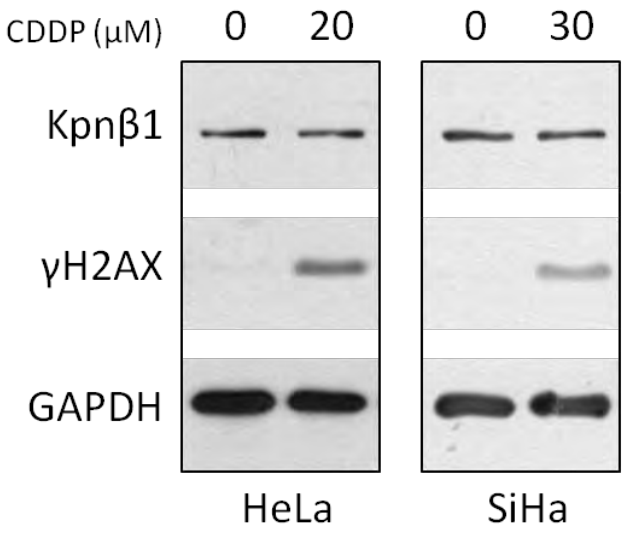

Figure 4.6. Kpnβ1 expression in response to CDDP-induced DNA damage in cervical cancer cell lines. HeLa and SiHa cells were treated with CDDP at their respective CDDP IC_{50} values for 24 hours. Protein lysate were examined for changes in Kpnβ1 level, alongside γH2AX to confirm for DNA damage by western blot. GAPDH was included for loading control. Each experiment was repeated at least two independent times.

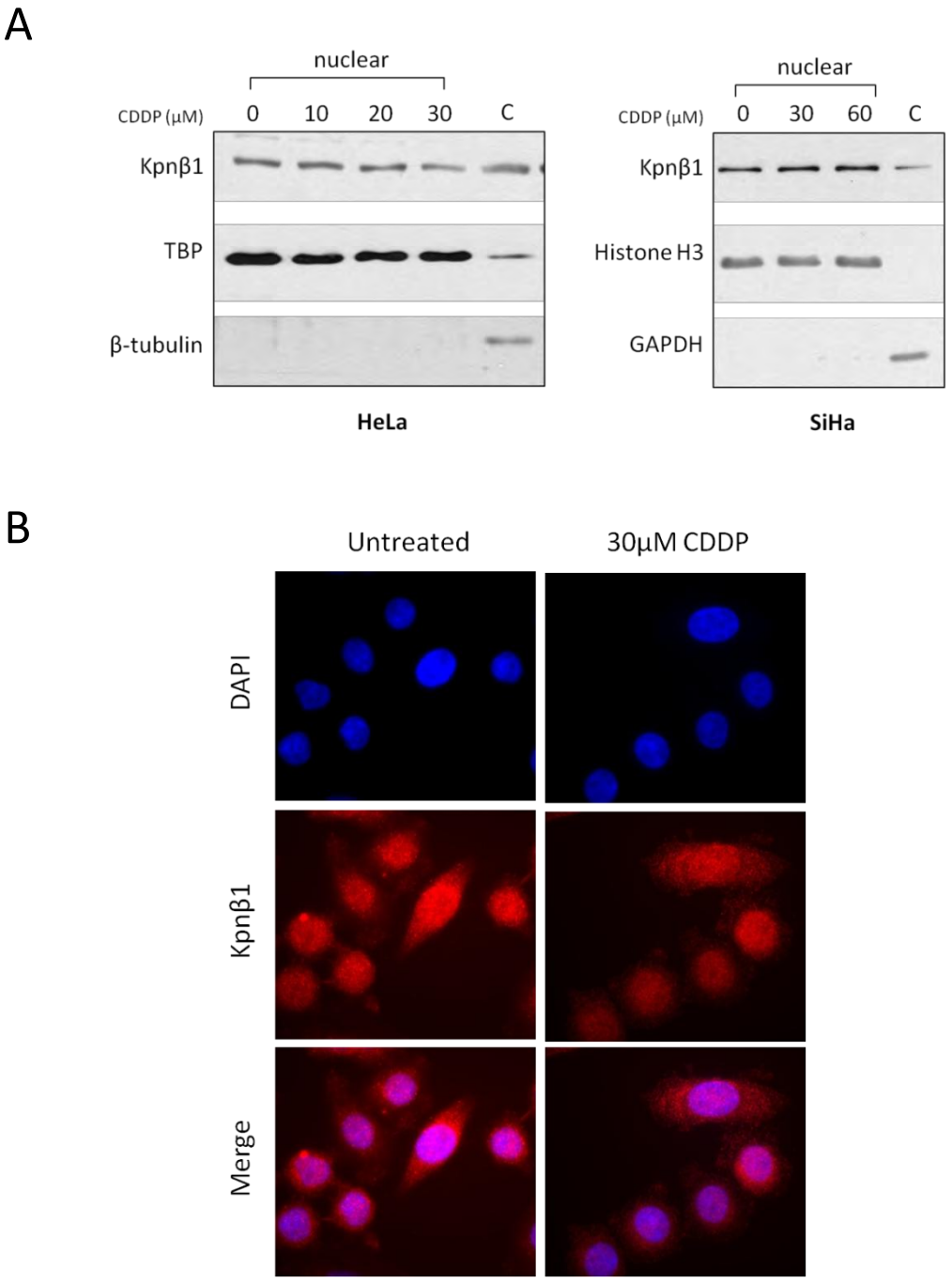

Figure 4.7. The effect of CDDP on Kpnβ1 nuclear localization in HeLa and SiHa cells. HeLa and SiHa cells were treated with a range of CDDP concentrations around their own respective CDDP IC_{50} values for 24 hours, followed by nuclear and cytoplasmic protein fractionation. Nuclear fractions were analyzed by western blot for Kpnβ1 content, TBP and Histone H3 were detected for nuclear loading control, and β-tubulin and GAPDH were included to confirm that clean nuclear lysates were obtained in comparison to a cytoplasmic protein sample 'C' from each experiment (A). Kpnβ1 was stained with Alexa-647 conjugated secondary antibody in CDDP treated and fixed SiHa cells. Localization was analyzed by fluorescent microscopy, and images were captured. At least 6 different field of views were captured for each treatment, and one representative is shown (B). Nuclear fractionation experiment was repeated three independent times (A) and immunofluorescence analysis was performed two independent times (B).

Although CDDP has been used in anti-cancer therapy for both cervical and ovarian malignancies, our results suggest different Kpnβ1 responses to CDDP treatment in these two cancers. While the effects of CDDP on Kpnβ1 expression and localization were apparent in ovarian cancer cells, this was not observed in cervical cancer cells. However, we have shown earlier that Kpnβ1 knock-down in cervical cancer cells exhibited increased sensitivity to CDDP, confirming its involvement in CDDP-induced cellular response. As Kpnβ1 expression and localization was unaffected by CDDP in cervical cancer cells, this suggests that Kpnβ1 in CDDP-induced response occurs via other mechanisms.

4.2.5. The role of p53 and p21 in the INI-43 and CDDP combination treatment

Both p53 and p21 proteins are highly investigated factors in cancer, and their significance in cancer and response to chemotherapeutic agents have been repeatedly demonstrated. To elucidate whether, and how, these proteins may play a role in CDDP response, and furthermore, whether the enhanced CDDP effects in INI-43 pre-treated cells involve these two proteins, we examined the effects of p21 and p53 knock-down on cellular response to single and combination treatments. The knock-down was confirmed for both p21 and p53 48 hours post transfection, which is the time point when cells receive treatments in subsequent experiments (Fig. 4.8.A).

4.2.5.1. p21 protects cells from CDDP-induced cell death while p53 does not affect CDDP-induced cell death in SiHa cells

We first examined cell viability after CDDP treatment in p21 or p53 knock-down cells. We found that p21 knock-down cells showed increased sensitivity to CDDP treatment, indicated by the significant decrease in cell viability compared to the control cells after CDDP treatment (Fig. 4.8.B). p53 knock-down, on the other hand, did not affect CDDP-induced reduction in cell viability (Fig. 4.8.C). To examine whether the decrease in cell viability was associated with apoptosis, we investigated PARP

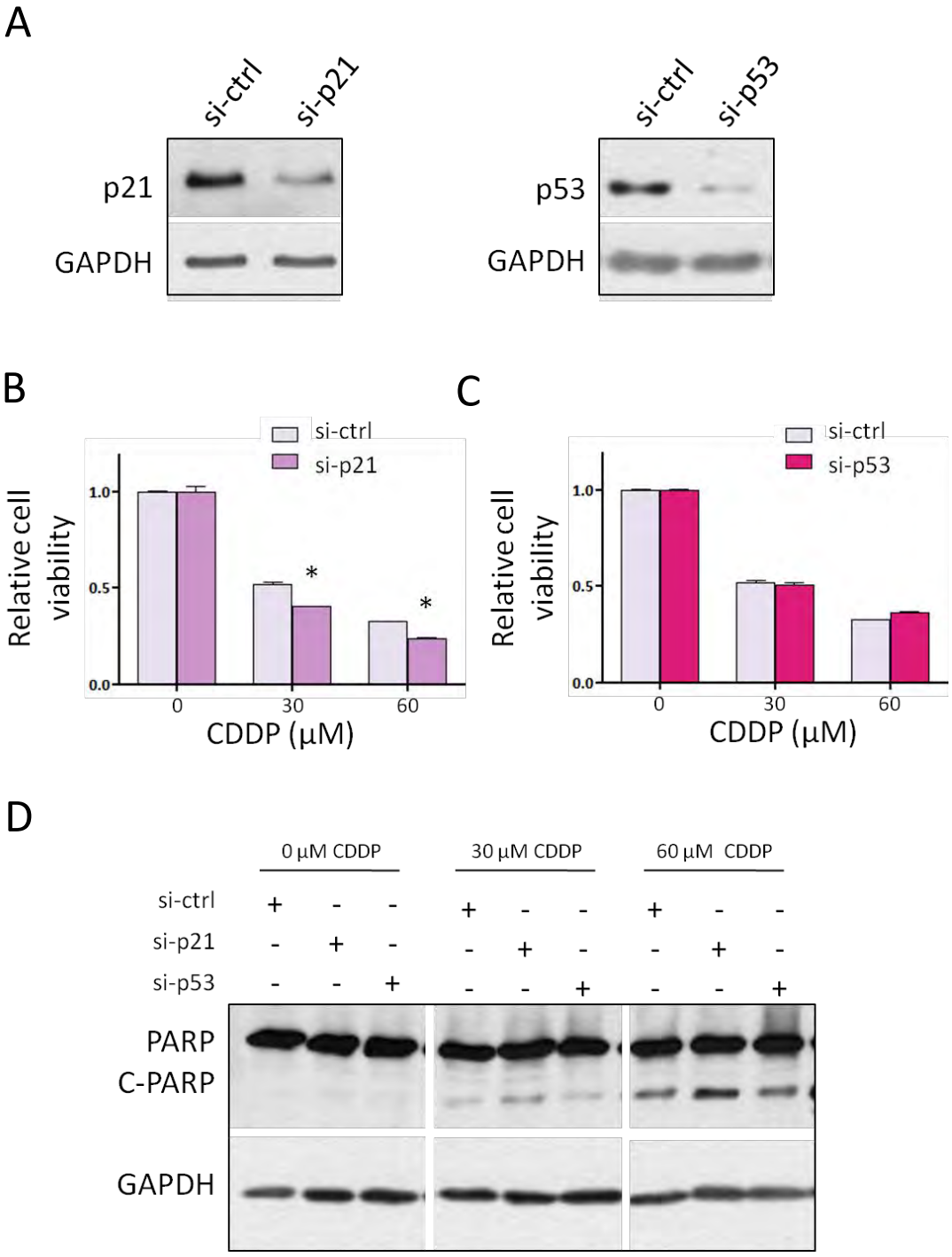

Figure 4.8. CDDP sensitivity in p21 or p53 knock-down SiHa cells. SiHa cells were transfected with 30 nM of control siRNA (si-ctrl), p21 targeting siRNA (si-p21) or p53 targeting siRNA (si-p53) and knock-down was confirmed by western 48 hours post transfection, GAPDH was included for loading control (A). Cell viability in p21 knock-down and p53 knock-down cells were examined after 48 hours of 30 μM and 60 μM CDDP treatment by MTT assay, and viable cells were normalized to the viability of untreated cells in each transfection group (B and C). CDDP-induced PARP cleavage was examined in p21 and p53 knock-down cells by western blot, with GAPDH as the loading control (D). Results shown are mean ± SEM of experiment conducted in triplicates (B and C) and repeated at least two independent times (B - D), *$p < 0.05$.

cleavage using western blot. This showed that after a 48 hour CDDP treatment, p21 knock-down cells exhibited increased levels of cleaved PARP compared to the control cells, whereas p53 showed similar levels of cleaved PARP to the control cells (Fig. 4.8.D). These results indicated that in CDDP-treated SiHa cells, the decrease in cell viability observed in p21 knock-down cells was a result of increased apoptosis. Furthermore, it confirmed the cell viability result for p53 knock-down cells, as no increased PARP cleavage was observed compared to si-ctrl transfected cells. These data suggest that p21 exerts a protective effect against CDDP-induced cell death, but p53 appears to not have a role in response to CDDP as a single treatment.

4.2.5.2. INI-43 induced enhancement in CDDP-cytotoxicity is dependent on p53 function

Next, the role of p21 and p53 in the enhancement of cell death in combination treatment was investigated. The degree of reduction in cell viability as a result of combination treatment were compared to single treatment for each knock-down via MTT assays. Cells with p21 or p53 knock-down, together with the control cells were treated with CDDP only or 5 μM INI-43 and CDDP for 48 hours, and cell viability was monitored using the MTT reagent. To quantify the enhancement of cell death associated with the combination treatment, the results were normalized to viability of cells receiving the CDDP single treatment. As expected, significant reduction in cell viability was observed for the control cells receiving the combination treatment, compared to single treatment (Fig. 4.9.A). In p21 knock-down cells, the degree of reduction in cell viability observed in combination treatment was more prominent than the control cells (Fig. 4.9.A). In p53 knock-down cells, however, cell viability was similar between single and combination treatment (Fig. 4.9.A). Examination of PARP cleavage is in accordance with these results - while the control cells showed moderate increase in PARP cleavage in combination treatment compared to single treatment, the degree of increase in cleaved PARP was more substantial in p21 knock-down cells, and no difference in PARP cleavage was observed between single and combination treatment in p53 knock-down cells (Fig. 4.9.B).

Densitometrical quantification of cleaved PARP relative to total PARP for single and combination treatments at 60 µM CDDP confirmed these interpretation (Fig. 4.9.C).

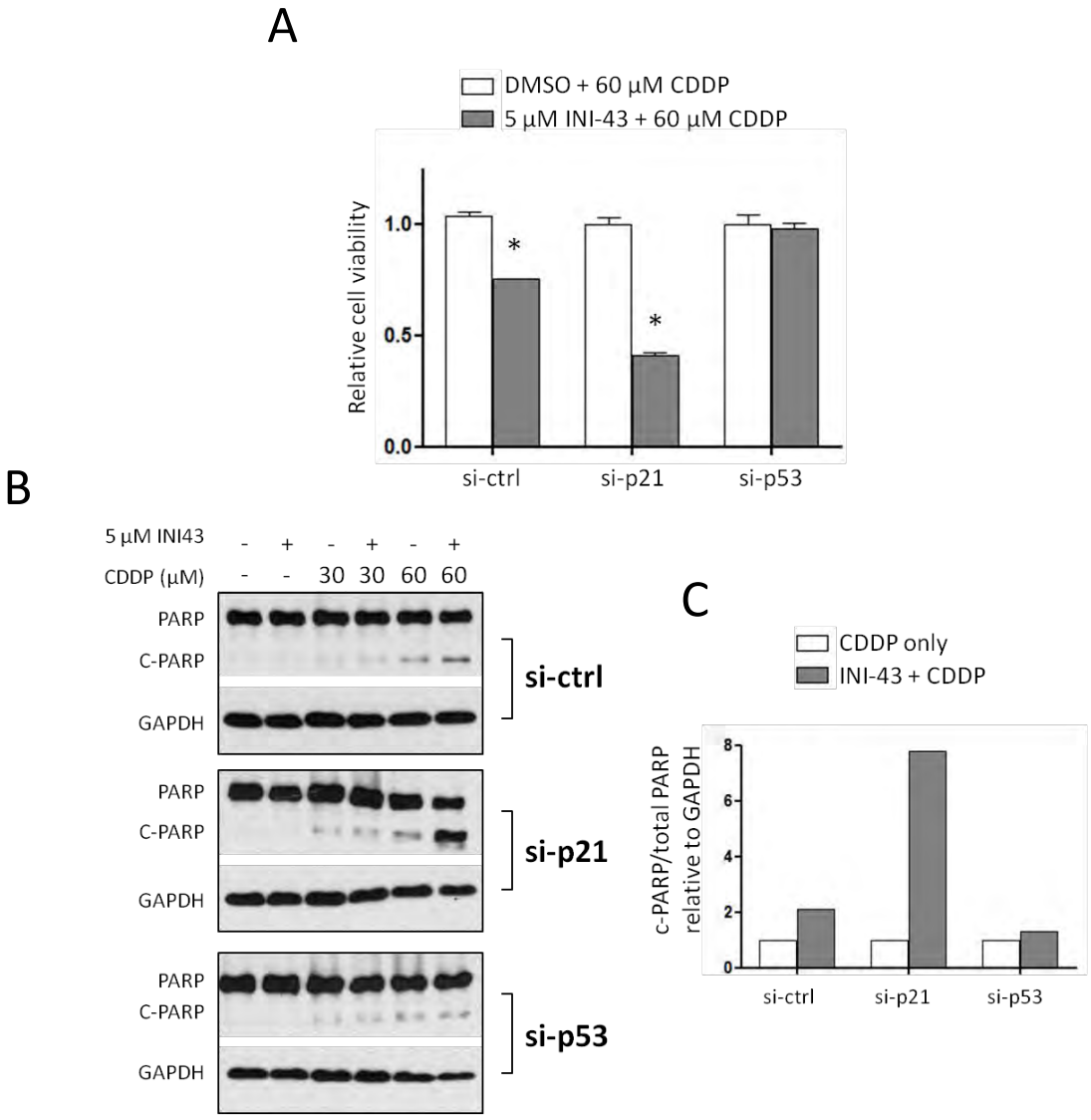

Figure 4.9. The effect of p21 and p53 knock-down on INI-43 enhanced CDDP sensitivity in SiHa cells. p21 and p53 knock-down SiHa cells were subjected to single CDDP or combined INI-43 plus CDDP treatment for 48 hours, followed by cell viability determination (A) and PARP cleavage evaluation (B and C). Cell viability was determined using the MTT assay, and to compare the degree of increase in cell death as a result of the combination treatment, viability was normalized to the cells receiving single CDDP treatment (A). PARP cleavage was investigated via western blot as an indication of apoptosis, with GAPDH as loading control (B). Densitometrical quantification of cleaved PARP relative to total PARP and normalized to GAPDH for the 60 µM CDDP treated cells (C). Results shown are mean ± SEM of experiments performed in triplicates (A), and repeated at least two independent times (A and B), *$p < 0.05$.

These results show that in p21 depleted cells, single CDDP treatment led to increased apoptosis compared to control cells. Furthermore, the degree of increase in cell death between single and combination treatment was more pronounced in p21 knock-down cells compared to control cells. These suggest a protective role for p21 in both single and combination treatment-induced cell death, as its inhibition resulted in increased cell death for both treatments. On the other hand, p53 appears not to have a role in the single CDDP induced cell death, as its inhibition resulted in similar CDDP sensitivity to the control cells. However, the combination treatment result suggests that p53 function is required for the enhanced CDDP cytotoxicity when cells are pre-treated with INI-43, as in p53 knock-down cells, the combination treatment no longer showed greater killing effects.

4.2.5.3. INI-43 pre-treatment stabilized p53 via Kpnβ1 inhibition

We next questioned the mechanism of action of INI-43, which enabled p53 to become a requirement for CDDP-induced apoptosis. We considered the possibility that INI-43 pre-treatment stabilized p53 protein, thereby allowing p53 to induce downstream pathways when subsequently exposed to CDDP.

To test this, we examined the levels of p53 in cycloheximide (CHX) treated cells. CHX is an inhibitor of protein synthesis, therefore the changes in p53 levels after CHX treatment directly reflect the rate of degradation. Cells were either treated with DMSO (control) or 5 μM INI-43 for 2 hours, consistent with the time and concentration used in the combination treatment prior to CDDP exposure. Proteins were harvested at various time points following CHX treatment, and p53 levels were measured. Western blot analysis showed an increase in p53 stability in INI-43 treated cells, which was indicated by the prolonged presence of p53 (Fig. 4.10.A). Densitometrical scanning of p53 levels relative to GAPDH were then used to calculate the half-life of p53, which showed a 3.4-fold increase from 7 minutes to 24 minutes (Fig. 4.10.B). To confirm that p53 stabilization by INI-43 treatment is

A

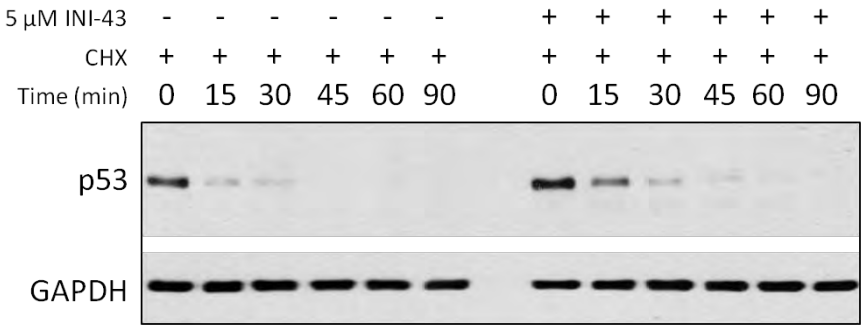
5 μM INI-43 - - - - - - + + + + + +
CHX + + + + + + + + + + + +
Time (min) 0 15 30 45 60 90 0 15 30 45 60 90
p53
GAPDH

B

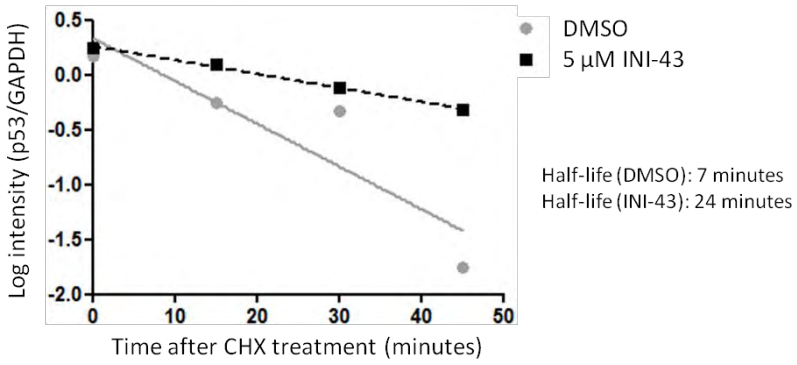
Log intensity (p53/GAPDH)
0.5
0.0
-0.5
-1.0
-1.5
-2.0
0 10 20 30 40 50
Time after CHX treatment (minutes)
DMSO
5 μM INI-43
Half-life (DMSO): 7 minutes
Half-life (INI-43): 24 minutes

C

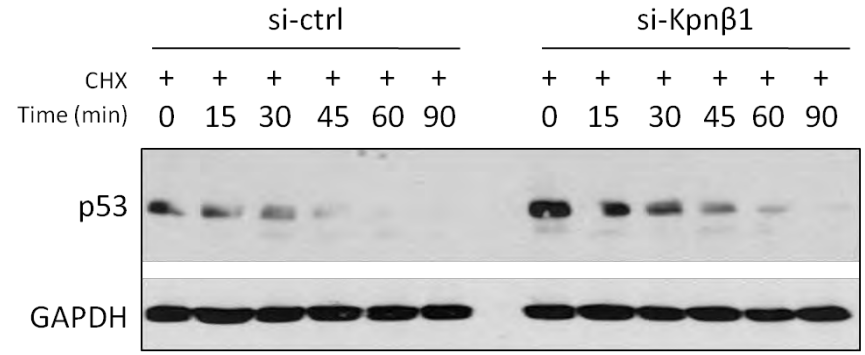
si-ctrl
si-Kpnβ1
CHX + + + + + + + + + + + +
Time (min) 0 15 30 45 60 90 0 15 30 45 60 90
p53
GAPDH

D

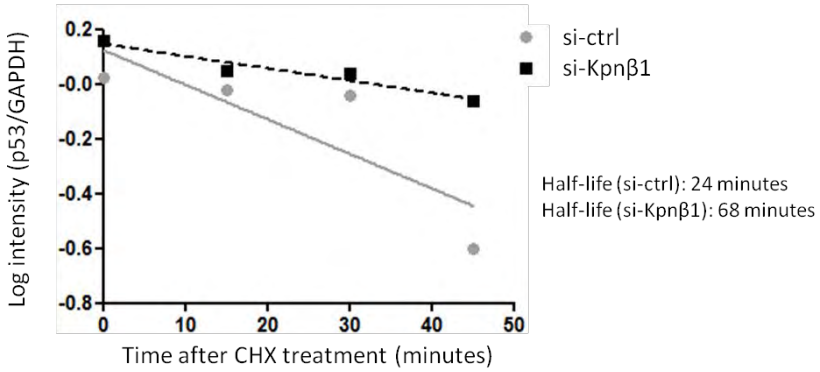
Log intensity (p53/GAPDH)
0.2
-0.0
-0.2
-0.4
-0.6
-0.8
0 10 20 30 40 50
Time after CHX treatment (minutes)
si-ctrl
si-Kpnβ1
Half-life (si-ctrl): 24 minutes
Half-life (si-Kpnβ1): 68 minutes

E

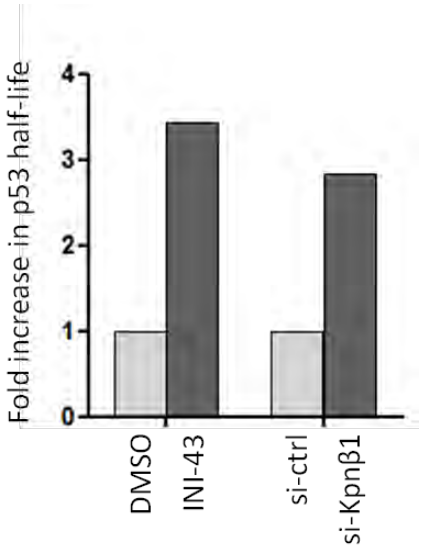

Figure 4.10. The effect of INI-43 treatment and Kpnβ1 inhibition on p53 stability. The half-life of p53 was examined in INI-43 treated (A and B) and Kpnβ1 knock-down cells (C and D). Cells were incubated with DMSO or 5 µM INI-43 for two hours (A); or transfected with 20 nM si-ctrl or si-Kpnβ1 for 48 hours (C), followed by treatment with 50 µg/mL cycloheximide (CHX). Proteins were harvested from each treatment at the indicated time points after CHX treatment, and analyzed for p53 content by western blot, with GAPDH as the loading control (A and C). Quantitative analysis of p53 protein was carried out by densitometrical scanning, and band intensities were plotted in log scale relative to p53 at time = 0 min for INI-43 treated (B) and Kpnβ1 knock-down cells (D). p53 protein half-life was determined using the equation (Log2)/[slope]. Results shown are representative of experiments performed at least twice. The fold increase in p53 stability is shown for the representative experiment in both INI-43 treated and si-Kpnβ1 transfected cells, normalized to their respective controls (E).

associated with Kpnβ1 inhibition, we examined p53 levels in Kpnβ1 knock-down cells after treatment with CHX. Similar to the INI-43 treated cells, Kpnβ1 knock-down cells sustained p53 for longer periods after CHX treatment, with a half-life of 68 minutes compared to the 24 minutes in the control cells. This represented a 2.8-fold increase in the calculated half-life in Kpnβ1 knock-down cells (Fig. 4.10.C and D). Although the absolute values for p53 half-life in the control cells differed in the two experiments, this is likely an experimental variation. In both experiments, however, approximately 3-fold increase in the half-life of p53 were observed when compared to their respective controls (Fig. 4.10.E), suggesting that INI-43 pre-treatment in SiHa cells stabilized p53, and that this stabilization is associated with Kpnβ1 inhibition.

So far, our results suggest differing roles for p53 and p21 in the CDDP-response pathway in cervical cancer cells. While p53 appears not to be involved in CDDP single treatment induced apoptosis, p21 was found to counteract this process. Furthermore, the enhancement of CDDP cytotoxicity by INI-43 was opposed by p21, but promoted by p53.

We next investigated whether INI-43 enhanced CDDP cytotoxicity via elevating p53 or repressing p21 levels. SiHa cells were subjected to single or combination treatment as previously described for 24 hours, and p53 and p21 levels were determined via western blotting. The result showed that in cells treated with single CDDP, a decrease in p21 level and increase in p53 level were observed (Fig. 4.11.A). Surprisingly, in cells treated with both INI-43 and CDDP, we observed elevated levels of p21 compared to cells receiving CDDP only, suggesting that the enhanced CDDP cytotoxicity in the combination treatment was not mediated through repression of p21 (Fig. 4.11.A). On the other hand, p53 levels were similar between single and combination treated cells. This suggest that the transcription or translation of p53 is likely repressed in the combination treated cells to maintain constant p53 levels as the rate of p53 degradation is slowed.

To investigate whether the stabilization of p53 represented increased p53 activity even though global increase in p53 levels was not observed, we examined the expression of Mcl-1 in single and combination treated cells, as Mcl-1 is transcriptionally repressed by p53[419]. Western blot analysis showed that at 30 μM and 60 μM CDDP concentrations, lower Mcl-1 levels were observed in INI-43 pre-treated cells compared to non-pre-treated cells (Fig. 4.11.B). These result suggest that INI-43 pre-treatment enhanced CDDP sensitivity in SiHa cells via stabilizing p53, which associated with the repression of the pro-survival factor Mcl-1 known to be negatively regulated by p53.

A

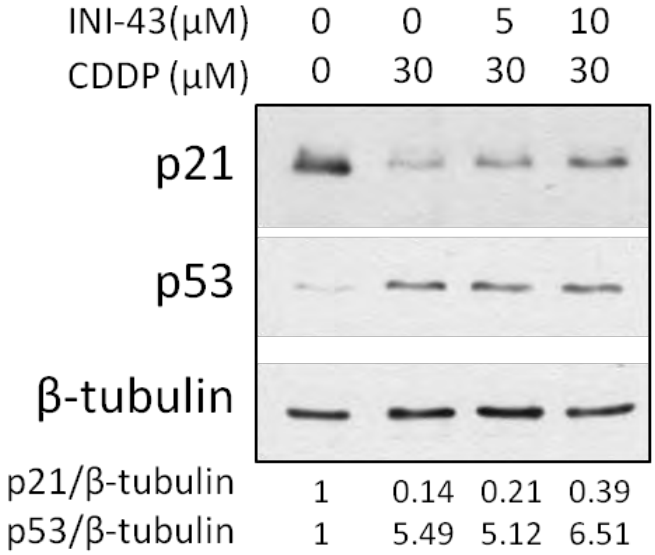

B

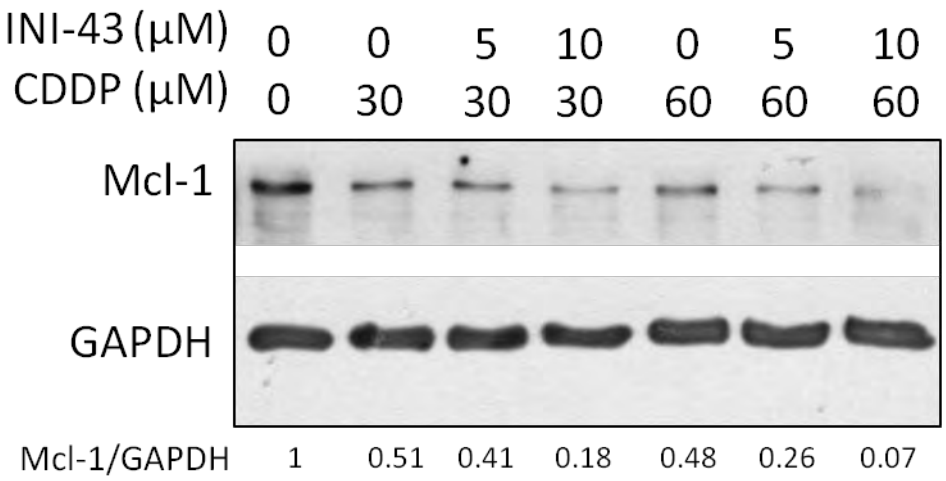

Figure 4.11. Expression of p53, p21, and the p53-downstream target Mcl-1 in response to single CDDP and combined INI-43 plus CDDP treatments. SiHa cells were subjected to single or combination treatment as previously described for 24 hours. Proteins were harvested and analyzed with western blot for p53 and p21 expression, with β-tubulin as the loading control (A). Mcl-1 expression was measured via western blot for single and combination treatment, with GAPDH as the loading control (B). Densitometrical quantification was conducted and expressed as protein of interest relative to their respective loading controls, and normalized to the untreated samples for both experiments. Results shown are representatives of experiments performed two independent times.

4.2.6. The effect of single CDDP treatment and INI-43 plus CDDP combination treatment on Nuclear Factor Kappa B (NFκB)

NFκB is a transcription factor best known for its role in the pro-inflammatory signalling pathway. In response to environmental stimuli, it relocates into the nucleus where it activates the transcription of various genes. It is generally considered a pro-survival factor[420], and has been shown to contribute to CDDP-resistance in many cancers[421, 422]. NFκB has been reported to enter the nucleus in a Kpnβ1/Karyopherinα-dependent manner[169, 270, 423], and we have previously found INI-43 to inhibit NFκB nuclear import[333]. As NFκB is an oncogenic factor known to mediate CDDP resistance, and that its nuclear entry is reliant on Kpnβ1, we investigated the effect of combination INI-43 and CDDP treatment on NFκB.

4.2.6.1. CDDP induced nuclear localization of p50 and p65, which is repressed by INI-43 pre-treatment

To investigate the activity of NFκB, we examined the localization of two subunits, p50 and p65, after cells were treated with CDDP or INI-43 plus CDDP as previously described. Immunofluorescence and fluorescent microscopy analysis showed that in the untreated cells, p50 stained with similar intensities in the nucleus and cytoplasm, indicating an even distribution between the two cellular compartments. In cells subjected to 30 μM CDDP treatment, p50 localization became more nuclear compared to untreated cells, and in cells receiving pre-treatment with 5 μM INI-43 followed by CDDP, p50 exhibited predominantly cytoplasmic distribution (Fig. 4.12.A). p50 fluorescence intensities were measured and expressed as nuclear fluorescence relative to cytoplasmic fluorescence (p50 Fc(Nu/Cy)), which showed a significant increase in single CDDP treated cells compared to untreated cells, and a significant decrease in combination treated cells compared to single treated cells (Fig. 4.12.B). Analysis of p65 localization showed a strong cytoplasmic localization in the untreated cells, and treatment with CDDP increased p65 nuclear accumulation, resulting in some cells showing nuclear p65 distribution and some cells showing even distribution. Pre-treatment with INI-43

decreased the CDDP-induced nuclear accumulation of p65, leading to predominant cytoplasmic localization (Fig. 4.12.C and D).

A

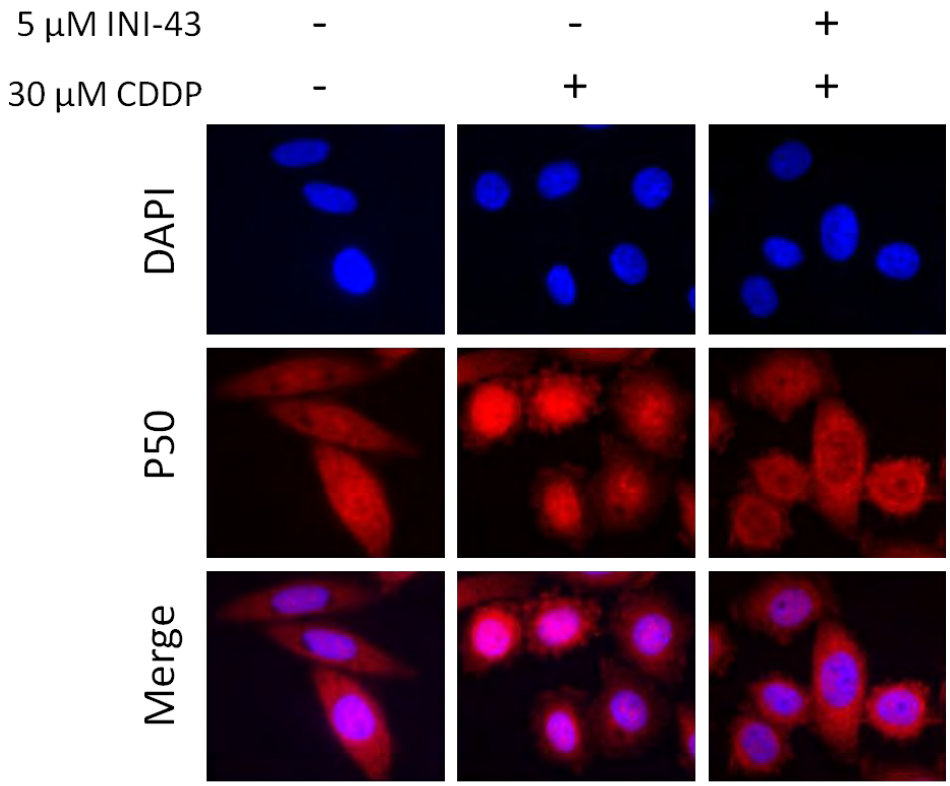

B

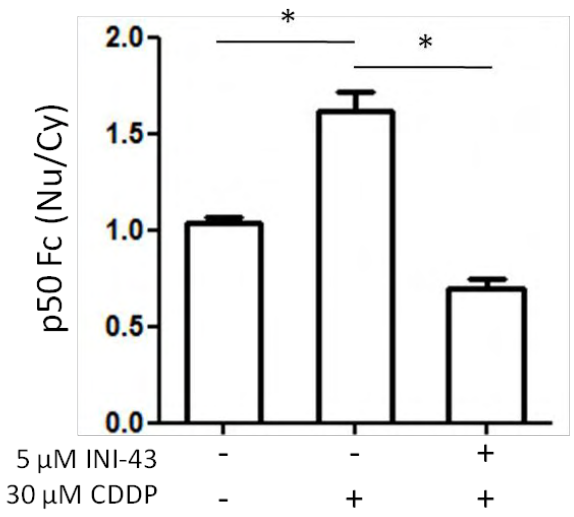

C

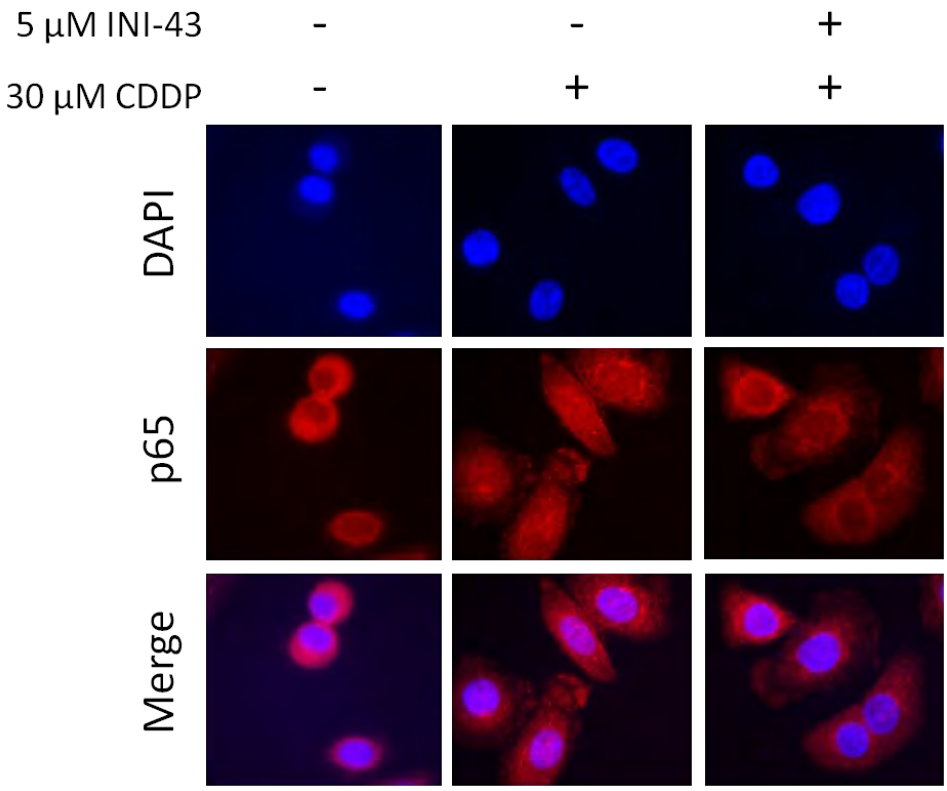

D

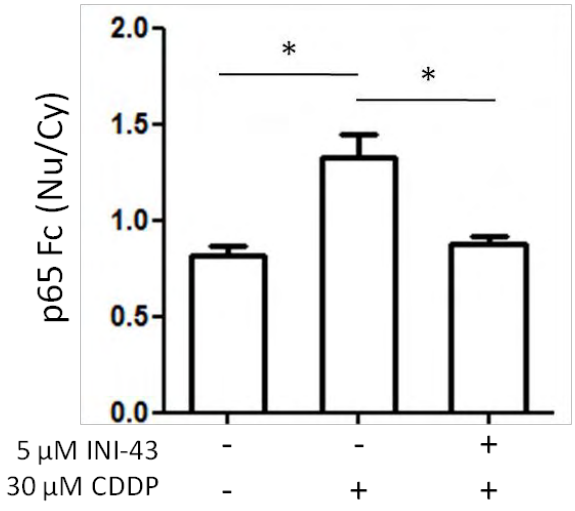

Figure 4.12. Cellular localization of NFκB p50 and p65 in response to single and combination treatment. SiHa cells were subjected to single or combination treatment for 24 hours, followed by fixation. NFκB-p50 (A) and NFκB-p65 (C) localization were then analyzed using immunofluorescence and fluorescent microscopy. A representing field of view is shown for each treatment. Fluorescence intensities were quantified using ImageJ and expressed as nuclear fluorescence relative to cytoplasmic fluorescence (Fc(Nu/Cy)) for p50 (B) and p65 (D). Results shown are mean ± SEM of 6 cells, *$p < 0.05$ (B and D).

These findings were independently confirmed using protein fractionation and western blot analysis, which showed similar results. There was an increase of nuclear p50 and p65 when cells were subjected to CDDP-only treatment, however, if the cells had received INI-43 prior to CDDP treatment, a reduction in CDDP-induced nuclear localization of p50 and p65 were observed, compared to those receiving CDDP only (Fig. 4.13). Nuclear p65 however, did not return to basal levels in the INI-43 pre-treated cells, as higher levels were still observed in the nuclear fraction after the combination treatment compared to the untreated cells. This is possibly due to alternative importing activities by other members of the Karyopherin family[169].

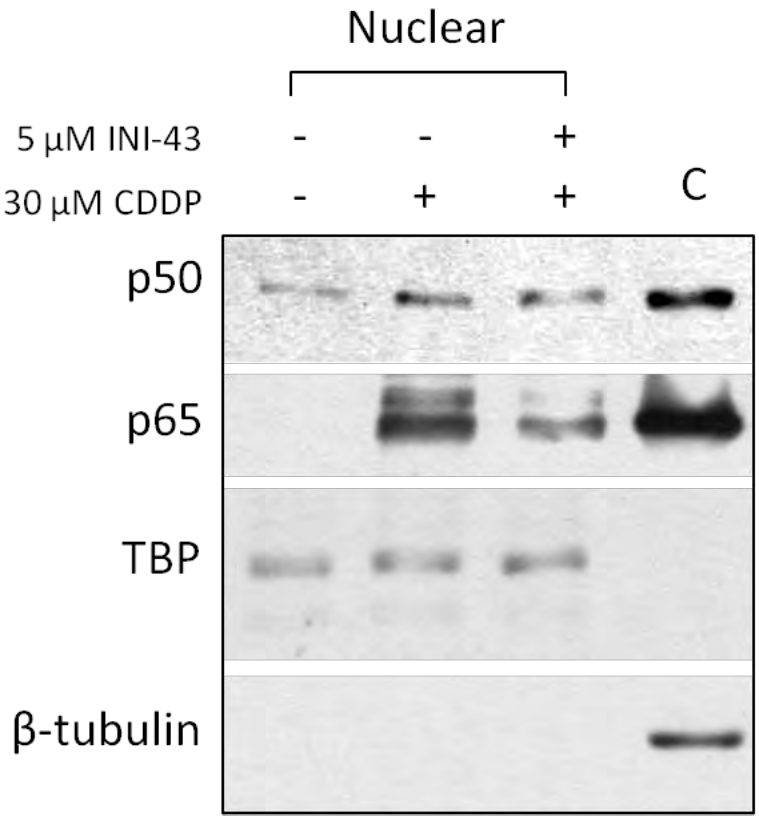

Figure 4.13. Nuclear p50 and p65 levels in SiHa cells treated with single CDDP or combination of INI-43 plus CDDP. SiHa cells were subjected to single and combination treatment as previously described for 24 hours, followed by nuclear protein extraction. Nuclear protein samples were analyzed for p50 and p65 levels, and TBP was used as the nuclear loading control. β-tubulin was included to confirm that clean nuclear lysates were obtained in comparison to a cytoplasmic protein sample 'C'. The experiment was repeated three independent times.

4.2.6.2. INI-43 pre-treatment decreased the levels of CDDP-induced NFκB target gene expression

To investigate whether the altered localization of p50 and p65 translated into functional significance, we examined the expression of three downstream targets of NFκB, namely cyclinD1, c-Myc, and X-chromosome linked inhibitor of apoptosis (XIAP), which are all known to be involved in CDDP-induced response[424-428]. Western blot analysis revealed that, with the exception in XIAP, single CDDP treatment led to increased levels of both cyclinD1 and c-Myc (Fig. 4.14.A). Furthermore, the levels of cyclinD1, c-Myc and XIAP were all repressed in a concentration dependent manner in combination treated cells, compared to CDDP only treated cells (Fig. 4.14.A). As both cyclinD1 and c-Myc have been reported to confer chemoresistance by increasing the cell's DNA repair capacity[429, 430], we examined whether their decreased expression in INI-43 pre-treated cells had an impact on CDDP-induced DNA damage. The level of γH2AX after 24 hours treatment with CDDP or INI-43 plus CDDP were measured using western blot, and the result showed increased γH2AX levels in the cells receiving combination treatment compared to single treatment (Fig. 4.14.B), suggesting increased DNA damage in these cells.

Taken together, these results suggest that in response to CDDP-induced DNA damage, NFκB relocates into the nucleus where it increased expression of target genes such as cyclinD1 and c-Myc. Pre-treatment of cells with INI-43 attenuated NFκB response by repressing its nuclear entry, as well as repressing p50 expression. This could consequently lead to decreased levels of cyclinD1 and c-Myc, and possibly XIAP resulting in enhanced DNA damage and apoptosis.

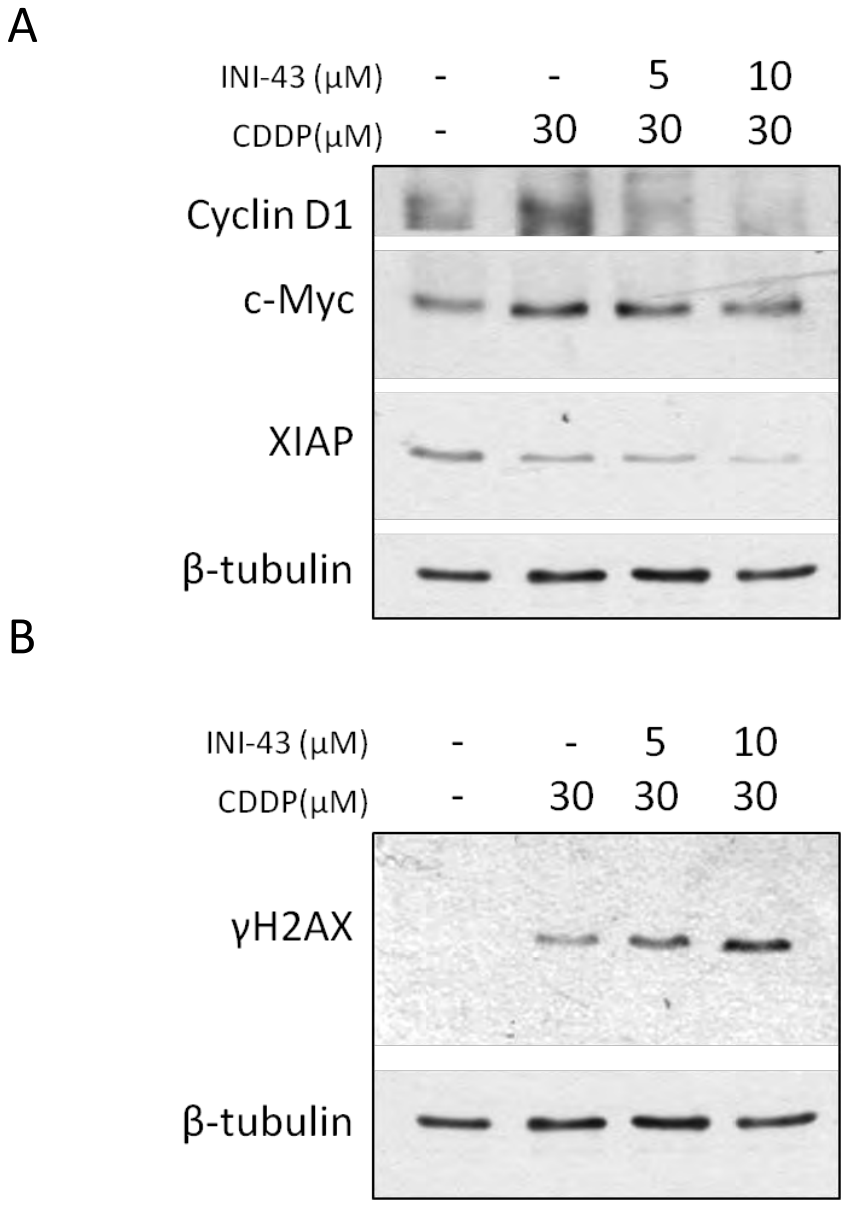

Figure 4.14. Expression of NFκB target genes cyclin D1, c-Myc and XIAP; as well as DNA damage marker γH2AX in SiHa cells subjected to single and combination treatment. SiHa cells were treated with CDDP only or a combination of INI-43 plus CDDP for 24 hours, followed by western blot analysis to determine levels of cyclinD1, c-Myc and XIAP (A). To examine the impact of decreased cyclinD1 and c-Myc expression on DNA damage, γH2AX expression was determined via western blot (B). β-tubulin was included for loading control. Results shown are representative of two independent experiments.

4.2.7. Kpnβ1 over-expression sensitized HeLa cells to CDDP

So far we have shown that Kpnβ1 inhibition via siRNA or INI-43 restored CDDP sensitivity in SiHa cells, with alterations in various molecular pathways involved in survival and apoptosis. These results suggest that the function of Kpnβ1 is important in CDDP-induced cellular response and may contribute to CDDP resistance. This led us to question whether increasing the expression of Kpnβ1 (and thereby its function) could increase the cells' tolerance to CDDP. To investigate this, we used the CDDP-sensitive and Kpnβ1 over-expressing cell line, HeLa-pEFIRES-Kpnβ1-GFP and the control cell line HeLa-pEFIRES-GFP, of which the former was previously shown to express approximately twice as much Kpnβ1 as the control GFP expressing cells (see Fig. 2.9 in Chapter 2).

4.2.7.1. Kpnβ1 over-expressing cells exhibited increased sensitivity to CDDP

CDDP sensitivity in the Kpnβ1-overpressing and control cells were first assessed by examining CDDP IC_{50}, which was 12.0 μM in Kpnβ1 over-expressing cells compared to 19.8 μM in the control cells (Fig. 4.15.A and B), suggesting increased CDDP sensitivity in Kpnβ1 over-expressing cells. Examination of cell viability confirmed these results, whereby significant decrease in cell viability was observed in Kpnβ1 over-expressing cells compared to control cells at all concentrations of CDDP (Fig. 4.15.C).

To determine whether the increased sensitivity to CDDP treatment in the Kpnβ1 over-expressing cells was associated with increased apoptosis, we investigated PARP cleavage in both cell lines after CDDP treatment via western blotting. The result showed enhanced PARP cleavage in Kpnβ1 over-expressing cells compared to the control cells when treated with the same concentration CDDP (Fig. 4.15.D), which was confirmed by densitometrical quantification (Fig. 4.15.E). This suggest that the enhanced decrease in cell viability of Kpnβ1 over-expressing cells observed after CDDP treatment associated with increased apoptosis.

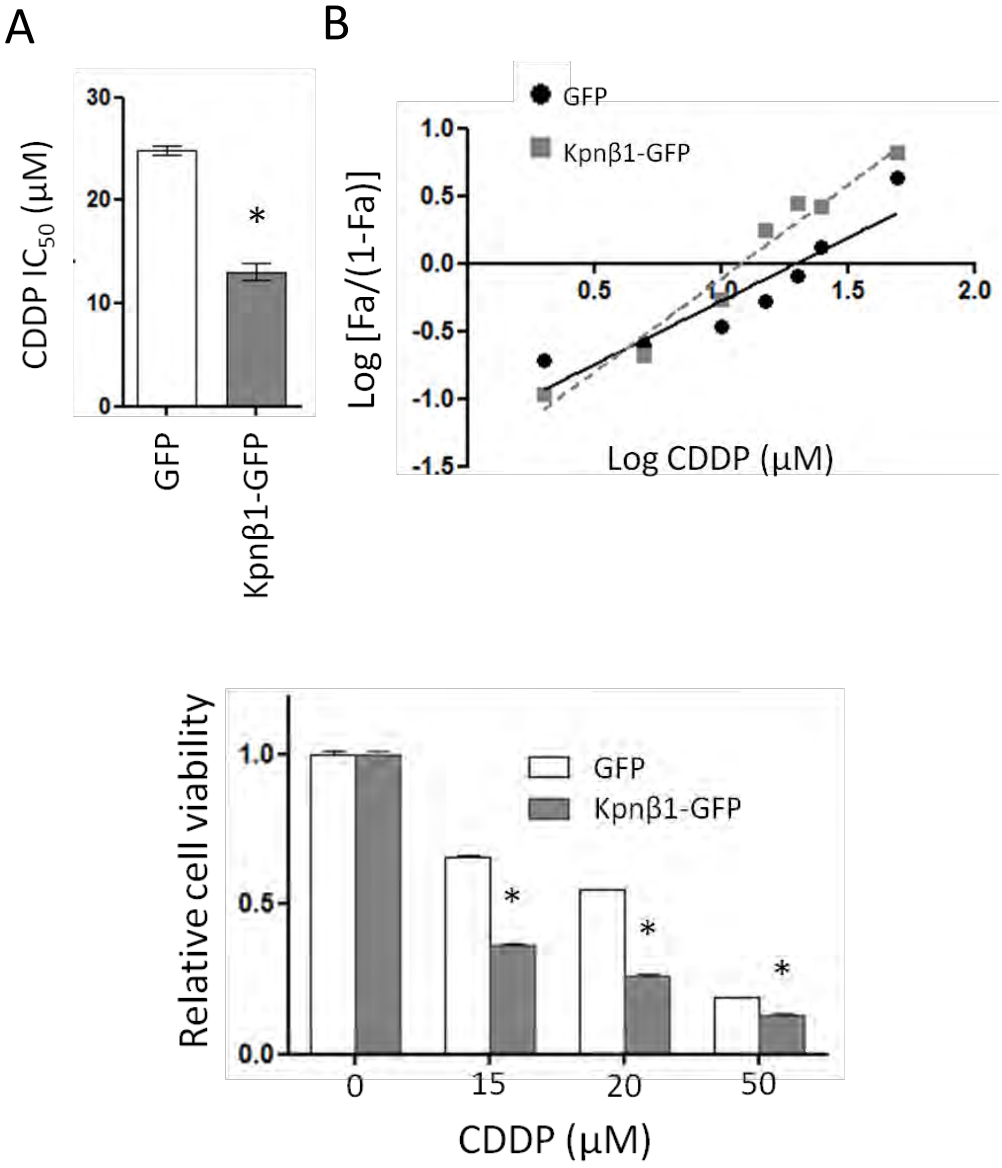
A
B
CDDP IC50 (μM)
30
20
10
0
*
GFP
Kpnβ1-GFP
GFP
Kpnβ1-GFP
Log [Fa/(1-Fa)]
1.0
0.5
0.0
-0.5
-1.0
-1.5
0.5
1.0
1.5
2.0
Log CDDP (μM)
C
Relative cell viability
1.0
0.5
0.0
GFP
Kpnβ1-GFP
*
*
*
0
15
20
50
CDDP (μM)
D
E
GFP
Kpnβ1-GFP
0 10 20 30 0 10 20 30
PARP
C-PARP
GAPDH
C-PARP relative to GAPDH
300
200
100
0
GFP
Kpnβ1-GFP
CDDP (μM)
0 10 20 30 0 10 20 30

Figure 4.15. CDDP sensitivity in Kpnβ1-over expressing cells. CDDP IC_{50} was determined for HeLa-pEFIRES-GFP (GFP) and HeLa-pEFIRES-Kpnβ1-GFP (Kpnβ1-GFP) cells (A). Results shown are the mean ± SEM of 4 independent experiments. A representing IC_{50} determination plot is shown (B), results are mean ± SEM of 6 replicates. Cell viability for the control and Kpnβ1 over-expressing cells were analyzed after 48-hour CDDP treatment via MTT assay, and results were normalized to viability of the untreated cells (C). Results shown are mean ± SEM of 6 replicates, and the experiment was repeated 4 independent times, $*p < 0.05$. PARP-cleavage was analyzed as an indication of apoptosis in both cell lines after 48-hour CDDP treatment, GAPDH was included as the loading control (D). The results were quantified densitometrically (E), and the experiment was repeated two independent times.

4.2.7.2. Effect of CDDP on p53, p21, Mcl-1 and γH2AX in Kpnβ1 over-expressing cells

Having shown earlier that inhibition of Kpnβ1 in combination with CDDP treatment led to alterations in p53, p21, Mcl-1 and γH2AX, we next explored effects of CDDP treatment on these proteins in Kpnβ1 over-expressing cells. Examination of p53, p21 and Mcl-1 showed that CDDP treatment led to similar trends of expression in these proteins in both cell lines, with increased p53 levels and decreased p21 and Mcl-1 levels in a concentration-dependent manner. The changes were, however, more prominent in Kpnβ1 over-expressing cells compared to the control cells (Fig. 4.16). Furthermore, Kpnβ1 over-expressing cells showed higher p53 levels and lower p21 and Mcl-1 levels without CDDP treatment, suggesting that Kpnβ1 over-expressing cells are more sensitive to apoptotic signals. As Kpnβ1 over expression has been reported to cause mitotic abnormalities and induce genomic instability, we investigated DNA damage marker γH2AX after CDDP treatment in comparison to the control cells. Western blot analysis showed enhanced γH2AX elevation in Kpnβ1 over-expressing cells compared to the control cells, indicative of enhanced DNA damage in these cells.

These results indicate that over-expression of Kpnβ1 enhanced CDDP sensitivity by enhancing DNA damage effects; as well as amplifying the effects of apoptotic factor p53 and suppressing anti-apoptotic factors p21 and Mcl-1. This was a surprising finding, as inhibition of Kpnβ1 increased the sensitivity of cervical cancer cells to CDDP treatment, we postulated that over-expression might have

a rescue effect. Our data, however, show that Kpnβ1 over-expression sensitized cancer cells to CDDP similarly to that observed in Kpnβ1 inhibited cells, suggesting interfering with Kpnβ1 expression in both directions disadvantaged cervical cancer cells to CDDP treatment.

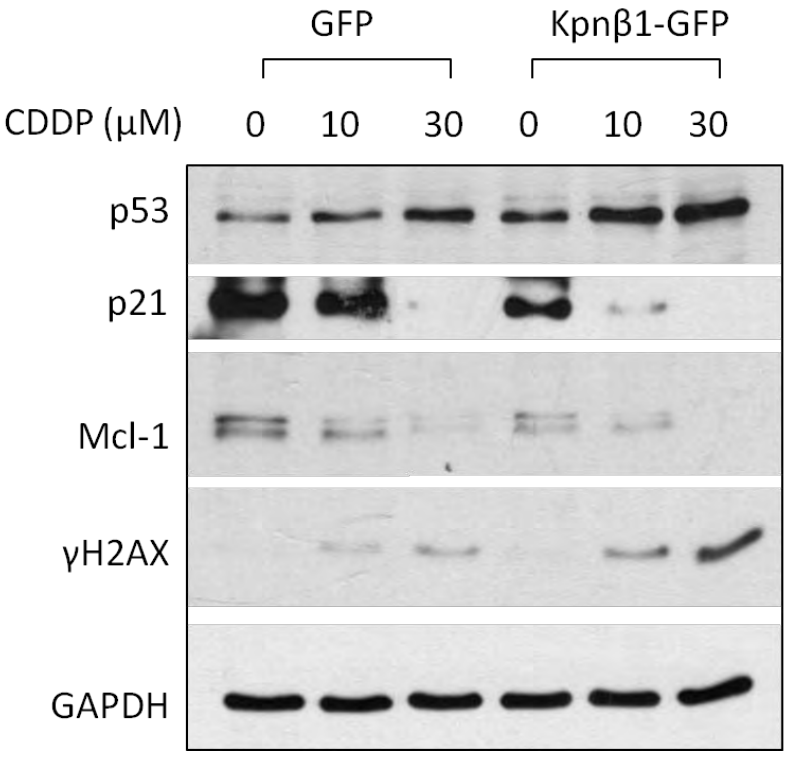

Figure 4.16. Levels of p53, p21, Mcl-1 and γH2AX in control and Kpnβ1 over-expressing cells after CDDP treatment. HeLa cells over-expressing Kpnβ1-GFP or GFP were treated with CDDP for 24 hours followed by western blot analysis to determine levels of γH2AX, p53, p21 and Mcl-1. GAPDH was included as loading control, and the experiment was repeated two independent times.

4.3. Discussion

In this chapter we report that sub-lethal concentrations of INI-43 effectively enhanced CDDP-induced apoptosis, as shown by decreased cell viability and increased apoptosis. These findings were observed in both CDDP-sensitive (HeLa) and CDDP-resistant (SiHa) cell lines. Kpnβ1 knock-down experiments showed similar results to that of INI-43 pre-treated cells, whereby CDDP sensitivity was significantly enhanced. This suggest that INI-43 acts in a manner similar to Kpnβ1 knock-down. We concluded that Kpnβ1 functions in the pro-survival pathway, and speculated that its over-expression can possibly increase CDDP resistance. To our surprise, Kpnβ1 over-expressing HeLa cells showed no survival advantage in comparison to the control GFP-expressing cells, but instead were more prone to CDDP-induced apoptosis. Although unexpected, this result could possibly explain why HeLa cells did not elevate Kpnβ1 levels in response to CDDP, since this proved to confer no advantage for cell survival. Whilst we have previously shown that Kpnβ1 inhibition genetically or pharmacologically induced cervical cancer cell death[128, 333], others have reported that exogenously expressed Kpnβ1 induced mitotic abnormalities, resulting in genomic instability[282, 286]. This could provide an explanation as to why Kpnβ1 over-expressing cells exhibited increased CDDP sensitivity. It is likely that cancer cells require a fine balance in Kpnβ1 expression, and that artificial perturbation of this fine balance in either directions could have deleterious effects on cell survival.

To understand the mechanism of action underlying the increased CDDP sensitivity observed in the combination treated cells, we investigated various proteins that are known to be involved in CDDP response; including p21, p53 and NFκB. The roles of p21 and p53 in CDDP-induced apoptosis were elucidated using knock-down experiments, and CDDP-induced alterations in NFκB localization was evaluated.

Evaluating the roles for p53 and p21 is challenging, as these proteins have been reported to support both pro- and anti-apoptotic effects of these cell cycle regulators. The role of p21 as a pro-apoptotic factor has been reported by various groups, including Chen *et al*., who have demonstrated that the upregulation of p21 enhanced apoptosis in ovarian cancer cells subjected to combination treatment incorporating CDDP[431]. Stordal and Davey showed decreased p21 promoted small cell lung cancer survival when challenged with DNA damage[432], and Taguchi *et al*. reported increased p21 expression in correlation with CDDP sensitivity in head and neck squamous cell carcinoma[433]. On the other hand, there are also substantial evidence suggesting that p21 can oppose apoptosis, conferring drug resistance. For instance, He *et al*. reported increased p21 in association with CDDP resistance in oesophageal squamous carcinoma through kinase-7[434], and other downstream kinases which are positively regulated by p21, including both PAK1 and PAK4, which have also been shown to increase cancerous phenotypes and CDDP resistance[435, 436]. p53, on the other hand, has been widely accepted as a tumour suppressor protein important for guarding the genome and regulating apoptosis. However, evidence are emerging to demonstrate that p53 can also promote oncogenesis in various cases[437-439]. These findings are suggestive that both p21 and p53 are involved in CDDP resistance and CDDP-induced apoptosis, yet their roles in the apoptotic pathway may not be absolute, and varies in each case.

To determine the role of p21 in our model system, we inhibited p21 expression via siRNA and examined cellular response to CDDP single treatment and INI-43 plus CDDP combination treatment. Our results suggest that p21 exhibited a protective role against cell death induced by both single and combination treatments. Interestingly, we found p21 levels to be elevated in the combination treatment compared to the single treatment, which seemingly contradicts the increased apoptosis observed in the combination treatment. We proposed the possibility that the combination treatment caused molecular alterations in numerous pathways, including both pro- and anti-survival. However, as the net outcome was greater killing effect, the activation of apoptotic pathways is likely

more potent than anti-apoptotic pathways. This finding also proposes a potential for co-targeting both Kpnβ1 and p21 in combination with CDDP, which further enhanced apoptosis compared to Kpnβ1 inhibition and CDDP.

The siRNA mediated p53 knock-down experiment demonstrated its pro-apoptotic role in our model system, but only in the combination treatment. We then showed that this was achieved through increased p53 stability by INI-43 pre-treatment or Kpnβ1 knock-down, which associated with increased responsiveness to CDDP treatment. SiHa is a HPV16 positive cell line harbouring the viral oncogenes E6[440], which has been reported to directly associate with p53 and induce its degradation[441]. This results in the highly unstable p53, which is supported by our observation where p53 level is rapidly diminished after CHX treatment. Furthermore, stabilization of p53 has also been observed in HPV16 and HPV18 positive CaSki cells after transfection with si-Kpnβ1[300], and interestingly, inhibition of CRM1 via KPT-185 or LMB has been shown to stabilize p53 in other cancer models[346, 442]. Together with our findings, these data suggest that interfering with the nuclear transport system in both directions may have stabilizing effect on p53. It is likely that under normal conditions in SiHa cells, p53 is rapidly degraded making the p53-associated apoptotic pathway less accessible to CDDP-induced DNA damage response. This is supported by our finding that p53 inhibition did not alter CDDP sensitivity in SiHa cells. INI-43 pre-treatment stabilized p53, thereby making p53 activity available for apoptotic induction when cells were subsequently treated with CDDP. This could also explain why the combination treatment does not augment apoptosis in C33A cells, as C33A cells contain mutant p53 which is non-functional[443].

Although INI-43 pre-treatment moderately stabilized p53, we did not observe global increase in p53 levels in the combination treatment compared to single treatment. This suggests that p53 levels are maintained in the cells even though it was stabilized after INI-43 pre-treatment. Previous work from

our laboratory, however, showed that lethal concentrations of INI-43 (≥10 μM), as well as siRNA-mediated Kpnβ1 knock-down increased cellular p53 levels, suggesting that greater inhibition of Kpnβ1 does lead to increased global p53 levels[**]. This was however, not observed at the sub-lethal dose of INI-43 used in our experiments. We theorize that even though the overall p53 level was not increased by INI-43 at 5 μM, it is the enhanced stability of p53 that associated with increased apoptosis in combination treated cells. The increased p21 levels as well as decreased Mcl-1 levels in INI-43 treated cells may be supporting evidence of this, as p53 is known to positively regulate p21 and repress Mcl-1[419, 444]. Furthermore, the elevated caspase-3/7 activities observed in the combination treatment could be associated with the decreased level of Mcl-1, as Mcl-1 is known to promote survival by inhibiting events preceding mitochondrial release of cytochrome C[445]. Whilst the link between Kpnβ1 inhibition and p53 stabilization is demonstrated in our results, further experiments should be carried out to determine how nuclear import inhibition leads to p53 stabilization, and whether this is mediated through interfering with HPV E6 activity.

NFκB is an important response factor to a variety of stress-signals, including CDDP induced DNA damage[446]. Under such conditions, NFκB is activated and relocates into the nucleus where it promotes the transcription of various genes involved in DNA repair and survival[447]. Its pro-survival and anti-apoptotic effects were first demonstrated by Wang *et al.*, shedding light on NFκB as a contributor to chemoresistance[448-450]. Subsequently, various groups have reported similar findings where increased chemosensitivity was observed after NFκB inhibition (for details, see review by Nakanishi and Toi, 2005[310, 451-453]). As NFκB is reliant on Kpnβ1/Karyopherinα for nuclear entry, we addressed the possibility that the enhanced sensitivity to CDDP observed in Kpnβ1 inhibited cells may involve inhibiting NFκB nuclear entry and activities. Supporting this, we found that INI-43 exhibited inhibitory effects on CDDP-induced nuclear import of NFκB, as well as the expression of its transcriptional targets cyclinD1, c-Myc and XIAP. Both c-Myc and XIAP are oncoproteins known to

[**] Stowell, C. "Identification of Nuclear Import Inhibitors That Display Anti-cancer activity." University of Cape Town, 2011

promote cell survival and are frequently dysregulated in cancer. c-Myc confers chemoresistance via suppressing Bridging Integrator 1 (BIN1), an inhibitor of PARP-1 involved in DNA repair activity. c-Myc thus allow increased tolerance to DNA damage, thereby conferring CDDP resistance[429]. XIAP promotes survival by directly binding to and inhibiting the activities of caspase-3, caspase-7 and possibly caspase-9[454, 455]. While cyclinD1 is best known for driving cell cycle from G1 to S phase[456], more recent work by Jirawatnotai *et al.* have demonstrated that cyclinD1 is also involved in DNA damage repair in association with Rad51[430], and that cyclinD1 inhibition impaired repairing capacity, leading to sensitization of cancer cells to CDDP[457]. Our results showed that INI-43 may indirectly repress the levels of these DNA-repair and anti-apoptotic proteins via decreasing NFκB nuclear import, and thus its transcriptional activity. We also found that at the same concentration of CDDP, cells pre-treated with INI-43 showed enhanced levels of γH2AX compared to non-pre-treated cells. This result could be explained in two ways; firstly, it could suggest that Kpnβ1 inhibition augmented the DNA-damaging capacity of CDDP, so that a fixed amount of CDDP is able to cause more harm in INI-43 pre-treated cells compared to control cells. Alternatively, we speculate that INI-43 pre-treatment impaired DNA repair response (potentially through decreasing levels c-Myc and cyclinD1), and as a result, these cells require more time to repair DNA damage. The elevated levels of γH2AX as a result of DNA damage is thus sustained in these cells 24 hours after treatment, while the cells receiving CDDP only were able to execute the repair more rapidly, allowing levels of γH2AX to fall after 24 hours. In support of our finding, Olive and Banath have reported that cells which retained γH2AX 24 hours after CDDP treatment correlated with their failure to survive and form colonies in clonogenic assays[458], and we similarly found that the enhanced cell death observed in the combination treatment correlated with higher γH2AX levels 24 hours after treatment. Interestingly, with opposing roles in apoptosis, NFκB and p53 have been shown to mutually antagonize the transcriptional activity of each other[459, 460], suggesting that INI-43 pre-treatment may impair NFκB mediated survival pathways by preventing its nuclear entry, as well as through stabilizing p53.

Taken together, we have shown here that Kpnβ1 inhibition sensitized cervical cancer cells to CDDP treatment, and we propose that the combined use of INI-43 and CDDP may be an effective approach for anti-cancer treatment. This is mediated through stabilization of p53 and preventing NFκB nuclear localization, leading to alterations in various downstream targets such as XIAP, c-Myc, and Mcl-1. These proteins are known to confer CDDP resistance in a variety of cancers, and their inhibition through genetic or pharmacological approaches have been demonstrated to increase sensitivity to chemotherapeutic agents[461-467]. The abrogation of enhanced cell death in combination treated cells via p53 knock-down suggest that p53 is likely upstream of NFκB induced survival response. Interestingly, CRM1 inhibition via LMB has similarly been demonstrated to enhance CDDP sensitivity in p53-wildtype cervical cancer cells[468], suggesting that p53 may play a crucial role in nuclear transport inhibition induced CDDP sensitivity.

CHAPTER 5

CONCLUSION

5.1. Main conclusions

The nuclear transport machinery in eukaryotic cells serve vital functions important for normal cellular processes, and abnormalities in this system is linked to pathogenesis such as cancer. The active participant in this system, the Karyopherins have shown therapeutic potentials in recent studies with the majority of the investigations revolving around the Exportin CRM1. In this study, we addressed the feasibility of targeting nuclear import associated with Kpnβ1, via the use of a small molecule INI-43, and investigated two main areas: the anti-cancer effect of nuclear import inhibition using a cell culture and an *in vivo* model system; and the effect of nuclear import inhibition on CDDP sensitivity in cancer cells in culture. The former provides evidence for the potential of INI-43 as a single agent in cancer treatment, while the latter sets the ground work for its combined use with other chemotherapeutic agents in current practice.

The anti-cancer effects of INI-43 were evident through a series of cell culture based assays. These included its negative impact on cancer cell viability, survival, and proliferative activities under different growth conditions. In particular, the ability of cancer cells to grow anchorage-independently is an indication of anoikis resistance, which is associated with invasiveness and metastasis[469]. The ability of INI-43 to inhibit cancer growth of this nature is an indication that INI-43 could be effective at treating tumours with invasive and migratory properties. Genetic manipulations to alter Kpnβ1 levels showed that while Kpnβ1 knock-down induced apoptotic events in cancer cells similar to that observed after INI-43 treatment, Kpnβ1 over-expression was able to partially reverse

this. The molecular events associated with INI-43 induced cell death were mitochondrial release of cytochrome C and PARP cleavage, indicating that cell death was mediated through the intrinsic mitochondrial pathway, which were similarly observed in Kpnβ1 knock-down cancer cells[300]. These findings further demonstrate that Kpnβ1 inhibition and INI-43 treatment triggered similar cellular events and phenotypes, supporting that INI-43 induced-cancer cell death is mediated through Kpnβ1.

INI-43 appeared less toxic to non-cancer cells, with IC_{50} values 2-3 fold higher in non-cancer fibroblast cells compared to cancer cells. At concentrations between 10 μM and 15 μM, INI-43 inhibited cancer cells by 100% whilst not affecting non-cancer cells. The selectivity of INI-43 may derive from the increased reliance of cancer cells on Kpnβ1 function[296]; which could be its nuclear import function in interphase cells and/or its mitotic involvement in dividing cells. As Kpnβ1 inhibition with siRNA and INI-43 both induced apoptosis related to G2/M cell cycle arrest[300, 333], it is likely that the apoptotic event is at least due partly to interference of the mitotic functions of Kpnβ1. Interestingly, the mechanism of cell death and selectivity of nuclear import inhibition is similarly observed in CRM1 inhibited cells, implying that altered nuclear transport in both directions caused similar deleterious effects on cancer cells[238].

Liver microsome and toxicology analyses of INI-43 revealed moderate stability and tolerability in athymic nude mice of up to 50 mg/kg, although 50 mg/kg may not be the maximum tolerated dose. The approved use of Ivermectin for treating parasitic infections, a compound with recently identified nuclear import inhibitory effects further demonstrates the systemic safety of nuclear import inhibitors. The promising data obtained from *in vitro* and toxicology studies prompted further experimentation in preclinical models, where the three dimensional development of tumours and interactions with its microenvironment is recapitulated. We showed that in the ectopic xenograft mouse model, intraperitoneally administered INI-43 hindered tumour growth, and the effects were

more pronounced in CaSki and WHCO6 cells. Both CaSki and KYSE30 tumours developed necrosis, a characteristic of aggressive tumours that strongly correlates to invasiveness[353]. INI-43 treatment in mice bearing those tumours showed reduced necrotic occurrence, suggesting that INI-43 may potentially be effective at treating aggressive epithelial neoplasm, although further experimental validation is needed. The selective anti-cancer effects of INI-43 *in vitro* and *in vivo* adds significance to its clinical potentials, yet further modification of its chemical structure may be necessary, as INI-43 is a compound with low solubility, which may compromise its deliverance systemically. Nonetheless, our findings show that INI-43 could be a useful lead parent compound for future generations of Kpnβ1 inhibitors with cancer therapeutic purposes.

As current anti-cancer treatment frequently employ the use of multiple chemotherapeutic agents, we examined the possibility of using INI-43 in combination with CDDP, a widely available first-line drug used in treating various cancers including small cell-lung cancer, ovarian cancer and cervical cancer. This compound was chosen for analysis in combination with INI-43 as it is a DNA-damaging agent, which meets the criteria where two agents used in combination should not have overlapping mechanisms of action. We hypothesized that nuclear trafficking of proteins is an important response under DNA damage conditions, and may play a role in drug resistance. Crippling this mechanism could therefore produce favourable outcomes in cancer cells less responsive to CDDP. Studies in the ovarian cancer model revealed elevated levels and altered localization of Kpnβ1 in response to CDDP treatment, suggesting that Kpnβ1 is responsive to DNA damage. Similar observations were made in HEK293 cells, where hydrogen-peroxide stress evoked a response in Kpnβ1 and its transport activity[384], suggesting that Kpnβ1 is involved in stress response in general.

As INI-43 has been shown to inhibit nuclear translocation of Kpnβ1 within 45-minute of treatment, and that 1.5-hour treatment was sufficient to impede nuclear import of Kpnβ1 cargoes[333], the combined treatment of INI-43 and CDDP was designed with 2-hour INI-43 pre-treatment at a sub-

lethal concentration (5 μM) followed by exposure to CDDP. Using this treatment protocol, both ovarian cancer and cervical cancer cells showed increased sensitivity to CDDP compared to cells which didn't receive the INI-43 pre-treatment. In both cancer models, this was attributed to increased apoptosis, which correlated with increased caspase-3/7 activity in SiHa cells, indicative of an escalation in the intrinsic apoptotic pathway. Furthermore, siRNA mediated Kpnβ1 knock-down in both cancer models led to increased CDDP sensitivity, illustrating that Kpnβ1 directly contributed to CDDP resistance.

In the combination treatment regimen, the dose of INI-43 used (5 μM) was not sufficient to cause cell death on its own, yet in combination it significantly enhanced CDDP-induced cell death in both cancer models, suggesting a synergistic relationship between the two drugs. CI determination in SiHa cells confirmed this, where the majority of the combinations produced superior killing effects compared to the additive effects of either drugs used on its own. These findings suggest that this combinatory pair may have potential and warrants further research.

In the ovarian cancer cell lines OVCAR4 and OVCAR5, CDDP treatment induced Kpnβ1 expression and nuclear localization, although whether this results in increased transport rates remain to be investigated. The enhanced apoptotic activities observed in the combination treatment correlated with a decrease in CDDP-induced nuclear Kpnβ1 accumulation, suggesting that the nuclear localization of Kpnβ1 may promote survival in cancer cells under stress conditions. Our findings suggest that Kpnβ1 associated activities favour the survival of ovarian cancer cells when exposed to CDDP. This was similarly observed in cervical cancer cells, although Kpnβ1 itself did not show a significant increase in nuclear localization or expression after CDDP treatment. It is possible that other regulatory mechanisms exist in HeLa cells that prevents the uncoordinated elevation in Kpnβ1 levels in response to CDDP, as this has been shown to cause mitotic disadvantages in this cell line[282, 286]. Although increased Kpnβ1 levels was not observed in cervical cancer cells in response to CDDP,

the increase in nuclear accumulation of the Kpnβ1 cargo NFκB-p50 and NFκB-p65 suggest that there was a change in substrate specificity or increase in Kpnβ1 activity in response to CDDP. Associated with this, an increase in cyclinD1 and c-Myc levels were observed in response to CDDP, both of which are transcriptionally regulated by NFκB[424-428]. INI-43 pre-treatment decreased the CDDP-induced nuclear localization of NFκB presumably by interfering with Kpnβ1 activity, and the expression of both cyclinD1 and c-Myc were accordingly reduced. These findings provides a possible explanation to the enhanced CDDP sensitivity, whereby INI-43 decreases the activation of pro-survival factors like NFκB by preventing their nuclear entry.

Using the cervical cancer cell line SiHa, we found that siRNA mediated p53 inhibition abrogated the enhanced cell death observed in the combination treatment. This suggest that the enhanced cell death observed in the combination treatment compared to the single treatment may in part result from p53 activity. We hypothesized that a change in p53 stability may account for the differences observed between single and combination treatment, and in support, we found an increase in p53 stability in the presence of INI-43. Kpnβ1 knock-down experiments further demonstrated that INI-43 induced p53 stability was a result of Kpnβ1 inhibition. We also speculate that there may be a overlap between the p53 and NFκB pathway, as both proteins negatively regulate the transcriptional activity of each other[459]. The decreased levels of NFκB-target genes in INI-43 treated cells could thus result from a combined effect of decreased NFκB nuclear localization as well as p53 stabilization. Furthermore, the combination treatment was ineffective at sensitizing C33A to CDDP, a p53 mutant cell line, suggesting that the presence of wildtype p53 may be the determining factor for the synergistic interaction between INI-43 and CDDP in cervical cancer cells.

The involvement of p53 in the responsiveness to the combination treatment for ovarian cancer cell lines OVCAR4 and OVCAR5 remains unclear, as contradicting evidence exist in literature regarding the p53 status for these two cell lines[470, 471]. However, if either cell lines harbour a mutant p53, this

would suggest an alternative, p53-independent mechanism for the enhanced cell death observed in combination treatment of these cells.

The decreased expression of both cyclinD1 and c-Myc associated with sustained γH2AX expression 24 hours after CDDP treatment. This could be an indication of enhanced DNA damage or prolonged DNA damage repair. As Kpnβ1 is also known to transport various cargoes involved in DNA repair, the enhanced level of γH2AX could result from the weakened DNA damage repair capacity as Kpnβ1 inhibition would prevent the nuclear entry of these cargoes. A decrease in other pro-survival factors, including XIAP and Mcl-1 were also observed in INI-43 pre-treated cells, which correlated with elevated apoptosis. The fact that p53 knock-down abrogated the ability of INI-43 to sensitize cancer cells to CDDP suggest that p53 is likely the key regulator in this network of events, and that the changes observed in c-Myc, XIAP and Mcl-1, NFκB and cyclinD1 is likely dependent on p53 activities in SiHa cells.

Whilst the enhanced killing effects of the combination treatment are linked to suppression of various anti-apoptotic factors, we also observed elevation of p21, which showed pro-survival effects. We speculate that the combined use of INI-43 and CDDP, as opposed to CDDP only, elicited alterations in numerous cellular events, some of which promoted cell death and others antagonizing it. However, the net outcome of enhanced cell death compared to the single use of CDDP demonstrated the feasibility of combining nuclear import inhibition and CDDP. Additionally, these results suggest a potential for targeting p21 and Kpnβ1 simultaneously in combination with CDDP, which further improved treatment outcome in SiHa cells.

We demonstrated that the combined use of INI-43 and CDDP achieved greater killing effects compared to CDDP alone, which occurred through alteration of multiple cellular events. Amongst these, p53 appears to be an important mediator for the enhanced killing in the combination

treatment in the cervical cancer model. The role of p53 in the combination treatment in other cancer models should, however be determined empirically using cells with known p53 status. If the benefit of this combination treatment is dependent on the presence of wildtype p53, this approach would then be more effective at treating cancers with lower occurrence of p53 mutations, such as cervical cancer. The main etiology for cervical cancer is HPV infection, where the viral E6 protein directly inactivates p53, thereby alleviating the selection pressure for loss-of-p53 function in this type of cancer. Indeed, mutations in p53 is observed more frequently in HPV negative cervical cancer than HPV positive cervical cancer (70.8% versus 36.4%)[472]. Other cancers known to present with low p53 mutation events include myeloid leukemia and skin squamous cell carcinoma[472], which could potentially be treated using this approach. However, if OVCAR4 and OVCAR5 are p53 mutant cells, our data suggest that INI-43 could sensitize cancer cells to CDDP via alternative pathways independent of p53, and that this approach could be effective at treating cancers with non-functional p53.

In conclusion, our study provides evidence for nuclear import inhibition as a novel class of anti-cancer targets. This is illustrated through the use of INI-43, a potential inhibitor of Kpnβ1 which targeted cancer cells and sensitized cancer cells to CDDP. We propose that further development of this compound may result in clinically useful anti-cancer therapies. On the other hand, coupling nuclear import inhibition to current therapeutic regimens could significantly enhance cancer cell death, or alternatively, the same treatment outcome could be achieved with lower doses of CDDP, thereby easing the undesired side effects associated with CDDP.

5.2. Summary of key findings

1. At concentrations around 10 μM, the small molecule INI-43 inhibited proliferation and induced apoptosis in cancer cells whilst having minimal effect on non-cancer cells proliferation *in vitro*.

2. The effects of INI-43 are likely mediated through interfering with Kpnβ1 function, as both INI-43 treatment Kpnβ1 knock-down induced similar phenotypes, and Kpnβ1 over-expression partially reversed the cancer-killing effect of INI-43.

3. INI-43 decreased tumour growth in both cervical and oesophageal cancer in xenograft mouse models.

4. INI-43 sensitized ovarian cancer cells to CDDP treatment, which correlated with decreased nuclear localization of Kpnβ1.

5. INI-43 sensitized cervical cancer cells to CDDP treatment synergistically, and the enhanced CDDP sensitivity is associated with p53 activity and repression of various anti-apoptotic factors including Mcl-1, c-Myc and XIAP.

5.3. Future experiments

Recommended future work include dissecting out the mechanism by which INI-43 induces cancer cell apoptosis, and to conduct comparable cell viability assays using more suitable controls such as non-cancer epithelial cells. As we speculate and have data to suggest that INI-43 acts by interfering with Kpnβ1 function, further experiments to support this could include examining the effects of INI-43 on localization of cargoes known to be exclusively ferried by Kpnβ1 (such as SREBP1[316]). Moreover, as Kpnβ1 also play important roles in many mitotic events[282, 286], the effects of INI-43 on mitotic processes should be investigated, including spindle assembly, chromosome segregation, nuclear envelope degradation and reformation. Investigating the effect of INI-43 on other members of the Karyopherin family known to co-operate with Kpnβ1 in importing cargoes (such as Karyopherinα) could provide more insight into understanding how INI-43 affects Kpnβ1.

The interaction between INI-43 and Kpnβ1 could be confirmed by targeted mutation in the predicted binding region of INI-43 to Kpnβ1, i.e. amino acids 331-363. Other experiments to confirm direct binding of INI-43 to Kpnβ1 is currently being investigated in our laboratory through circular dichroism, fluorescence resonance energy transfer and isothermal titration calorimetry. As discussed earlier, the pharmacokinetic and pharmacodynamic properties of INI-43 is another area to focus on, including examining the absorption, distribution and excretion of INI-43 in a living system. For extensive *in vivo* testing, the structure of INI-43 could be modified to improve its chemical property such as solubility.

The combination treatment of INI-43 and CDDP have generated promising results, and could be furthered by testing in an *in vivo* system such as in xenograft mouse models. The mechanism by which INI-43 stabilizes p53 should be addressed, these experiments include investigating the effects

of INI-43 on p53 and other proteins known to be involved in determining p53 stability (such as HPV E6 and MDM2). The combination treatment should also be tested in a suitable non-cancer system to address whether the enhanced killing effect is specific to cancer.

CHAPTER 6

MATERIALS AND METHODS

6.1. Materials

6.1.1. Cell lines

The following cell lines were obtained from the American Type Culture Collection (ATCC, Rockville, MD, USA): human cervical carcinoma cell lines, HeLa (HPV18), CaSki (HPV16 and HPV18), SiHa (HPV16) and C33A (HPV negative); and normal breast skin fibroblasts CCD-1068SK. Oesophageal carcinoma cell lines WHCO5 and WHCO6 were originally derived from South African patients with oesophageal squamous cell carcinoma, and were acquired from Prof. R. Veale (University of Witwatersrand)[473]. KYSE30 was established by Shimada *et al*. and were purchased from German Resource Centre for Biological Materials, DSMZ GmbH (Braunschweig, Germany)[474]. Normal skin fibroblasts FG_0 and DMB were obtained from the Department of Medicine, University of Cape Town. All the ovarian epithelial carcinoma cell lines; including A2780, OVCAR3, OVCAR4, OVCAR5, OVCAR8, SKOV3 and CP70, as well as the immortalized ovarian surface epithelial cell line T29 were provided by Prof. M. Birrer (Harvard Medical School, MA, USA), and were originally obtained as previously described[475-477].

6.1.2. siRNA (Kpnβ1, p53, p21)

Inhibition of gene expression was achieved using small-interfering RNA (siRNA). All siRNAs were purchased as lyophilized powders from Santa Cruz Biotechnology (Santa Cruz, CA, USA), including Kpnβ1 siRNA (sc-35736), p21 (sc-29427), p53 (sc-29435) and the control siRNA (sc-37007). The

lyophilized powder was resuspended in RNase-free water to a concentration of 10 µM and stored at -20^{O}C.

6.1.3. Compounds

6.1.3.1. Inhibitor of Nuclear Import-43 (INI-43)

Inhibitor of Nuclear Import-43 (INI-43, chemical name *3-(1H-benzimidazol-2-yl)-1-(3-dimethylaminopropyl)pyrrolo[5,4-b]quinoxalin-2-amine*)) was purchased in powder form from Chembridge (ZINC identification number 20547783, San Diego, CA, USA) and MolPort Chemicals (MolPort-000-492-602, Riga Latvia). The compound was dissolved in DMSO to a stock concentration of 10 mM and stored at -20^{O}C.

6.1.3.2. Ivermectin

Nuclear import inhibitor Ivermectin was purchased from Sigma-Aldrich (St Louis, MO, USA) and dissolved in DMSO to a stock concentration of 50 mM and stored at -20^{O}C.

6.1.3.3. Importazole

Nuclear import inhibitor Importazole was purchased from Sigma-Aldrich (St Louis, MO, USA) and dissolved in DMSO to a stock concentration of 50 mM and stored at 4^{O}C.

6.1.3.4. CDDP

Cisplatin (CDDP) was purchased as a powder form from Sigma-Aldrich (St Louis, MO, USA), and dissolved in 0.9% NaCl to a concentration of 1 mg/mL. Solutions were filter sterilized through a 0.22 µm filter and kept at room temperature protected from light.

6.1.3.5. Doxycycline

Doxycycline (Dox) was purchased as a powder form from Sigma-Aldrich (St Louis, MO, USA), and dissolved in water to a concentration of 10 mg/mL. The solution was filter sterilized through a 0.22 µm filter and kept at -20^{O}C protected from light.

6.1.3.6. Puromycin

Puromycin was purchased as a powder form from Calbiochem (Merck), and dissolved in water to a concentration of 10 mg/mL. The solution was filter sterilized through a 0.22 µm filter and kept at -20^{O}C protected from the light.

6.1.4. Plasmids

6.1.4.1. pHIV7-TetR-IRES-GFP-shRNA

To conditionally inhibit the expression of Kpnβ1 in cancer cells, the lentiviral construct for doxycycline-inducible shRNA expression, the pHIV7-TetR-IRES-GFP (pTIG) plasmid was used. The construct pTIG-shRNA-Kpnβ1 (pTIG-shKpnβ1) was cloned using the pTIG-shRNA-TBX2 (pTIG-shTBX2) as the starting material (see section 6.2.9), which was a kind gift from A/Prof. S. Prince (University of Cape Town, South Africa). The pTIG plasmid was originally designed by A/Prof. M. Weinberg (University of Witwatersrand, South Africa, see Appendix Fig. A.2)[338]. The control plasmid used in these experiments, pTIG-scrambled sequence (pTIG-scr) was a kind gift from Dr A. Cooper and A/Prof. S. Prince.

6.1.4.2. pEFIRES-GFP plasmids

Kpnβ1 over-expressing HeLa cells and control cells (HeLa-pEFIRES-Kpnβ1-GFP and HeLa-pEFIRES-GFP) were established using the pEFIRES-GFP construct as previously described[333]. The pEFIRES plasmid was kindly provided by Yosef Shaul (Weizmann Institute of Science, Isreal)[478], and the Kpnβ1 sequence was released from the pEGFP-Kpnβ1 plasmid kindly provided by Prof. P. Lavia (Institute of Molecular Biology and Pathology, CNR National Research Council, Rome, Italy)[282]. Cloning of the pEFIRES-Kpnβ1-GFP, and establishment of the pEFIRES stable cell lines were achieved by Dr P. van der Watt and Dr K. Hadley.

6.1.4.3. pQC-NLS-mCherry IX

Kpnβ1 activity was assessed in ovarian cancer cells using the pQC-NLS-mCherry IX construct purchased from Addgene Repository, and a kind gift from Connie Cepko (plasmid #37354)[479].

6.1.5. Antibodies

The following antibodies used for the western blot and immunofluorescence experiments were purchased from Santa Cruz Biotechnology: rabbit anti-Kpnβ1 (H300, sc-11367), rabbit anti-β-tubulin (H-235, sc-9104), mouse anti-GAPDH (0411, sc-47724), rabbit anti-GFP (FL, c-8334), rabbit anti-PARP-1 (H-250, sc-7150), rabbit anti-TBP (TFIID, N-12, sc-204), rabbit anti-p21 (H-164, sc-756), rabbit anti-Mcl-1 (H-260, sc-20679), rabbit anti-NFκB p50 (H-119, sc-7178), rabbit anti-NFκB p65 (H-286, sc-7151), mouse anti-cyclinD1 (HD11, sc-246) and rabbit anti-c-Myc (N-262, sc-764). Other antibodies used for western blot experiments include mouse anti-cytochrome C (Clone 7H8.2C12, 556433, BD Pharmingen, San Diego, CA, USA), rabbit anti-Peroxiredoxin-3 (Prdx-3, raised against synthetic peptide corresponding to amino acids 241-256 of human Prdx-3, p1247, Sigma), rabbit anti-Histone H3 (D1H2, raised against carboxy terminus of human histone H3 protein #4499, Cell Signal), rabbit

anti-phospho-Histone H2A.X (γH2AX, Ser139, 20E3, #9718, Cell Signal), anti-cleaved PARP (Asp214, D64E10, #5625, cell signal), mouse anti-XIAP (raised against human XIAP amino acid 268-426, 610763, BD Biosciences) and mouse anti-p53 (DO-7, raised against recombinant human wildtype p53, M7001, DakoCytomation, Glostrup, Denmark). Secondary antibodies used were Goat anti-Rabbit IgG (H + L)-HRP Conjugate (#1706515, Bio-Rad), Goat anti-Mouse IgG (H + L)-HRP Conjugate (#1706516, Bio-Rad), Goat anti-Rabbit IgG (H + L), FITC conjudate (#65-6111, Thermofisher Scientific), Alexa Fluor 647 Chicken anti-Rabbit IgG antibody (#A-21443, Molecular Probes), and Cy3-conjugated Goat anti-Rabbit (#111-165-144, Jackson ImmunoResearch).

6.1.6. Animals

Animal ethics approval was obtained from the Faculty of Health Sciences Animal Ethics Committee, University of Cape Town, South Africa (reference number 012/009) for all animal experiments. Male and female athymic nu/nu mice (UCT 21) of 4 - 6 weeks age were obtained from the animal breeding unit (Health Sciences, University of Cape Town, South Africa) and all procedures were carried out in strict accordance with the guidelines of the Animal Ethics Committee, University of Cape Town. The mice were housed 6 per cage in autoclaved polysulfone cages in a room maintained at constant temperature and humidity. Mice were housed under 12-hour light and darkness cycles and were fed a regular autoclaved chow diet with water containing antibiotics and multi-vitamins.

6.2. Methods

6.2.1. INI-43 mass and purity confirmation

To ensure the identity and quality of INI-43 used in this study, INI-43 was dissolved in 100% DMSO (Sigma) and analyzed by reverse-phase high performance liquid chromatography tandem mass spectrometry. INI-43 was separated on a 2.1 mm x 150 mm column (Kinetex C_{18}, particle size 2.6 µM) using a gradient flow, from 5 mM ammonium formate (pH 3) in 5% acetonitrile to 95% acetonitrile, at an eluent flow rate of 0.4 mL/min. Detection was accomplished using a diode array detector (DAD) coupled to an AB SCIEX 4000 QTRAP MS and equipped with electrospray positive ionization capacity (Turbo V^{TM} ion source).The sample volume was 300 µL, and the acquisition mode was single quadrupole full scan, scanning from m/z 100 to 500 at 1 sec/scan. The target compound was detected at 33.33 µM. Analyst 1.5.2 software was used for instrument control and data acquisition.

6.2.2. Cell culture

6.2.2.1. Medium requirements

The cervical cancer, oesophageal cancer, and normal skin fibroblasts cell lines (HeLa, CaSki, SiHa, C33A, WHCO5, WHCO6, KYSE30, CCD-1068SK, DMB and FG_0) were maintained in Dulbecco's Modified Eagle's Medium (DMEM, Gibco, Life Technologies, Carlsbad, CA, USA) supplemented with 100 U/mL penicillin, 100 µg/mL streptomycin and 10% Fetal Calf Serum (Gibco, Life Technologies, Carlsbad, CA, USA). The HeLa-pEFIRES stable cell lines were maintained in full growth medium supplemented with 1.5 µg/mL Puromycin (Calbiochem, Merck). The ovarian cell lines (A2780, OVCAR3, OVCAR4, OVCAR5, OVCAR8, SKOV3, CP70 and T29) were maintained in RPMI-1640 (Invitrogen Life Technologies) supplemented with 10% Fetal Calf Serum (Gibco, Life technologies, CA, USA), 1% L-glutamine, 100 U/mL penicillin and 100 mg/mL streptomycin. All cells were cultured at 37^{O}C in a humidified chamber with 5% CO_2.

6.2.2.2. Subculturing cells

Cells grown in a 10 cm tissue culture dish were washed with PBS before trypsinization with 4 mL of trypsin-EDTA solution. After detachment, the trypsin-EDTA-cell suspension was neutralized with the addition of 4 mL fresh culture medium. Cell suspension were centrifuged at 250 x G for approximately 5 minutes at room temperature or $4^{O}C$ to pellet the cells. The supernatant was aspirated off and cells were resuspended in fresh culture medium at appropriate volumes and placed in new culture dishes.

6.2.2.3. Freezing and thawing cells

For long term storage, cells grown to approximately 80% confluency were collected by trypsinization, neutralization and centrifugation as above described. After aspiration, cell pellet was resuspended in pre-chilled freezing medium at a concentration of approximately 1 x 10^{6} cells per mL freezing medium. Cells were transferred into cryotubes and kept at $-80^{O}C$ for two weeks before placing it in the liquid nitrogen.

To revive the cells, 1 mL frozen cell suspension was thawed to $37^{O}C$ in a waterbath and rapidly added to 9 mL fresh growth medium in a 10 cm culture dish.

6.2.2.4. Mycoplasma checks

To ensure that the cells were free of mycoplasma contamination, cells were routinely checked for mycoplasma as follows: cells were grown in penicillin-free and streptomycin-free culture medium for 3-4 days, and plated onto coverslips. Cells were fixed and stained with Hoechst fluorescent DNA-binding stain before mounting and visualization on a Zeiss Axiovert 200 Fluorescent Microscope (Carl Zeiss, Jena, Germany).

6.2.3. Performing the single (CDDP) and combination (INI-43 and CDDP) treatments

To assess whether nuclear import inhibition via INI-43 treatment had an effect on CDDP sensitivity in cancer cells, we investigated the single CDDP treatment and combination of INI-43 and CDDP treatment. All combination treatments were achieved by pre-treating cells with INI-43 for 2 hours, followed by CDDP treatment without removing INI-43 from the media. This was achieved through 2 serial steps - a pre-treatment using half of the total media volume with 1 x INI-43 concentration for 2 hours, followed by a second treatment using half the total media volume with 1 x INI-43 concentration and 2 x CDDP concentration. For treatment with 5 μM INI-43 and 30 μM CDDP in a 96-well plate where the total media volume was 100 μL, the cells were first treated with 50 μL media containing 5 μM INI-43 for 2 hours, followed by addition of another 50 μL media containing 5 μM INI-43 and 60 μM CDDP, giving a final total volume of 100 μL, with 5 μM INI-43 and 30 μM CDDP. The control cells were subjected to exactly the same procedure, except equivalent volumes of DMSO were administered in place of INI-43.

6.2.4. Half inhibitory concentration (IC_{50}) determination

The IC_{50} for the different agents were determined as follows: cells were plated at 5000 cells/well in a 96-well dish and left overnight to adhere. Cells were then treated with the agent of interest at ranging concentrations for 48 hours, followed by addition of the MTT reagent (3-[4,5-dimethylthiazol-2-yl]-2,5-diphenyltetrazolium bromide, Sigma) for four hours. Crystals were solubilized using Solubilization Reagent for 24 hours. The absorbance, which is indicative of cell viability were measured at OD_{595nm} using a Biotek microplate spectrophotometer (Winooski, VT, USA), and the IC_{50} value was calculated by plotting the [Fa/(1-Fa)] in log scale against log drug concentration, where $Fa = \frac{100 - \%\ viable\ cells\ relative\ to\ the\ untreated}{100}$. The half inhibitory concentration was calculated using the formula $IC_{50} = 10^{x\text{-}intercept}$.

6.2.5. Cell viability assay

Cell viability was examined after incubation with drug of interest for a period of 48 hours unless otherwise stated. Briefly, cells were seeded to settle overnight. After drug treatment for the appropriate time period, MTT reagent was added at 1/10 total volume for 4 hours, and crystals were solubilized with Solubilization Reagent for approximately 24 hours. Cell viability was then determined by absorbance at OD_{595nm} as previously described.

6.2.6. Proliferation assay

To assay for cell proliferation, cells were seeded in 96-well plates at 1000 cells/well. After attachment, cells were treated with INI-43 at various concentrations, and viable cells were examined using the MTT reagent and Solubilization Reagent as previously described, every 24 hours for a period of 5 days.

6.2.7. Clonogenic assay

Cells were seeded sparsely (1000 to 2000 cells per 35 mm dish), followed by INI-43 treatment the next day. Cells were incubated in the presence of INI-43 for 24 hours, before the drug-containing media is replaced with fresh growth media. The viable cells were left to proliferate and form colonies with the growth media replenished every 48 hours, until the control cells have formed colonies with approximately 50 cells per colony. Cells were rinsed with 2 mL PBS and fixed with 2 mL Fixation Solution for 5 minutes at room temperature. Colonies were stained with 1 mL 0.5% Crystal Violet Solution for 2 hours at room temperature, after which crystal violet solution was removed, and the plates were rinsed in tap water. The plates were left to air-dry overnight before images were captured using a standard camera.

6.2.8. Anchorage-independent proliferation assay

Anchorage-independent proliferation of cancer cells were assayed as previously described[480]. Briefly, 10 000 cells were resuspended in 100 µL full growth media containing INI-43 and 1% methylcellulose (Sigma) and plated in triplicates per well of a 96-well plate. Prior to plating, 96-well dishes were coated with 100 µL poly-(HEMA) (Sigma) per well for at least 16 hours to prevent cell adhesion. Colonies were monitored daily, and upon the control cells reaching reasonable colony sizes, the colonies were stained with MTT reagent (Sigma) for several hours at 37^{O}C. Colonies were photographed using brightfield microscope with the Moticam 2500 camera (Motic, British Columbia, Canada) on a Zeiss Telaval microscope.

6.2.9. Cloning of the pTIG- plasmids

To conditionally inhibit the expression of Kpnβ1, an inducible shRNA system was employed. Three Kpnβ1 targeting shRNAs (shKpnβ1-1, shKpnβ1-2 and shKpnβ1-3) were separately cloned into the pHIV7-TetR-IRES-GFP-shRNA vector (pTIG), which expresses shKpnβ1 under the control of the tetracycline/doxycycline-inducible U6 promoter. The starting material, pTIG-shTBX2 was digested with restriction enzyme *BamHI*, which cleaved the plasmid into three segments of 7539bp, 1388bp and 1038bp (Fig. 6.1). The 1038bp fragment which contained the U6 promoter and the shTBX2 was then separated from the other fragments by electrophoresis on a 1% agarose gel (Fig. 6.2.A), and purified using the Wizard® SV Gel and PCR clean-up system (Promega). Using this fragment as the template, primers were designed for PCR to amplify the U6 promoter, with the shKpnβ1 sequence incorporated into the reverse primer (Fig. 6.1). Restriction sites *NotI* and *SphI* were included into the forward primer (1038_forward) and reverse primer (1038_reverse), respectively, along with a few extra base pairs for restriction enzyme digestion (Fig. 6.1). The PCR product was confirmed by electrophoresis to be the right size of approximately 350 bp on a 2% agarose gel (Fig. 6.2.B), and purified using the Wizard® SV Gel and PCR clean-up system (Promega). The PCR product and the

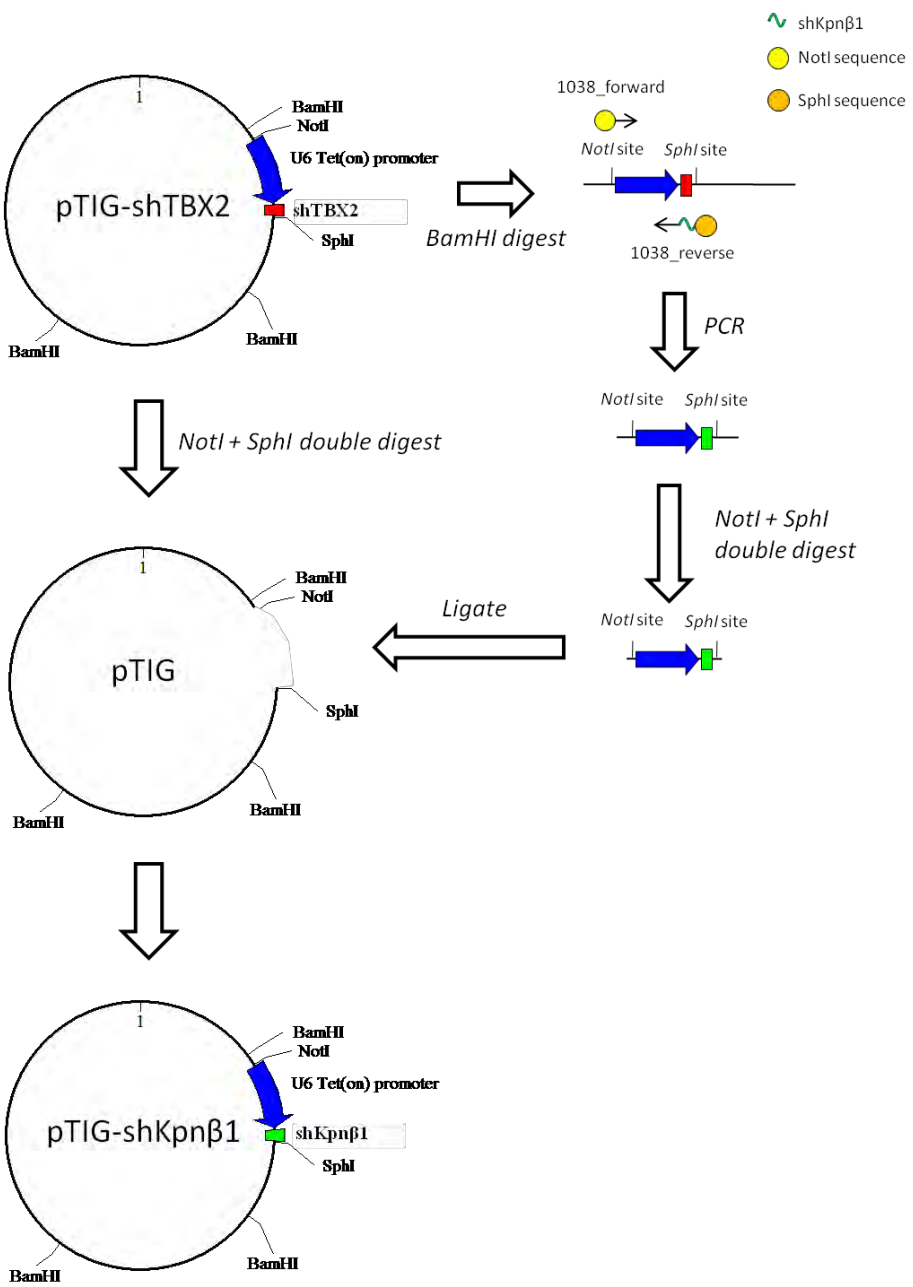

Figure 6.1. Cloning of the doxycycline inducible pHIV7-TetR-IRES-GFP-shRNA-Kpnβ1 (pTIG-shKpnβ1) using the pTIG-shTBX2 plasmid. The pTIG-shTBX2 plasmid was digested with *BamHI* to release a 1038 bp fragment containing both the U6 promoter and shTBX2. Using this fragment as a PCR template, primers were designed with restriction sites *NotI* and *SphI*, and the shKpnβ1 sequence was incorporated into the reverse primer to amplify PCR product containing the U6 promoter and the shKpnβ1 sequence. The PCR product and pTIG-shTBX2 were then both digested with *NotI* and *SphI* independently, followed by ligation to produce pTIG-shKpnβ1.

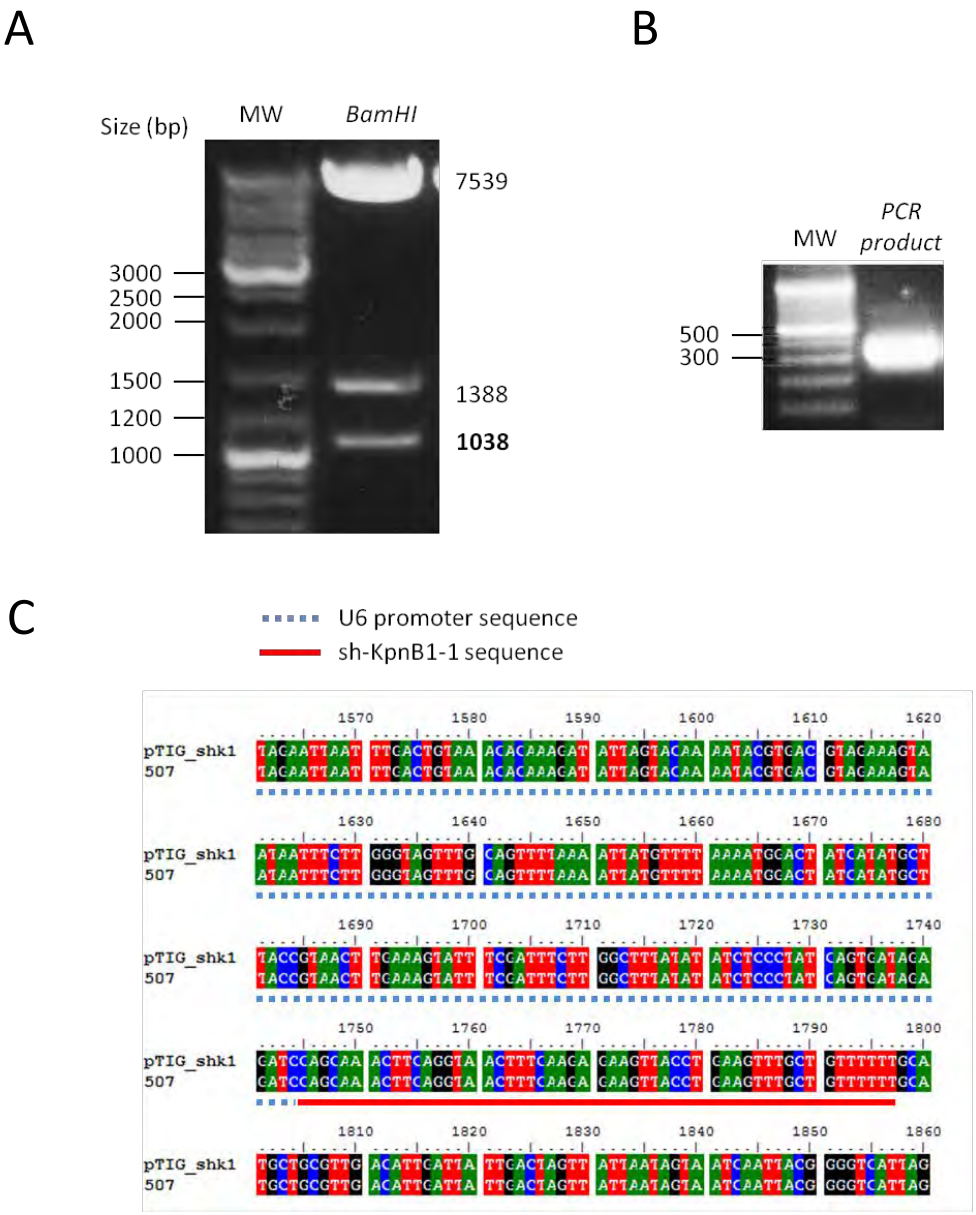

Figure 6.2. Cloning of the doxycycline inducible pHIV7-TetR-IRES-GFP-shRNA-Kpnβ1 (pTIG-shKpnβ1) using the pTIG-shTBX2 plasmid. Gel electrophoresis of *BamHI* digested pTIG-shTBX2, with the 1038bp fragment containing the U6 promoter and shTBX2 (A). Gel electrophoresis of the PCR product ran using the 1038 bp fragment from the *BamHI* digested pTIG-shTBX2, and the 1038_forward and 1038_reverse primers (B). Alignment of cloning product and target sequence in the U6 promoter (blue dotted line) and shKpnβ1-1 region (red solid line), confirming the sequence identity.

pTIG-shTBX2 plasmid were then both digested with *NotI* and *SphI*, followed by ligation of the two fragments together (Fig. 6.1). The resultant plasmid was transformed into competent *E.coli* JM109 cells (Promega), and prepared on large scale using the Maxiprep Kit (Qiagen). Resulting plasmid were then confirmed by sequencing and showed 100% match to the target sequence (Fig. 6.2.C). Details regarding the above mentioned steps were as follows:

(i) Primer sequences:

Forward primer:

5' – GATCGAATTCGGATCCGCGGCCGC*AAGGTCGGGCAGGAAGAGGGCC -3'

Reverse primer:

5' – GTCAACGCAGCATGC**(shRNA sequence)GATCTCTATCACTGATAGGGA -3'

shRNA sequences:

shKpnβ1-1

5' - AAAAAACAGCAAACTTCAGGTAACTTCTCTTGAAAGTTACCTGAAGTTTGCTG -3'

shKpnβ1-2

5' – AAAAAAGCGGCGCAGAAGTTCCTGGTCTCTTGAACCAGGAACTTCTGCGCCGC – 3'

shKpnβ1-3

5' – AAAAAAGGATGTTCCAAAGCACAGCTCTCTTGAAGCTGTGCTTTGGAACATCC – 3'

*GCGGCCGC – *NotI* restriction site

**GCATGC – *SphI* restriction site

(ii) Restriction enzyme digestion were all performed at 37^{O}C for 1 hour per µg of DNA.

(iii) The agarose gels were prepared by adding 1 g (for 1%) or 2 g (for 2%) of agarose powder (Sigma) into 100 mL TAE buffer, followed by microwave heating until completely dissolved. The solution was left at room temperature to reach approximately 60^{O}C, followed by addition of 5 µL of 10 mg/mL ethidium bromide. The solution was then poured into the gel tank to set. DNA materials with loading dye were loaded into the wells and electrophoresed at 90-100 V for a time period sufficient to separate the DNA fragment, alongside a molecular weight marker.

(iv) DNA clean-up and purification from PCR reactions and agarose gels were achieved using the Wizard® SV Gel and PCR clean-up system (Promega); and the large-scale plasmid preparation from *E.coli* were achieved using Maxiprep Kit (Qiagen). Both were used according to the manufacturer's instructions.

(v) PCR was performed in a total volume of 50 µL with 20 pmole of each of the primers, 200 µM dNTP, 2 mM $MgSO_4$, 1 U of Taq *pfu* DNA polymerase (Fermentas), 5% DMSO and 2 ng template DNA in sterile water. PCR conditions were denaturation at 95^{O}C for 5 minutes; followed by 35 cycles of 30-second denaturation at 95^{O}C, 30-second annealing at 50.5^{O}C, 3-minute elongation at 72^{O}C; and a final elongation at 72^{O}C for 15 minutes. The annealing temperature was chosen based on empirical testing, and the temperature cycles were performed using the GeneAmpPCR machine (PCR System 2700, Applied Biosystems).

(vi) Ligation was performed using 500 ng linearized pTIG vector and 30 ng insert (U6-shKpnβ1), 2.5 U T4 DNA ligase (Promega) in a total reaction volume of 20 µL. Reaction was incubated at room temperature for 16 hours.

(vii) Transformation was performed by addition of the entire ligation product into 50 µL of competent *E.coli* JM109 (Promega) and mixed by flicking. The tubes were placed on ice for 20 minutes, followed by a heat shock in a 42^{O}C waterbath for 2 minutes. The tube was placed back on ice for another 2 minutes, and 450 µL of LB was added. The cells were incubated at 37^{O}C for 1 hour with 150 rpm shaking. A volume of 100 µL from the transformation reaction was then plated onto selective LA plates containing 100 µg/mL ampicillin, and the plates were incubated at 37^{O}C overnight. Viable colonies indicated the successful uptake of plasmid DNA.

(viii) The BigDye® Terminator V3.1 Cycle Sequencing Kit (Applied Biosystems) was used to confirm the sequence of the clones, where all procedures performed were in strict accordance with the manufacturer's instructions and temperature cycles were performed using the GeneAmpPCR machine (PCR System 2700, Applied Biosystems). DNA was cleaned up by ethanol precipitation and the DNA pellet was electrophoresed at the Human Genetics department (Health Sciences faculty, University of Cape Town).

6.2.10. siRNA and plasmid transfection (siRNA, pEFIRES, pTIG, mCherry)

To insert siRNA into cells, the transfection reagent Transfectin (Bio-Rad) or Lipofectamine^{R} 2000 Reagent (Invitrogen Life Technologies) were used for cervical and ovarian cancers, respectively. Transfection mixes were prepared according to the final siRNA concentration and size of dish been transfected. Generally, for transfection of 20 nM siRNA, 1 µL of Transfectin or 0.9 µL of

Lipofectamine^{R} 2000 Reagent per mL total media volume were used. Cells were generally seeded in 10 cm dishes on day 0, followed by transfection on day 1. On day 2, the transfected cells were sub-cultured into smaller dishes for the subsequent experiments, unless otherwise stated. For si-Kpnβ1 transfection (20 nM) in a 10 cm dish, 10 µL Transfectin was added to 800 µL DMEM and incubated at room temperature for 5 minutes. A volume of 20 µL 10 µM si-Kpnβ1 was then added to the mix and gently mixed by flicking the tube. The mixture was incubated at room temperature for 15 - 20 minutes, and added dropwise to the cells in 5 mL penicillin-free and streptomycin-free growth media, giving a final siRNA concentration of 20 nM. For transfection of si-p21 and si-53 (30 nM) in the same size dish, 15 µL Transfectin and 30 µL of 10 µM siRNA were used. After 5 - 6 hours of incubation, the transfection mix-containing media was replaced with fresh growth media containing penicillin and streptomycin. For transfection of 20 nM si-Kpnβ1 using Lipofectamine^{R} 2000 Reagent in ovarian cancer cells, 9 µL of Lipofectamine^{R} 2000 Reagent was gently mixed with 1.5 mL DMEM and incubated at room temperature for 5 minutes, after which 20 µL of 10 µM si-Kpnβ1 diluted in 1.5 mL DMEM was added. The transfection mix were gently tapped and incubated at room temperature for 20 minutes, and all 3 mL were then added dropwise to cells in the 10 cm dish containing 7 mL penicilline-free and streptomycin-free growth media. Successful knock-down is verified via western blotting 48 hours after transfection.

For transfection of the pTIG series of plasmid, the transfection reagent GencCellin^{TM} Transfection Reagent (Celtic Molecular Diagnostics, South Africa) was used. Briefly, 4 µL of GencCellin^{TM} Transfection Reagent was used per µg of plasmid DNA transfected. For transfection in a 60 mm culture dish, 2 µg of pTIG plasmid was diluted in 200 µL DMEM, to which 8 µL of GencCellin^{TM} Transfection Reagent was added. The mixture was vortexed for 2 - 3 seconds, and incubated at room temperature for 15 minutes, after which the mixture was added dropwise to the cells giving a final DNA concentration of 500 ng/mL.

For transfection of the pQC-NLS-mCherry-IX plasmid in ovarian cancer cells, Lipofectamine^{R} 2000 Reagent was used. Cells were seeded in 24-well plates in total volumes of 300 µL, followed by transfection of 800 ng pQC-NLS-mCherry-IX using 3 µL of Lipofectamine^{R} 2000 Reagent, each diluted in 50 µL of DMEM and the rest of the procedure is identical to above-described.

6.2.11. Protein harvest from cultured cells and quantification

To analyze protein levels under various conditions, proteins were harvested from cells. Depending on the question addressed in each experiment, proteins were harvested from different cellular fractions.

All buffers and solutions used in protein extraction procedures were added with 1 x complete protease inhibitor cocktail (Roche, Basel, Switzerland) and 0.1 M Sodium Orthovanadata (Na_3VO_4) to inhibit phosphatases prior to use.

6.2.11.1. Whole cell lysates from live cells

To analyze protein expression in viable cells, whole cell lysate were extracted using the RIPA buffer on ice. Cells were grown and subjected to the required treatment for a period of time. Before protein extraction, cells were washed with ice-cold PBS twice, followed by addition of RIPA buffer. The RIPA buffer-cell mix was scraped from the dish and placed into eppendorf tubes. The lysates were then sonicated for 3 - 5 seconds to shear the DNA strands, which were then removed together with other cellular debris by centrifugation at 10 000 x G for 10 minutes. The supernatant containing the proteins were then placed into new pre-chilled eppendorf tubes, and the entire procedure was performed strictly on ice. Protein samples were stored at -80^{O}C until ready for quantification and western blotting.

6.2.11.2. Whole cell lysates from live and dead cells

To analyze PARP cleavage as an indication of apoptosis, lysates from both live and dead cells were extracted. After the required treatment for the required time (generally 48 hours, unless otherwise stated), the culture media containing the floating dead cells were collected into a falcon tube and pelleted by centrifugation at 250 x G for 5 minutes. The dead-cell pellet and the viable adherent cells were both washed twice in ice-cold PBS, followed by addition of RIPA. Proteins from the live and dead cells were then combined, and subsequently subjected to sonication and centrifugation as previously described. The entire procedure was performed strictly on ice.

6.2.11.3. Mitochrondrial fractionation

To investigate the mitochondrial release of cytochrome C after INI-43 treatment, cells were grown and treated with INI-43 in 10 cm dishes. After the required length of incubation period, cells were washed twice in cold PBS, followed by lysis in Subcellular Fractionation Buffer and passed through a 25 Ga needle ten times. The samples were then incubated on ice for 20 minutes, and centrifuged at 720 x G for 5 minutes. The supernatant was further centrifuged at 10 000 x G, and the pellet was washed in Subcellular Fractional Buffer and passed ten times through a 25 Ga needle again, followed by centrifugation at 10 000 x G. The resulting pellet containing the mitochondrial material was resuspended in RIPA buffer, and stored at -80^{O}C until ready for analysis.

6.2.11.4. Nuclear and cytoplasmic fractionation

To examine the changes in nuclear content of certain proteins after CDDP and INI-43 treatment, the nuclear proteins were harvested separately from the cytoplasm. Cells were grown in 10 cm dishes and subjected to the required treatment. At time of harvesting, cells were washed twice in ice-cold PBS, and collected by trypsinization as previously described. The cell pellets were resuspended in Harvest Buffer on ice for 5 minutes, followed by centrifugation at 1000 x G for 10 minutes which

separated the cytoplasmic fraction (supernatant) and the nuclear fraction (pellet). The cytoplasmic fraction was centrifuged again at 14 000 x G for 15 minutes, and the supernatant stored at -80^{O}C. The nuclear pellet was washed in Buffer A, and centrifuged at 1000 x G for 5 minutes. The pellet was then resuspended in Buffer C and vortexed for 15 minutes at 4^{O}C to extract the nuclear protein, followed by centrifugation at 14 000 x G for 10 minutes. The supernatant containing the nuclear protein was moved into a new eppendorf and stored at -80^{O}C.

All protein samples were quantified in 96-well plates using the BCA Protein Assay Kit (Pierce, Thermo Scientific, Rockford, IL, USA), according to the manufacturer's instructions. The absorbencies at OD_{595nm} were determined using a Biotek microplate spectrophotometer (Winooski, VT, USA), alongside the BSA protein standards.

6.2.12. Western blot analysis

6.2.12.1. Sodium dodecyl sulphate polyacrylamide gel electrophoresis (SDS-PAGE) and protein transfer

SDS-polyacrylamide gels were prepared with 4% stacking gel on top of the 7.5% - 15% resolving gel. 1-50 µg of protein samples were heat denatured in the presence of 1 x Laemmli Loading Dye at 95^{O}C for 5 minutes, and loaded into the wells of the stacking gel. The protein molecular weight marker, Kaleidoscope (Bio-Rad) was loaded alongside to determine the size of the proteins. Samples were electrophoresed at 150 V-180 V for a period of time sufficient to separate the protein of interest, using the Bio-Rad Mini Protein II System (Bio-Rad, Hercules, CA, USA). Following electrophoresis, proteins were transferred onto a Hybond^{TM}-ECL^{TM} nitrocellulose membrane (Amersham Biosciences, Buckinghamshire, U.K.) using a tank transfer system (Bio-Rad) at 100V for 70 minutes.

6.2.12.2. Immunoblotting and chemiluminescent detection

After transfer, the nitrocellulose membranes were blocked in 5% (w/v) fat-free milk prepared in TBST at room temperature for 1 hour. Membranes were then incubated with the primary antibody (refer to Table 6.1 for antibody conditions) at $4^{O}C$ overnight with shaking. The membranes were then washed 3 x 10 minutes in TBST with shaking, and the secondary antibody was applied for 1 - 3 hours at room temperature with shaking. The membranes were again washed 3 x 5 minutes, where after the antibody was detected using the Lumiglo, Lumiglo Reserve (KPL, Inc., Gaithersburg, MD, USA) or Super Signal™ West Pico Chemiluminescent Substrate (Thermo Fisher Scientific) depending on the strength of the signal. The chemiluminescent light emission was detected by exposing X-ray films (AGFA) to the nitrocellulose membrane for a period of time, followed by immersing the film in developer (AGFA G128), water, then fixative (AGFA G333C) and water.

6.2.12.3. Stripping and reprobing blots

For stripping and reprobing, membranes were immersed in Stripping Buffer for 10 - 20 minutes, replacing with fresh Stripping Buffer halfway. Membranes were then washed in PBS 2 x 10 minutes, followed by 2 x 5 minutes in TBST, after which blocking and incubation with primary antibody can proceed.

6.2.13. Immunofluorescence

To analyze the cellular distribution of proteins, cells were grown on glass coverslips and subjected to the appropriate treatments. Cells were then washed twice in ice-cold PBS, and fixed in 4% paraformaldehyde prepared in PBS for 10 minutes at room temperature. The cells were then washed with PBS, and permeabilized by a 5 minute incubation with 0.5% Triton-X-100 prepared in PBS at room temperature. After one wash in PBST, the cells were blocked using Blocking Buffer for

Table 6.1. Antibody concentrations and incubation conditions for western blot analysis

Primary antibody	Primary antibody conditions	Secondary antibody	Secondary antibody conditions	Substrate
Rabbit anti-Kpnβ1 (Santa Cruz)	1:2000, 5% milk	Goat anti Rabbit (Bio-Rad)	1:5000, TBST	Lumiglo Super Signal
Mouse anti-GAPDH (Santa Cruz)	1:10000, TBST	Goat anti Mouse (Bio-Rad)	1:5000, 5 % milk	Lumiglo Super Signal
Rabbit anti-β-tubulin (Santa Cruz)	1:1000, TBST	Goat anti Rabbit (Bio-Rad)	1:5000, TBST	Lumiglo Super Signal
Rabbit anti-GFP (Santa Cruz)	1:1000, TBST	Goat anti Rabbit (Bio-Rad)	1:5000, TBST	Lumiglo
Rabbit anti-PARP-1 (Santa Cruz)	1:1000, 5% milk	Goat anti Rabbit (Bio-Rad)	1:5000, TBST	Lumiglo
Rabbit anti-TFIID (TBP) (Santa Cruz)	1:1000, TBST	Goat anti Rabbit (Bio-Rad)	1:5000, TBST	Lumiglo
Rabbit anti-p21 (Santa Cruz)	1:200, 5% milk	Goat anti Rabbit (Bio-Rad)	1:5000, TBST	Lumiglo
Rabbit anti-Mcl-1 (Santa Cruz)	1:250, TBST	Goat anti Rabbit (Bio-Rad)	1:5000, TBST	Lumiglo
Rabbit anti-NFκB p50 (Santa Cruz)	1:5000, TBST	Goat anti Rabbit (Bio-Rad)	1:5000, 5% milk	Lumiglo

Table 6.1. Antibody concentrations and incubation conditions for western blot analysis (continued)

Rabbit anti-NFκB p65 (santa cruz)	1:5000, 5% milk	Goat anti Rabbit	1:5000, 5% milk	Lumiglo Reserve
Mouse anti-cyclinD1 (santa cruz)	1:250, 2.5% milk	Goat anti Mouse	1:2500, 5% milk	Lumiglo Reserve
Mouse anti-c-Myc (santa cruz)	1:200, 5% milk	Goat anti Mouse	1:2000, 5% milk	Lumiglo
Mouse anti-cytochrome C (BD Pharmingen)	1:250, TBST	Goat anti Mouse	1:2500, 5% milk	Lumiglo Reserve
Rabbit anti-Peroxiredoxin-3 (Sigma)	1:4000, TBST	Goat anti Rabbit	1:5000, TBST	Lumiglo
Rabbit anti-Histone H3 (D1H2) (cell signal)	1:5000, TBST	Goat anti Rabbit	1:5000, TBST	Lumiglo Super Signal
Rabbit anti-Phospho-Histone H2A.X (ser139) (cell signaling)	1:500, TBST	Goat anti Rabbit	1:5000, TBST	Lumiglo, Super Signal
Mouse anti-p53 (Dako)	1:500, TBST	Goat anti Mouse	1:2000, 5% milk	Lumiglo
Rabbit anti-Cleaved PARP (cell signal)	1:1000, 5% BSA	Goat anti Rabbit	1:5000, 5% milk	Super Signal
Mouse anti-XIAP (BD Biosciences)	1:500, TBST	Goat anti Mouse	1:2000, 5% milk	Lumiglo

15 minutes at 37^{O}C (Blocking Buffer: 5% Normal Horse Serum (Sigma) and 0.2% Gelatin from cold water fish skin (Sigma) prepared in 1 x PBST). After blocking, cells were incubated with the primary antibody and secondary antibody diluted in Blocking Buffer or 1% BSA (Table 6.2), each for 60 minutes at 37^{O}C with 3 x 5 minute PBST washes in between. The cells were washed one final time with PBST at room temperature, and the nuclei were labelled with 500 ng/mL DAPI. The slides were mounted and coverslipped, and images were visualized using a Zeiss Inverted Fluorescence Microscope under 100 x oil immersion. For confocal imaging, a spinning disk confocal microscopy (Nikon Ti2000 and Yokugawa CSU-X1) was used. Images were acquired using a EMCCD camera (Hamamatsu).

Table 6.2. Antibody concentrations and incubation conditions for immunofluorescence

Primary antibody	Primary antibody conditions	Secondary antibody	Secondary antibody conditions	Cell lines
Rabbit anti Kpnβ1 (Santa Cruz)	1:400, blocking buffer	Goat anti Rabbit IgG, FITC conjugate (Thermofisher Scientific)	1:200, blocking buffer*	Ovarian cancer cell lines
Rabbit anti Kpnβ1 (Santa Cruz)	1:400, blocking buffer	Alexa Fluor 647 Chicken anti Rabbit IgG (Molecular Probes)	1:200, blocking buffer*	Ovarian cancer cell lines
Rabbit anti Kpnβ1 (Santa Cruz)	1:100, 1% BSA in PBST	Cy3 Goat anti Rabbit (Jackson ImmunoResearch)	1:300, 1% BSA in PBST	Cervical cancer cell lines
Rabbit anti NFκB p50 (Santa Cruz)	1:200, 1% BSA in PBST	Cy3 Goat anti Rabbit (Jackson ImmunoResearch)	1:300, 1% BSA in PBST	SiHa
Rabbit anti NFκB p65 (Santa Cruz)	1:200, 1% BSA in PBST	Cy3 Goat anti Rabbit (Jackson ImmunoResearch)	1:300, 1% BSA in PBST	SiHa

6.2.14. Microsomal assay

To determine the metabolic stability of INI-43, human liver microsome (pool of 50, mixed gender, Batch number H0610, Lot number 1110413, Xenotech) and mouse liver microsome (pool of 600 male Mouse BALB/c, Batch number M3000, Lot number 0810197, Xenotech) were used to set up reactions containing 0.5 mg/mL microsomes, 10 µM INI-43 and 5 mM $MgCl_2$ made up to 475 µL with 0.1 M phosphate buffer. Reactions were initiated by adding 1 mM co-factor NADPH and incubated at $37^{O}C$ for 30 minutes. The reaction was stopped by adding equal volumes of pre-chilled acetonitrile to precipitate the proteins. The samples were vortexed and centrifuged, and supernatant was filtered through a 0.22 µm filter. The centrifuged and filtered samples of microsomal incubations were then analysed by HPLC-MS/MS to determine the remaining concentrations of the parent compound. A reverse-phase high performance liquid chromatography (HPLC) on a high-pressure chromatogram (Agilent 1200 Rapid Resolution, 600 bar, USA) with a diode array detector (DAD) coupled to an AB SCIEX 4000 QTRAP MS, equipped with a Turbo V^{TM} ion source and a 2.1 mm x 150 mm column (Kinetex C18, particle size 2.6 µM) were used. The column was eluted in a gradient flow, from 5 mM ammonium formate (pH 3) in 5% acetonitrile to 95% acetonitrile, at an eluent flow rate of 0.4 mL/min. Analyst 1.5.2 software was used for instrument control and data acquisition. Lightsight 2.2.1 software was used for metabolite identification and data processing. The % INI-43 remaining were calculated using the formula $\%\ INI\text{-}43\ remaining = \frac{peak\ area\ after\ incubation}{peak\ area\ at\ T=0}\ x\ 100$, and the projected half-life ($T_{1/2}$) was determined using the formula $T_{1/2}\ (minutes) = absolute\left(\frac{ln\ 2\ x\ (incubation\ time)}{ln\left(\frac{\%remaining}{100}\right)}\right)$ as previously described[481].

6.2.15. INI-43 toxicology analysis

To confirm that INI-43 is suitable for testing in nude mice, toxicology studies were performed. Experiments were initiated with low dose INI-43 (1 mg/kg), where twelve mice were randomized

into the control and test group of 6 each. The test mice received 1 mg/kg INI-43 dissolved in DMSO, and the control mice received an equivalent amount of DMSO. INI-43 and DMSO were delivered via intraperitoneal injections every 48 hours for a duration of 28 days, through which the animals' wellbeing and body mass were monitored daily. At the end of the experiment, the mice were euthanized by halothane overdose and autopsies were performed for regular checks. The liver was then removed and weighed, and sent for pathological examination. After confirming that the mice were tolerant to 1 mg/kg INI-43, intermediate dose at 10 mg/kg were tested, followed by high dose at 50 mg/kg. All experiments were carried out in identical format.

6.2.16. Tumour formation analysis

To optimize the conditions for tumour induction in nude mice using xenografted cancer cells, nine mice were used for each of the cell lines HeLa, CaSki, WHCO6 and KYSE30. Mice were divided into three groups of 3, receiving 5, 7.5 and 10 million cancer cells via subcutaneous injections. Cells for inoculation were prepared by culturing in 15 cm dishes until approximately 80% confluent. Cells were harvested by trypsinization, washed twice in ice-cold PBS and resuspended in PBS to a final concentration of 25 000 cells/µL, 37 500 cells/µL and 50 000 cells/µL. A volume of 200 µL cell suspension was subcutaneously implanted into the hind flanks of each nude mice, equivalent to 5 million, 7.5 million and 10 million cells, respectively. The mice were monitored daily for wellbeing and tumour development, where the tumour length and width were recorded using a calliper. Tumour volume was calculated using the formula $tumour\ volume\ (mm^3) = \frac{length \times width \times width}{2}$. For irregularly shaped tumours, length refers to the longest diameter and width refers to the shortest diameter. Upon the tumour length reaching 20 mm, appearance of necrosis in the tumour tissues, or observation of distress in the mice, whichever occurred first, the animal was euthanized by halothane overdose and the endpoint of each experiment was marked by the death of the last mouse in that group.

6.2.17. Tumourigenesis assay

The tumourigenesis assay was carried out using the cervical cancer cell line CaSki and oesophageal cancer cell lines WHCO6 and KYSE30. Cancer cells (5 x 10^6 per mouse) were subcutaneously implanted into the hind flanks of nude mice as previously described. Once the tumours had reached a palpable size, drug treatment was initiated. Tumour bearing mice were randomized into two groups of six each, and dosed intraperitoneally with either the vehicle control (DMSO) or INI-43 (50 mg/kg), every 2-3 days for 3 (WHCO6 and KYSE30) or 4 (CaSki) weeks. The WHCO6 and KYSE30 tumours grew more rapidly, and either reached 20 mm or developed necrosis before the pre-scheduled 4-week experimental duration, and hence had to be euthanized earlier. Tumours were measured on day 0 (first treatment) and twice a week thereafter, using a calliper as previously described. At the end of each studies, tumours were dissected out, weighed and photographed.

6.2.18. Combination index determination

To elucidate the nature of the combined use of INI-43 and CDDP (i.e. synergistic, additive or antagonistic), the Chou-Talalay method was employed. Briefly, cells were seeded in 96-well plates at 5000 cells per well in five replicates. The cells were then subjected to INI-43 only, CDDP only or a combination of INI-43 and CDDP as previously described. The concentration of drugs used are summarized in Appendix Table 7.1, where three ratios were tested, 1 INI-43 : 3 CDDP, 1 INI-43 : 4 CDDP and 1 INI-43 : 5 CDDP. Cells were incubated in the presence of drugs for 48 hours, after which cell viability for each treatment were determined using the MTT reagent and Solubilization Reagent. Cell viabilities for each treatment were normalized to the untreated, and converted to Fa as previously described. The Fa values were then used to calculate the CI values using the CompuSyn software (ComboSyn, Inc., Paramus, NJ), and plotted against Fa.

6.2.19. Caspase-3/7 activity

SiHa cells were seeded in 96-well plates and treated with DMSO or INI-43 for 2 hours, followed by CDDP at various concentrations for 48 hours. Caspase-3/7 activity was monitored using the Caspase-Glo^{R} 3/7 assay, according to the manufacturer's instructions. Luminescence was measured using the Veritas^{TM} microplate luminometer (Promega) and normalized to cell viability measured by the MTT performed in parallel.

6.2.20. p53 half-life determination

To determine the half-life of p53 in INI-43 treated and Kpnβ1 knock-down cells, SiHa cells were treated with 5 µM of INI-43 for two hours or transfected with si-Kpnβ1 for 48 hours, consistent with the pre-treatment prior to CDDP exposure. Cells were then treated with 50 µg/mL cycloheximide (CHX), where after proteins were harvested at 0, 15, 30, 45, 60 and 90 minutes. Proteins were quantified by the BCA kit (Pierce), as previously described, and p53 expression were examined via western blotting. Resulting protein bands were densitometrically quantified by ImageJ, followed by normalization to p53 band intensity at time = 0. The band intensities were plotted in log scale relative to time, and the half life $T_{1/2}$ was calculated using the following equation $T_{1/2}\ (minutes) = \frac{Log2}{[slope]}$, where *[slope]* is the absolute value of the gradient of the linear trendline drawn.

6.2.21. Statistical analysis

Experiments were performed in triplicates, quadruplicates, 5 or 6 replicates, and expressed as the mean ± standard error of the mean (SEM), unless otherwise stated. All *in vitro* experiments were performed at least two independent times. For data analysis, the Student's t-test (unpaired or paired) was performed with a p value of <0.05 considered statistically significant. For the *in vivo* experiments,

changes in mice's body mass and liver mass were analyzed using non-parametric Mann-Whitney *U* test, and a p value of <0.05 was considered statistically significant.

6.3. Solutions

6.3.1. Tissue culture solutions

Trypsin-EDTA

0.5 g Trypsin

8 g NaCl

1.45 g $Na_2HPO_4.2H_2O$

0.2 g KCl

0.2 g KH_2PO_4

10 mM EDTA, pH 8.0

Adjust volume to 1 L with PBS

Cell-freezing media

90% Growth media

10% DMSO

MTT reagent (IC_{50}, viability and proliferation assays)

100 mg MTT

20 mL PBS

Vortex and incubate in 37^{O}C waterbath for 15 minutes

Filter sterilize through 0.22 µm filter

Store at 4^{O}C protected from light for a maximum period of one month

Solubilization Reagent (IC_{50}, viability and proliferation assays)

25 g SLS

Adjust volume to 250 mL with dH_2O

Add 76.6 µL concentrated HCl

Fixation Solution (clonogenic assay)

12.5 mL glacial acetic acid

87.5 mL methanol

Crystal Violet Solution (clonogenic assay)

500 mg crystal violet

25 mL methanol

75 mL dH_2O

1% methylcellulose growth media (anchorage-independent colony formation assay)

1 g methylcellulose powder

Autoclave

100 mL pre-warmed complete growth media

Vortex and shake at $4^{O}C$ overnight

Poly-(HEMA) solution (anchorage-independent colony formation assay)

2.4 g poly(2-hydroxyethyl methacrylate)

200 mL 96% ethanol

Dissolve with constant stirring in $65^{O}C$ waterbath

6.3.2. Protein solutions

6.3.2.1. Protein extraction solutions

Prior to use, complete protease inhibitor cocktail (Roche, Basel, Switzerland) and Sodium Orthovanadate (Na_3VO_4) were added to a final concentration of 1 x and 0.1 M respectively, to all protein extraction solutions.

RIPA Buffer (50 mL)

	Volume	Final concentration
5 M NaCl	1.5 mL	150 mM
1 M Tris, pH 7.5	2.5 mL	50 mM
Triton-X-100	0.5 mL	1% (v/v)
Sodium deoxycholate	0.5 g powder	1% (w/v)
10% SDS	0.5 mL	0.1% (v/v)
500 mM EGTA	0.2 mL	2 mM
500 mM EDTA	0.2 mL	2 mM
500 mM NaF	5 mL	50 mM
100 mM $Na_2P_2O_7$	2.5 mL	5 mM
ddH_2O to 50 mL		

Subcellular Fractionation Buffer (Mitochondrial protein extraction, 50 mL)

4.28 g Sucrose

1 mL 1 M HEPES (pH 7.4)

5 mL 100 mM KCl

7.5 µL 1 M $MgCl_2$

100 µL 500 mM EDTA

100 µL 500 mM EGTA

Up to 50 mL with dH_2O

Harvest Buffer (Nuclear protein extraction, 50 mL)

500 µL 1 M HEPES pH 7.9

2.5 mL 1 M NaCl

10 µL 500 mM EDTA

250 µL Triton-X-100

Up to 50 mL with dH_2O

Buffer A (Nuclear protein extraction, 50 mL)

500 µL 1 M HEPES pH 7.9

500 µL 1 M KCl

10 µL 500 mM EDTA

10 µL 500 mM EGTA

Up to 50 mL with dH_2O

Buffer C (Nuclear protein extraction, 50 mL)

50 µL 1 M HEPES pH 7.9

2.5 mL 1 M NaCl

5 µL 100 mM EDTA

5 µL 100 mM EGTA

100 µL 5% NP-40

Up to 5 mL with dH_2O

6.3.2.2. Western Blot solutions

4% Stacking Gel

1.25 mL 1 M Tris-Cl, pH 6.8

100 µL 10% SDS

1.3 mL 30% Acrylamide

7.3 mL dH_2O

120 µL 10% APS

12 µL Temed

Resolving Gel

Component	7.5%	10.0%	12.5%	15.0%
ddH_2O	7.3 mL	5.7 mL	4.3 mL	2.3 mL
1 M Tris pH 8.8	7.5 mL	7.5 mL	7.5 mL	7.5 mL
30% acrylamide	5 mL	6.6 mL	8 mL	10 mL
10% SDS	100 µL	100 µL	100 µL	100 µL
10% APS	350 µL	350 µL	350 µL	350 µL
TEMED	35 µL	35 µL	35 µL	35 µL

4% Laemmli Loading Dye (10 mL)

2.5 mL 1 M Tris-Cl, pH 6.8

3 mL 20% SDS

0.5 mL 0.1% Bromophenol Blue

4 mL Glycerol

Prior to use, 50 µL of β-mercaptoethanol was added into 450 µL of the dye solution and kept at room temperature for a maximum period of 1 month

1 x Running Buffer

2.9 g Tris

14.4 g Glycine

1 g SDS

Up to 1 L with dH_2O

1 x Transfer Buffer

3.03 g Tris

14.4 g Glycine

500 mL dH_2O

200 mL Isopropanol/Methanol

Up to 1 L with dH_2O

TBST

6.05 g Tris

8.77 g NaCl

800 mL dH_2O

Adjust pH to 7.5

500 µL Tween-20

Up to 1 L with dH_2O

Stripping Buffer

15 g glycine

1 g SDS

10 mL Tween-20

Adjust pH to 2.2

up to 1 L with dH_2O

6.3.3. DNA solutions

TE Buffer

1 mL 1 M Tris-Cl, pH 8.0

200 µL 500 mM EDTA, pH 8.0

98.8 mL dH_2O

TAE Buffer

4.84 g Tris

1.14 mL Glacial acetic acid

2 mL 500 mM EDTA

Up to 1 L with dH_2O

6.3.4. Bacterial solutions

Luria Broth (LB)

10 g Tryptone

5 g Yeast Extract

10 g NaCl

950 mL dH_2O

Adjust to pH 7.0 with 5 N NaOH

Up to 1 L with dH_2O

Autoclave

Luria Agar (LA)

10 g Tryptone

5 g Yeast Extract

10 g NaCl

15 g Agar

Up to 1 L with dH_2O

Autoclave

Ampicillin (10 mg/mL)

1 mg Ampicillin

10 mL dH_2O

Filter sterilize using 0.22 µm filter

Stored at -20^{O}C

6.3.5. Others

4% Paraformaldehyde (Immunofluorescence)

40 g paraformaldehyde

900 mL PBS

Heat to approximately 60^{O}C with constant stirring

Raise pH by adding 1 N NaOH dropwise, until solution clears

Up to 1 L with PBS

Filter sterilize

Mowiol Mounting Solution

2.4 g Mowiol-488

6 g Glycerol

6 mL dH_2O

Stir vigorously

12 mL 200 mM Tris-Cl, pH 8.5

Heat to 60^{O}C with stirring for 10 minutes

Remove undissolved particles by centrifugation at 5000 x G for 15 minutes

Store at -20^{O}C

Prior to use, dissolve 2.5 mg of n-propyl gallate in 1 mL thawed Mowiol by vortexing

6.3.6. General

PBS

8.0 g NaCl

0.2 g KCl

0.24 g KH_2PO_4

1.44 g Na_2HPO_4

800 mL dH_2O

Adjust to pH 7.4 with HCl

Up to 1 L with dH_2O

Autoclave

PBST

1 L PBS

2 mL Tween-20

0.5 M EDTA

186.12 g $Na_2EDTA\text{-}2H_2O$

800 mL dH_2O

Adjust to pH 8.0 with NaOH

Up to 1 L with dH_2O

Autoclave

0.5 M EGTA

190.18 g EGTA

800 mL dH_2O

Adjust to pH 8.0 with NaOH

Up to 1 L with dH_2O

Autoclave

1 M Tris-Cl

121 g Tris base

800 mL dH_2O

Adjust to pH 8.0 with conc. HCl

Up to 1 L with dH_2O

Autoclave

1 M HEPES

238.80 g HEPES

800 mL dH_2O

Adjust to desired pH using KOH pellets

Up to 1 L with dH_2O

Filter sterilize

REFERENCES

1. Siegel RL, Miller KD, Jemal A. Cancer statistics, 2016. *CA Cancer J Clin.* 2016;66:7-30.

2. Bertuzzi M, Marelli C, Bagnati R, et al. Plasma clusterin as a candidate pre-diagnosis marker of colorectal cancer risk in the Florence cohort of the European Prospective Investigation into Cancer and Nutrition: a pilot study. *BMC Cancer.* 2015;15:56.

3. Boccardi V, Marano L, Rossetti RR, Rizzo MR, di Martino N, Paolisso G. Serum CD26 levels in patients with gastric cancer: a novel potential diagnostic marker. *BMC Cancer.* 2015;15:703.

4. Hung CH, Hu TH, Lu SN, et al. Circulating microRNAs as biomarkers for diagnosis of early hepatocellular carcinoma associated with hepatitis B virus. *Int J Cancer.* 2016;138:714-720.

5. Kumar P, Nandi S, Tan TZ, et al. Highly sensitive and specific novel biomarkers for the diagnosis of transitional bladder carcinoma. *Oncotarget.* 2015;6:13539-13549.

6. Terzi H, Kale E, Kale A, Turkay U, Chong GO, Lee YS. New method: Are tumor markers in vaginal-washing fluid significant in the diagnosis of primary ovarian carcinoma? *Eur J Gynaecol Oncol.* 2015;36:560-563.

7. Tong YS, Wang XW, Zhou XL, et al. Identification of the long non-coding RNA POU3F3 in plasma as a novel biomarker for diagnosis of esophageal squamous cell carcinoma. *Mol Cancer.* 2015;14:3.

8. Yin J, Hou P, Wu Z, Wang T, Nie Y. Circulating miR-375 and miR-199a-3p as potential biomarkers for the diagnosis of hepatocellular carcinoma. *Tumour Biol.* 2015;36:4501-4507.

9. Zhang G, Zong J, Lin S, et al. Circulating Epstein-Barr virus microRNAs miR-BART7 and miR-BART13 as biomarkers for nasopharyngeal carcinoma diagnosis and treatment. *Int J Cancer.* 2015;136:E301-312.

10. Blanco LZ, Thurow TA, Mahajan A, et al. Multinucleation is an objective feature useful in the diagnosis of pleomorphic lobular carcinoma in situ. *Am J Clin Pathol.* 2015;144:722-726.

11. Hirobe M, Masumori N, Tanaka T, et al. Clinicopathological characteristics of Xp11.2 translocation renal cell carcinoma in adolescents and adults: Diagnosis using immunostaining of transcription factor E3 and fluorescence in situ hybridization analysis. *Int J Urol.* 2015;23:140-145.

12. Huang CH, Kuo CJ, Liang SS, et al. Onco-proteogenomics identifies urinary S100A9 and GRN as potential combinatorial biomarkers for early diagnosis of hepatocellular carcinoma. *BBA Clin.* 2015;3:205-213.

13. Yang DW, Zhang Y, Hong QY, et al. Role of a serum-based biomarker panel in the early diagnosis of lung cancer for a cohort of high-risk patients. *Cancer.* 2015;121 Suppl 17:3113-3121.

14. Zhao Y, Liu X, Zhong L, et al. The combined use of miRNAs and mRNAs as biomarkers for the diagnosis of papillary thyroid carcinoma. *Int J Mol Med.* 2015;36:1097-1103.

15. Zhao Y, Wang M, Cui C, et al. Significance of combined tests of serum golgi glycoprotein 73 and other biomarkers in diagnosis of small primary hepatocellular carcinoma. *Cancer Biomark.* 2015;15:677-683.

16. Liu WH, Ren LN, Wang X, et al. Combination of exosomes and circulating microRNAs may serve as a promising tumor marker complementary to alpha-fetoprotein for early-stage hepatocellular carcinoma diagnosis in rats. *J Cancer Res Clin Oncol.* 2015;141:1767-1778.

17. Melo SA, Luecke LB, Kahlert C, et al. Glypican-1 identifies cancer exosomes and detects early pancreatic cancer. *Nature.* 2015;523:177-182.

18. Thery C. Cancer: Diagnosis by extracellular vesicles. *Nature.* 2015;523:161-162.

19. An T, Qin S, Xu Y, et al. Exosomes serve as tumour markers for personalized diagnostics owing to their important role in cancer metastasis. *J Extracell Vesicles.* 2015;4:27522.
20. Properzi F, Logozzi M, Fais S. Exosomes: the future of biomarkers in medicine. *Biomark Med.* 2013;7:769-778.
21. El Khachibi M, Diakite B, Hamzi K, et al. Screening of exon 11 of BRCA1 gene using the high resolution melting approach for diagnosis in Moroccan breast cancer patients. *BMC Cancer.* 2015;15:81.
22. Meder L, Konig K, Fassunke J, et al. Implementing amplicon-based next generation sequencing in the diagnosis of small cell lung carcinoma metastases. *Exp Mol Pathol.* 2015;99:682-686.
23. Yu JP, Xu XG, Ma RJ, et al. Development of a clinical chemiluminescent immunoassay for serum GPC3 and simultaneous measurements alone with AFP and CK19 in diagnosis of hepatocellular carcinoma. *J Clin Lab Anal.* 2015;29:85-93.
24. Kahn N, Lavie O, Paz M, Segev Y, Haick H. Dynamic Nanoparticle-Based Flexible Sensors: Diagnosis of Ovarian Carcinoma from Exhaled Breath. *Nano Lett.* 2015;15:7023-7028.
25. Lerner SP, Goh A. Novel endoscopic diagnosis for bladder cancer. *Cancer.* 2015;121:169-178.
26. Liu JJ, Li HX, Chen ZB, et al. Consistency analysis of contrast-enhanced ultrasound and contrast-enhanced CT in diagnosis of small hepatocellular carcinoma. *Int J Clin Exp Med.* 2015;8:21466-21471.
27. Fischer MA, Raptis DA, Donati OF, et al. MR imaging features for improved diagnosis of hepatocellular carcinoma in the non-cirrhotic liver: Multi-center evaluation. *Eur J Radiol.* 2015;84:1879-1887.
28. Zhou HL, Xiang H, Duan L, et al. Application of Combined Two-Dimensional and Three-Dimensional Transvaginal Contrast Enhanced Ultrasound in the Diagnosis of Endometrial Carcinoma. *Biomed Res Int.* 2015;2015:292743.
29. Wang Y, Zhang X, Cao K, et al. Diffusion-tensor imaging as an adjunct to dynamic contrast-enhanced MRI for improved accuracy of differential diagnosis between breast ductal carcinoma in situ and invasive breast carcinoma. *Chin J Cancer Res.* 2015;27:209-217.
30. Liu Y, Li J, Liu F, Feng L, Yu D, Zhang N. Theranostic Polymeric Micelles for the Diagnosis and Treatment of Hepatocellular Carcinoma. *J Biomed Nanotechnol.* 2015;11:613-622.
31. Baskar R, Lee KA, Yeo R, Yeoh KW. Cancer and radiation therapy: current advances and future directions. *Int J Med Sci.* 2012;9:193-199.
32. Peyrone M. Ueber die Einwirkung des Ammoniaks auf Platinchlorür. *Justus Liebigs Annalen der Chemie.* 1844;51:1-29.
33. Werner A. Beitrag zur Konstitution anorganischer Verbindungen. *Zeitschrift für anorganische Chemie.* 1893;3:267-330.
34. Rosenberg B, Vancamp L, Krigas T. Inhibition of cell division in escherichia coli by electrolysis products from a platinum electrode. *Nature.* 1965;205:698-699.
35. Rosenberg B, VanCamp L, Trosko JE, Mansour VH. Platinum compounds: a new class of potent antitumour agents. *Nature.* 1969;222:385-386.
36. Kelland L. The resurgence of platinum-based cancer chemotherapy. *Nat Rev Cancer.* 2007;7:573-584.
37. Goodsell DS. The molecular perspective: cisplatin. *Oncologist.* 2006;11:316-317.
38. Dasari S, Tchounwou PB. Cisplatin in cancer therapy: molecular mechanisms of action. *Eur J Pharmacol.* 2014;740:364-378.
39. Weiss RB, Christian MC. New cisplatin analogues in development. A review. *Drugs.* 1993;46:360-377.
40. Parker WB. Enzymology of purine and pyrimidine antimetabolites used in the treatment of cancer. *Chem Rev.* 2009;109:2880-2893.
41. Tiwari M. Antimetabolites: established cancer therapy. *J Cancer Res Ther.* 2012;8:510-519.

42. Hortobagyi GN. Anthracyclines in the treatment of cancer. An overview. *Drugs.* 1997;54 Suppl 4:1-7.
43. Nitiss JL. Targeting DNA topoisomerase II in cancer chemotherapy. *Nat Rev Cancer.* 2009;9:338-350.
44. Honore S, Pasquier E, Braguer D. Understanding microtubule dynamics for improved cancer therapy. *Cell Mol Life Sci.* 2005;62:3039-3056.
45. Dumontet C, Jordan MA. Microtubule-binding agents: a dynamic field of cancer therapeutics. *Nat Rev Drug Discov.* 2010;9:790-803.
46. Sawyers C. Targeted cancer therapy. *Nature.* 2004;432:294-297.
47. Baselga J, Arribas J. Treating cancer's kinase 'addiction'. *Nat Med.* 2004;10:786-787.
48. Fausel C. Targeted chronic myeloid leukemia therapy: Seeking a cure. *Am J Health Syst Pharm.* 2007;64:S9-15.
49. Hermans A, Heisterkamp N, von Linden M, et al. Unique fusion of bcr and c-abl genes in Philadelphia chromosome positive acute lymphoblastic leukemia. *Cell.* 1987;51:33-40.
50. Paez JG, Janne PA, Lee JC, et al. EGFR mutations in lung cancer: correlation with clinical response to gefitinib therapy. *Science.* 2004;304:1497-1500.
51. Rosell R, Carcereny E, Gervais R, et al. Erlotinib versus standard chemotherapy as first-line treatment for European patients with advanced EGFR mutation-positive non-small-cell lung cancer (EURTAC): a multicentre, open-label, randomised phase 3 trial. *Lancet Oncol.* 2012;13:239-246.
52. Zhou C, Wu YL, Chen G, et al. Erlotinib versus chemotherapy as first-line treatment for patients with advanced EGFR mutation-positive non-small-cell lung cancer (OPTIMAL, CTONG-0802): a multicentre, open-label, randomised, phase 3 study. *Lancet Oncol.* 2011;12:735-742.
53. Nicholson RI, Gee JM, Harper ME. EGFR and cancer prognosis. *Eur J Cancer.* 2001;37 Suppl 4:S9-15.
54. Russo J, Russo IH. The role of estrogen in the initiation of breast cancer. *J Steroid Biochem Mol Biol.* 2006;102:89-96.
55. Gann PH, Hennekens CH, Ma J, Longcope C, Stampfer MJ. Prospective study of sex hormone levels and risk of prostate cancer. *J Natl Cancer Inst.* 1996;88:1118-1126.
56. Fabian CJ. The what, why and how of aromatase inhibitors: hormonal agents for treatment and prevention of breast cancer. *Int J Clin Pract.* 2007;61:2051-2063.
57. Burish TG, Tope DM. Psychological techniques for controlling the adverse side effects of cancer chemotherapy: findings from a decade of research. *J Pain Symptom Manage.* 1992;7:287-301.
58. Coates A, Abraham S, Kaye SB, et al. On the receiving end--patient perception of the side-effects of cancer chemotherapy. *Eur J Cancer Clin Oncol.* 1983;19:203-208.
59. Griffin AM, Butow PN, Coates AS, et al. On the receiving end. V: Patient perceptions of the side effects of cancer chemotherapy in 1993. *Ann Oncol.* 1996;7:189-195.
60. Carelle N, Piotto E, Bellanger A, Germanaud J, Thuillier A, Khayat D. Changing patient perceptions of the side effects of cancer chemotherapy. *Cancer.* 2002;95:155-163.
61. Lindley C, McCune JS, Thomason TE, et al. Perception of chemotherapy side effects cancer versus noncancer patients. *Cancer Pract.* 1999;7:59-65.
62. Partridge AH, Burstein HJ, Winer EP. Side effects of chemotherapy and combined chemohormonal therapy in women with early-stage breast cancer. *J Natl Cancer Inst Monogr.* 2001;2001:135-142.
63. Gottesman MM. Mechanisms of cancer drug resistance. *Annu Rev Med.* 2002;53:615-627.
64. Xu Y, Villalona-Calero MA. Irinotecan: mechanisms of tumor resistance and novel strategies for modulating its activity. *Ann Oncol.* 2002;13:1841-1851.
65. Santos A, Zanetta S, Cresteil T, et al. Metabolism of irinotecan (CPT-11) by CYP3A4 and CYP3A5 in humans. *Clin Cancer Res.* 2000;6:2012-2020.

66. Pluen A, Boucher Y, Ramanujan S, et al. Role of tumor-host interactions in interstitial diffusion of macromolecules: cranial vs. subcutaneous tumors. *Proc Natl Acad Sci U S A.* 2001;98:4628-4633.
67. Yauch RL, Dijkgraaf GJ, Alicke B, et al. Smoothened mutation confers resistance to a Hedgehog pathway inhibitor in medulloblastoma. *Science.* 2009;326:572-574.
68. Atwood SX, Chang AL, Oro AE. Hedgehog pathway inhibition and the race against tumor evolution. *J Cell Biol.* 2012;199:193-197.
69. Kasper M, Toftgard R. Smoothing out drug resistance. *Cancer Cell.* 2013;23:3-5.
70. Galmarini CM, Mackey JR, Dumontet C. Nucleoside analogues: mechanisms of drug resistance and reversal strategies. *Leukemia.* 2001;15:875-890.
71. Damaraju VL, Damaraju S, Young JD, et al. Nucleoside anticancer drugs: the role of nucleoside transporters in resistance to cancer chemotherapy. *Oncogene.* 2003;22:7524-7536.
72. Longo-Sorbello GS, Bertino JR. Current understanding of methotrexate pharmacology and efficacy in acute leukemias. Use of newer antifolates in clinical trials. *Haematologica.* 2001;86:121-127.
73. Klanova M, Lorkova L, Vit O, et al. Downregulation of deoxycytidine kinase in cytarabine-resistant mantle cell lymphoma cells confers cross-resistance to nucleoside analogs gemcitabine, fludarabine and cladribine, but not to other classes of anti-lymphoma agents. *Mol Cancer.* 2014;13:159.
74. Song JH, Kim SH, Kweon SH, et al. Defective expression of deoxycytidine kinase in cytarabine-resistant acute myeloid leukemia cells. *Int J Oncol.* 2009;34:1165-1171.
75. Rathe SK, Largaespada DA. Deoxycytidine kinase is downregulated in Ara-C-resistant acute myeloid leukemia murine cell lines. *Leukemia.* 2010;24:1513-1515.
76. Cai J, Damaraju VL, Groulx N, et al. Two distinct molecular mechanisms underlying cytarabine resistance in human leukemic cells. *Cancer Res.* 2008;68:2349-2357.
77. McLellan LI, Wolf CR. Glutathione and glutathione-dependent enzymes in cancer drug resistance. *Drug Resist Updat.* 1999;2:153-164.
78. Townsend DM, Tew KD. The role of glutathione-S-transferase in anti-cancer drug resistance. *Oncogene.* 2003;22:7369-7375.
79. Traverso N, Ricciarelli R, Nitti M, et al. Role of glutathione in cancer progression and chemoresistance. *Oxid Med Cell Longev.* 2013;2013:972913.
80. Endresen L, Bakka A, Rugstad HE. Increased resistance to chlorambucil in cultured cells with a high concentration of cytoplasmic metallothionein. *Cancer Res.* 1983;43:2918-2926.
81. Doz F, Roosen N, Rosenblum ML. Metallothionein and anticancer agents: the role of metallothionein in cancer chemotherapy. *J Neurooncol.* 1993;17:123-129.
82. Kasahara K, Fujiwara Y, Nishio K, et al. Metallothionein content correlates with the sensitivity of human small cell lung cancer cell lines to cisplatin. *Cancer Res.* 1991;51:3237-3242.
83. Kelley SL, Basu A, Teicher BA, Hacker MP, Hamer DH, Lazo JS. Overexpression of metallothionein confers resistance to anticancer drugs. *Science.* 1988;241:1813-1815.
84. Hughes TP, Kaeda J, Branford S, et al. Frequency of major molecular responses to imatinib or interferon alfa plus cytarabine in newly diagnosed chronic myeloid leukemia. *N Engl J Med.* 2003;349:1423-1432.
85. Lynch TJ, Bell DW, Sordella R, et al. Activating mutations in the epidermal growth factor receptor underlying responsiveness of non-small-cell lung cancer to gefitinib. *N Engl J Med.* 2004;350:2129-2139.
86. Shepherd FA, Rodrigues Pereira J, Ciuleanu T, et al. Erlotinib in previously treated non-small-cell lung cancer. *N Engl J Med.* 2005;353:123-132.

87. Taron M, Ichinose Y, Rosell R, et al. Activating mutations in the tyrosine kinase domain of the epidermal growth factor receptor are associated with improved survival in gefitinib-treated chemorefractory lung adenocarcinomas. *Clin Cancer Res.* 2005;11:5878-5885.
88. Gorre ME, Mohammed M, Ellwood K, et al. Clinical resistance to STI-571 cancer therapy caused by BCR-ABL gene mutation or amplification. *Science.* 2001;293:876-880.
89. Soverini S, Martinelli G, Rosti G, et al. ABL mutations in late chronic phase chronic myeloid leukemia patients with up-front cytogenetic resistance to imatinib are associated with a greater likelihood of progression to blast crisis and shorter survival: a study by the GIMEMA Working Party on Chronic Myeloid Leukemia. *J Clin Oncol.* 2005;23:4100-4109.
90. Jabbour E, Kantarjian H, Jones D, et al. Frequency and clinical significance of BCR-ABL mutations in patients with chronic myeloid leukemia treated with imatinib mesylate. *Leukemia.* 2006;20:1767-1773.
91. Apperley JF. Part I: mechanisms of resistance to imatinib in chronic myeloid leukaemia. *Lancet Oncol.* 2007;8:1018-1029.
92. Blencke S, Ullrich A, Daub H. Mutation of threonine 766 in the epidermal growth factor receptor reveals a hotspot for resistance formation against selective tyrosine kinase inhibitors. *J Biol Chem.* 2003;278:15435-15440.
93. Kobayashi S, Boggon TJ, Dayaram T, et al. EGFR mutation and resistance of non-small-cell lung cancer to gefitinib. *N Engl J Med.* 2005;352:786-792.
94. Pao W, Miller VA, Politi KA, et al. Acquired resistance of lung adenocarcinomas to gefitinib or erlotinib is associated with a second mutation in the EGFR kinase domain. *PLoS Med.* 2005;2:e73.
95. Balak MN, Gong Y, Riely GJ, et al. Novel D761Y and common secondary T790M mutations in epidermal growth factor receptor-mutant lung adenocarcinomas with acquired resistance to kinase inhibitors. *Clin Cancer Res.* 2006;12:6494-6501.
96. Bean J, Riely GJ, Balak M, et al. Acquired resistance to epidermal growth factor receptor kinase inhibitors associated with a novel T854A mutation in a patient with EGFR-mutant lung adenocarcinoma. *Clin Cancer Res.* 2008;14:7519-7525.
97. Arribas J, Baselga J, Pedersen K, Parra-Palau JL. p95HER2 and breast cancer. *Cancer Res.* 2011;71:1515-1519.
98. Nagy P, Friedlander E, Tanner M, et al. Decreased accessibility and lack of activation of ErbB2 in JIMT-1, a herceptin-resistant, MUC4-expressing breast cancer cell line. *Cancer Res.* 2005;65:473-482.
99. Fessler SP, Wotkowicz MT, Mahanta SK, Bamdad C. MUC1* is a determinant of trastuzumab (Herceptin) resistance in breast cancer cells. *Breast Cancer Res Treat.* 2009;118:113-124.
100. Berns K, Horlings HM, Hennessy BT, et al. A functional genetic approach identifies the PI3K pathway as a major determinant of trastuzumab resistance in breast cancer. *Cancer Cell.* 2007;12:395-402.
101. Razis E, Bobos M, Kotoula V, et al. Evaluation of the association of PIK3CA mutations and PTEN loss with efficacy of trastuzumab therapy in metastatic breast cancer. *Breast Cancer Res Treat.* 2011;128:447-456.
102. Lu Y, Zi X, Zhao Y, Mascarenhas D, Pollak M. Insulin-like growth factor-I receptor signaling and resistance to trastuzumab (Herceptin). *J Natl Cancer Inst.* 2001;93:1852-1857.
103. Gajria D, Chandarlapaty S. HER2-amplified breast cancer: mechanisms of trastuzumab resistance and novel targeted therapies. *Expert Rev Anticancer Ther.* 2011;11:263-275.
104. Sergina NV, Rausch M, Wang D, et al. Escape from HER-family tyrosine kinase inhibitor therapy by the kinase-inactive HER3. *Nature.* 2007;445:437-441.
105. Lee-Hoeflich ST, Crocker L, Yao E, et al. A central role for HER3 in HER2-amplified breast cancer: implications for targeted therapy. *Cancer Res.* 2008;68:5878-5887.
106. Munoz M, Henderson M, Haber M, Norris M. Role of the MRP1/ABCC1 multidrug transporter protein in cancer. *IUBMB Life.* 2007;59:752-757.

107. Zahreddine H, Borden KL. Mechanisms and insights into drug resistance in cancer. *Front Pharmacol.* 2013;4:28.
108. Holohan C, Van Schaeybroeck S, Longley DB, Johnston PG. Cancer drug resistance: an evolving paradigm. *Nat Rev Cancer.* 2013;13:714-726.
109. Michor F, Polyak K. The origins and implications of intratumor heterogeneity. *Cancer Prev Res (Phila).* 2010;3:1361-1364.
110. Marusyk A, Polyak K. Tumor heterogeneity: causes and consequences. *Biochim Biophys Acta.* 2010;1805:105-117.
111. Jiang T, Shi W, Natowicz R, et al. Statistical measures of transcriptional diversity capture genomic heterogeneity of cancer. *BMC Genomics.* 2014;15:876.
112. Marusyk A, Almendro V, Polyak K. Intra-tumour heterogeneity: a looking glass for cancer? *Nat Rev Cancer.* 2012;12:323-334.
113. Merlo LM, Maley CC. The role of genetic diversity in cancer. *J Clin Invest.* 2010;120:401-403.
114. de Bruin EC, McGranahan N, Mitter R, et al. Spatial and temporal diversity in genomic instability processes defines lung cancer evolution. *Science.* 2014;346:251-256.
115. Park SY, Gonen M, Kim HJ, Michor F, Polyak K. Cellular and genetic diversity in the progression of in situ human breast carcinomas to an invasive phenotype. *J Clin Invest.* 2010;120:636-644.
116. Tajiri R, Ooi A, Fujimura T, et al. Intratumoral heterogeneous amplification of ERBB2 and subclonal genetic diversity in gastric cancers revealed by multiple ligation-dependent probe amplification and fluorescence in situ hybridization. *Hum Pathol.* 2014;45:725-734.
117. Natrajan R, Sailem H, Mardakheh FK, et al. Microenvironmental Heterogeneity Parallels Breast Cancer Progression: A Histology-Genomic Integration Analysis. *PLoS Med.* 2016;13:e1001961.
118. Polyak K. Heterogeneity in breast cancer. *J Clin Invest.* 2011;121:3786-3788.
119. Merlo LM, Shah NA, Li X, et al. A comprehensive survey of clonal diversity measures in Barrett's esophagus as biomarkers of progression to esophageal adenocarcinoma. *Cancer Prev Res (Phila).* 2010;3:1388-1397.
120. Bhamidipati PK, Kantarjian H, Cortes J, Cornelison AM, Jabbour E. Management of imatinib-resistant patients with chronic myeloid leukemia. *Ther Adv Hematol.* 2013;4:103-117.
121. Bixby D, Talpaz M. Seeking the causes and solutions to imatinib-resistance in chronic myeloid leukemia. *Leukemia.* 2011;25:7-22.
122. Cardoso F, Bedard PL, Winer EP, et al. International guidelines for management of metastatic breast cancer: combination vs sequential single-agent chemotherapy. *J Natl Cancer Inst.* 2009;101:1174-1181.
123. Miles D, Vukelja S, Moiseyenko V, et al. Survival benefit with capecitabine/docetaxel versus docetaxel alone: analysis of therapy in a randomized phase III trial. *Clin Breast Cancer.* 2004;5:273-278.
124. O'Shaughnessy J, Miles D, Vukelja S, et al. Superior survival with capecitabine plus docetaxel combination therapy in anthracycline-pretreated patients with advanced breast cancer: phase III trial results. *J Clin Oncol.* 2002;20:2812-2823.
125. Albain KS, Nag SM, Calderillo-Ruiz G, et al. Gemcitabine plus Paclitaxel versus Paclitaxel monotherapy in patients with metastatic breast cancer and prior anthracycline treatment. *J Clin Oncol.* 2008;26:3950-3957.
126. Moore MJ, Goldstein D, Hamm J, et al. Erlotinib plus gemcitabine compared with gemcitabine alone in patients with advanced pancreatic cancer: a phase III trial of the National Cancer Institute of Canada Clinical Trials Group. *J Clin Oncol.* 2007;25:1960-1966.
127. du Bois A, Herrstedt J, Hardy-Bessard AC, et al. Phase III trial of carboplatin plus paclitaxel with or without gemcitabine in first-line treatment of epithelial ovarian cancer. *J Clin Oncol.* 2010;28:4162-4169.

128. van der Watt PJ, Maske CP, Hendricks DT, et al. The Karyopherin proteins, Crm1 and Karyopherin beta1, are overexpressed in cervical cancer and are critical for cancer cell survival and proliferation. *Int J Cancer.* 2009;124:1829-1840.
129. Chahine MN, Pierce GN. Therapeutic targeting of nuclear protein import in pathological cell conditions. *Pharmacol Rev.* 2009;61:358-372.
130. Hung MC, Link W. Protein localization in disease and therapy. *J Cell Sci.* 2011;124:3381-3392.
131. Mor A, White MA, Fontoura BM. Nuclear trafficking in health and disease. *Curr Opin Cell Biol.* 2014;28:28-35.
132. Alber F, Dokudovskaya S, Veenhoff LM, et al. The molecular architecture of the nuclear pore complex. *Nature.* 2007;450:695-701.
133. Wente SR, Rout MP. The nuclear pore complex and nuclear transport. *Cold Spring Harb Perspect Biol.* 2010;2:a000562.
134. Ribbeck K, Lipowsky G, Kent HM, Stewart M, Gorlich D. NTF2 mediates nuclear import of Ran. *Embo j.* 1998;17:6587-6598.
135. Clarke PR, Zhang C. Spatial and temporal coordination of mitosis by Ran GTPase. *Nat Rev Mol Cell Biol.* 2008;9:464-477.
136. Carazo-Salas RE, Guarguaglini G, Gruss OJ, Segref A, Karsenti E, Mattaj IW. Generation of GTP-bound Ran by RCC1 is required for chromatin-induced mitotic spindle formation. *Nature.* 1999;400:178-181.
137. Ohba T, Nakamura M, Nishitani H, Nishimoto T. Self-organization of microtubule asters induced in Xenopus egg extracts by GTP-bound Ran. *Science.* 1999;284:1356-1358.
138. Wilde A, Zheng Y. Stimulation of microtubule aster formation and spindle assembly by the small GTPase Ran. *Science.* 1999;284:1359-1362.
139. Hetzer M, Bilbao-Cortes D, Walther TC, Gruss OJ, Mattaj IW. GTP hydrolysis by Ran is required for nuclear envelope assembly. *Mol Cell.* 2000;5:1013-1024.
140. Dasso M. The role of the Ran GTPase pathway in cell cycle control and interphase nuclear functions. *Prog Cell Cycle Res.* 1995;1:163-172.
141. Simon DN, Rout MP. Cancer and the nuclear pore complex. *Adv Exp Med Biol.* 2014;773:285-307.
142. Chow KH, Factor RE, Ullman KS. The nuclear envelope environment and its cancer connections. *Nat Rev Cancer.* 2012;12:196-209.
143. Barres V, Ouellet V, Lafontaine J, Tonin PN, Provencher DM, Mes-Masson AM. An essential role for Ran GTPase in epithelial ovarian cancer cell survival. *Mol Cancer.* 2010;9:272.
144. Yuen HF, Chan KK, Grills C, et al. Ran is a potential therapeutic target for cancer cells with molecular changes associated with activation of the PI3K/Akt/mTORC1 and Ras/MEK/ERK pathways. *Clin Cancer Res.* 2012;18:380-391.
145. Xu S, Powers MA. Nuclear pore proteins and cancer. *Semin Cell Dev Biol.* 2009;20:620-630.
146. Yuen HF, Gunasekharan VK, Chan KK, et al. RanGTPase: a candidate for Myc-mediated cancer progression. *J Natl Cancer Inst.* 2013;105:475-488.
147. Deng L, Lu Y, Zhao X, et al. Ran GTPase protein promotes human pancreatic cancer proliferation by deregulating the expression of Survivin and cell cycle proteins. *Biochem Biophys Res Commun.* 2013;440:322-329.
148. Woo IS, Jang HS, Eun SY, et al. Ran suppresses paclitaxel-induced apoptosis in human glioblastoma cells. *Apoptosis.* 2008;13:1223-1231.
149. Milano SK, Kwon W, Pereira R, Antonyak MA, Cerione RA. Characterization of a novel activated Ran GTPase mutant and its ability to induce cellular transformation. *J Biol Chem.* 2012;287:24955-24966.
150. Ly TK, Wang J, Pereira R, et al. Activation of the Ran GTPase is subject to growth factor regulation and can give rise to cellular transformation. *J Biol Chem.* 2010;285:5815-5826.

151. Angeline M, Merle E, Moroianu J. The E7 oncoprotein of high-risk human papillomavirus type 16 enters the nucleus via a nonclassical Ran-dependent pathway. *Virology.* 2003;317:13-23.
152. Takahashi N, van Kilsdonk JW, Ostendorf B, et al. Tumor marker nucleoporin 88 kDa regulates nucleocytoplasmic transport of NF-kappaB. *Biochem Biophys Res Commun.* 2008;374:424-430.
153. Martinez N, Alonso A, Moragues MD, Ponton J, Schneider J. The nuclear pore complex protein Nup88 is overexpressed in tumor cells. *Cancer Res.* 1999;59:5408-5411.
154. Mosammaparast N, Pemberton LF. Karyopherins: from nuclear-transport mediators to nuclear-function regulators. *Trends Cell Biol.* 2004;14:547-556.
155. Forbes DJ, Travesa A, Nord MS, Bernis C. Nuclear transport factors: global regulation of mitosis. *Curr Opin Cell Biol.* 2015;35:78-90.
156. Gorlich D, Henklein P, Laskey RA, Hartmann E. A 41 amino acid motif in importin-alpha confers binding to importin-beta and hence transit into the nucleus. *EMBO J.* 1996;15:1810-1817.
157. Bayliss R, Littlewood T, Stewart M. Structural basis for the interaction between FxFG nucleoporin repeats and importin-beta in nuclear trafficking. *Cell.* 2000;102:99-108.
158. Moroianu J, Blobel G, Radu A. Nuclear protein import: Ran-GTP dissociates the karyopherin alphabeta heterodimer by displacing alpha from an overlapping binding site on beta. *Proc Natl Acad Sci U S A.* 1996;93:7059-7062.
159. Gorlich D, Pante N, Kutay U, Aebi U, Bischoff FR. Identification of different roles for RanGDP and RanGTP in nuclear protein import. *EMBO J.* 1996;15:5584-5594.
160. Kutay U, Bischoff FR, Kostka S, Kraft R, Gorlich D. Export of importin alpha from the nucleus is mediated by a specific nuclear transport factor. *Cell.* 1997;90:1061-1071.
161. Hieda M, Tachibana T, Yokoya F, Kose S, Imamoto N, Yoneda Y. A monoclonal antibody to the COOH-terminal acidic portion of Ran inhibits both the recycling of Ran and nuclear protein import in living cells. *J Cell Biol.* 1999;144:645-655.
162. Palmeri D, Malim MH. Importin beta can mediate the nuclear import of an arginine-rich nuclear localization signal in the absence of importin alpha. *Mol Cell Biol.* 1999;19:1218-1225.
163. Cingolani G, Bednenko J, Gillespie MT, Gerace L. Molecular basis for the recognition of a nonclassical nuclear localization signal by importin beta. *Mol Cell.* 2002;10:1345-1353.
164. Kau TR, Way JC, Silver PA. Nuclear transport and cancer: from mechanism to intervention. *Nat Rev Cancer.* 2004;4:106-117.
165. Turner JG, Dawson J, Sullivan DM. Nuclear export of proteins and drug resistance in cancer. *Biochem Pharmacol.* 2012;83:1021-1032.
166. Bischoff FR, Gorlich D. RanBP1 is crucial for the release of RanGTP from importin beta-related nuclear transport factors. *FEBS Lett.* 1997;419:249-254.
167. Ben-Efraim I, Gerace L. Gradient of increasing affinity of importin beta for nucleoporins along the pathway of nuclear import. *J Cell Biol.* 2001;152:411-417.
168. Baake M, Bauerle M, Doenecke D, Albig W. Core histones and linker histones are imported into the nucleus by different pathways. *Eur J Cell Biol.* 2001;80:669-677.
169. Liang P, Zhang H, Wang G, et al. KPNB1, XPO7 and IPO8 mediate the translocation ofNF-kappaB/p65 into the nucleus. *Traffic.* 2013;14:1132-1143.
170. Kohler M, Speck C, Christiansen M, et al. Evidence for distinct substrate specificities of importin alpha family members in nuclear protein import. *Mol Cell Biol.* 1999;19:7782-7791.
171. Jakel S, Gorlich D. Importin beta, transportin, RanBP5 and RanBP7 mediate nuclear import of ribosomal proteins in mammalian cells. *EMBO J.* 1998;17:4491-4502.
172. Connor MK, Kotchetkov R, Cariou S, et al. CRM1/Ran-mediated nuclear export of p27(Kip1) involves a nuclear export signal and links p27 export and proteolysis. *Mol Biol Cell.* 2003;14:201-213.

173. Gaubatz S, Lees JA, Lindeman GJ, Livingston DM. E2F4 is exported from the nucleus in a CRM1-dependent manner. *Mol Cell Biol.* 2001;21:1384-1392.
174. Yang J, Bardes ES, Moore JD, Brennan J, Powers MA, Kornbluth S. Control of cyclin B1 localization through regulated binding of the nuclear export factor CRM1. *Genes Dev.* 1998;12:2131-2143.
175. Dickmanns A, Monecke T, Ficner R. Structural Basis of Targeting the Exportin CRM1 in Cancer. *Cells.* 2015;4:538-568.
176. van der Watt PJ, Leaner VD. The nuclear exporter, Crm1, is regulated by NFY and Sp1 in cancer cells and repressed by p53 in response to DNA damage. *Biochim Biophys Acta.* 2011;1809:316-326.
177. Zhao H, Faltermeier CM, Mendelsohn L, Porter PL, Clurman BE, Roberts JM. Mislocalization of p27 to the cytoplasm of breast cancer cells confers resistance to anti-HER2 targeted therapy. *Oncotarget.* 2014;5:12704-12714.
178. Ho JY, Hsu RJ, Wu CL, et al. BRCA1 mislocalization associated with breast carcinogenesis and poor prognosis in Taiwanese women. *Eur J Cancer Prev.* 2015;24:407-415.
179. Ahmad A, Enzlin JH, Bhagwat NR, et al. Mislocalization of XPF-ERCC1 nuclease contributes to reduced DNA repair in XP-F patients. *PLoS Genet.* 2010;6:e1000871.
180. Jiao W, Lin HM, Datta J, et al. Aberrant nucleocytoplasmic localization of the retinoblastoma tumor suppressor protein in human cancer correlates with moderate/poor tumor differentiation. *Oncogene.* 2007;27:3156-3164.
181. Wang X, Li S. Protein mislocalization: mechanisms, functions and clinical applications in cancer. *Biochim Biophys Acta.* 2014;1846:13-25.
182. Varini K, Benzaria A, Taieb N, et al. Mislocalization of the exitatory amino-acid transporters (EAATs) in human astrocytoma and non-astrocytoma cancer cells: effect of the cell confluence. *J Biomed Sci.* 2012;19:10.
183. Falini B, Bolli N, Liso A, et al. Altered nucleophosmin transport in acute myeloid leukaemia with mutated NPM1: molecular basis and clinical implications. *Leukemia.* 2009;23:1731-1743.
184. Yang W, Musser SM. Nuclear import time and transport efficiency depend on importin beta concentration. *J Cell Biol.* 2006;174:951-961.
185. Kuusisto HV, Wagstaff KM, Alvisi G, Roth DM, Jans DA. Global enhancement of nuclear localization-dependent nuclear transport in transformed cells. *FASEB J.* 2012;26:1181-1193.
186. Sakai M, Sohda M, Miyazaki T, et al. Significance of karyopherin-{alpha} 2 (KPNA2) expression in esophageal squamous cell carcinoma. *Anticancer Res.* 2010;30:851-856.
187. Alshareeda AT, Negm OH, Green AR, et al. KPNA2 is a nuclear export protein that contributes to aberrant localisation of key proteins and poor prognosis of breast cancer. *Br J Cancer.* 2015;112:1929-1937.
188. Zhang Y, Zhang M, Yu F, et al. Karyopherin alpha 2 is a novel prognostic marker and a potential therapeutic target for colon cancer. *J Exp Clin Cancer Res.* 2015;34:145.
189. Laurila E, Vuorinen E, Savinainen K, Rauhala H, Kallioniemi A. KPNA7, a nuclear transport receptor, promotes malignant properties of pancreatic cancer cells in vitro. *Exp Cell Res.* 2014;322:159-167.
190. Grupp K, Habermann M, Sirma H, et al. High nuclear karyopherin alpha 2 expression is a strong and independent predictor of biochemical recurrence in prostate cancer patients treated by radical prostatectomy. *Mod Pathol.* 2014;27:96-106.
191. He L, Ding H, Wang JH, et al. Overexpression of karyopherin 2 in human ovarian malignant germ cell tumor correlates with poor prognosis. *PLoS One.* 2012;7:e42992.
192. Yang L, Hu B, Zhang Y, et al. Suppression of the nuclear transporter-KPNbeta1 expression inhibits tumor proliferation in hepatocellular carcinoma. *Med Oncol.* 2015;32:128.
193. Stelma T, Chi A, van der Watt PJ, Verrico A, Lavia P, Leaner VD. Targeting nuclear transporters in cancer: Diagnostic, prognostic and therapeutic potential. *IUBMB Life.* 2016;68:268-280.

194. van der Watt PJ, Ngarande E, Leaner VD. Overexpression of Kpnbeta1 and Kpnalpha2 importin proteins in cancer derives from deregulated E2F activity. *PLoS One.* 2011;6:e27723.
195. Nevins JR. The Rb/E2F pathway and cancer. *Hum Mol Genet.* 2001;10:699-703.
196. Yim EK, Park JS. The role of HPV E6 and E7 oncoproteins in HPV-associated cervical carcinogenesis. *Cancer Res Treat.* 2005;37:319-324.
197. Hwang SG, Lee D, Kim J, Seo T, Choe J. Human papillomavirus type 16 E7 binds to E2F1 and activates E2F1-driven transcription in a retinoblastoma protein-independent manner. *J Biol Chem.* 2002;277:2923-2930.
198. Lin J, Zhang L, Huang H, et al. MiR-26b/KPNA2 axis inhibits epithelial ovarian carcinoma proliferation and metastasis through downregulating OCT4. *Oncotarget.* 2015;6:23793-23806.
199. Zhang P, Garnett J, Creighton CJ, et al. EZH2-miR-30d-KPNB1 pathway regulates malignant peripheral nerve sheath tumour cell survival and tumourigenesis. *J Pathol.* 2014;232:308-318.
200. Kallioniemi A, Kallioniemi OP, Sudar D, et al. Comparative genomic hybridization for molecular cytogenetic analysis of solid tumors. *Science.* 1992;258:818-821.
201. Brinkmann U, Gallo M, Polymeropoulos MH, Pastan I. The human CAS (cellular apoptosis susceptibility) gene mapping on chromosome 20q13 is amplified in BT474 breast cancer cells and part of aberrant chromosomes in breast and colon cancer cell lines. *Genome Res.* 1996;6:187-194.
202. Winkler J, Ori A, Holzer K, et al. Prosurvival function of the cellular apoptosis susceptibility/importin-alpha1 transport cycle is repressed by p53 in liver cancer. *Hepatology.* 2014;60:884-895.
203. Muller PAJ, Vousden KH. p53 mutations in cancer. *Nat Cell Biol.* 2013;15:2-8.
204. Brinkmann U, Brinkmann E, Gallo M, Pastan I. Cloning and characterization of a cellular apoptosis susceptibility gene, the human homologue to the yeast chromosome segregation gene CSE1. *Proc Natl Acad Sci U S A.* 1995;92:10427-10431.
205. Wellmann A, Krenacs L, Fest T, et al. Localization of the cell proliferation and apoptosis-associated CAS protein in lymphoid neoplasms. *Am J Pathol.* 1997;150:25-30.
206. Stawerski P, Wagrowska-Danilewicz M, Stasikowska O, Danilewicz M. Immunoexpression of CAS protein is augmented in high grade serous ovarian tumors. *Pol J Pathol.* 2010;61:219-223.
207. Kahle J, Baake M, Doenecke D, Albig W. Subunits of the heterotrimeric transcription factor NF-Y are imported into the nucleus by distinct pathways involving importin beta and importin 13. *Mol Cell Biol.* 2005;25:5339-5354.
208. Zhou F, Qiu W, Yao R, et al. CRM1 is a novel independent prognostic factor for the poor prognosis of gastric carcinomas. *Med Oncol.* 2013;30:726.
209. Zhu J, Wang Y, Huang H, et al. Upregulation of KPNbeta1 in gastric cancer cell promotes tumor cell proliferation and predicts poor prognosis. *Tumour Biol.* 2015;37:661-672.
210. Lorenzato A, Martino C, Dani N, et al. The cellular apoptosis susceptibility CAS/CSE1L gene protects ovarian cancer cells from death by suppressing RASSF1C. *Faseb j.* 2012;26:2446-2456.
211. Scherf U, Kalab P, Dasso M, Pastan I, Brinkmann U. The hCSE1/CAS protein is phosphorylated by HeLa extracts and MEK-1: MEK-1 phosphorylation may modulate the intracellular localization of CAS. *Biochem Biophys Res Commun.* 1998;250:623-628.
212. Kim IS, Kim DH, Han SM, et al. Truncated form of importin alpha identified in breast cancer cell inhibits nuclear import of p53. *J Biol Chem.* 2000;275:23139-23145.
213. Melo SA, Moutinho C, Ropero S, et al. A genetic defect in exportin-5 traps precursor microRNAs in the nucleus of cancer cells. *Cancer Cell.* 2010;18:303-315.
214. Shtivelman E. A link between metastasis and resistance to apoptosis of variant small cell lung carcinoma. *Oncogene.* 1997;14:2167-2173.

215. Yu Y, Xu F, Peng H, et al. NOEY2 (ARHI), an imprinted putative tumor suppressor gene in ovarian and breast carcinomas. *Proc Natl Acad Sci U S A.* 1999;96:214-219.
216. Mazumder Indra D, Mitra S, Singh RK, et al. Inactivation of CHEK1 and EI24 is associated with the development of invasive cervical carcinoma: clinical and prognostic implications. *Int J Cancer.* 2011;129:1859-1871.
217. Huang S, Chang IS, Lin W, et al. ARHI (DIRAS3), an imprinted tumour suppressor gene, binds to importins and blocks nuclear import of cargo proteins. *Biosci Rep.* 2010;30:159-168.
218. Muthu K, Panneerselvam M, Topno NS, Jayaraman M, Ramadas K. Structural perspective of ARHI mediated inhibition of STAT3 signaling: an insight into the inactive to active transition of ARHI and its interaction with STAT3 and importinbeta. *Cell Signal.* 2015;27:739-755.
219. King FW, Shtivelman E. Inhibition of nuclear import by the proapoptotic protein CC3. *Mol Cell Biol.* 2004;24:7091-7101.
220. Lieu KG, Shim EH, Wang J, et al. The p53-induced factor Ei24 inhibits nuclear import through an importin beta-binding-like domain. *J Cell Biol.* 2014;205:301-312.
221. Dahl E, Kristiansen G, Gottlob K, et al. Molecular profiling of laser-microdissected matched tumor and normal breast tissue identifies karyopherin alpha2 as a potential novel prognostic marker in breast cancer. *Clin Cancer Res.* 2006;12:3950-3960.
222. Jensen JB, Munksgaard PP, Sorensen CM, et al. High expression of karyopherin-alpha2 defines poor prognosis in non-muscle-invasive bladder cancer and in patients with invasive bladder cancer undergoing radical cystectomy. *Eur Urol.* 2011;59:841-848.
223. Noetzel E, Rose M, Bornemann J, Gajewski M, Knuchel R, Dahl E. Nuclear transport receptor karyopherin-alpha2 promotes malignant breast cancer phenotypes in vitro. *Oncogene.* 2012;31:2101-2114.
224. Parikh K, Cang S, Sekhri A, Liu D. Selective inhibitors of nuclear export (SINE)--a novel class of anti-cancer agents. *J Hematol Oncol.* 2014;7:78.
225. Lu C, Figueroa JA, Liu Z, et al. Nuclear Export as a Novel Therapeutic Target: The CRM1 Connection. *Curr Cancer Drug Targets.* 2015;15:575-592.
226. Ishizawa J, Kojima K, Hail N, Jr., Tabe Y, Andreeff M. Expression, function, and targeting of the nuclear exporter chromosome region maintenance 1 (CRM1) protein. *Pharmacol Ther.* 2015;153:25-35.
227. Mao L, Yang Y. Targeting the nuclear transport machinery by rational drug design. *Curr Pharm Des.* 2013;19:2318-2325.
228. Lapalombella R, Sun Q, Williams K, et al. Selective inhibitors of nuclear export show that CRM1/XPO1 is a target in chronic lymphocytic leukemia. *Blood.* 2012;120:4621-4634.
229. Cheng Y, Holloway MP, Nguyen K, et al. XPO1 (CRM1) inhibition represses STAT3 activation to drive a survivin-dependent oncogenic switch in triple-negative breast cancer. *Mol Cancer Ther.* 2014;13:675-686.
230. Gravina GL, Tortoreto M, Mancini A, et al. XPO1/CRM1-selective inhibitors of nuclear export (SINE) reduce tumor spreading and improve overall survival in preclinical models of prostate cancer (PCa). *J Hematol Oncol.* 2014;7:46.
231. Gao W, Lu C, Chen L, Keohavong P. Overexpression of CRM1: A Characteristic Feature in a Transformed Phenotype of Lung Carcinogenesis and a Molecular Target for Lung Cancer Adjuvant Therapy. *J Thorac Oncol.* 2015;10:815-825.
232. Noske A, Weichert W, Niesporek S, et al. Expression of the nuclear export protein chromosomal region maintenance/exportin 1/Xpo1 is a prognostic factor in human ovarian cancer. *Cancer.* 2008;112:1733-1743.
233. Shen A, Wang Y, Zhao Y, Zou L, Sun L, Cheng C. Expression of CRM1 in human gliomas and its significance in p27 expression and clinical prognosis. *Neurosurgery.* 2009;65:153-160.
234. Huang WY, Yue L, Qiu WS, Wang LW, Zhou XH, Sun YJ. Prognostic value of CRM1 in pancreas cancer. *Clin Invest Med.* 2009;32:E315.

235. Yao Y, Dong Y, Lin F, et al. The expression of CRM1 is associated with prognosis in human osteosarcoma. *Oncol Rep.* 2009;21:229-235.
236. Tiedemann RE, Zhu YX, Schmidt J, et al. Identification of molecular vulnerabilities in human multiple myeloma cells by RNA interference lethality screening of the druggable genome. *Cancer Res.* 2012;72:757-768.
237. Inoue H, Kauffman M, Shacham S, et al. CRM1 blockade by selective inhibitors of nuclear export attenuates kidney cancer growth. *J Urol.* 2013;189:2317-2326.
238. Etchin J, Sun Q, Kentsis A, et al. Antileukemic activity of nuclear export inhibitors that spare normal hematopoietic cells. *Leukemia.* 2013;27:66-74.
239. Nishi K, Yoshida M, Fujiwara D, Nishikawa M, Horinouchi S, Beppu T. Leptomycin B targets a regulatory cascade of crm1, a fission yeast nuclear protein, involved in control of higher order chromosome structure and gene expression. *J Biol Chem.* 1994;269:6320-6324.
240. Kudo N, Matsumori N, Taoka H, et al. Leptomycin B inactivates CRM1/exportin 1 by covalent modification at a cysteine residue in the central conserved region. *Proc Natl Acad Sci U S A.* 1999;96:9112-9117.
241. Tunac JB, Graham BD, Dobson WE, Lenzini MD. Novel antitumor antibiotics, CI-940 (PD 114,720) and PD 114,721. Taxonomy, fermentation and biological activity. *J Antibiot (Tokyo).* 1985;38:460-465.
242. Newlands ES, Rustin GJ, Brampton MH. Phase I trial of elactocin. *Br J Cancer.* 1996;74:648-649.
243. Mutka SC, Yang WQ, Dong SD, et al. Identification of nuclear export inhibitors with potent anticancer activity in vivo. *Cancer Res.* 2009;69:510-517.
244. Sakakibara K, Saito N, Sato T, et al. CBS9106 is a novel reversible oral CRM1 inhibitor with CRM1 degrading activity. *Blood.* 2011;118:3922-3931.
245. Liu X, Niu M, Xu X, et al. CRM1 is a direct cellular target of the natural anti-cancer agent plumbagin. *J Pharmacol Sci.* 2014;124:486-493.
246. Niu M, Xu X, Shen Y, et al. Piperlongumine is a novel nuclear export inhibitor with potent anticancer activity. *Chem Biol Interact.* 2015;237:66-72.
247. Breit MN, Kisseberth WC, Bear MD, et al. Biologic activity of the novel orally bioavailable selective inhibitor of nuclear export (SINE) KPT-335 against canine melanoma cell lines. *BMC Vet Res.* 2014;10:160.
248. Etchin J, Sanda T, Mansour MR, et al. KPT-330 inhibitor of CRM1 (XPO1)-mediated nuclear export has selective anti-leukaemic activity in preclinical models of T-cell acute lymphoblastic leukaemia and acute myeloid leukaemia. *Br J Haematol.* 2013;161:117-127.
249. Mendonca J, Sharma A, Kim HS, et al. Selective inhibitors of nuclear export (SINE) as novel therapeutics for prostate cancer. *Oncotarget.* 2014;5:6102-6112.
250. Ranganathan P, Yu X, Na C, et al. Preclinical activity of a novel CRM1 inhibitor in acute myeloid leukemia. *Blood.* 2012;120:1765-1773.
251. Sun H, Hattori N, Chien W, et al. KPT-330 has antitumour activity against non-small cell lung cancer. *Br J Cancer.* 2014;111:281-291.
252. Zhang K, Wang M, Tamayo AT, et al. Novel selective inhibitors of nuclear export CRM1 antagonists for therapy in mantle cell lymphoma. *Exp Hematol.* 2013;41:67-78.
253. London CA, Bernabe LF, Barnard S, et al. Preclinical evaluation of the novel, orally bioavailable Selective Inhibitor of Nuclear Export (SINE) KPT-335 in spontaneous canine cancer: results of a phase I study. *PLoS One.* 2014;9:e87585.
254. Azmi AS, Muqbil I, Wu J, et al. Targeting the Nuclear Export Protein XPO1/CRM1 Reverses Epithelial to Mesenchymal Transition. *Sci Rep.* 2015;5:16077.
255. Yang J, Bill MA, Young GS, et al. Novel small molecule XPO1/CRM1 inhibitors induce nuclear accumulation of TP53, phosphorylated MAPK and apoptosis in human melanoma cells. *PLoS One.* 2014;9:e102983.

256. Turner JG, Sullivan DM. CRM1-mediated nuclear export of proteins and drug resistance in cancer. *Curr Med Chem.* 2008;15:2648-2655.
257. El-Tanani M, Dakir el H, Raynor B, Morgan R. Mechanisms of Nuclear Export in Cancer and Resistance to Chemotherapy. *Cancers (Basel).* 2016;8:35.
258. Tai YT, Landesman Y, Acharya C, et al. CRM1 inhibition induces tumor cell cytotoxicity and impairs osteoclastogenesis in multiple myeloma: molecular mechanisms and therapeutic implications. *Leukemia.* 2014;28:155-165.
259. Turner JG, Engel R, Derderian JA, Jove R, Sullivan DM. Human topoisomerase IIalpha nuclear export is mediated by two CRM-1-dependent nuclear export signals. *J Cell Sci.* 2004;117:3061-3071.
260. Turner JG, Dawson J, Emmons MF, et al. CRM1 Inhibition Sensitizes Drug Resistant Human Myeloma Cells to Topoisomerase II and Proteasome Inhibitors both In Vitro and Ex Vivo. *J Cancer.* 2013;4:614-625.
261. Salas Fragomeni RA, Chung HW, Landesman Y, et al. CRM1 and BRAF inhibition synergize and induce tumor regression in BRAF-mutant melanoma. *Mol Cancer Ther.* 2013;12:1171-1179.
262. Turner JG, Marchion DC, Dawson JL, et al. Human multiple myeloma cells are sensitized to topoisomerase II inhibitors by CRM1 inhibition. *Cancer Res.* 2009;69:6899-6905.
263. Gong LH, Chen XX, Wang H, et al. Piperlongumine induces apoptosis and synergizes with cisplatin or paclitaxel in human ovarian cancer cells. *Oxid Med Cell Longev.* 2014;2014:906804.
264. Kojima K, Kornblau SM, Ruvolo V, et al. Prognostic impact and targeting of CRM1 in acute myeloid leukemia. *Blood.* 2013;121:4166-4174.
265. Adam EJ, Adam SA. Identification of cytosolic factors required for nuclear location sequence-mediated binding to the nuclear envelope. *J Cell Biol.* 1994;125:547-555.
266. Gorlich D, Kostka S, Kraft R, et al. Two different subunits of importin cooperate to recognize nuclear localization signals and bind them to the nuclear envelope. *Curr Biol.* 1995;5:383-392.
267. Chi NC, Adam EJ, Adam SA. Sequence and characterization of cytoplasmic nuclear protein import factor p97. *J Cell Biol.* 1995;130:265-274.
268. Ayala-Madrigal ML, Doerr S, Ramirez-Duenas ML, Hansmann I. Assignment of KPNA4 and KPNB1 encoding karyopherin alpha 4 and beta 1 to human chromosome bands 11q22 and 17q21 respectively, by in situ hybridization. *Cytogenet Cell Genet.* 2000;89:258-259.
269. Cook A, Bono F, Jinek M, Conti E. Structural biology of nucleocytoplasmic transport. *Annu Rev Biochem.* 2007;76:647-671.
270. Yan W, Li R, He J, Du J, Hou J. Importin beta1 mediates nuclear factor-kappaB signal transduction into the nuclei of myeloma cells and affects their proliferation and apoptosis. *Cell Signal.* 2015;27:851-859.
271. Szczepny A, Wagstaff KM, Dias M, et al. Overlapping binding sites for importin beta1 and suppressor of fused (SuFu) on glioma-associated oncogene homologue 1 (Gli1) regulate its nuclear localization. *Biochem J.* 2014;461:469-476.
272. Russell MW, Soliman MA, Schriemer D, Riabowol K. ING1 protein targeting to the nucleus by karyopherins is necessary for activation of p21. *Biochem Biophys Res Commun.* 2008;374:490-495.
273. Lo HW, Ali-Seyed M, Wu Y, Bartholomeusz G, Hsu SC, Hung MC. Nuclear-cytoplasmic transport of EGFR involves receptor endocytosis, importin beta1 and CRM1. *J Cell Biochem.* 2006;98:1570-1583.
274. Cimica V, Chen HC, Iyer JK, Reich NC. Dynamics of the STAT3 transcription factor: nuclear import dependent on Ran and importin-beta1. *PLoS One.* 2011;6:e20188.
275. Odaka Y, Mally A, Elliott LT, Meyers S. Nuclear import and subnuclear localization of the proto-oncoprotein ETO (MTG8). *Oncogene.* 2000;19:3584-3597.
276. Xiao Z, Liu X, Lodish HF. Importin beta mediates nuclear translocation of Smad 3. *J Biol Chem.* 2000;275:23425-23428.

277. Theodore M, Kawai Y, Yang J, et al. Multiple nuclear localization signals function in the nuclear import of the transcription factor Nrf2. *J Biol Chem.* 2008;283:8984-8994.
278. Le Roux LG, Moroianu J. Nuclear entry of high-risk human papillomavirus type 16 E6 oncoprotein occurs via several pathways. *J Virol.* 2003;77:2330-2337.
279. Darshan MS, Lucchi J, Harding E, Moroianu J. The l2 minor capsid protein of human papillomavirus type 16 interacts with a network of nuclear import receptors. *J Virol.* 2004;78:12179-12188.
280. Ems-McClung SC, Zheng Y, Walczak CE. Importin alpha/beta and Ran-GTP regulate XCTK2 microtubule binding through a bipartite nuclear localization signal. *Mol Biol Cell.* 2004;15:46-57.
281. Roostalu J, Cade NI, Surrey T. Complementary activities of TPX2 and chTOG constitute an efficient importin-regulated microtubule nucleation module. *Nat Cell Biol.* 2015;17:1422-1434.
282. Ciciarello M, Mangiacasale R, Thibier C, et al. Importin beta is transported to spindle poles during mitosis and regulates Ran-dependent spindle assembly factors in mammalian cells. *J Cell Sci.* 2004;117:6511-6522.
283. Blower MD, Nachury M, Heald R, Weis K. A Rae1-containing ribonucleoprotein complex is required for mitotic spindle assembly. *Cell.* 2005;121:223-234.
284. Schmitz MH, Held M, Janssens V, et al. Live-cell imaging RNAi screen identifies PP2A-B55alpha and importin-beta1 as key mitotic exit regulators in human cells. *Nat Cell Biol.* 2010;12:886-893.
285. Harel A, Chan RC, Lachish-Zalait A, Zimmerman E, Elbaum M, Forbes DJ. Importin beta negatively regulates nuclear membrane fusion and nuclear pore complex assembly. *Mol Biol Cell.* 2003;14:4387-4396.
286. Roscioli E, Di Francesco L, Bolognesi A, et al. Importin-beta negatively regulates multiple aspects of mitosis including RANGAP1 recruitment to kinetochores. *J Cell Biol.* 2012;196:435-450.
287. Neumayer G, Belzil C, Gruss OJ, Nguyen MD. TPX2: of spindle assembly, DNA damage response, and cancer. *Cell Mol Life Sci.* 2014;71:3027-3047.
288. Xia F, Lee CW, Altieri DC. Tumor cell dependence on Ran-GTP-directed mitosis. *Cancer Res.* 2008;68:1826-1833.
289. Zhong Y, Wang Y, Yang H, et al. Importin beta interacts with the endoplasmic reticulum-associated degradation machinery and promotes ubiquitination and degradation of mutant alpha1-antitrypsin. *J Biol Chem.* 2011;286:33921-33930.
290. Bauerle M, Doenecke D, Albig W. The requirement of H1 histones for a heterodimeric nuclear import receptor. *J Biol Chem.* 2002;277:32480-32489.
291. Lowe AR, Tang JH, Yassif J, et al. Importin-beta modulates the permeability of the nuclear pore complex in a Ran-dependent manner. *Elife.* 2015;4:e04052.
292. Yasuhara N, Takeda E, Inoue H, Kotera I, Yoneda Y. Importin alpha/beta-mediated nuclear protein import is regulated in a cell cycle-dependent manner. *Exp Cell Res.* 2004;297:285-293.
293. Zeng Y, Wang Y, Wu Z, et al. miR-9 enhances the transactivation of nuclear factor of activated T cells by targeting KPNB1 and DYRK1B. *Am J Physiol Cell Physiol.* 2015;308:C720-728.
294. Kaur G, Ly-Huynh JD, Jans DA. Intracellular calcium levels can regulate Importin-dependent nuclear import. *Biochem Biophys Res Commun.* 2014;450:812-817.
295. Di Paola S, Micaroni M, Di Tullio G, Buccione R, Di Girolamo M. PARP16/ARTD15 is a novel endoplasmic-reticulum-associated mono-ADP-ribosyltransferase that interacts with, and modifies karyopherin-ss1. *PLoS One.* 2012;7:e37352.
296. Kuusisto HV, Jans DA. Hyper-dependence of breast cancer cell types on the nuclear transporter Importin beta1. *Biochim Biophys Acta.* 2015;1853:1870-1878.

297. Smith ER, Cai KQ, Smedberg JL, et al. Nuclear entry of activated MAPK is restricted in primary ovarian and mammary epithelial cells. *PLoS One.* 2010;5:e9295.
298. Yan WQ, Du J, Jiang H, Hou J. [Effect of nuclear receptor inhibitor importazole on the proliferation and apoptosis of multiple myeloma cells]. *Zhonghua Xue Ye Xue Za Zhi.* 2013;34:323-326.
299. Martens-de Kemp SR, Nagel R, Stigter-van Walsum M, et al. Functional genetic screens identify genes essential for tumor cell survival in head and neck and lung cancer. *Clin Cancer Res.* 2013;19:1994-2003.
300. Angus L, van der Watt PJ, Leaner VD. Inhibition of the nuclear transporter, Kpnbeta1, results in prolonged mitotic arrest and activation of the intrinsic apoptotic pathway in cervical cancer cells. *Carcinogenesis.* 2014;35:1121-1131.
301. Liang SH, Clarke MF. Regulation of p53 localization. *Eur J Biochem.* 2001;268:2779-2783.
302. Thompson ME. BRCA1 16 years later: nuclear import and export processes. *Febs j.* 2010;277:3072-3078.
303. Hu W, Kemp BE, Jans DA. Kinetic properties of nuclear transport conferred by the retinoblastoma (Rb) NLS. *J Cell Biochem.* 2005;95:782-793.
304. Siegel D, Martin T, Nooka A, et al. Integrated safety profile of single-agent carfilzomib: experience from 526 patients enrolled in 4 phase II clinical studies. *Haematologica.* 2013;98:1753-1761.
305. O'Connor OA, Wright J, Moskowitz C, et al. Phase II clinical experience with the novel proteasome inhibitor bortezomib in patients with indolent non-Hodgkin's lymphoma and mantle cell lymphoma. *J Clin Oncol.* 2005;23:676-684.
306. Drinyaev VA, Mosin VA, Kruglyak EB, et al. Antitumor effect of avermectins. *Eur J Pharmacol.* 2004;501:19-23.
307. Malilas W, Koh SS, Kim S, et al. Cancer upregulated gene 2, a novel oncogene, enhances migration and drug resistance of colon cancer cells via STAT1 activation. *Int J Oncol.* 2013;43:1111-1116.
308. Kumar K, Raza SS, Knab LM, et al. GLI2-dependent c-MYC upregulation mediates resistance of pancreatic cancer cells to the BET bromodomain inhibitor JQ1. *Sci Rep.* 2015;5:9489.
309. Bentires-Alj M, Barbu V, Fillet M, et al. NF-kappaB transcription factor induces drug resistance through MDR1 expression in cancer cells. *Oncogene.* 2003;22:90-97.
310. Godwin P, Baird AM, Heavey S, Barr MP, O'Byrne KJ, Gately K. Targeting nuclear factor-kappa B to overcome resistance to chemotherapy. *Front Oncol.* 2013;3:120.
311. Sahin K, Tuzcu M, Basak N, et al. Sensitization of Cervical Cancer Cells to Cisplatin by Genistein: The Role of NFkappaB and Akt/mTOR Signaling Pathways. *J Oncol.* 2012;2012:461562.
312. Xu Y, Fang F, St Clair DK, Sompol P, Josson S, St Clair WH. SN52, a novel nuclear factor-kappaB inhibitor, blocks nuclear import of RelB:p52 dimer and sensitizes prostate cancer cells to ionizing radiation. *Mol Cancer Ther.* 2008;7:2367-2376.
313. Lin YZ, Yao SY, Veach RA, Torgerson TR, Hawiger J. Inhibition of nuclear translocation of transcription factor NF-kappa B by a synthetic peptide containing a cell membrane-permeable motif and nuclear localization sequence. *J Biol Chem.* 1995;270:14255-14258.
314. Torgerson TR, Colosia AD, Donahue JP, Lin YZ, Hawiger J. Regulation of NF-kappa B, AP-1, NFAT, and STAT1 nuclear import in T lymphocytes by noninvasive delivery of peptide carrying the nuclear localization sequence of NF-kappa B p50. *J Immunol.* 1998;161:6084-6092.
315. Zienkiewicz J, Armitage A, Hawiger J. Targeting nuclear import shuttles, importins/karyopherins alpha by a peptide mimicking the NFkappaB1/p50 nuclear localization sequence. *J Am Heart Assoc.* 2013;2:e000386.
316. Nagoshi E, Imamoto N, Sato R, Yoneda Y. Nuclear import of sterol regulatory element-binding protein-2, a basic helix-loop-helix-leucine zipper (bHLH-Zip)-containing transcription

factor, occurs through the direct interaction of importin beta with HLH-Zip. *Mol Biol Cell.* 1999;10:2221-2233.

317. Kosugi S, Hasebe M, Entani T, Takayama S, Tomita M, Yanagawa H. Design of peptide inhibitors for the importin alpha/beta nuclear import pathway by activity-based profiling. *Chem Biol.* 2008;15:940-949.

318. Hashimoto H, Messerli SM, Sudo T, Maruta H. Ivermectin inactivates the kinase PAK1 and blocks the PAK1-dependent growth of human ovarian cancer and NF2 tumor cell lines. *Drug Discov Ther.* 2009;3:243-246.

319. Melotti A, Mas C, Kuciak M, Lorente-Trigos A, Borges I, Ruiz i Altaba A. The river blindness drug Ivermectin and related macrocyclic lactones inhibit WNT-TCF pathway responses in human cancer. *EMBO Mol Med.* 2014;6:1263-1278.

320. Wagstaff KM, Rawlinson SM, Hearps AC, Jans DA. An AlphaScreen(R)-based assay for high-throughput screening for specific inhibitors of nuclear import. *J Biomol Screen.* 2011;16:192-200.

321. Wagstaff KM, Sivakumaran H, Heaton SM, Harrich D, Jans DA. Ivermectin is a specific inhibitor of importin alpha/beta-mediated nuclear import able to inhibit replication of HIV-1 and dengue virus. *Biochem J.* 2012;443:851-856.

322. Nishio M, Sugimachi K, Goto H, et al. Dysregulated YAP1/TAZ and TGF-beta signaling mediate hepatocarcinogenesis in Mob1a/1b-deficient mice. *Proc Natl Acad Sci U S A.* 2016;113:E71-80.

323. Menez C, Mselli-Lakhal L, Foucaud-Vignault M, Balaguer P, Alvinerie M, Lespine A. Ivermectin induces P-glycoprotein expression and function through mRNA stabilization in murine hepatocyte cell line. *Biochem Pharmacol.* 2012;83:269-278.

324. Hintersteiner M, Ambrus G, Bednenko J, et al. Identification of a small molecule inhibitor of importin beta mediated nuclear import by confocal on-bead screening of tagged one-bead one-compound libraries. *ACS Chem Biol.* 2010;5:967-979.

325. Soderholm JF, Bird SL, Kalab P, et al. Importazole, a small molecule inhibitor of the transport receptor importin-beta. *ACS Chem Biol.* 2011;6:700-708.

326. Ambrus G, Whitby LR, Singer EL, et al. Small molecule peptidomimetic inhibitors of importin alpha/beta mediated nuclear transport. *Bioorg Med Chem.* 2010;18:7611-7620.

327. Galal SA, Abdelsamie AS, Soliman SM, et al. Design, synthesis and structure-activity relationship of novel quinoxaline derivatives as cancer chemopreventive agent by inhibition of tyrosine kinase receptor. *Eur J Med Chem.* 2013;69:115-124.

328. Ghattass K, El-Sitt S, Zibara K, et al. The quinoxaline di-N-oxide DCQ blocks breast cancer metastasis in vitro and in vivo by targeting the hypoxia inducible factor-1 pathway. *Mol Cancer.* 2014;13:12.

329. Lee SH, Kim N, Kim SJ, Song J, Gong YD, Kim SY. Anti-cancer effect of a quinoxaline derivative GK13 as a transglutaminase 2 inhibitor. *J Cancer Res Clin Oncol.* 2013;139:1279-1294.

330. Al-Douh MH, Sahib HB, Osman H, Abd Hamid S, Salhimi SM. Anti-proliferation effects of benzimidazole derivatives on HCT-116 colon cancer and MCF-7 breast cancer cell lines. *Asian Pac J Cancer Prev.* 2012;13:4075-4079.

331. Chu B, Liu F, Li L, et al. A benzimidazole derivative exhibiting antitumor activity blocks EGFR and HER2 activity and upregulates DR5 in breast cancer cells. *Cell Death Dis.* 2015;6:e1686.

332. Youssef AM, Malki A, Badr MH, Elbayaa RY, Sultan AS. Synthesis and anticancer activity of novel benzimidazole and benzothiazole derivatives against HepG2 liver cancer cells. *Med Chem.* 2012;8:151-162.

333. van der Watt PJ, Chi A, Stelma T, et al. Targeting the Nuclear Import Receptor Kpnbeta1 as an Anticancer Therapeutic. *Mol Cancer Ther.* 2016;15:560-573.

334. Puck TT, Marcus PI. Action of x-rays on mammalian cells. *J Exp Med.* 1956;103:653-666.

335. Rafehi H, Orlowski C, Georgiadis GT, Ververis K, El-Osta A, Karagiannis TC. Clonogenic assay: adherent cells. *J Vis Exp.* 2011;13:2573.

336. Shin SI, Freedman VH, Risser R, Pollack R. Tumorigenicity of virus-transformed cells in nude mice is correlated specifically with anchorage independent growth in vitro. *Proc Natl Acad Sci U S A.* 1975;72:4435-4439.
337. Paddison PJ, Caudy AA, Bernstein E, Hannon GJ, Conklin DS. Short hairpin RNAs (shRNAs) induce sequence-specific silencing in mammalian cells. *Genes Dev.* 2002;16:948-958.
338. Aagaard L, Amarzguioui M, Sun G, et al. A facile lentiviral vector system for expression of doxycycline-inducible shRNAs: knockdown of the pre-miRNA processing enzyme Drosha. *Mol Ther.* 2007;15:938-945.
339. Kaufmann SH, Desnoyers S, Ottaviano Y, Davidson NE, Poirier GG. Specific proteolytic cleavage of poly(ADP-ribose) polymerase: an early marker of chemotherapy-induced apoptosis. *Cancer Res.* 1993;53:3976-3985.
340. van de Waterbeemd H, Gifford E. ADMET in silico modelling: towards prediction paradise? *Nat Rev Drug Discov.* 2003;2:192-204.
341. Barka T, Popper H. Liver enlargement and drug toxicity. *Medicine (Baltimore).* 1967;46:103-117.
342. Caruso R, Parisi A, Bonanno A, et al. Histologic coagulative tumour necrosis as a prognostic indicator of aggressiveness in renal, lung, thyroid and colorectal carcinomas: A brief review. *Oncol Lett.* 2012;3:16-18.
343. Liu X, Chong Y, Liu H, Han Y, Niu M. CRM1 inhibitor S109 suppresses cell proliferation and induces cell cycle arrest in renal cancer cells. *Korean J Physiol Pharmacol.* 2016;20:161-168.
344. Liu X, Chong Y, Liu H, Han Y, Niu M. Novel reversible selective inhibitor of CRM1 for targeted therapy in ovarian cancer. *J Ovarian Res.* 2015;8:35.
345. Niu M, Chong Y, Han Y, Liu X. Novel reversible selective inhibitor of nuclear export shows that CRM1 is a target in colorectal cancer cells. *Cancer Biol Ther.* 2015;16:1110-1118.
346. Wang S, Han X, Wang J, Yao J, Shi Y. Antitumor effects of a novel chromosome region maintenance 1 (CRM1) inhibitor on non-small cell lung cancer cells in vitro and in mouse tumor xenografts. *PLoS One.* 2014;9:e89848.
347. Wang Y, Wang Y, Xiang J, et al. Knockdown of CRM1 inhibits the nuclear export of p27(Kip1) phosphorylated at serine 10 and plays a role in the pathogenesis of epithelial ovarian cancer. *Cancer Lett.* 2014;343:6-13.
348. Pathria G, Wagner C, Wagner SN. Inhibition of CRM1-mediated nucleocytoplasmic transport: triggering human melanoma cell apoptosis by perturbing multiple cellular pathways. *J Invest Dermatol.* 2012;132:2780-2790.
349. Sengupta S, Lohse CM, Leibovich BC, et al. Histologic coagulative tumor necrosis as a prognostic indicator of renal cell carcinoma aggressiveness. *Cancer.* 2005;104:511-520.
350. Proskuryakov SY, Gabai VL. Mechanisms of tumor cell necrosis. *Curr Pharm Des.* 2010;16:56-68.
351. Vakkila J, Lotze MT. Inflammation and necrosis promote tumour growth. *Nat Rev Immunol.* 2004;4:641-648.
352. Seitz C, Gupta A, Shariat SF, et al. Association of tumor necrosis with pathological features and clinical outcome in 754 patients undergoing radical nephroureterectomy for upper tract urothelial carcinoma: an international validation study. *J Urol.* 2010;184:1895-1900.
353. Zigeuner R, Shariat SF, Margulis V, et al. Tumour necrosis is an indicator of aggressive biology in patients with urothelial carcinoma of the upper urinary tract. *Eur Urol.* 2010;57:575-581.
354. Simone G, Papalia R, Loreto A, Leonardo C, Sentinelli S, Gallucci M. Independent prognostic value of tumour diameter and tumour necrosis in upper urinary tract urothelial carcinoma. *BJU Int.* 2009;103:1052-1057.
355. Pichler M, Hutterer GC, Chromecki TF, et al. Histologic tumor necrosis is an independent prognostic indicator for clear cell and papillary renal cell carcinoma. *Am J Clin Pathol.* 2012;137:283-289.

356. Pollheimer MJ, Kornprat P, Lindtner RA, et al. Tumor necrosis is a new promising prognostic factor in colorectal cancer. *Hum Pathol.* 2010;41:1749-1757.
357. Swinson DE, Jones JL, Richardson D, Cox G, Edwards JG, O'Byrne KJ. Tumour necrosis is an independent prognostic marker in non-small cell lung cancer: correlation with biological variables. *Lung Cancer.* 2002;37:235-240.
358. Hiraoka N, Ino Y, Sekine S, et al. Tumour necrosis is a postoperative prognostic marker for pancreatic cancer patients with a high interobserver reproducibility in histological evaluation. *Br J Cancer.* 2010;103:1057-1065.
359. Siegel RL, Miller KD, Jemal A. Cancer statistics, 2015. *CA Cancer J Clin.* 2015;65:5-29.
360. Johnson SW, Ozols RF, Hamilton TC. Mechanisms of drug resistance in ovarian cancer. *Cancer.* 1993;71:644-649.
361. Agarwal R, Kaye SB. Ovarian cancer: strategies for overcoming resistance to chemotherapy. *Nat Rev Cancer.* 2003;3:502-516.
362. Kyrgiou M, Salanti G, Pavlidis N, Paraskevaidis E, Ioannidis JP. Survival benefits with diverse chemotherapy regimens for ovarian cancer: meta-analysis of multiple treatments. *J Natl Cancer Inst.* 2006;98:1655-1663.
363. McGuire WP, Hoskins WJ, Brady MF, et al. Cyclophosphamide and cisplatin compared with paclitaxel and cisplatin in patients with stage III and stage IV ovarian cancer. *N Engl J Med.* 1996;334:1-6.
364. Piccart MJ, Bertelsen K, Stuart G, et al. Long-term follow-up confirms a survival advantage of the paclitaxel-cisplatin regimen over the cyclophosphamide-cisplatin combination in advanced ovarian cancer. *Int J Gynecol Cancer.* 2003;13 Suppl 2:144-148.
365. Raja FA, Chopra N, Ledermann JA. Optimal first-line treatment in ovarian cancer. *Ann Oncol.* 2012;23 Suppl 10:x118-127.
366. Ozols RF, Bundy BN, Greer BE, et al. Phase III trial of carboplatin and paclitaxel compared with cisplatin and paclitaxel in patients with optimally resected stage III ovarian cancer: a Gynecologic Oncology Group study. *J Clin Oncol.* 2003;21:3194-3200.
367. du Bois A, Luck HJ, Meier W, et al. A randomized clinical trial of cisplatin/paclitaxel versus carboplatin/paclitaxel as first-line treatment of ovarian cancer. *J Natl Cancer Inst.* 2003;95:1320-1329.
368. van der Burg ME, de Wit R, van Putten WL, et al. Weekly cisplatin and daily oral etoposide is highly effective in platinum pretreated ovarian cancer. *Br J Cancer.* 2002;86:19-25.
369. Verborg WA, Campbell LR, Highley MS, Rankin EM. Weekly cisplatin with oral etoposide: a well-tolerated and highly effective regimen in relapsed ovarian cancer. *Int J Gynecol Cancer.* 2008;18:228-234.
370. Gounaris I, Iddawela M, Parkinson C, et al. Intensive cisplatin/oral etoposide for epithelial ovarian cancer: the Cambridge Gynae-Oncology Centre experience: too toxic for relapse? *Anticancer Drugs.* 2016;27:239-244.
371. Burger RA, Brady MF, Bookman MA, et al. Incorporation of bevacizumab in the primary treatment of ovarian cancer. *N Engl J Med.* 2011;365:2473-2483.
372. Perren TJ, Swart AM, Pfisterer J, et al. A phase 3 trial of bevacizumab in ovarian cancer. *N Engl J Med.* 2011;365:2484-2496.
373. Zheng M, Tang L, Huang L, et al. Overexpression of karyopherin-2 in epithelial ovarian cancer and correlation with poor prognosis. *Obstet Gynecol.* 2010;116:884-891.
374. Christiansen A, Dyrskjot L. The functional role of the novel biomarker karyopherin alpha 2 (KPNA2) in cancer. *Cancer Lett.* 2013;331:18-23.
375. Turner JG, Dawson J, Cubitt CL, Baz R, Sullivan DM. Inhibition of CRM1-dependent nuclear export sensitizes malignant cells to cytotoxic and targeted agents. *Semin Cancer Biol.* 2014;27:62-73.
376. Miyake TM, Pradeep S, Zand B, et al. Abstract 5541: Therapeutic targeting of CRM1 in ovarian cancer. *Cancer Research.* 2013;73:5541.

377. Chen Y, Kalir E, Camacho-Vanegas C, et al. Abstract 2163: Increased overall survival in platinum-resistant ovarian cancer: paradigmatic use of novel SINE (selective inhibitor of nuclear export), which restores p53 nuclear localization and activation. *Cancer Research.* 2013;73:2163.
378. Lange A, Mills RE, Lange CJ, Stewart M, Devine SE, Corbett AH. Classical nuclear localization signals: definition, function, and interaction with importin alpha. *J Biol Chem.* 2007;282:5101-5105.
379. Kuo LJ, Yang LX. Gamma-H2AX - a novel biomarker for DNA double-strand breaks. *In Vivo.* 2008;22:305-309.
380. Zheng J, Mercado-Uribe I, Rosen DG, et al. Induction of papillary carcinoma in human ovarian surface epithelial cells using combined genetic elements and peritoneal microenvironment. *Cell Cycle.* 2010;9:140-146.
381. Kodiha M, Chu A, Matusiewicz N, Stochaj U. Multiple mechanisms promote the inhibition of classical nuclear import upon exposure to severe oxidative stress. *Cell Death Differ.* 2004;11:862-874.
382. Crampton N, Kodiha M, Shrivastava S, Umar R, Stochaj U. Oxidative stress inhibits nuclear protein export by multiple mechanisms that target FG nucleoporins and Crm1. *Mol Biol Cell.* 2009;20:5106-5116.
383. Kodiha M, Banski P, Ho-Wo-Cheong D, Stochaj U. Dissection of the molecular mechanisms that control the nuclear accumulation of transport factors importin-alpha and CAS in stressed cells. *Cell Mol Life Sci.* 2008;65:1756-1767.
384. Sturchler E, Feurstein D, Chen W, McDonald P, Duckett D. Stress-induced nuclear import of apoptosis signal-regulating kinase 1 is mediated by karyopherin alpha2/beta1 heterodimer. *Biochim Biophys Acta.* 2013;1833:583-592.
385. Tristan C, Shahani N, Sedlak TW, Sawa A. The diverse functions of GAPDH: views from different subcellular compartments. *Cell Signal.* 2011;23:317-323.
386. Kodiha M, Banski P, Stochaj U. Interplay between MEK and PI3 kinase signaling regulates the subcellular localization of protein kinases ERK1/2 and Akt upon oxidative stress. *FEBS Lett.* 2009;583:1987-1993.
387. Sekimoto T, Yoneda Y. Intrinsic and extrinsic negative regulators of nuclear protein transport processes. *Genes Cells.* 2012;17:525-535.
388. Dietlein F, Reinhardt HC. Molecular pathways: exploiting tumor-specific molecular defects in DNA repair pathways for precision cancer therapy. *Clin Cancer Res.* 2014;20:5882-5887.
389. Helleday T, Petermann E, Lundin C, Hodgson B, Sharma RA. DNA repair pathways as targets for cancer therapy. *Nat Rev Cancer.* 2008;8:193-204.
390. Tkach JM, Yimit A, Lee AY, et al. Dissecting DNA damage response pathways by analysing protein localization and abundance changes during DNA replication stress. *Nat Cell Biol.* 2012;14:966-976.
391. Wood CD, Thornton TM, Sabio G, Davis RA, Rincon M. Nuclear localization of p38 MAPK in response to DNA damage. *Int J Biol Sci.* 2009;5:428-437.
392. Gildemeister OS, Sage JM, Knight KL. Cellular redistribution of Rad51 in response to DNA damage: novel role for Rad51C. *J Biol Chem.* 2009;284:31945-31952.
393. Abella N, Brun S, Calvo M, et al. Nucleolar disruption ensures nuclear accumulation of p21 upon DNA damage. *Traffic.* 2010;11:743-755.
394. Liu W, Nichols AF, Graham JA, Dualan R, Abbas A, Linn S. Nuclear transport of human DDB protein induced by ultraviolet light. *J Biol Chem.* 2000;275:21429-21434.
395. Li C, Chen L, Chen J. DNA damage induces MDMX nuclear translocation by p53-dependent and -independent mechanisms. *Mol Cell Biol.* 2002;22:7562-7571.
396. Lopez-Girona A, Furnari B, Mondesert O, Russell P. Nuclear localization of Cdc25 is regulated by DNA damage and a 14-3-3 protein. *Nature.* 1999;397:172-175.

397. Wan G, Zhang X, Langley RR, et al. DNA-damage-induced nuclear export of precursor microRNAs is regulated by the ATM-AKT pathway. *Cell Rep.* 2013;3:2100-2112.
398. Boulikas T. Nuclear import of DNA repair proteins. *Anticancer Res.* 1997;17:843-863.
399. Kirby TW, Gassman NR, Smith CE, et al. Nuclear Localization of the DNA Repair Scaffold XRCC1: Uncovering the Functional Role of a Bipartite NLS. *Sci Rep.* 2015;5:13405.
400. Ries F, Klastersky J. Nephrotoxicity induced by cancer chemotherapy with special emphasis on cisplatin toxicity. *Am J Kidney Dis.* 1986;8:368-379.
401. Pabla N, Dong Z. Cisplatin nephrotoxicity: mechanisms and renoprotective strategies. *Kidney Int.* 2008;73:994-1007.
402. Green JA, Lainakis G. Cytotoxic chemotherapy for advanced or recurrent cervical cancer. *Ann Oncol.* 2006;17 Suppl 10:x230-232.
403. Leitao MM, Jr., Chi DS. Recurrent cervical cancer. *Curr Treat Options Oncol.* 2002;3:105-111.
404. Gadducci A, Tana R, Cosio S, Cionini L. Treatment options in recurrent cervical cancer (Review). *Oncol Lett.* 2010;1:3-11.
405. Heijkoop ST, van Doorn HC, Stalpers LJ, et al. Results of concurrent chemotherapy and hyperthermia in patients with recurrent cervical cancer after previous chemoradiation. *Int J Hyperthermia.* 2014;30:6-10.
406. Lorusso D, Petrelli F, Coinu A, Raspagliesi F, Barni S. A systematic review comparing cisplatin and carboplatin plus paclitaxel-based chemotherapy for recurrent or metastatic cervical cancer. *Gynecol Oncol.* 2014;133:117-123.
407. Long HJ, 3rd, Bundy BN, Grendys EC, Jr., et al. Randomized phase III trial of cisplatin with or without topotecan in carcinoma of the uterine cervix: a Gynecologic Oncology Group Study. *J Clin Oncol.* 2005;23:4626-4633.
408. Takekida S, Fujiwara K, Nagao S, et al. Phase II study of combination chemotherapy with docetaxel and carboplatin for locally advanced or recurrent cervical cancer. *Int J Gynecol Cancer.* 2010;20:1563-1568.
409. Tsuda H, Hashiguchi Y, Nishimura S, et al. Phase I-II study of irinotecan (CPT-11) plus nedaplatin (254-S) with recombinant human granulocyte colony-stimulating factor support in patients with advanced or recurrent cervical cancer. *Br J Cancer.* 2004;91:1032-1037.
410. Burnett AF, Roman LD, Garcia AA, Muderspach LI, Brader KR, Morrow CP. A phase II study of gemcitabine and cisplatin in patients with advanced, persistent, or recurrent squamous cell carcinoma of the cervix. *Gynecol Oncol.* 2000;76:63-66.
411. Pariente R, Pariente JA, Rodriguez AB, Espino J. Melatonin sensitizes human cervical cancer HeLa cells to cisplatin-induced cytotoxicity and apoptosis: effects on oxidative stress and DNA fragmentation. *J Pineal Res.* 2016;60:55-64.
412. Kilic U, Sahin K, Tuzcu M, et al. Enhancement of Cisplatin sensitivity in human cervical cancer: epigallocatechin-3-gallate. *Front Nutr.* 2014;1:28.
413. Lin WM, Li ZG. Blockage of cisplatin-induced autophagy sensitizes cervical cancer cells to cisplatin. *Genet Mol Res.* 2015;14:16905-16912.
414. Yeh PY, Yeh KH, Chuang SE, Song YC, Cheng AL. Suppression of MEK/ERK signaling pathway enhances cisplatin-induced NF-kappaB activation by protein phosphatase 4-mediated NF-kappaB p65 Thr dephosphorylation. *J Biol Chem.* 2004;279:26143-26148.
415. Chan YY, Kalpana S, Chang WC, Chang WC, Chen BK. Expression of aryl hydrocarbon receptor nuclear translocator enhances cisplatin resistance by upregulating MDR1 expression in cancer cells. *Mol Pharmacol.* 2013;84:591-602.
416. Elmore S. Apoptosis: a review of programmed cell death. *Toxicol Pathol.* 2007;35:495-516.
417. Chou TC, Talalay P. Quantitative analysis of dose-effect relationships: the combined effects of multiple drugs or enzyme inhibitors. *Adv Enzyme Regul.* 1984;22:27-55.
418. Chou TC. Drug combination studies and their synergy quantification using the Chou-Talalay method. *Cancer Res.* 2010;70:440-446.

419. Pietrzak M, Puzianowska-Kuznicka M. p53-dependent repression of the human MCL-1 gene encoding an anti-apoptotic member of the BCL-2 family: the role of Sp1 and of basic transcription factor binding sites in the MCL-1 promoter. *Biol Chem.* 2008;389:383-393.
420. Papa S, Zazzeroni F, Pham CG, Bubici C, Franzoso G. Linking JNK signaling to NF-kappaB: a key to survival. *J Cell Sci.* 2004;117:5197-5208.
421. Almeida LO, Abrahao AC, Rosselli-Murai LK, et al. NFkappaB mediates cisplatin resistance through histone modifications in head and neck squamous cell carcinoma (HNSCC). *FEBS Open Bio.* 2014;4:96-104.
422. Oiso S, Ikeda R, Nakamura K, Takeda Y, Akiyama S, Kariyazono H. Involvement of NF-kappaB activation in the cisplatin resistance of human epidermoid carcinoma KCP-4 cells. *Oncol Rep.* 2012;28:27-32.
423. Fagerlund R, Kinnunen L, Kohler M, Julkunen I, Melen K. NF-{kappa}B is transported into the nucleus by importin {alpha}3 and importin {alpha}4. *J Biol Chem.* 2005;280:15942-15951.
424. La Rosa FA, Pierce JW, Sonenshein GE. Differential regulation of the c-myc oncogene promoter by the NF-kappa B rel family of transcription factors. *Mol Cell Biol.* 1994;14:1039-1044.
425. Lee H, Arsura M, Wu M, Duyao M, Buckler AJ, Sonenshein GE. Role of Rel-related factors in control of c-myc gene transcription in receptor-mediated apoptosis of the murine B cell WEHI 231 line. *J Exp Med.* 1995;181:1169-1177.
426. Hinz M, Krappmann D, Eichten A, Heder A, Scheidereit C, Strauss M. NF-kappaB function in growth control: regulation of cyclin D1 expression and G0/G1-to-S-phase transition. *Mol Cell Biol.* 1999;19:2690-2698.
427. Stehlik C, de Martin R, Kumabashiri I, Schmid JA, Binder BR, Lipp J. Nuclear factor (NF)-kappaB-regulated X-chromosome-linked iap gene expression protects endothelial cells from tumor necrosis factor alpha-induced apoptosis. *J Exp Med.* 1998;188:211-216.
428. Guttridge DC, Albanese C, Reuther JY, Pestell RG, Baldwin AS, Jr. NF-kappaB controls cell growth and differentiation through transcriptional regulation of cyclin D1. *Mol Cell Biol.* 1999;19:5785-5799.
429. Pyndiah S, Tanida S, Ahmed KM, Cassimere EK, Choe C, Sakamuro D. c-MYC suppresses BIN1 to release poly(ADP-ribose) polymerase 1: a mechanism by which cancer cells acquire cisplatin resistance. *Sci Signal.* 2011;4:ra19.
430. Jirawatnotai S, Hu Y, Michowski W, et al. A function for cyclin D1 in DNA repair uncovered by protein interactome analyses in human cancers. *Nature.* 2011;474:230-234.
431. Chen H, Landen CN, Li Y, Alvarez RD, Tollefsbol TO. Enhancement of Cisplatin-Mediated Apoptosis in Ovarian Cancer Cells through Potentiating G2/M Arrest and p21 Upregulation by Combinatorial Epigallocatechin Gallate and Sulforaphane. *J Oncol.* 2013;2013:872957.
432. Stordal B, Davey M. Understanding cisplatin resistance using cellular models. *IUBMB Life.* 2007;59:696-699.
433. Taguchi T, Kato Y, Baba Y, et al. Protein levels of p21, p27, cyclin E and Bax predict sensitivity to cisplatin and paclitaxel in head and neck squamous cell carcinomas. *Oncol Rep.* 2004;11:421-426.
434. He S, Feng M, Liu M, et al. P21-activated kinase 7 mediates cisplatin-resistance of esophageal squamous carcinoma cells with Aurora-A overexpression. *PLoS One.* 2014;9:e113989.
435. Huynh N, Liu KH, Yim M, Shulkes A, Baldwin GS, He H. Demonstration and biological significance of a gastrin-P21-activated kinase 1 feedback loop in colorectal cancer cells. *Physiol Rep.* 2014;2:e12048.
436. Fu X, Feng J, Zeng D, Ding Y, Yu C, Yang B. PAK4 confers cisplatin resistance in gastric cancer cells via PI3K/Akt- and MEK/Erk-dependent pathways. *Biosci Rep.* 2014;34:e00094.

437. di Pietro A, Koster R, Boersma-van Eck W, et al. Pro- and anti-apoptotic effects of p53 in cisplatin-treated human testicular cancer are cell context-dependent. *Cell Cycle.* 2012;11:4552-4562.
438. Stubbert LJ, Smith JM, Hamill JD, Arcand TL, McKay BC. The anti-apoptotic role for p53 following exposure to ultraviolet light does not involve DDB2. *Mutat Res.* 2009;663:69-76.
439. Janicke RU, Sohn D, Schulze-Osthoff K. The dark side of a tumor suppressor: anti-apoptotic p53. *Cell Death Differ.* 2008;15:959-976.
440. Meissner JD. Nucleotide sequences and further characterization of human papillomavirus DNA present in the CaSki, SiHa and HeLa cervical carcinoma cell lines. *J Gen Virol.* 1999;80 (Pt 7):1725-1733.
441. Crook T, Tidy JA, Vousden KH. Degradation of p53 can be targeted by HPV E6 sequences distinct from those required for p53 binding and trans-activation. *Cell.* 1991;67:547-556.
442. Lecane PS, Kiviharju TM, Sellers RG, Peehl DM. Leptomycin B stabilizes and activates p53 in primary prostatic epithelial cells and induces apoptosis in the LNCaP cell line. *Prostate.* 2003;54:258-267.
443. Crook T, Wrede D, Vousden KH. p53 point mutation in HPV negative human cervical carcinoma cell lines. *Oncogene.* 1991;6:873-875.
444. He G, Siddik ZH, Huang Z, et al. Induction of p21 by p53 following DNA damage inhibits both Cdk4 and Cdk2 activities. *Oncogene.* 2005;24:2929-2943.
445. Clohessy JG, Zhuang J, de Boer J, Gil-Gomez G, Brady HJ. Mcl-1 interacts with truncated Bid and inhibits its induction of cytochrome c release and its role in receptor-mediated apoptosis. *J Biol Chem.* 2006;281:5750-5759.
446. Volcic M, Karl S, Baumann B, et al. NF-kappaB regulates DNA double-strand break repair in conjunction with BRCA1-CtIP complexes. *Nucleic Acids Res.* 2012;40:181-195.
447. Janssens S, Tschopp J. Signals from within: the DNA-damage-induced NF-kappaB response. *Cell Death Differ.* 2006;13:773-784.
448. Wang CY, Mayo MW, Baldwin AS, Jr. TNF- and cancer therapy-induced apoptosis: potentiation by inhibition of NF-kappaB. *Science.* 1996;274:784-787.
449. Wang CY, Cusack JC, Jr., Liu R, Baldwin AS, Jr. Control of inducible chemoresistance: enhanced anti-tumor therapy through increased apoptosis by inhibition of NF-kappaB. *Nat Med.* 1999;5:412-417.
450. Lagunas VM, Melendez-Zajgla J. Nuclear Factor-kappa B as a Resistance Factor to Platinum-Based Antineoplasic Drugs. *Met Based Drugs.* 2008;2008:576104.
451. Nakanishi C, Toi M. Nuclear factor-kappaB inhibitors as sensitizers to anticancer drugs. *Nat Rev Cancer.* 2005;5:297-309.
452. Morais C, Gobe G, Johnson DW, Healy H. Inhibition of nuclear factor kappa B transcription activity drives a synergistic effect of pyrrolidine dithiocarbamate and cisplatin for treatment of renal cell carcinoma. *Apoptosis.* 2010;15:412-425.
453. Venkatraman M, Anto RJ, Nair A, Varghese M, Karunagaran D. Biological and chemical inhibitors of NF-kappaB sensitize SiHa cells to cisplatin-induced apoptosis. *Mol Carcinog.* 2005;44:51-59.
454. Deveraux QL, Takahashi R, Salvesen GS, Reed JC. X-linked IAP is a direct inhibitor of cell-death proteases. *Nature.* 1997;388:300-304.
455. Salvesen GS, Duckett CS. IAP proteins: blocking the road to death's door. *Nat Rev Mol Cell Biol.* 2002;3:401-410.
456. Connell-Crowley L, Harper JW, Goodrich DW. Cyclin D1/Cdk4 regulates retinoblastoma protein-mediated cell cycle arrest by site-specific phosphorylation. *Mol Biol Cell.* 1997;8:287-301.
457. Jirawatnotai S, Hu Y, Livingston DM, Sicinski P. Proteomic identification of a direct role for cyclin d1 in DNA damage repair. *Cancer Res.* 2012;72:4289-4293.

458. Olive PL, Banath JP. Kinetics of H2AX phosphorylation after exposure to cisplatin. *Cytometry B Clin Cytom.* 2009;76:79-90.
459. Webster GA, Perkins ND. Transcriptional cross talk between NF-kappaB and p53. *Mol Cell Biol.* 1999;19:3485-3495.
460. Rocha S, Martin AM, Meek DW, Perkins ND. p53 represses cyclin D1 transcription through down regulation of Bcl-3 and inducing increased association of the p52 NF-kappaB subunit with histone deacetylase 1. *Mol Cell Biol.* 2003;23:4713-4727.
461. Biroccio A, Benassi B, Amodei S, Gabellini C, Del Bufalo D, Zupi G. c-Myc down-regulation increases susceptibility to cisplatin through reactive oxygen species-mediated apoptosis in M14 human melanoma cells. *Mol Pharmacol.* 2001;60:174-182.
462. Leonetti C, Biroccio A, Candiloro A, et al. Increase of cisplatin sensitivity by c-myc antisense oligodeoxynucleotides in a human metastatic melanoma inherently resistant to cisplatin. *Clin Cancer Res.* 1999;5:2588-2595.
463. Xu B, Liu P, Li J, Lu H. c-MYC depletion potentiates cisplatin-induced apoptosis in head and neck squamous cell carcinoma: involvement of TSP-1 up-regulation. *Ann Oncol.* 2010;21:670-672.
464. Checinska A, Hoogeland BS, Rodriguez JA, Giaccone G, Kruyt FA. Role of XIAP in inhibiting cisplatin-induced caspase activation in non-small cell lung cancer cells: a small molecule Smac mimic sensitizes for chemotherapy-induced apoptosis by enhancing caspase-3 activation. *Exp Cell Res.* 2007;313:1215-1224.
465. Qu Y, Xia P, Zhang S, Pan S, Zhao J. Silencing XIAP suppresses osteosarcoma cell growth, and enhances the sensitivity of osteosarcoma cells to doxorubicin and cisplatin. *Oncol Rep.* 2015;33:1177-1184.
466. Dean EJ, Ward T, Pinilla C, et al. A small molecule inhibitor of XIAP induces apoptosis and synergises with vinorelbine and cisplatin in NSCLC. *Br J Cancer.* 2010;102:97-103.
467. You L, Wang Y, Jin Y, Qian W. Downregulation of Mcl-1 synergizes the apoptotic response to combined treatment with cisplatin and a novel fiber chimeric oncolytic adenovirus. *Oncol Rep.* 2012;27:971-978.
468. Naniwa J, Kigawa J, Akeshima R, et al. Leptomycin B enhances CDDP-sensitivity via nuclear accumulation of p53 protein in HPV-positive cells. *Cancer Sci.* 2003;94:1099-1103.
469. Guadamillas MC, Cerezo A, Del Pozo MA. Overcoming anoikis--pathways to anchorage-independent growth in cancer. *J Cell Sci.* 2011;124:3189-3197.
470. O'Connor PM, Jackman J, Bae I, et al. Characterization of the p53 tumor suppressor pathway in cell lines of the National Cancer Institute anticancer drug screen and correlations with the growth-inhibitory potency of 123 anticancer agents. *Cancer Res.* 1997;57:4285-4300.
471. Forbes S, Clements J, Dawson E, et al. Cosmic 2005. *Br J Cancer.* 2006;94:318-322.
472. Petitjean A, Mathe E, Kato S, et al. Impact of mutant p53 functional properties on TP53 mutation patterns and tumor phenotype: lessons from recent developments in the IARC TP53 database. *Hum Mutat.* 2007;28:622-629.
473. Jones GJ, Heiss NS, Veale RB, Thornley AL. Amplification and expression of the TGF-alpha, EGF receptor and c-myc genes in four human oesophageal squamous cell carcinoma lines. *Biosci Rep.* 1993;13:303-312.
474. Shimada Y, Imamura M, Wagata T, Yamaguchi N, Tobe T. Characterization of 21 newly established esophageal cancer cell lines. *Cancer.* 1992;69:277-284.
475. Godwin AK, Meister A, O'Dwyer PJ, Huang CS, Hamilton TC, Anderson ME. High resistance to cisplatin in human ovarian cancer cell lines is associated with marked increase of glutathione synthesis. *Proc Natl Acad Sci U S A.* 1992;89:3070-3074.
476. Sabichi AL, Hendricks DT, Bober MA, Birrer MJ. Retinoic acid receptor beta expression and growth inhibition of gynecologic cancer cells by the synthetic retinoid N-(4-hydroxyphenyl) retinamide. *J Natl Cancer Inst.* 1998;90:597-605.

477. Liu J, Yang G, Thompson-Lanza JA, et al. A genetically defined model for human ovarian cancer. *Cancer Res.* 2004;64:1655-1663.
478. Hobbs S, Jitrapakdee S, Wallace JC. Development of a bicistronic vector driven by the human polypeptide chain elongation factor 1alpha promoter for creation of stable mammalian cell lines that express very high levels of recombinant proteins. *Biochem Biophys Res Commun.* 1998;252:368-372.
479. Beier KT, Samson ME, Matsuda T, Cepko CL. Conditional expression of the TVA receptor allows clonal analysis of descendents from Cre-expressing progenitor cells. *Dev Biol.* 2011;353:309-320.
480. Fukazawa H, Mizuno S, Uehara Y. A microplate assay for quantitation of anchorage-independent growth of transformed cells. *Anal Biochem.* 1995;228:83-90.
481. Di L, Kerns EH, Gao N, et al. Experimental design on single-time-point high-throughput microsomal stability assay. *J Pharm Sci.* 2004;93:1537-1544.

APPENDIX I

INI-43 IC_{50} determination plots in additional ovarian cancer cell lines

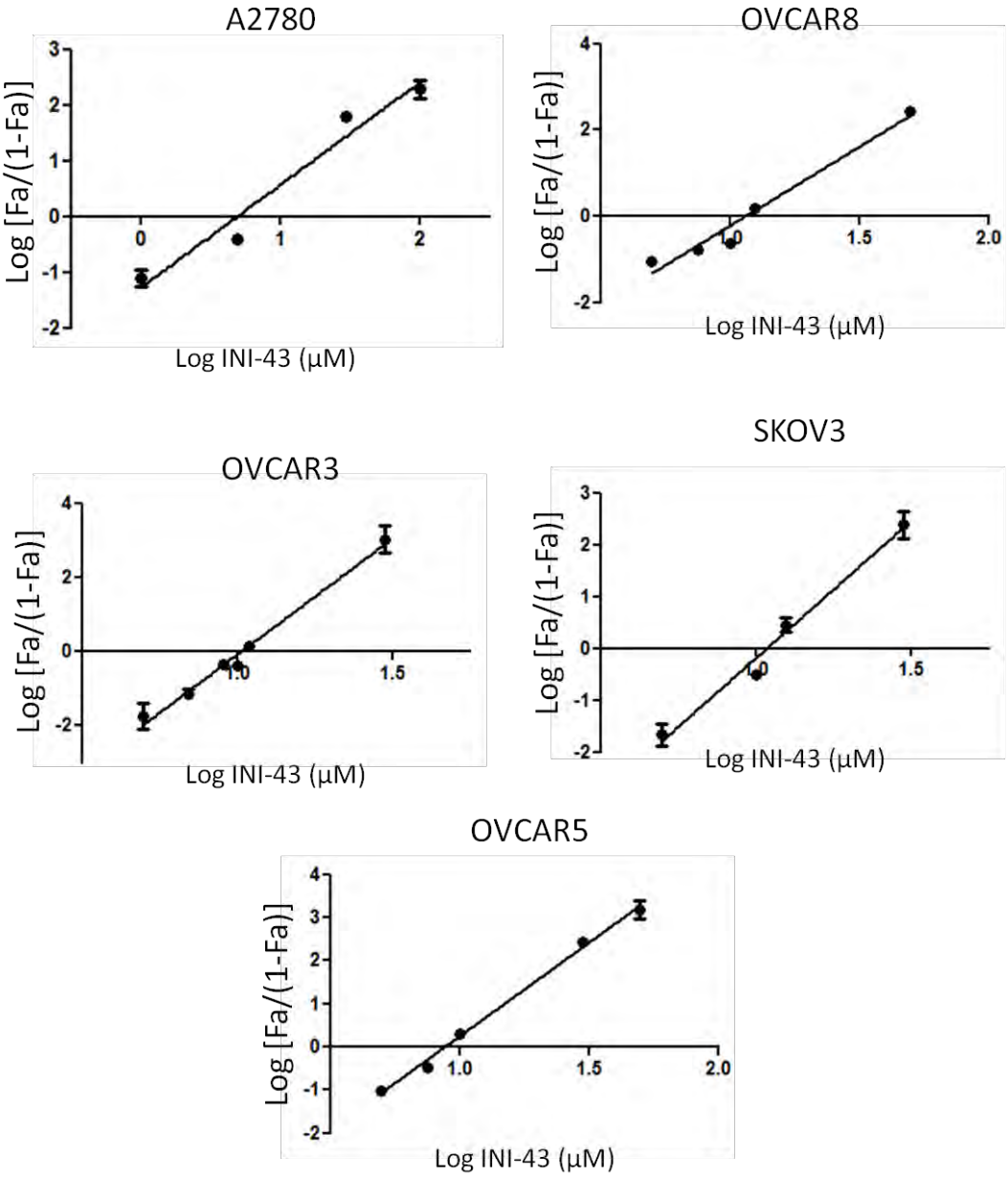

INI-43 IC_{50} determination plots in additional oesophageal cancer cell lines

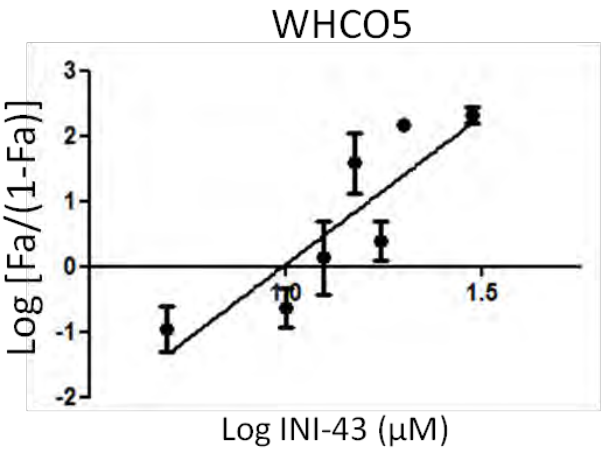

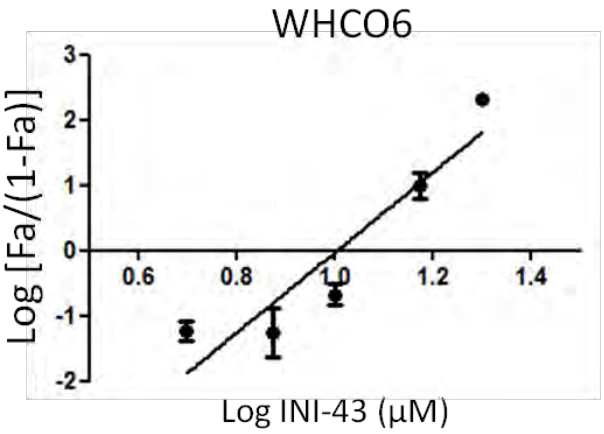

INI-43 IC_{50} determination plots in additional non-cancer cell lines

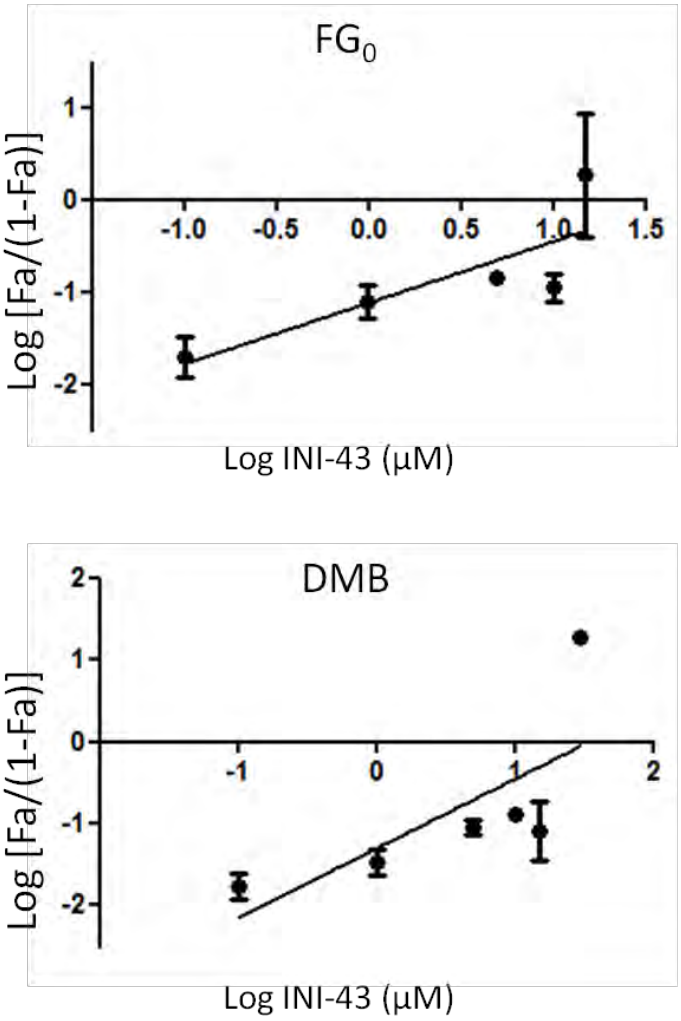

Figure A.1. INI-43 IC_{50} determination in ovarian cancer, oesophageal cancer and non-cancer fibroblast cell lines. Five-thousand cells were seeded per well in 96-well plates and allowed to settle overnight. Cells were then treated with INI-43 at various concentrations, and viable cells were assayed 48 hours later using the MTT reagent as previously described. Cell viability was standardized to the untreated cells, and plotted as log [Fa/(1-Fa)] against INI-43 concentration in log scale as previously described. Results shown are mean ± SEM of experiments performed in 5 replicates repeated at least two independent times.

APPENDIX II

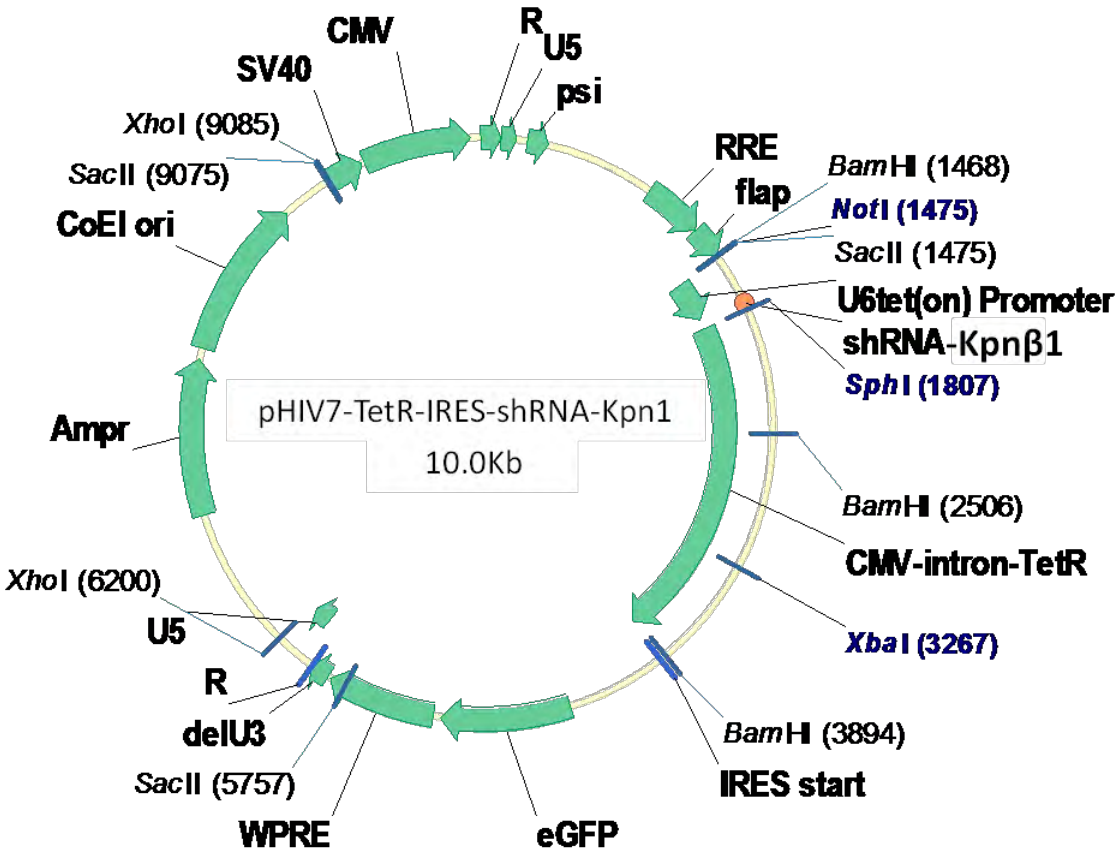

Figure A.2. pHIV7-TetR-IRES-shRNA-Kpnβ1 (pTIG-shKpnβ1). The conditional shRNA expressing plasmid containing the shKpnβ1 under the control of the tetracycline/doxycycline-inducible U6 promoter, spanned by *NotI* and *SphI* restriction sites. The plasmid also contains IRES for expression of GFP as a selection marker in eukaryotic cells, and Ampicillin resistance gene (AmpR) for selection in bacterial cells.

APPENDIX III

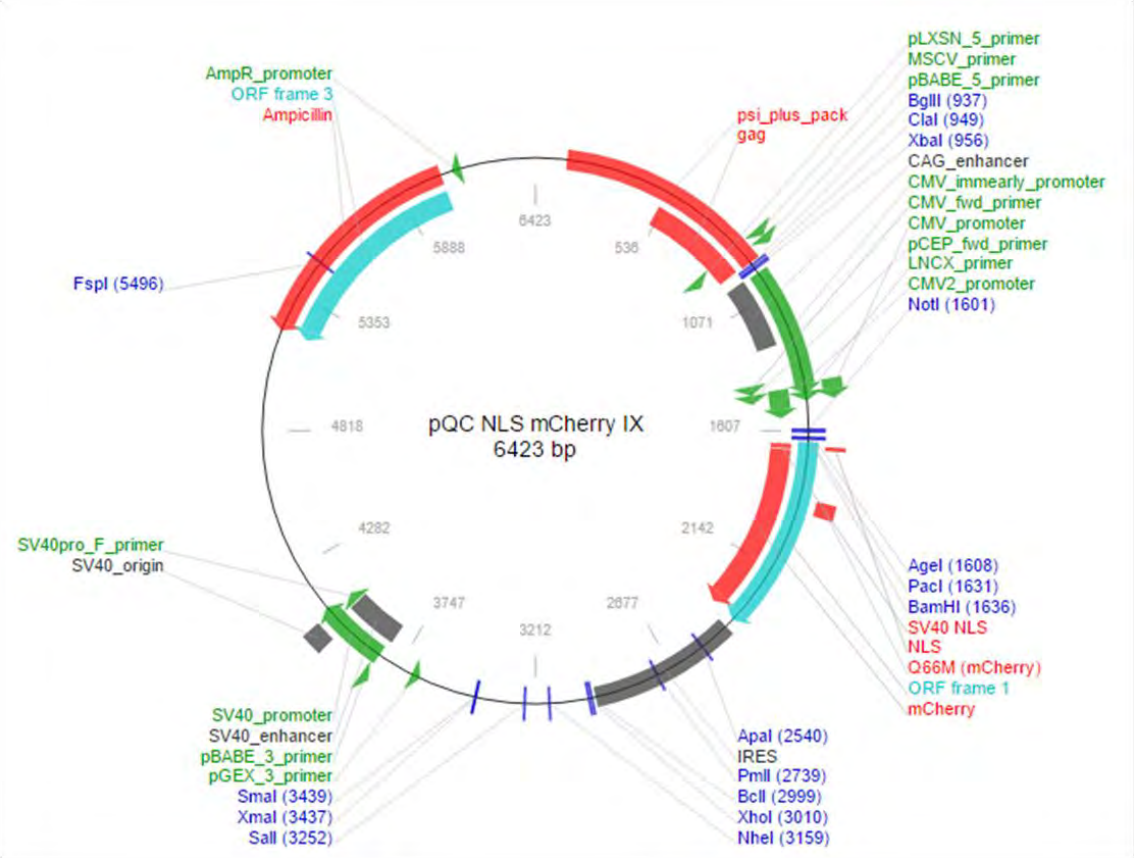

Figure A.3. pQC-NLS-mCherry-IX. The pQC construct which constitutively expressed the NLS-tagged mCherry fluorescent protein under the control of the CMV promoter.

APPENDIX IV

Table A.1. Combination Index determination: CDDP and INI-43 concentrations used in cell viability assays

CDDP (μM)	INI-43 (μM)		
	1INI-43:3CDDP	1INI-43:4CDDP	1INI-43:5CDDP
3	1	0.75	0.6
7.5	2.5	1.875	1.5
15	5	3.75	3
22.5	7.5	5.625	4.5
30	10	7.5	6
45	15	11.25	9

Table A.1. CDDP and INI-43 concentrations used in determining the nature of interaction between the two drugs. Cells were subjected to treatment with single INI-43, single CDDP or a combination of INI-43 and CDDP. The combination treatment was carried out where the ratio of the two drugs remain constant in each experiment, and the INI-43 to CDDP ratios tested were 1:3, 1:4 and 1:5.